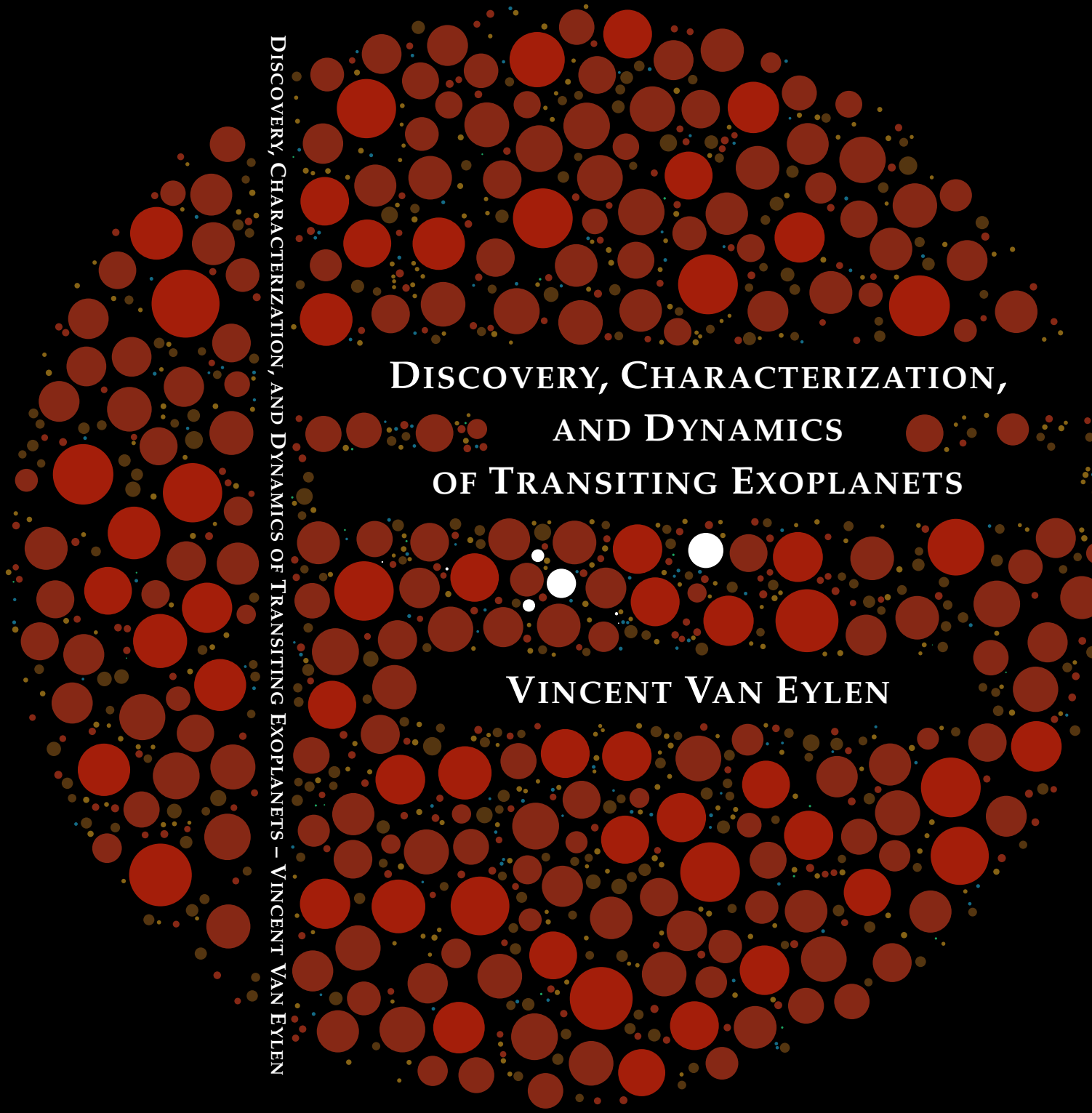
Discovery, Characterization, and Dynamics of Transiting Exoplanets – Vincent Van Eylen
Discovery, Characterization, and Dynamics of Transiting Exoplanets
Vincent Van Eylen

Discovery, Characterization, and Dynamics of Transiting Exoplanets

Vincent Van Eylen

PhD Thesis, November 2015

Advisor: Prof. Simon Albrecht
Co-advisors: Prof. Hans Kjeldsen, Prof. Josh Winn

Stellar Astrophysics Centre (SAC)
Department of Physics and Astronomy
Faculty of Science and Technology
Aarhus University, Denmark

Vincent Van Eylen
Discovery, Characterization, and Dynamics of Transiting Exoplanets

November 2015

PHD THESIS ADVISORS:
Prof. Simon Albrecht
Prof. Hans Kjeldsen
Prof. Josh Winn

Aarhus University – Faculty of Science and Technology
Department of Physics and Astronomy – Stellar Astrophysics Centre (SAC)
Ny Munkegade 120, Building 1520, Aarhus, Denmark

FRONT IMAGE:
All known transiting exoplanets to date. The size of the circles is proportional to the size of the planets, while the colors range from orange for planets larger than Jupiter, to blue for planets smaller than Earth. The eight planets in the solar system are shown in white.

PREFACE

When doing astronomy for a few years, at some point you inevitably find yourself dragged down to tiny details - stuck at a computer, writing, calculating, computing. It can be easy to forget about *cool science*. But there is a cure! Fly to *Gran Canaria*. Ignore all the tour operators and the families on their way to an all-inclusive hotel, instead, take the next plane to *La Palma*. Say hello to the beach. Drive up the *Roque de los Muchachos*: enjoy an hour cruising up on the windy road from sea level up to 2000 meter. Make sure that *Radio Quarenta* keeps you company. Get handed over keys, accompanied by the words, *it's your telescope now*. Feel the building move as you point to a star. Be amazed as you realize the light you are now seeing has traveled hundreds of years to get here. Observe binary stars. Observe the effect of planets on stars. Split the light into a full spectrum of colors. Don't be upset when a bit of your observing time gets taken away for a *target of opportunity*, instead realize that you are pointing your telescope elsewhere to look at a *gamma ray burst*. As you get more tired, blast several entire *Muse* concerts through the speakers and sing along – no one can hear you – and eat your *super snacks*. Go outside and realize that this is one of the darkest places in the world. No sound but the wind. Look up! See so many stars! See the milky way! Stay longer, and see even more as your eyes adapt! Wonder if all those stars have Earths? Identify the *summer triangle* – you don't need to be in La Palma for this – where the *Kepler* field is and where we know of the existence of thousands of planets. Do they have forests and deserts and beautiful beaches? Bacteria or dinosaurs? Do you know? Realize that within our lifetime, we may find out. Wonder if there's an *exoplanet's astronomer* right now, who's looking back at you? Look up once again, smile! Hurry back to the control room, worry that something may have gone wrong in your absence, but find that the telescope has been flawlessly compensating for the Earth's rotation and tracking your star's movement on the sky. Collect the last photons, they've traveled hundreds of years, so don't be late! Close down the dome well into twilight. Enjoy the sunrise! *This is the big picture* – this is why I do astronomy. For the past three years, I've had the pleasure to learn about exoplanets in the universe. Whether it was about the big picture or the tiny details, I have not done so alone.

Thank you Simon, because I could not have wished for a better thesis advisor. I started as your first student, and if I am a scientist today it is in no small part due to your guidance. You've made me better in countless ways. I will take what you taught me with me through the rest of my career, in science or otherwise. Hans, *tusind tak* for the help and advice throughout the years, in the beginning of my degree, and even before. You taught me my first exoplanet course and supervised my masterthesis project. Without that, I wouldn't be doing astronomy today, let alone studying exoplanets. I owe

a great deal of gratitude to Josh, for being a mentor and a source of scientific creativity and encouragement during six months at MIT. You went above and beyond what I could hope for. Thank you Sara, for hosting me in Boston during the early days of my PhD, and for being an example and a source of inspiration. There's a countless number of researchers and collaborators who have my gratitude for teaching me, helping me, guiding me. Science can rarely be done alone, and I've had the pleasure to work with many brilliant people. Thank you Conny, my first astronomy mentor, without whom I would have never even made it to Denmark.

Throughout the years in Aarhus I've met many wonderful people. Sandra, my first real friend in Denmark – now that my thesis is done you can expect me in Spain. Catalina, my fantastic flatmate, friend and so much more. Tina, for inspiring me to think outside the box and for making me take things less seriously. Gulnur, for always being there, and for countless conversations. Thank you Angela, for making me feel home away from home, and thank you to your beautiful dog Nevada – we've lived the snowiest Boston winter *ever* together. Lisa, my exoplanet friend on the other side of the ocean!

None of what's in this thesis would have ever materialized without so many colleagues at the Stellar Astrophysics Centre, and the morning coffee breaks. You and coffee are the best way to start the day and I am glad to call so many of you my friends. Mikkel, I've been grateful to rely on your scientific wisdom during so much of my PhD. Rikke: *tak for kagen*! Ditte, thank you for being so awesome. You, Tushar, Jakob, Chen, Michael, Rasmus, Bram, we've made the greatest office over the years. Jens and Fatemeh, for showing me the joys of La Palma, and so much more. What would work be without Fridays? Mikkel, Jens and Ditte, it's been a pleasure to build a little office Fridaybar, as well as a friendship which will outlast my time in Aarhus. Vichi, Karsten, Christoffer, Magnus, Victor, Brandon, Caro, I appreciate your regular contributions, be them talking or drinking. Mia, ever helpful with every little PhD struggle. Thank you Brigitte, for always compensating for my lack of administrative discipline, and for doing so with a smile. Louise, you've made many days just a little bit sunnier. Thank you, Jørgen, our center leader, and thanks to all the students in the exoplanet group! Thanks again to countless of the aforementioned people, for proofreading and improving this thesis in so many ways.

Mum and dad, Wout, I enormously appreciate your encouragement regardless of what it is I choose to undertake – I bet you didn't expect I would ever become an astronomer. Sara, a friend in Belgium and beyond, for giving me a dinner to look forward to every few months. Michael, Christophe, Hanne, Christophe, Thomas, Pieter, Natascha, Sofie, Lynn, Kristien, Jorien, for making me remember what beer tastes like whenever I come home to Belgium and for being my friend as if I never left.

Rhita: *Parce que c'est toi le seul à qui j'peux dire, qu'avec toi je n'ai plus peur de vieillir!*

Vincent Van Eylen
Aarhus, 1 November 2015

SUMMARY

Are we alone in the Universe? So far, the question remains unanswered, but a significant leap forward was achieved two decades ago, with the discovery of the first planets orbiting stars other than our Sun. Almost 2000 exoplanets have now been detected. They are diverse in radius, mass and orbital period, but beyond those basic parameters very little is known about them. In this context, I have worked on the discovery and characterization of new, interesting planets, on the one hand, and on the other hand on studying the properties of known planets in much greater detail. To this end, in this thesis I make use of the transit method, which is based on the observed brightness drop of a star as a planet crosses in front of it.

This thesis consists of two parts. The first part focuses on the discovery of new planets and the understanding of exoplanet properties. I report the discovery of the planet Kepler-410A b, a Neptune-sized planet in a 17 day orbit. Kepler-410 is composed of two stars, one of which hosts a transiting planet, and an additional non-transiting planet. The latter was discovered due to its gravitational influence on Kepler-410A b, which causes a variation in the timing of the transits. I was able to identify which of the two stars hosts the planet by using observations from the *Kepler* spacecraft, as well as infrared transit measurements using the *Spitzer* satellite. Furthermore, I found six new planets observed by *Kepler*, which were detected by precisely timing the duration of their transits to identify their host stars. I use asteroseismology, the study of stellar pulsations, to accurately measure the properties of the host stars and the planets. A radial velocity study is presented to follow up candidate planets observed transiting with the *K2* mission, and I present the first results of this study, constraining the masses and bulk compositions of three planets.

The second part of this thesis focuses on dynamics of exoplanets. All the solar system planets orbit in nearly the same plane, and that plane is also aligned with the equatorial plane of the Sun. That is not true for all exoplanets, where misaligned (oblique) planets and even retrograde planet orbits have been discovered. Making use of a novel technique, I measure the inclination angle of Kepler-410A using asteroseismology and find it to be aligned with the orbital plane of the transiting planet. The measurement joins a handful of obliquity measurements, so far suggesting multi-planet systems are mostly aligned. This favors theories suggesting that hot Jupiter migration is responsible for creating misaligned planets. Moreover, unlike the planets in the solar system, which have nearly circular orbits, some exoplanets exhibit highly elliptical orbits. I present the first study of eccentricity focused on small planets in multi-planet systems, and show that their eccentricity is low, while I find that the eccentricity of transiting single-planet systems is slightly higher. These eccentricities are similar to the solar system, but differ from the highly eccentric orbits seen for some massive planets.

CONTENTS

PREFACE v

SUMMARY vii

1 FOR NON-ASTRONOMERS 1
- 1.1 What exoplanets are . . . 1
- 1.2 How exoplanets are found . . . 2
- 1.3 What is known about exoplanets . . . 3
- 1.4 Thesis outline . . . 5

2 SCIENTIFIC FRAMEWORK 7
- 2.1 The space telescope revolution . . . 7
- 2.2 The science of exoplanet transits . . . 10
  - 2.2.1 Transit occurrence . . . 10
  - 2.2.2 Physical transit parameters . . . 11
  - 2.2.3 Transit timing variations . . . 14
  - 2.2.4 Radial velocity follow-up . . . 14
  - 2.2.5 A word about exoplanet atmospheres . . . 15
- 2.3 Understanding host stars through asteroseismology . . . 16
- 2.4 This thesis . . . 18
  - 2.4.1 Part one . . . 18
  - 2.4.2 Part two . . . 19

I EXOPLANET DISCOVERY & CHARACTERIZATION 21

3 TRANSITING EXOPLANETS AND FALSE POSITIVES 23
- 3.1 Transit search for planet candidates . . . 23
- 3.2 False alarms and false positives . . . 25
- 3.3 Planet candidate validation and confirmation strategies . . . 26

4 TWO COLORS: *kepler* AND *spitzer* 31
- 4.1 Planet validation . . . 31
  - 4.1.1 Constraints . . . 32
  - 4.1.2 Scenarios . . . 38
- 4.2 Knowing the star: asteroseismology . . . 41
  - 4.2.1 Frequency analysis . . . 41
  - 4.2.2 Asteroseismic modeling . . . 42
- 4.3 Knowing the planet . . . 44
- 4.4 Transit timing variations: a second planet? . . . 46
- 4.5 Summary . . . 48

5 KNOWING THE STAR, FINDING THE PLANET 49
- 5.1 How to use the transit duration to find the host star . . . 49
- 5.2 Application: six new planets . . . 50
  - 5.2.1 KOI-5 . . . 50
  - 5.2.2 Kepler-92 (KOI-285) . . . 51

5.2.3 Kepler-449 (KOI-270) . . . 52
5.2.4 Kepler-450 (KOI-279) . . . 52
5.3 Discussion . . . 52
6 SYSTEMATIC EFFECTS IN *kepler* DATA 55
6.1 Introduction . . . 56
6.2 Observations . . . 57
6.3 Results . . . 58
6.3.1 Global transit modeling . . . 58
6.3.2 Transit depth variations . . . 60
6.4 Discussion . . . 61
6.4.1 The true planetary radius . . . 61
6.4.2 Other targets . . . 61
6.4.3 Possible causes . . . 63
6.5 Conclusions . . . 65
7 THE SPECTROSCOPIC FOLLOW-UP OF *k2* OBSERVATIONS 67
7.1 Introduction . . . 68
7.2 Photometry . . . 69
7.3 Ground based follow-up observations . . . 71
7.4 Results . . . 74
7.4.1 EPIC 201295312 . . . 74
7.4.2 EPIC 201546283 . . . 76
7.4.3 EPIC 201577035 . . . 76
7.5 Discussion . . . 77

II EXOPLANET DYNAMICS 79
8 EXOPLANETS AND THE SOLAR SYSTEM 81
8.1 The solar system . . . 81
8.2 Large exoplanets . . . 83
8.2.1 Obliquity: the star-planet (mis)alignment . . . 83
8.2.2 Eccentricity: circular and elliptical orbits . . . 84
8.3 Why we need to observe dynamics of small planets . . . 86
9 STAR-PLANET (MIS)ALIGNMENT 89
9.1 Host star inclinations from asteroseismology . . . 90
9.2 Results . . . 92
9.2.1 The case of Kepler-410 . . . 93
9.2.2 Other asteroseismic inclination measurements . . . 95
9.3 Alignment: an emerging trend for small planets in multi-planet systems? . . . 97
10 ECCENTRICITY OF MULTI-PLANET SYSTEMS 101
10.1 Introduction . . . 102
10.2 Methods . . . 105
10.2.1 Pipeline . . . 105
10.2.2 Parameter correlations . . . 109
10.2.3 Transit insertion tests . . . 114

10.3 Results . . . 115
10.3.1 Multi-planet systems with small planets have low eccentricities . . . 116
10.3.2 Homogeneous stellar and planetary parameters and new TTVs . . . 119
10.4 Discussion . . . 123
10.4.1 Habitability . . . 127
10.4.2 Occurrence rates . . . 127
10.5 Conclusions . . . 128
11 ECCENTRICITY OF SINGLE-PLANET SYSTEMS 131
11.1 Sample of "single-planet" systems . . . 132
11.1.1 False positives . . . 132
11.1.2 Single-planet systems vs. multi-planet systems . . . 133
11.2 Analysis method . . . 134
11.3 Results . . . 137
11.3.1 Short-period planets . . . 137
11.3.2 Longer period single-planet systems . . . 138
11.3.3 Eccentricity distribution . . . 143
11.4 Discussion . . . 145
12 ECCENTRICITY OF BINARY STARS 147
12.1 Introduction . . . 148
12.2 Theoretical expectations . . . 150
12.3 Methods . . . 153
12.3.1 Measuring $e \cos \omega$ . . . 153
12.4 Results . . . 154
12.5 Discussion . . . 157

13 CONCLUSIONS AND OUTLOOK 161
DANSK RESUMÉ 169
VITAE 171
PUBLICATIONS 173

BIBLIOGRAPHY 175

1 FOR NON-ASTRONOMERS

This chapter briefly situates this thesis within its context. The chapter aims to provide a brief introduction for non-experts. Readers more familiar with the topic may wish to skip it. In Section 1.1 I explain what exoplanets are, in Section 1.2 I describe how they are found, and in Section 1.3 I briefly summarize some of what is currently known about exoplanets. Finally, in Section 1.4 I provide an outline of this thesis, and give some information about the order in which the subsequent chapters can best be read.

1.1 WHAT EXOPLANETS ARE

Extrasolar planets, or in short exoplanets, are planets which exist outside the solar system. The solar system consists of eight planets in orbit around the Sun: Mercury, Venus, Earth, Mars, Jupiter, Saturn, Uranus, and Neptune. Other stars can, like the Sun, have planets in orbit too, and those planets are called exoplanets. To first order, exoplanet systems are similar to the solar system. Like the Sun, stars are large shining objects. Because of its proximity, the Sun provides the Earth with far more light than stars do, but the most nearby stars can nevertheless be seen with the naked eye in the night sky, while fainter stars require binoculars or telescopes. In contrast to stars, planets are much smaller, and because they don't have an internal nuclear heat source, they are typically also much colder and darker.

The solar system planets are relatively nearby, so that high-resolution images showing the surface of the planets exist for all eight. In addition, the planets' proximity allows them to be visited, e.g. by the unmanned Curiosity Rover on Mars. The same is not true for exoplanets because they are far away. The nearest star other than the Sun is Proxima Centauri at a distance of 4.24 light years, which means that light takes 4.24 years to reach Earth from this star. Reaching the star would take thousands of years with current technology, and even in the foreseeable future it would likely take several decades of travel.

Since visiting exoplanets is not an option, the information we have about these planets is far more limited than for planets in the solar system. The situation is worse, because we cannot typically make images of exoplanets either. This is because the planets are too faint and too close to their much brighter host stars, a difficulty which can be compared to trying to see a fly right next to a car light. This has complicated the discovery of exoplanets and the first planet orbiting a star similar to the Sun was only found relatively recently, in 1995.

1.2 HOW EXOPLANETS ARE FOUND

Initially most planets were discovered by monitoring the movement they induce on their host stars under the influence of gravity. As the Earth describes a circle around the Sun, the Sun also undergoes a (much) smaller movement, as both Sun and Earth orbit their common center of gravity. Therefore, the Sun undergoes a movement which is caused by the eight solar system planets. The same is true for other stars when planets orbit around them. The movement of a star relative to an observer can be measured using a method known as the *radial velocity (RV) method*, which is illustrated in the left panel of Figure 1. The larger the movement, the easier it is to measure. Consequentially, the RV method is mostly sensitive to large, relatively close-in planets, as they cause the largest movement of their host stars. The movement of a star is measured making use of the Doppler effect, where the observed color of a star changes when it is approaching to or receding from an observer, just as the pitch of an ambulance's sound appears different when the ambulance is approaching or receding.

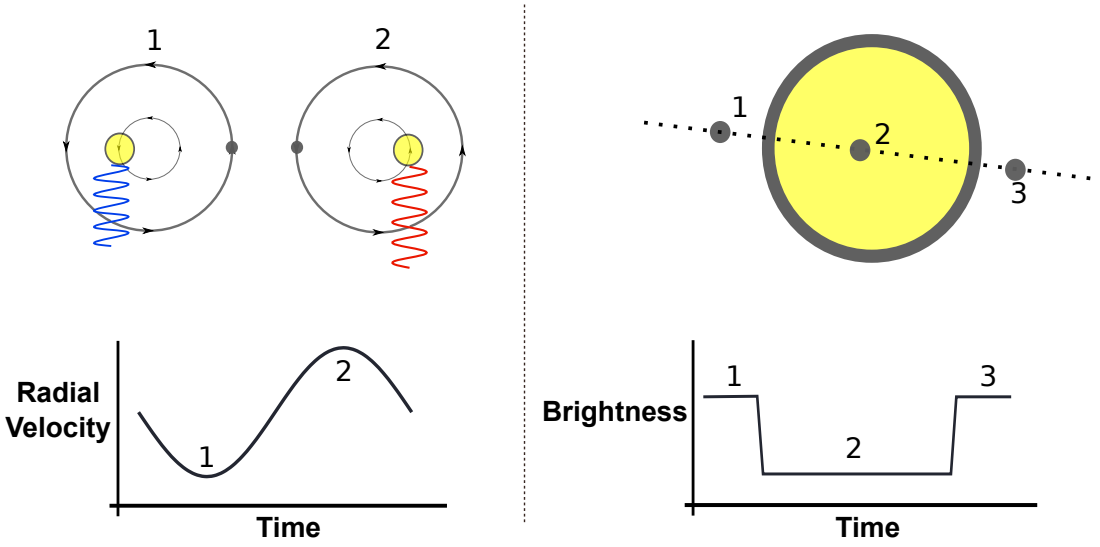

Figure 1 – Cartoon showing the two most common methods to detect exoplanets. The star is indicated in yellow, and the planet in grey. *Left:* the radial velocity (RV) method. As the star and planet orbit their common center of mass, the stellar light is periodically blueshifted and redshifted. *Right:* the transit method. As a planet passes between the star and an observer, the total observed brightness of the star temporarily decreases because part of the star's light is physically blocked.

The most important other detection method is called the *transit method*, which is illustrated in the right panel of Figure 1. The transit method is used during most of this thesis. The method uses the fact that the brightness of a star is observed to drop because a planet moves in front of it, physically blocking a part of the star's light. The phenomenon is comparable to a solar eclipse, in which the Sun's brightness is dimmed as an object (e.g. the Moon)

moves in between an observer and the Sun. The situation is similar for exoplanets. If the brightness of a star is observed over time, a lucky observer may see the overall brightness of the star suddenly decrease and thereby infer the presence of an exoplanet. It is worth emphasizing that in contrast to a solar eclipse, an exoplanet is not actually seen crossing the star's surface, because only the total integrated light of a star can be measured. Not all planets transit, since a large fraction of them have orbital orientations which imply that they do not pass in front of their stars, relative to an observer on Earth.

In practice transits can be very shallow, because planets are usually much smaller than stars. The larger the planet, the deeper its transit, and the easier it is to detect, but even Jupiter-sized planets cause a drop in brightness of only a fraction of a percent when they transit a star similar to the Sun. Moreover, the atmosphere of our own Earth makes it harder to reliably detect exoplanets transiting, because atmospheric instabilities cause apparent variations in the brightness of a star. As a result, most transiting planets are not discovered using ground-based telescopes, but rather utilizing satellites or space telescopes. An example of such a space telescope is the NASA *Kepler* mission, which was launched in 2009, and whose data is used throughout this thesis.

Although the RV and transit methods are by far the most prolific, a few other methods have been employed to detect new exoplanets. They include microlensed planets which are discovered making use of a relativistic gravitational effect, and direct imaging. The direct imaging method is the only one which allows for a planet to be directly seen in an image. While the method holds great promise, it has so far only been used to detect a few very young, hot exoplanets traveling on large orbits at great distances from their host stars, because these planets offer the best contrast ratio relative to their stars.

1.3 WHAT IS KNOWN ABOUT EXOPLANETS

During the past twenty years almost 2000 exoplanets have been found. The number of known exoplanets is small compared to the much larger amount of known stars in the universe, but this is because planets are hard to find. In fact, planets are very common and recent studies suggest almost every star may have at least one planet.

Some exoplanet systems are very similar to the solar system, while others are not. It is important to keep in mind that the solar system planets are themselves very different from each other. For example, the Earth has a rocky surface, while Jupiter and Saturn are gas planets. Jupiter is also 11 times larger than Earth and 318 times more massive. The Earth itself is more than double the size of Mercury, and 18 times Mercury's mass. Exoplanets occur with a similar diversity in mass and size. The mass and radius are not always

simultaneously known for an exoplanet, but when they are, they can be used to constrain the mean density of the planet. It appears that small planets are often rocky, while large planets have a lower density and must therefore contain more volatile elements, such as gases or ices. This is similar to the solar system where small planets, like Earth, are rocky, while the giant planets are not.

The orbits of the solar system have periods ranging from 88 days (Mercury) to 165 years (Neptune), while the Earth completes an orbit around the Sun in approximately 365 days. The longest period exoplanets are difficult to detect – for one, because they require very patient astronomers – but there are known planets with periods much shorter than Mercury's. In fact, some exoplanets are known to have periods less than one day! The solar system planets have orbits which are mostly circular, while this is not necessarily true for exoplanets where some have very elliptical orbits. In some cases, multiple planets are found to orbit the same star, while in other cases only a single planet has been detected. Planets also occur in binary star systems, sometimes orbiting around one component of a double star, in other cases planets are in orbit around both stars. Beyond mass, size and period, often very little information is available about an exoplanet, because almost all planets are found using indirect methods inferring their existence from their influence on the stars they orbit.

The stars which are orbited by planets are not all like the Sun. In fact, although the first known exoplanets is often said to be 51 Peg (Mayor and Queloz 1995), a planet was discovered a few years earlier orbiting a so-called pulsating radio star or pulsar (Wolszczan and Frail 1992). Planets are found around stars both younger and older than the Sun, including more evolved giant stars which are several times larger than the Sun. Recently, small stars known as K and M dwarf stars have received increased attention in the search for new planets. These stars are interesting because they are relatively cool, which implies that orbiting planets receive less light. As a consequence close-in planets orbiting these stars on relatively short orbital periods may be cool enough to be potentially habitable. Such short-period planets are easier to find. In addition, because K and M dwarf stars are smaller, the relative size of the planets compared to the stars is larger, which also makes detecting them easier.

To date, not much is known about exoplanetary atmospheres, although in a few cases molecules have been detected. The most common way in which this is done is utilizing a technique known as *transmission spectroscopy*. When star light passes through the planet's atmosphere during a planetary transit, some wavelengths of light pass through the atmosphere, while others are absorbed. The details of this depend on the molecules in the atmosphere, so

that their presence can be studied in this way. A few detections of sodium and water molecules in exoplanet atmospheres have been made, although these observations have mostly been limited to relatively large exoplanets. Eventually, information about a planet's atmosphere may reveal indications about the presence of life on these planets, through the detection of specific molecules, so called bio-signatures or bio-indicators.

1.4 THESIS OUTLINE

This thesis is structured in two parts. The first part is focused on the discovery of new transiting planets, and the detailed characterization of planet properties. The second part deals with planetary dynamics, more specifically with the ellipticity of exoplanet orbits and the orientation of their stars' rotation axes. Before diving into those two parts, a general scientific introduction about transiting exoplanets is provided in the next chapter. In addition, the first chapter of each part provides a more specific introduction.

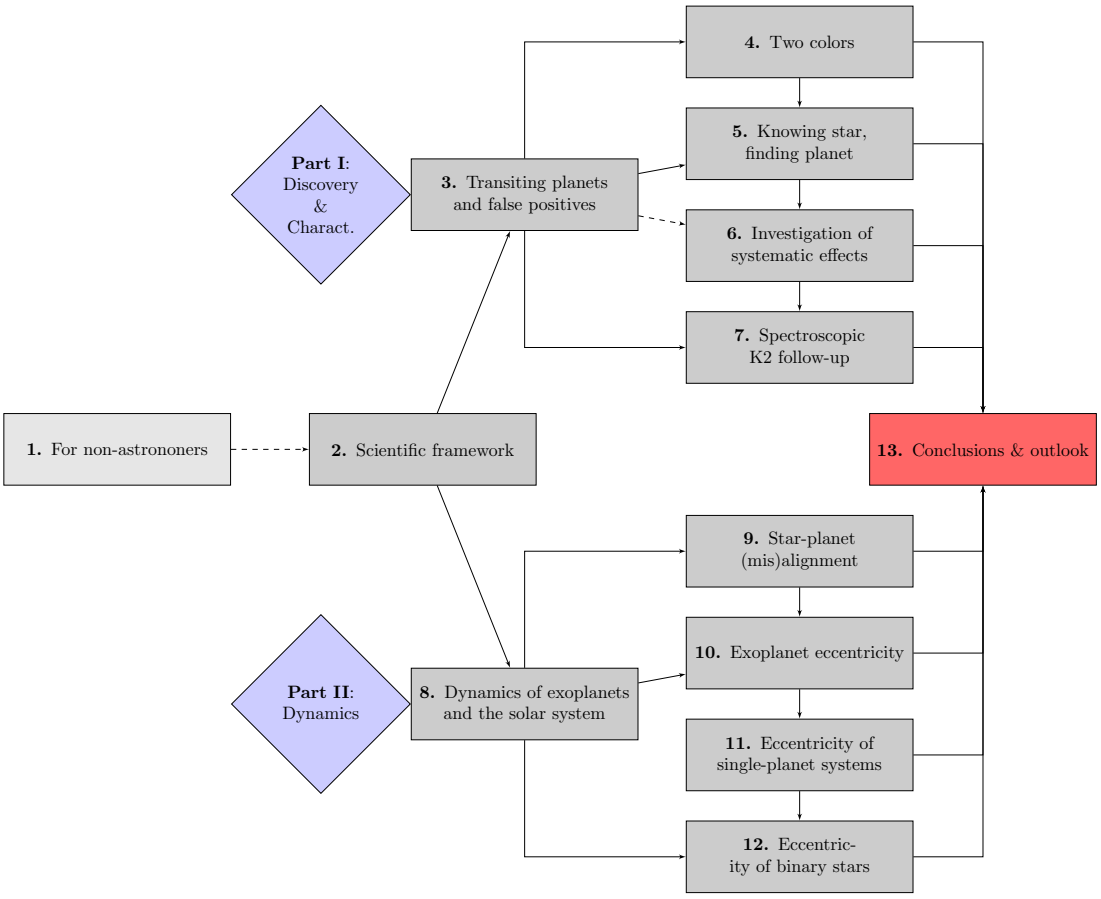

Figure 2 – Flowchart describing the different chapters of this thesis and the order in which they can ideally be read.

The other chapters in each part are structured such that they can be read independently or in order of appearance, and the two parts are themselves

mutually independent. Chapter 6 is fairly technical, as detailed properties of *Kepler* data are discussed, and some readers may wish to skip it. The final chapter of this thesis provides conclusions and a future outlook, which span both parts of the thesis. A schematic view of this thesis is shown in Figure 2.

2 SCIENTIFIC FRAMEWORK

This chapter aims to set the scientific stage for the rest of this thesis, by introducing the concepts which are widely used in the next chapters. I have chosen brevity over completeness, so that this chapter makes no attempt to be a complete introduction to the broad field exoplanet research entails, but rather focuses on concepts that are the most relevant here. For readers interested in a more general introduction a large body of excellent literature exists (e.g. the monograph by Seager and Lissauer 2010).

In Section 2.1 I describe the revolution which has taken place during the past few years, because of the availability of high-quality photometry from space-based instruments. The quality of the photometry of these instruments – *Kepler* in particular – makes it possible to observe transits of small planets. More details about the science behind exoplanet transits is given in Section 2.2. When and how often do transits happen? Which planetary properties can be derived from transit observations? I also briefly describe how radial velocity measurements can be used to detect planets and why they remain important even in the context of transiting exoplanets. In Section 2.3, I turn my attention to determining the properties of planet host stars. I outline how understanding host stars is crucial for understanding the planets, and focus in particular on the role of asteroseismology to understand stars. Finally, in Section 2.4, I describe an outline of the remainder of this thesis, which is structured in two parts that each come with their own brief introductory chapter, and a final chapter presenting some conclusions as well as a future outlook.

2.1 THE SPACE TELESCOPE REVOLUTION

During the past few years, exoplanet science has been revolutionized by the advent of photometry from space. Prior to this, detecting planets through their transits was challenging because the Earth's atmosphere's stability makes it difficult to detect tiny variations in the observed brightness of a star. As a consequence, only transits of large exoplanets can be observed from ground. Spacecrafts like MOST (Walker et al. 2003), CoRoT (Auvergne et al. 2009) and *Kepler* (Borucki et al. 2010) have changed the landscape by providing photometry of stars from space, measuring the brightness of selected stars over time.

MOST was primarily concerned with measuring stellar oscillations (see Section 2.3). CoRoT detected its first transiting exoplanet in 2007 and has since found several dozen. The main source of observations used in this thesis comes from the *Kepler* mission, a NASA mission which was launched in

March 2009. Its primary goal is the discovery of exoplanets, including earth-sized planets in the habitable zone. *Kepler* detected transiting exoplanets by monitoring the brightness of approximately 150,000 stars simultaneously and looking for periodic dips in brightness. For about four years, it has observed the same field of view and largely the same stars (in the Cygnus-Lyra region, see Figure 3). The large majority of stars were observed in a long cadence sampling mode, in which their brightness was recorded in 29.4 minute intervals (Borucki et al. 2008), while a small subset of (several hundred) stars were observed in short cadence, i.e. every 58.8 seconds.

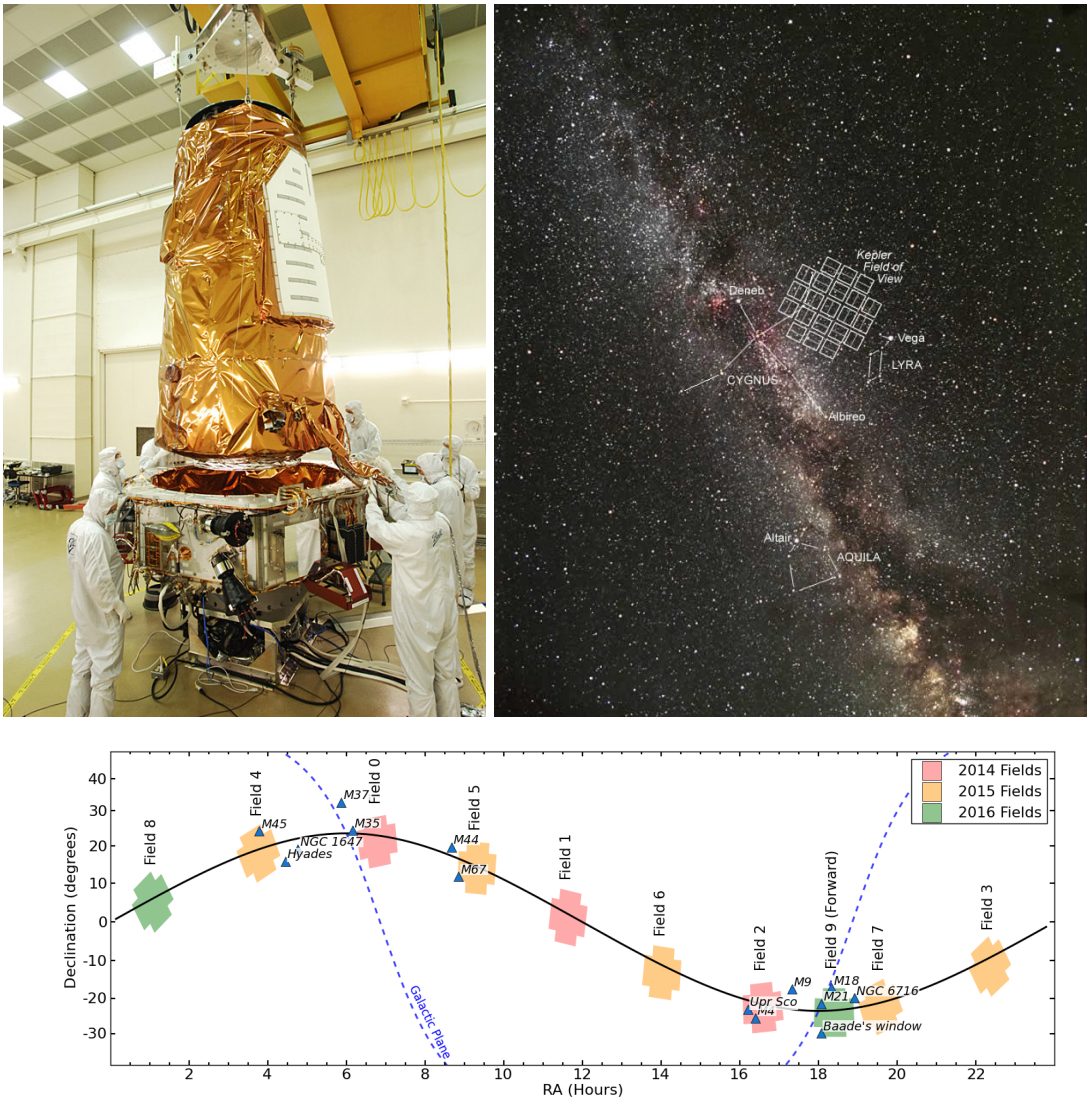

Figure 3 – The *Kepler* mission. *Top left: Kepler* spacecraft construction prior to launch (credit: Ball Aerospace). *Top right:* the field of view of the original *Kepler* mission, which it observed continuously for four years. *Bottom:* the *K2* mission (which uses the same *Kepler* spacecraft) observes a planned 10 different fields, each for about 80 days.

As the satellite orbits in a heliocentric, Earth-trailing orbit, its 42 charge-coupled device (CCD) cameras have observed in a wavelength band ranging from 450 to 900 nm. The field of view is 110 square degrees and images are collected on 4 arcsecond pixels. A 6-hour photometric precision of 18 parts per million can be achieved (ppm, Koch et al. 2010), allowing the detection of the smallest (i.e. Earth-sized) planets.

The *Kepler* mission has been very prolific: at the time of writing, the NASA exoplanet archive[1] lists 1892 confirmed planets, of which 1030 are discovered by *Kepler*. There's a further 3666 planet candidates for which transits are detected but which await further vetting to prove or disprove their validity. A large majority of these candidates are expected to be genuine planets (e.g. Fressin et al. 2013).

The *Kepler* nominal mission ceased operation in May 2014 after a second reaction wheel failed, making it impossible to maintain the required pointing accuracy. However, the *Kepler* spacecraft was reused for a different mission dubbed *K2*, making use of only two functional reaction wheels. The refurbished mission points in the ecliptic plane (rather than the *Kepler* Cygnus-Lyra field) because in this way the solar flux helps to stabilize the two-wheel mission and a total of at least 10 different fields are currently set for observation (see Figure 3; bottom). Each of the fields will be monitored for about 80 days. Because the pointing is less stable than in the original *Kepler* mission, the data quality is not as exquisite and more elaborate data reduction techniques are needed. Nevertheless, at the time of writing, with data for the first four campaigns available, 24 transiting planets have already been securely detected with many more candidates awaiting further analysis. The ongoing *K2* mission provides what is in some way a preparation for the upcoming MIT-NASA TESS mission (Ricker et al. 2014), which after launch in 2017 will cover the full sky within two years, observing each 1/24th of the sky for about one month. This approach allows for the discovery of transiting planets around the brightest, most nearby stars. In the more distant future the European PLATO mission (Rauer et al. 2014) is scheduled for launch in 2024.

Apart from exerting a major influence on exoplanet science, space photometry has also revolutionized asteroseismology, the science of stellar oscillations. As stars oscillate, they vary in brightness, so that the ultra-precise photometric missions, with long time series of observations, are ideally suited to detect stellar oscillations. Furthermore asteroseismology turns out to be a very useful tool to characterize exoplanet host stars, so that there is not only an observational but also a scientific synergy.

1 http://kepler.nasa.gov/Mission/discoveries/

In Section 2.2, I describe the science behind exoplanet transits. I detail the physics that can be derived from transits, as well as those properties for which additional exoplanet detection and characterization methods are required. In Section 2.3, I describe the need for characterizing planet host stars to learn about the planets, and I focus in particular on asteroseismology.

2.2 THE SCIENCE OF EXOPLANET TRANSITS

In this section scientific background about exoplanet transits is provided. In Section 2.2.1 I describe when and how often planets transit. I discuss some of the properties of exoplanet transits and the physics that can be derived from them, with a focus on those parameters that are relevant for the subsequent chapters. For a more general introduction to exoplanet transits, as well as more details, I refer the reader to the excellent discussion by Winn (2010). In Section 2.2.2 I explore the physical parameters that can be derived from transit observations. Section 2.2.3 deals with the mutual gravitational influence of multiple planets in the same system, which can sometimes be observed in a phenomenon known as transit timing variations (TTVs). In Section 2.2.4 I explain the limitations of transits, and the additional techniques which are needed to fully characterize transiting exoplanets. Finally, although not at the core of this thesis, in Section 2.2.5 I briefly outline how transits can be used to study the atmospheres of planets.

2.2.1 *Transit occurrence*

A planetary transit occurs when the observed brightness of a star drops as a planet moves in front of it and physically blocks a fraction of the light, a phenomenon which is somewhat comparable to a solar eclipse. We use the term *transit* rather than *eclipse* because planets are typically one or two orders of magnitude smaller than stars, causing a planet to block only a small fraction of a star's light.

While transits yield a wealth of information, far from all exoplanets are observed transiting. This is because orbits are oriented randomly, but a transit comes into view only for a privileged observer, who happens to look at the orbit nearly edge-on. This implies that for an observer at any location (e.g. Earth or a satellite close to Earth), only a fraction of all planets can ever be observed in transit. The transit probability p_{tra} depends on the distance of the planet to the star (the semi-major axis a) relative to the radius of the star ($R_\star$)

and the planet (R_p), as well as the eccentricity (e) and orientation (given by the angle of periastron ω) of the orbit:

$$p_{tra} = \left(\frac{R_\star + R_p}{a}\right)\left(\frac{1 + e\sin\omega}{1 - e^2}\right). \tag{2.1}$$

The orbital parameters e and ω aren't always known for individual planets, and the distribution of e for samples of exoplanets is a matter of active research (see also Chapter 10). This is important when attempting to measure the occurrence rate of exoplanets from transit surveys, because to do so one needs to estimate the fraction of planets which transit their star. It follows clearly from Equation 2.1 that the transit probability depends on e and ω. To understand the general influence of eccentricity, we can average over ω, which is distributed uniformly under the assumption that the place of Earth in the universe is not a special one. This leads to $1 + e\sin\omega \to 1$, while the factor $(1 - e^2)^{-1}$ remains, i.e. eccentric planets transit more often than planets on circular orbits.

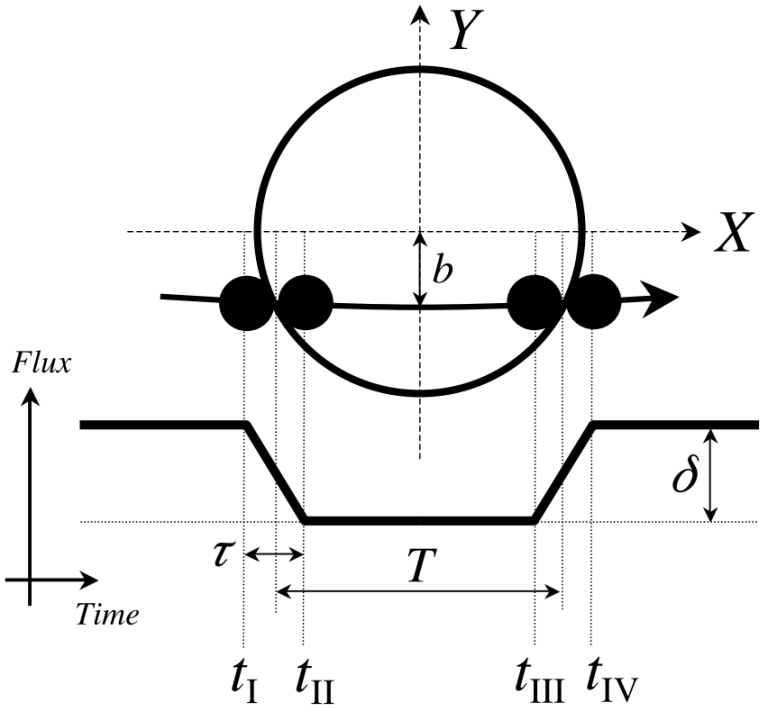

Figure 4 – Illustration of a transit, which is observed as a drop in flux over time as a planet (solid black circle) crosses a star (large circle). The various parameters are discussed in the main text. Figure courtesy Winn (2010).

2.2.2 *Physical transit parameters*

The most straightforward property to derive from a planet transit is the orbital period P, which can simply be derived from the time between subse-

quent transits. Furthermore the planet's radius relative to the radius of the star follows directly from the transit depth δ (see Figure 4):

$$\delta = \left(\frac{R_p}{R_\star}\right)^2. \tag{2.2}$$

In reality, however, transits are typically not flat-bottomed, which complicates the estimate of the transit depth. This is caused by a phenomenon known as *limb darkening*, in which the edges (limbs) of a star appear darker than its center. This occurs because near the limb the same optical depth corresponds to more outer, cooler layers of the stellar atmosphere, resulting in a lower apparent surface brightness near the limb, in particular for short (optical) observing wavelength. A good and simple way to describe the limb darkening is by using a quadratic law (see e.g. Kipping 2013a, for a more general discussion). Following the coordinates shown in Figure 4, the intensity I of the star at a point (X, Y) can then be described as

$$I \propto 1 - u(1 - \sqrt{1 - X^2 - Y^2}) - v(1 - \sqrt{1 - X^2 - Y^2})^2, \tag{2.3}$$

where the parameters u and v can either be determined (fitted) from the transit light curve itself, or looked up in tables compiled from computations based on stellar models (e.g. Claret 2004; Claret and Bloemen 2011).

While conceptually simple, the inclusion of limb darkening significantly complicates the calculation of light curves from transits. One solution is to numerically calculate light curves, but the seminal work by Mandel and Agol (2002) has provided analytical expressions for transit light curves for a range of common limb darkening laws. Beyond the aforementioned parameters P, $R_p/R_\star$ and (u, v), it turns out that transit light curves also constrain the impact parameter b and the parameter $R_\star/a$. Although their exact derivation makes for relatively complicated expressions, I attempt to provide some intuition below.

The impact parameter b (see Figure 4) is the minimal sky-projected distance between the stellar and planetary disk during transit and has units of stellar radius, taking values between 0, for a central transit, and 1, for a grazing transit configuration. The value of b depends on the orbital inclination (i) and the relative distance of the planet to the star, i.e. for a circular orbit $b = (a/R_\star)\cos i$. The parameter influences the shape of the transit, i.e. the contact times t_I, t_{II}, t_{III} and t_{IV}, such that b can be determined from a transit light curve by measuring the transit duration T and the duration of the

ingress or egress τ. For non-grazing transits and assuming $R_p \ll R_{star} \ll a$ (Winn 2010), we have

$$b = \sqrt{1 - \frac{R_p}{R_\star}\frac{T}{\tau}}. \tag{2.4}$$

The transit light curve provides further information through its total duration T (once again, see Figure 4). The duration of the transit can be inferred from the length of the path of the star which is crossed by the planet, and the velocity with which the planet does so. Assuming again non-grazing transits and $R_p \ll R_{star} \ll a$, the path length is equal to $2R_\star\sqrt{1-b^2}$, while for a circular orbit, the planet's velocity v_p is constant and easily derived from the distance it travels during one period P, i.e. $2\pi a/P$. For eccentric orbits, the velocity during transit depends on e and ω. Taking this all together, we have:

$$T = \frac{R_\star P}{\pi a}\sqrt{1-b^2}\frac{\sqrt{1-e^2}}{1+e\sin\omega}. \tag{2.5}$$

From Equation 2.5 it follows that when the eccentricity is known independently (or can be assumed ≈ 0), the transit duration constrains $R_\star/a$. The latter is not just a useful parameter which sets the orbital scale, but also a proxi for the stellar density $\rho_\star$. This follows directly from Kepler's third law, which reads $P^2 \propto a^3/(M_\star + M_p)$. After neglecting the planetary mass M_p (which is much smaller than the stellar mass $M_\star$), dividing both sides by the volume of the star and rewriting, Kepler's third law reads:

$$\rho_\star \approx \frac{3\pi}{GP^2}\left(\frac{a}{R_\star}\right)^3. \tag{2.6}$$

Taking Equation 2.5 and 2.6 together, it follows that when the stellar density is known independently (e.g. from stellar isochrone models or from asteroseismology), a combination of e and ω can be determined from the transit duration. This is the principle used in Chapter 10 to determine the eccentricity of a sample of *Kepler* planets, combining transit photometry with stellar densities determined through asteroseismology.

To summarize, measuring a transit gives access to a number of physical parameters. The depth of the transit provides info on the planet-star radius ratio, while it is also affected by the stellar limb darkening. The shape of the transits (the duration of the ingress/egress relative to the total duration) provides information on the impact parameter and thus on the orbital inclination, while the total duration further constrains $R_\star/a$ as a function of (e, ω), and when the latter are known, the stellar density. The eccentricity cannot typically be

derived from transits alone, unless detailed information on the stellar density is available in which case it can in principle be derived through a careful measurement of the transit duration and shape.

2.2.3 *Transit timing variations*

As described above, transiting planets typically reveal their orbital period in a straightforward way: all that needs to be done is measuring the time between periodic transits. However, if a second planet orbits the same star, the orbit is no longer strictly Keplerian, and the transits are no longer exactly periodic. This phenomenon is known as transit timing variations (TTVs).

As a result, monitoring the timing of transits can be used to detect additional planets. The amplitude depends on the mass of the additional planet (as well as orbital properties), but was predicted to even allow the smallest, Earth-mass planets, to be detected (Holman and Murray 2005; Agol et al. 2005). These predictions turned out to be correct and the *Kepler* mission has made it possible to detect hundreds of TTVs (e.g. Mazeh et al. 2013), with amplitudes ranging from minutes to several hours. In some cases, the TTVs of a transiting planet can be used to reveal the presence of an additional, non-transiting planet. In other cases, the mutual TTVs of transiting planets can be used to measure the masses of the planets, which cannot usually be done from transit photometry alone. Notably, the technique has recently been used to measure the mass of a Mars-sized planet (Jontof-Hutter et al. 2015).

While measuring times of transits is straightforward, interpreting TTV signals often is not. In particular when only one planet is seen transiting, it is difficult to interpret a TTV signal unambiguously, with only a few successful cases to date (e.g. Nesvorný et al. 2012). One reason for this is that the modeling often requires n-body simulations which are computationally expensive. In some cases, analytical approximate formulae can be found, which is a field of ongoing research (e.g. Deck et al. 2014). For mutual TTV detections of transiting planets near resonance, it has been possible to measure masses and eccentricities in a statistical sense (Lithwick et al. 2012; Hadden and Lithwick 2014).

2.2.4 *Radial velocity follow-up*

The first exoplanets were not discovered by measuring their transits, but rather by the radial velocity (RV) signal they induce on their host stars as the star-planet system orbits its common center of mass (e.g. Mayor and Queloz 1995). Transiting planets have now picked up the pace of exoplanet discovery with the arrival of *Kepler* photometry, but even when transits are detected RV

monitoring remains important. There are two common reasons to conduct RV follow-up of a transiting planet:

1. to confirm that a transit-like signal is indeed caused by a planet, and is not a false positive;

2. to measure the planet's mass.

False positives are described in more detail in Chapter 3. When a periodic RV signal with semi-amplitude $K_\star$ is observed, under the assumption that $M_p \ll M_\star$ the mass of the planet can be derived as (e.g. Lovis and Fischer 2010)

$$M_p = \frac{K_\star}{\sin i} M_\star^{2/3} \sqrt{1-e^2} \left(\frac{P}{2\pi G}\right)^{1/3}. \tag{2.7}$$

In general, RV planet detections constrain the minimum mass $M_p \sin i$, but when measuring the RV signal of a transiting planet i is necessarily close to 90° so that the true M_p can be determined. As we saw above, transiting planets deliver information about the planet radius, so that RV follow-up of transiting planets constrains the compositions of exoplanets (e.g. Marcy et al. 2014; Rogers 2015). Indeed, RV follow-up of transiting planets is the most common way in which exoplanet compositions can be constrained, although an alternative exists in the interpretation of TTV signals (e.g. Hadden and Lithwick 2014). The relative faintness of many planet host stars observed by *Kepler* complicates the RV follow-up, and is part of the reason why ongoing and future missions such as *K2* and TESS have a stronger focus on the detection of planets around bright stars.

Planets in eccentric orbits have a velocity which varies with the orbital phase, and consequentially the shape of the RV curve is influenced. Therefore RV measurements can also be used to measure the orbital parameters e and ω, which cannot generally be constrained from transit photometry alone.

2.2.5 *A word about exoplanet atmospheres*

Although not at the heart of this thesis, it is impossible to discuss transiting exoplanets without at least mentioning the opportunities they pose towards understanding planetary atmospheres. The study of exoplanet atmospheres represents a whole field of research on its own. Rather than being complete, here I only briefly introduce two common methods related to transits that have been used to constrain planetary atmospheres.

One technique relies on the measurement of star light reflected on the planet, by monitoring the total brightness throughout a full period, as more

and more of the 'day' side of the planet comes into view. These phase curve studies can in principle map the day-night contrast of a planet and constrain its albedo, although studies so far have mostly been limited to hot Jupiters (e.g. Knutson et al. 2007; Demory et al. 2013; Esteves et al. 2013).

Another technique, known as transmission spectroscopy, follows a principle which is comparable to why the moon turns red during a lunar eclipse. During such an event, the light reaching the moon is filtered through the Earth's atmosphere, coloring red due to Rayleigh scattering. Similarly, during an exoplanet's transit, part of the observed star light crosses through the optically thin part of the planet's atmosphere, where it picks up absorption features of that planet. Because planets are small, the absorption features of the planet only contribute a fraction of the features of the star. For example, for a Jupiter-sized planet, the planet atmosphere's features are expected to contribute a fraction of 10^{-4} relative to the continuum flux of a Sun-like star (Seager and Sasselov 2000).

Even though such measurements are technologically challenging, the technique has already achieved some remarkable successes. The first detections were made for HD 209458, where sodium was detected (Charbonneau et al. 2002), and later atomic hydrogen (Vidal-Madjar et al. 2003). Snellen et al. (2010) detected carbon monoxide in the atmosphere of HD 209458b. Water absorption features have also been detected in exoplanet atmospheres (e.g. Deming et al. 2013; Birkby et al. 2013). For super-Earth planets, the detection of molecules is complicated due to the presence of clouds, which can wash out absorption lines and render spectra featureless (e.g. Kreidberg et al. 2014; Ehrenreich et al. 2014). Even when detections are made, interpreting them unambiguously is not straightforward (e.g. Benneke and Seager 2012; Benneke 2015, and references therin). Despite these complications, the ultimate hope is that transmission spectroscopy can be used to detect so-called bio-signatures, i.e. out-of-equilibrium chemistry indicative of the presence of biological processes. I refer to Seager and Deming (2010) and Seager et al. (2012) for more details.

2.3 UNDERSTANDING HOST STARS THROUGH ASTEROSEISMOLOGY

Because most exoplanets are discovered by indirect means such as transits, it is often said that you can only know a planet as well as you know the host star. That it is crucially important to understand the star a planet orbits around is also obvious from the physics that can be derived from planetary transits (see Section 2.2), which depends on the properties of the star which is transited.

The most common way in which the properties of stars – including planet host stars – are measured, is by analyzing high-resolution spectra. In prac-

tice, this means that when an interesting planetary transit is measured, one or more ground-based high-resolution spectra of the star will be sought and analyzed. The amount and strength of spectral absorption lines depend on the stellar temperature T, the surface gravity $\log g$ and the metallicity [Fe/H] of the star. In addition to these properties, more parameters can be determined by comparing the observations to stellar models. In this way, parameters such as the stellar mass $M_\star$ and stellar radius $R_\star$ can be constrained.

Another way to measure stellar properties relies on photometry. Beyond the search for transiting exoplanets, the *Kepler* satellite provides data which is excellent to perform asteroseismology. Asteroseismology is the study of stellar oscillations, and can tell us more about stellar evolution and stellar interiors, as well as provide detailed stellar properties. A general introduction to asteroseismology is beyond the scope of this section, but I refer the reader to Aerts et al. (2010). Here I focus on the interplay with exoplanet science, and in addition I limit the discussion to main-sequence and red giant stars exhibiting so-called solar-like oscillations, whose patterns are relatively well-understood.

Solar-like oscillations are stochastic in nature, i.e. they are damped oscillations which are continuously re-excited by convection. The oscillations can exhibit a wide range of frequencies. The Sun has a characteristic frequency of approximately five minutes, while red giant stars can have periods of several hours. Over the timescale of these periods, the stellar surface expands and contracts, giving rise to temperature fluctuations which can be observed if the brightness of the star is carefully monitored. With the long oscillation periods of red giants, the standard *Kepler* sampling of 30 minutes is adequate to resolve the pulsations, but for main sequence stars similar to the Sun, only *Kepler*'s short one minute cadence can be used – an important limitation because far fewer stars have been observed in this way.

Although other types of oscillations exist, here I will be exclusively concerned with acoustic modes for which the pressure force acts as the restoring force. These modes, which are also called p modes, exhibit a regular pattern of frequencies. To measure these, a Fourier transform of a light curve is taken, such that the different frequencies of individual oscillations can be measured. Mathematically, each p mode can be described using spherical harmonics, by three *quantum numbers*: the radial order n, the angular degree l and the azimuthal order m. The radial order n describes the number of nodal shells between the center and the surface of a star. The angular degree l describes the number of nodal lines at the surface. Because of cancellation effects in the integrated brightness of a star, high-order l modes are more difficult to observe and *Kepler* typically can only observe modes with $l = 0, 1, 2$. The azimuthal order m takes values between $m = -l$ and $m = l$. In the absence of

rotation these $(2l+1)$ modes with different m-values have the same frequency.

Asteroseismology cannot routinely be done on all exoplanet host stars. In addition to the observing cadence requirement mentioned above, the fainter stars observed by *Kepler* do not reach the signal-to-noise level required to observe oscillations. Despite these limitations, asteroseismology has been used to characterize the properties (e.g. mass and radius) of hundreds of exoplanet host stars (e.g. Huber et al. 2013b), and in rare cases it can also be used to constrain the inclination of host stars (see Chapter 9). The power of asteroseismology to characterize planet host stars is used throughout this thesis, and further asteroseismic concepts will be introduced when they arise.

2.4 THIS THESIS

This thesis is structured in two parts. The first part deals with the discovery and characterization of transiting exoplanets, while the second part focuses on exoplanet dynamics.

2.4.1 *Part one*

The topics of the first part are introduced in Chapter 3. I describe how transits are searched for in photometric data sets, what scenarios can lead to false positives and how we can ultimately validate or confirm planet candidates to be genuine planets.

In Chapter 4 I present the discovery of a Neptune-sized planet in the Kepler-410 system. The planet validation is interesting because Kepler-410 consists of two companion stars. Observations from the *Spitzer* satellite are used along with *Kepler* photometry to discover which star this planet transits. The host star (Kepler-410A) is characterized very accurately using asteroseismology, which allows the planet properties to be determined accurately as well. Transit timing variations reveal the presence of a second planet in the system.

I announce six more new exoplanets in Chapter 5. These planets orbit KOI-270 (Kepler-449), KOI-279 (Kepler-45) and KOI-285 (Kepler-92), and they are validated to be genuine owing to a detailed understanding of the host star, in combination with the duration of the planetary transits. I also discuss the transits of KOI-5, for which it was not possible to prove or disprove the planetary nature.

I make a small digression in Chapter 6, which is more technical, to investigate systematic effects in *Kepler* data. I compare transit depths observed in different quarters of *Kepler*, finding a seasonal, quarter-to-quarter variation. I

discuss the causes of this variation, and the influence on the accuracy and precision with which planet transits can be determined from *Kepler*.

In Chapter 7 I move beyond the main *Kepler* mission and turn my attention to the *K2* mission. I present the first results of a RV follow-up campaign, and constraints on the masses and bulk compositions of three planets which were observed in the first scientific *K2* campaign.

2.4.2 *Part two*

Part two is introduced in Chapter 8. In this chapter I describe the dynamical properties of the solar system, with a particular focus on the eccentricity of the planetary orbits, and the inclination of the Sun relative to these planets. These properties are compared to large exoplanets which have been observed over the last two decades to show, often striking, differences with the solar system. These differences are placed into a theoretical context, highlighting the need for dynamical measurements of smaller exoplanets, particularly for those in multi-planet systems. That is precisely the topic of the next chapters.

In Chapter 9, I outline how asteroseismology can be used to measure the alignment of exoplanets, specifically for small planets in multi-planet system. Much of the focus is on Kepler-410, the best example of such an asteroseismic measurement to date. This measurement is put into context of other asteroseismic inclination determinations, as well as measurements from other techniques, in an attempt to interpret the first results.

I move from studying the alignment to the study of eccentricity in Chapter 10. I present the results of a study to measure the eccentricity of 74 planets in multi-planet systems. These results are the first for which it was possible to measure the eccentricity of the smallest exoplanets, and made use of transit duration in combination with asteroseismically determined stellar densities. I describe the difference in eccentricity between the observed systems and systems with larger exoplanets, and compare with the solar system.

In Chapter 11 I continue along the same lines, now focussing efforts on single planet systems rather than systems with multiple transiting planets. I show that this results in several complications when interpreting this sample, because some of the single planet systems may in fact be multi-planet systems, while others may turn out to be false positives. I finally compare the single planet systems with other eccentricity determinations.

Finally, in Chapter 12 I turn my attention to measuring the eccentricity of binary stars. In particular, I attempt to compare the eccentricity of binaries with cool stars, to the eccentricity of binaries with hot components. The latter have

radiative outer layers rather than convective outer layers, which may influence the tidal circularisation efficiency. The results of our study are interpreted in this context, and a link with exoplanet dynamics is drawn.

Outlook

Within this thesis, several questions have been answered, while others are left open. Yet other new questions have arisen. Chapter 13 draws conclusions, and provides an outlook to what future research may be able to bring.

Several parts of this thesis have been previously published:

- Chapter 4 and Chapter 9 contain results which were previously published in Van Eylen et al. (2014);
- Chapter 6 is mildly adapted from Van Eylen et al. (2013);
- Chapter 7 is submitted for publication at the time of writing (Van Eylen et al. 2015);
- The main results of Van Eylen and Albrecht (2015) are presented in Chapter 10, while some others are described in Chapter 5.

The results in Chapter 11 and Chapter 12 are not yet published. An overview of my publications is provided at the end of this thesis.

Part I

EXOPLANET DISCOVERY & CHARACTERIZATION

"Exoplanets. We can't actually see them, but we infer their existence because of the effect they have on the star they orbit."

– Gregory House, MD

3 TRANSITING EXOPLANETS AND FALSE POSITIVES

The first part of this thesis deals with the discovery and characterization of transiting exoplanets. This chapter serves as an introduction to this broad topic. Previously, I discussed in Section 2.2 what can be learned from planetary transit observations and why it is crucial to understand the planet host stars. Here, I take a step back and I explain how planetary transits can be detected, and how false positives can mimick genuine planets. In Section 3.1 I describe how transit-like signals are searched for in large data sets, with a focus on *Kepler* and *K2* observations. Subsequently, in Section 3.2 I discuss a number of false positive scenarios that can mimic planetary transits, but are not. Finally, in Section 3.3 I present a number of ways in which genuine planets can be distinguished from false positives.

3.1 TRANSIT SEARCH FOR PLANET CANDIDATES

The first step in discovering exoplanets from a time series of photometry is to identify transit-like events. This step consists of identifying what *might* be a planet. Further vetting will usually be required to confirm this finding, which can be done either by obtaining additional observations or by ruling out all alternative interpretations – this next step is the subject of Section 3.2.

The transit search can be done in a variety of ways, the simplest of which is a visual search. Although manual search has its limitations (e.g. it is time consuming and likely to miss the smallest, most interesting planets), it has also seen some remarkable success. For example, the Planet Hunters project[1], in which non-astronomers scour *Kepler* data for planets (Fischer et al. 2012), was able to find a circumbinary planet in a quadruple system which was missed by algorithmic searches due to its non-periodic properties (Schwamb et al. 2013).

Transit search algorithms attempt to exploit typical properties of transits to discover them in vast amounts of data sets. One of the key properties of planet transits is their periodicity, i.e. transits recur every orbital period. Transit timing variations (see Section 2.2.3) can cause deviations from the strictly Keplerian periodicity, but are often small enough not to be a major source of concern.

One example of a code that exploits the periodicity is the box least-square (BLS) search (Kovács et al. 2002), which folds the data based on a specified

1 http://www.planethunters.org

range of periods that are searched for, and then attempts to fit a box (which serves as a simplified transit model) to the folded data set. It is particularly suitable for transits that are short compared to the orbital period. A different technique makes use of Fourier transforms and is very efficient at planets with periods less than a few days (so-called ultra-short period planets, e.g. Sanchis-Ojeda et al. 2014).

For the *Kepler* dataset, an 'official' candidate search is carried out by the *Kepler* team, with results which were updated as more data became available (Borucki et al. 2011; Batalha et al. 2013; Burke et al. 2014; Rowe et al. 2015; Mullally et al. 2015). Other groups carried out independent searches, finding largely the same, or at least reconcilible, results (e.g. Ofir and Dreizler 2013; Petigura et al. 2013; Sanchis-Ojeda et al. 2014). These searches are typically carried out on data where instrumental trends are already mitigated, which, for *Kepler*, is known as the Presearch Data Conditioned (PDC) version (Smith et al. 2012).

The result of such searches are catalogs of *Kepler objects of interest* (KOIs). Not all KOIs are actual planets, because not all transit-like signals picked up by the searches are truly transits, and not all transits are caused by exoplanets (many are instead eclipsing binaries). The latest catalog contains 7348 KOIs, of which 4175 survived further scrutiny and are termed *planet candidates*. To make sure such a candidate is indeed a genuine planet usually requires individual attention of the system (see Section 3.2). At the time of writing, the official list of confirmed *Kepler* planets[2] contains 1030 planets orbiting 453 stars.

For the *K2* mission, only the raw photometry is made available and the task of finding planet candidates lies solely with the exoplanet community. An additional complication for *K2* data is the removal of instrumental variations, in particular those caused by the movement of the spacecraft. Several teams have devised techniques to correct for these trends (Vanderburg and Johnson 2014; Lund et al. 2015; Sanchis-Ojeda et al. 2015) and carried out transit searches using BLS algorithms (Vanderburg and Johnson 2014; Van Eylen et al. 2015) and Fourier transforms (Sanchis-Ojeda et al. 2015). With no mission-led transit search, there is no clear current count of the total amount of candidates discovered by *K2*, although a number of planets have already been found using the first sets of data (see Chapter 7).

2 http://kepler.nasa.gov/Mission/discoveries/

3.2 FALSE ALARMS AND FALSE POSITIVES

Once transit-like events have been identified, the next step is to assess their validity. Is the observed feature indeed a transit caused by an exoplanet orbiting the star? To answer this question, it is necessary to be aware of the various alternatives. That is the topic of the current section. Broadly speaking, we can divide the alternative scenarios into two categories: *false alarms* and *false positives*.

False alarms are the result of noise or data processing errors. They can occur when the transit search algorithm picks up other (quasi-)periodic events such as star spots, in which case further vetting or visual inspection can usually dismiss these cases. More complicated are situations where features are caused by data with a low signal-to-noise (S/N) ratio. Here, what appears to be a transit is instead noise. This can be a concern for the smallest planets (which have shallow transits), as well as for long period planets where only a few transits are observed. These cases are usually sorted out as more data is acquired. When that is not feasible, one solution is to increase the S/N ratio required to claim a planet candidate detection, e.g. when requiring $S/N \geqslant 7.1$ only one false alarm is expected in the entire *Kepler* data set (Jenkins et al. 2002). Unfortunately, this approach can lead to false negatives, in which some of the most interesting planets are also missed (Mullally et al. 2015).

Nevertheless, the data quality of *Kepler* and *K2* is such that for many planets false alarms are not a major concern. Much more important, and much harder to avoid, are false positives. In this case, a transit is correctly observed, but is not caused by an exoplanet orbiting the observed star. Typically the transit event is instead occurring on a star which cannot be separated from the target star in the photometry. To understand this, we note that one pixel of the *Kepler* spacecraft measures 3.98×3.98 arcsec, and a typical star spans several pixels. This implies that stars that are separated by only a few arcseconds in the plane of the sky, cannot be independently identified when observed, although they may nevertheless be far away from the target star (in the background or foreground).

Together with the target star the *Kepler* spacecraft will typically observe one or more 'companion' stars in the background, along (approximately) the same line of sight. As a result, what appears like an exoplanet transit occurring at the target star, could instead be a nearby eclipsing binary (EB). This is illustrated in Figure 5. An EB will normally produce an eclipse which is much deeper than an exoplanet transit, but if the EB is much fainter than the target star the deep eclipse may be diluted to look identical to an exoplanet transit on the target star. This fainter binary star may be physically associated with the target star (i.e. a triple star system), or may occur in the background – a so-called chance alignment.

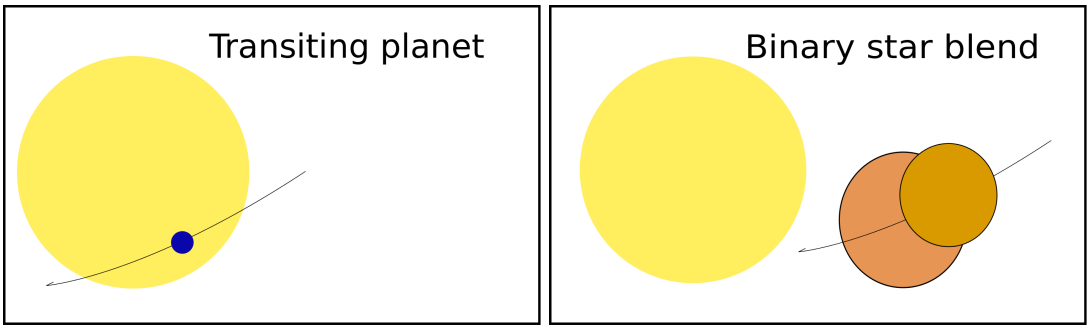

Figure 5 – Illustration of one of the most common false positive scenarios. A binary star causes a deep transit event, which is heavily diluted by flux from another star, causing the transit to look similar to a planet transit. If the binary star is spatially nearby in the plane of the sky, the two scenarios can often not be distinguished from (*Kepler*) photometry alone.

Confusion can also occur when a star – physically associated or coincidentally aligned – occurs nearby to the target star, and this companion star contains a transiting planet. The planet may then be misidentified to occur on the target star rather than on the companion. In some sense, this is not a false positive scenario because the transit is caused by a planet, but planet parameters such as its size or semi-major axis will be misidentified if the host star is misidentified.

Common to all of these scenarios is that transits occurring on the target star or a companion star can look perfectly identical, making it impossible to distinguish the different possibilities when looking at the transit light curve alone. Strategies to deal with false positives fall into two broad categories: on the one hand a planet can be confirmed by independently measuring its signal using a different instrument or method, and on the other hand planets can be validated statistically by ruling out all alternative transit scenarios beyond reasonable doubt. I discuss both of these categories in Section 3.3.

3.3 PLANET CANDIDATE VALIDATION AND CONFIRMATION STRATEGIES

The first method to confirm a planetary candidate is by conducting follow-up observations to detect the planet using a different set of data. The most straightforward way to do so is by measuring the RV signal of the host star caused by the gravitational influence of the planet (see Section 2.2.4). When a planet's RV signal is detected with the expected period, this unambiguously confirms its presence. An additional advantage of this confirming method is that it provides the mass of the planet. Together with the radius (which can be derived from the transit) the mass yields a measure of the mean density of the planet. Measuring planetary densities, in particular for small planets, is an area of active research because it provides information about the composition of planets, and their diversity.

Unfortunately, measuring the RV signal is unfeasible for small and/or distant planets, because their gravitational influence on the star is too small to detect with current instrumentation. In this case one has to resort to statistical arguments to find planets (here, we usually use the term *planet validation* rather than confirmation), in which the sum of the probability of every possible scenario is weighed against that of the transit being caused by a genuine exoplanet. One then hopes to conclude that the exoplanet probability is overwhelming. In practice, additional analysis and/or observations are usually needed to make such a claim.

Because all false positive scenarios depend on the presence of other nearby stars, usually it is useful to detect or rule out such objects. One interesting technique to limit the parameter space is known as *centroid vetting*. Here, one compares the center of light during transits with the center of light outside transits. If the transit occurs on the central target star, no difference between these two measurements should be expected. If, however, the transit occurs on a nearby object, the center of light will show a tiny shift during transit. While a centroid analysis cannot prove the planetary nature of a transit, it provides constraints on the maximum angular separation of stars on which the transit can occur. These constraints are often much tighter than what can be derived from the photometric aperture alone (see e.g. Batalha et al. 2010). We note that the *Kepler* Community Follow-Up Observing Program (CFOP) carries out centroid vetting for all KOIs and classifies systems with clear centroid offsets as false positives (e.g. Mullally et al. 2015).

After centroid vetting, the list of *Kepler* planet candidates has a low false positive rate (e.g. Morton and Johnson 2011). Fressin et al. (2013) estimate the global false positive rate of the sample of planet candidates to be 9.4%, while peaking at 17.7% for the largest planets, and at a low of 6.7% for small Neptunes. Follow-up observations with the *Spitzer* space telescope of a sample of 51 candidates, combined with other constraints, result in an upper limit on the false positive rate of 8.8% (Désert et al. 2015). The false positive rate is further lowered for multi-planet systems (Lissauer et al. 2012, 2014), and a group of 851 planets orbiting 340 stars has been mass-validated because (almost) all of these transit candidates are expected to be genuine planets (Rowe et al. 2014).

Often high resolution images are taken of the target star. Using ground-based instrumentation, images using adaptive optics (e.g. Adams et al. 2012) or Speckle imaging (e.g. Howell et al. 2011), can reveal or rule out the presence of companion stars which remain hidden in the *Kepler* photometry. When such images reveal the presence of more than one star, it can be very difficult to validate the transit signal, and in general detailed knowledge of the star is required.

To summarize, the overall false positive rate of *Kepler* planets is low. The presence of a planet can be directly confirmed using RV follow-up measurements, or indirectly validated by showing that it is highly unlikely that the transit is caused by anything else than a planet orbiting the star. For individual planet candidates of interest, sometimes none of these methods can easily be applied. Small planets, in systems with only a single transiting planet, can be particularly hard to validate or confirm, as can planet candidates in systems with nearby companion stars.

I have worked on techniques to validate planets that can be especially useful for complicated cases. In Chapter 4 I report on the discovery of Kepler-410A b, which was first published by Van Eylen et al. (2014). This is a bright binary star system where the Neptune-sized planet orbits one companion in 17.8 days. Owing to the power of asteroseismology, it was possible to extract detailed information about one of the host stars and find out that the companion star was significantly smaller and cooler. Using *Spitzer* transit measurements and comparing the depth with that observed by *Kepler*, we were able to decisively show that the planet orbits Kepler-410A and not Kepler-410B.

In Chapter 5, six additional new *Kepler* planets are presented (see Van Eylen and Albrecht 2015, for the original publication). All these planets are part of multi-planet systems, but were not previously validated because nearby companion stars were detected. I then show that, because multi-planet systems in *Kepler* have nearly circular orbits (see Chapter 10), the transit duration can be predicted from the stellar density. Making use of asteroseismology to precisely characterize the target star, the mean stellar density can be determined, and the predicted transit duration can be compared with the observations. In some cases the excellent agreement between prediction and observation allows the validation of the planets.

Chapter 6 digresses slightly from this track. There, I investigate systematic effects present in *Kepler* data sets. We show that between different seasons of observations, the spacecraft's measurement of exoplanet radii is different to a few percent. This provides an upper limit on the maximum accuracy of exoplanet radii which can be achieved with this instrument (see Van Eylen et al. 2013, for the original publication). This chapter is relatively technical and some readers may wish to skip it.

In Chapter 7, the final chapter of Part I of the thesis, I move beyond *Kepler* and present planets observed with its successor *K2*. I present a code used to detrend *K2* observations and search for planetary transits. Furthermore I show results of a follow-up campaign to measure the RV signal of interesting planets using three different ground-based telescopes. Even though this campaign has only just started, RV measurements for 3 stars in *K2* campaign 1 are

already presented, and lead to the confirmation of at least one new planet. At the time of writing, this chapter is submitted for publication (Van Eylen et al. 2015).

4 TWO COLORS: *KEPLER* AND *SPITZER*

In this chapter I describe the discovery and characterization of the planet Kepler-410A b. This object provides a particularly interesting but complicated case for planetary validation:

- Kepler-410 consists of a blend between two stars, Kepler-410A and Kepler-410B, complicating the analysis;
- The planet is small (2.8 $R_\oplus$) and in a relatively distant orbit (17.8 days), making radial velocity confirmation undesirable; and,
- Kepler-410A is a bright star (V = 9.4, the third-brightest confirmed *Kepler* planet host).

The validation was possible using a number of follow-up observations, including infrared transit measurements using the *Spitzer* telescope. These additional measurements are presented in Section 4.1, where I also describe how they can be combined to validate the planet Kepler-410A b. In Section 4.2, I describe the detailed characterization of the planet host star, which made use of asteroseismology. The transit photometry is then analyzed and the resulting planetary parameters are presented in Section 4.3. The system contains at least one additional planet which is revealed by the presence of transit timing variations (TTVs), which is the topic of Section 4.4. A short summary is presented in Section 4.5. The Kepler-410 system was first announced by Van Eylen et al. (2014) and this chapter is adapted from parts of that publication. A discussion of the obliquity measurement of Kepler-410 is postponed to Chapter 9.

4.1 PLANET VALIDATION

In this Section, I investigate the possible scenarios causing the transit-like features in the *Kepler* data for Kepler-410. For a general introduction to this topic, the reader is referred Section 3.2 and Section 3.3. In Section 4.1.1, I describe the constraints, as provided by the *Kepler* data, *Spitzer* data and additional observations from ground-based instruments. In Section 4.1.2, I use those constraints to assess the likelihood of various scenarios, to conclude that the transits are indeed caused by a planet in orbit around Kepler-410A.

4.1.1 *Constraints*

4.1.1.1 *Geometry of transit signal*

A first constraint on what could be causing the transit signal in the *Kepler* data, comes from the *geometry of the transit signal* itself. While the transit signal could be diluted by additional stellar flux (i.e. by Kepler-410B, or additional unseen blends), the shape of the transit, as governed by the four contact points, remains the same. We use T_{tot} for the total transit duration, T_{full} for the duration between contact points two and three (the transit duration minus ingress and egress, see Figure 4), b for the impact parameter, and find (see e.g. Winn 2010):

$$\frac{\sin(\pi T_{tot}/P)}{\sin(\pi T_{full}/P)} = \frac{\sqrt{(1+R_p/R_\star)^2 - b^2}}{\sqrt{(1-R_p/R_\star)^2 - b^2}}. \tag{4.1}$$

Here $R_\star$ and R_p indicate the stellar and planetary radii. This equation (which only strictly holds for a zero-eccentricity orbit) can be understood by considering the most extreme case, namely a binary with two stars of the same size and $b = 0$, causing the equation to go to infinity. The transit becomes fully V-shaped, half of the transit is in ingress, while the other half is in egress. As it turns out, the short-cadence data constrains the transit shape to be clearly different from a V-shape as can be seen in Figure 6. With the left-hand side of Equation 4.1 determined by the data and setting $b \equiv 0$, an upper limit on $R_p/R_\star$ can be determined. Given the observed transit depth this ratio can now be used to establish an upper limit on any light dilution.

We model the planetary transit for various degrees of dilution until the transit fits for the ingress and egress get significantly worse (3σ on a χ^2 distribution). We find that transits occurring at a star more than 3.5 magnitudes fainter than Kepler-410A can be rejected using this criterium, and therefore we exclude this region of the parameter space. This region is shown as the *geometric limit* in hatched-gray in Figure 7.

4.1.1.2 *Centroid*

Pixel analysis during transits can also unmask blends. Transits occurring around a slightly offset blended star would lead to centroid shifts on the *Kepler* CCD between in transit and out of transit data (see also Section 3.3). A non detection of such shifts can give an upper limit on the brightness of a potential blend as function of projected distance on the sky.

The *Kepler* team runs elaborate vetting procedures to determine if planetary signatures are caused by blends and centroid shifts are part of this procedure.

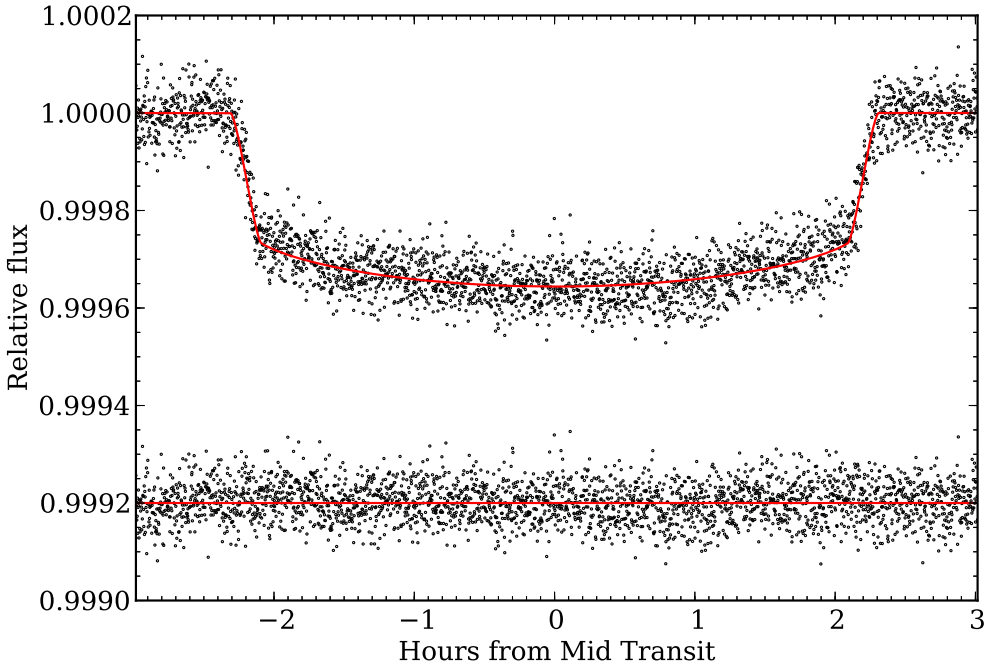

Figure 6 – Planetary transit using the phase-folded *Kepler* observations, which were binned for clarity. The best fit is shown with a red line, together with the residuals (offset).

These procedures are described in detail by Bryson et al. (2013). Kepler-410A, however, is a highly saturated star, which invalidates centroid shift measurements that appear in the Data Validation Report[1]. Visual inspection of the difference images (see Bryson et al. 2013, Section 5) in the Kepler-410 Data Validation report gives no indication that the transit source is not on the same pixel (3.98″ by 3.98″) as Kepler-410A. This analysis is qualitative, however, and does not rule out the companion star. We therefore rely on other evidence given in this paper that the transit occurs on Kepler-410A.

4.1.1.3 *Ground-based photometry*

Adams et al. (2012) and Howell et al. (2011) independently observed a blended object (Kepler-410B) at a distance of 1.6″. These observations can also be used to exclude further objects inside certain magnitude and separation limits. The limits from the adaptive optics (A.O.) observations by Adams et al. (2012) are shown in Figure 7. The inner spatial limit for detections is at 0.2″, where unseen objects up to a contrast of 4.2 magnitudes in the *Kepler* bandpass are excluded. This increases to 11.5 magnitudes at 6″.

Speckle images of Kepler-410 at 562 and 692 nm by Howell et al. (2011) provide even tighter spatial constraints (Figure 7), achieving a magnitude con-

1 http://exoplanetarchive.ipac.caltech.edu/docs/deprecated/KeplerDV.html

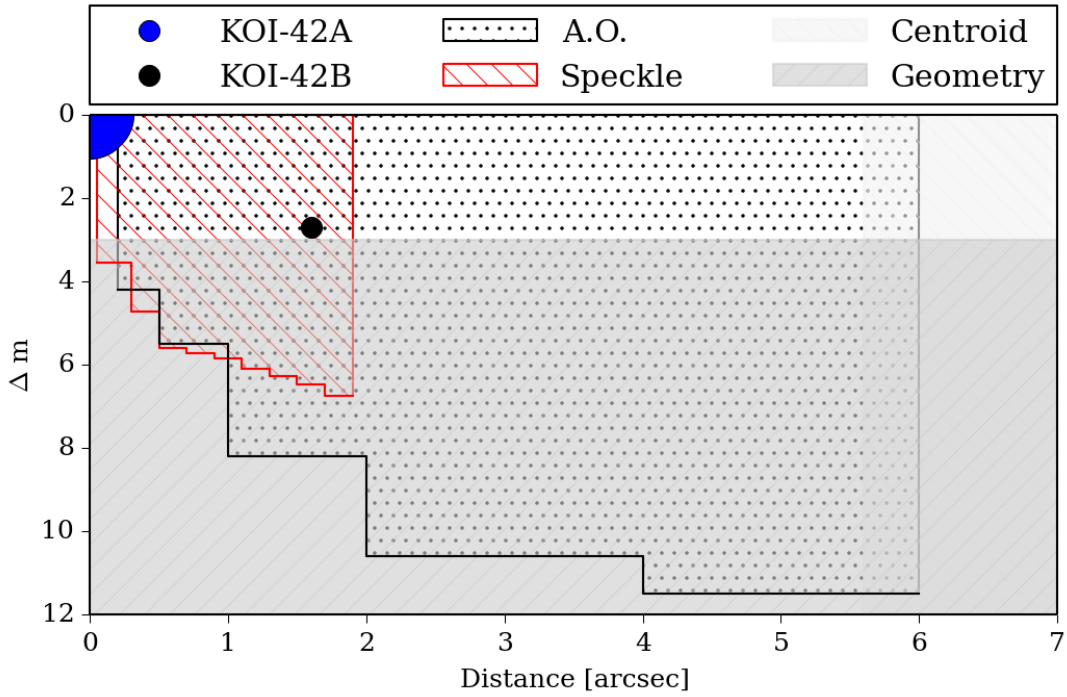

Figure 7 – Magnitude relative to Kepler-410A plotted versus the distance to the star. Kepler-410B is observed at 1.6″ and Δm = 2.7 (Adams et al. 2012). A large magnitude difference is excluded because of the transit geometry, while a large angular separation can be ruled out by analyzing the centroid. Finally, ground-based photometry using adaptive optics (A.O.) and Speckle imaging rules out all but a very small area of the parameter space.

trast of 3.55 magnitudes between 0.05″ and 0.30″, with an increasing contrast up to 1.9″. The limits in Figure 7 are 3σ limits for observations at 562 nm, while those for 692 nm are about 0.5 magnitudes tighter for the closest separations.

We further note that the 562 nm detection of Kepler-410B estimates it to be 4.24 magnitudes fainter than Kepler-410A, which, if the same difference holds in the broader *Kepler* band, would place it below our geometric limit of possible planet hosting stars. However, Howell et al. (2011) note that at 1.6″ separation, the magnitude estimation of detected targets might be underestimated and we choose to adopt the *Kepler* magnitude value for Kepler-410B as claimed in Adams et al. (2012), placing it just above our geometric limit.

4.1.1.4 *Spectroscopy*

Spectroscopic observations of Kepler-410 were taken with the HIRES[2] echelle spectrometer at the Keck I telescope and reduced following a procedure described in Chubak et al. (2012). The spectra have a spectral resolution of R = 55000 and stellar lines in the the near-IR wavelength region 654 - 800

2 High Resolution Echelle Spectrometer on the Keck observatory.

Ref.	T_{eff} (K)	log g	[Fe/H] (dex)	$v \sin(i)$ (km s^{-1})	Instrument
a	6325 ± 75	-	$+0.01 \pm 0.10$	15.0 ± 0.5	HiRES, McDonald
b	6195 ± 134	3.95 ± 0.21	-0.16 ± 0.21	11.0 ± 0.8	ESPaDOnS

Table 1 – Stellar parameters from spectroscopy. *a:* Huber et al. (2013b). *b:* Molenda-Żakowicz et al. (2013).

Date (JD)	Radial Velocity (km/s)
2454988.979733	-40.30 ± 0.4
2455318.048353	-40.995 ± 0.3
2455726.094382	-40.18 ± 0.6

Table 2 – Radial velocity measurements of Kepler-410.

nm were used to calculate the Doppler shift. The wavelength scale was determined from thorium-argon lamp spectra taken in twilight before and after each observing night while the wavelength zero-point was determined using telluric lines (from the A and B absorption bands) present in the target spectra. Due to the relatively high $v \sin i$ of the star (see Table 1), the errors listed here are slightly higher than the typical value (0.1 km s^{-1}) stated in Chubak et al. (2012). The data are listed in Table 2. We will use these RVs later to constrain scenarios involving binary systems.

4.1.1.5 *Spitzer observations*

Kepler-410 was observed on 11 July and 18 December 2010 in-transit with the *Spitzer Space telescope* (Werner et al. 2004). The first visit consists of full-frame images with a longer integration time and lower accuracy than the second visit, where *Spitzer*'s subarray mode was used. We only analyze the subarray data. They consist of 310 sets of 64 individual subarray images, obtained using IRAC's channel 2 (Fazio et al. 2004), which is centered at 4.5 µm. The data are available for download from the *Spitzer* Heritage Archive database[3] as basic calibrated data (BCD) files. The first observations (which are often more noisy due to the telescope's ramp up) are often ignored (see e. g. Knutson et al. 2008), but we omit the first 55 observations to keep an equal amount of observations before and after the transit (62 observations on each wing, with 131 in-transit observations).

We analyzed the data following a procedure described by Désert et al. (2009). A square aperture (11×11 pixels) is used to collect the stellar flux (where 64 images of each subarray observation are immediately combined)

3 http://sha.ipac.caltech.edu/applications/Spitzer/SHA

and the centroid position is calculated. Since a pixel spans 1.2″, the flux contains the combined light of Kepler-410A and Kepler-410B. Subsequently, a linear function in time is used to de-trend the data, in combination with a quadratic function of the x and y coordinates of the centroids, resulting in five free fitting parameters, (see e.g. Knutson et al. 2008; Désert et al. 2009; Demory et al. 2011) to correct for the pixel-phase effect. We fit only the out-of-transit data, but correct the full dataset.

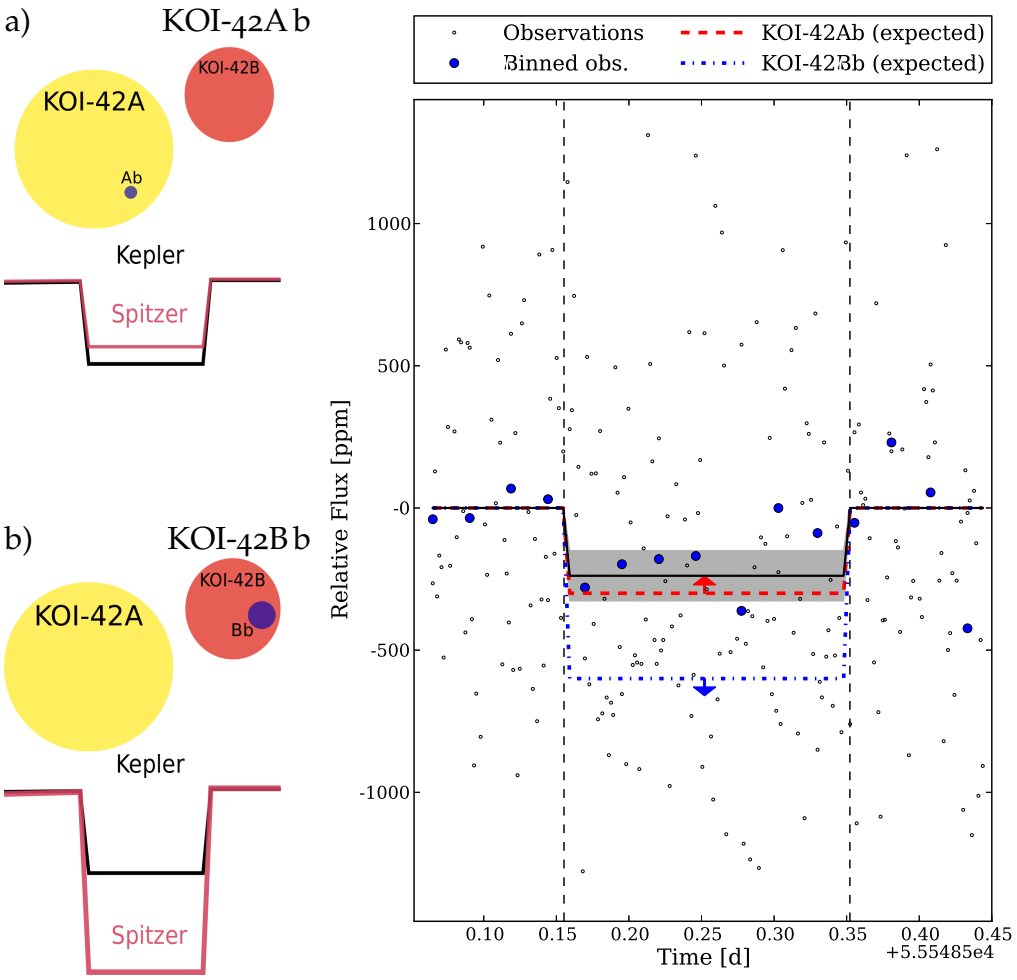

Figure 8 – **Left:** Illustration of two different scenarios: a planet orbiting the star KOI-42A (Kepler-410A), and a larger planet orbiting KOI-42B (Kepler-410B). The transits look the same when observed by *Kepler* because KOI-42B is fainter. However, because the two stars are different, the transits don't look the same when observed by the *Spitzer* telescope. **Right:** Transit observation using *Spitzer* in grey, with binned data points in blue. A confidence interval of the transit depth is shown in grey. The transit depth is consistent with the prediction for KOI-42A, but not with that for KOI-42B.

Now we compare the average flux level of the in-transit data to the out-of-transit data finding a transit depth of 240 ± 90 parts per million (ppm). The uncertainty is calculated by bootstrapping (we re-sample without replacement,

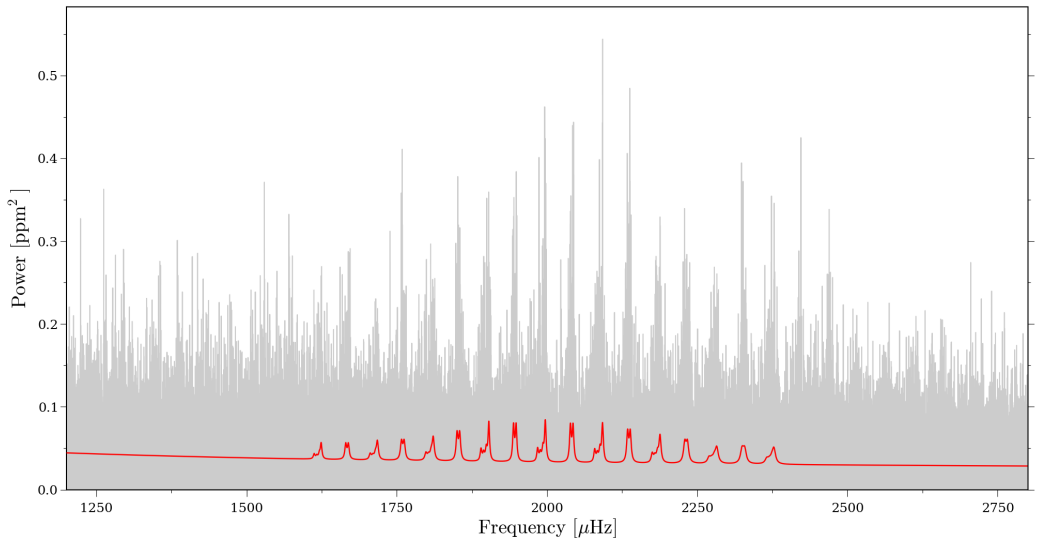

Figure 9 – Power spectrum of Kepler-410 (gray). Overlaid in red are the model fits (Equation 4.3) obtained from the MCMC peak-bagging (see Section 4.2.2.

treating the in-transit and out-of-transit data separately), which we find to result in a slightly higher error level compared to simply using the scatter on the data points. We adopt this value and show the result in Figure 8. A similar procedure, comparing median flux levels rather than mean flux levels, gives a transit depth of 260 ± 90 ppm.

4.1.1.6 *Asteroseismology*

Finally, the *Kepler* data provide an asteroseismic constraint on additional objects, by looking at the (absence of) stellar pulsations in the power spectrum (see Figure 9 and Section 4.2.1 for more information). We searched the power spectrum for excess power from stellar oscillations using the so-called *MWPS* method (see Lund et al. 2012). With this, only one set of (solar-like) pulsations was detected, which can be attributed to Kepler-410A because of their high amplitudes, and we can thereby rule out additional signal from bright, large stars to be present in the light curve. We exclude solar-like oscillations of main-sequence stars or red giants up to $K_p = 13$, the geometric exclusion limit (Figure 7).

We can translate this magnitude limit on additional solar-like oscillations into limits on the surface gravity using the method developed by Chaplin et al. (2011) (see also Campante et al. 2014). We estimate a lower limit for the value of ν_{max}[4] for a marginal detection of oscillations in the power spectrum. This

4 The frequency at which the oscillations have the largest amplitude.

lower limit on ν_{max} can in turn be translated into a lower limit for the surface gravity (g) of the star (or $\log g$ as most often used) via the simple relation:

$$g \simeq g_{\odot} \left(\frac{\nu_{max}}{\nu_{max,\odot}} \right) \left(\frac{T_{eff}}{T_{eff,\odot}} \right)^{1/2}. \tag{4.2}$$

The above relation builds on the proportionality between ν_{max} and the acoustic cut-off frequency (ν_{ac}; see e. g., Brown et al. 1991; Belkacem et al. 2011). In addition, the procedure uses various scaling relations for e.g. the amplitudes of the oscillations and the stellar noise background – we refer the reader to Chaplin et al. (2011) for further details.

For temperatures in the range $T_{eff} = 5500 - 5777$ K we estimate that non-detection of oscillations in any second component (i.e. a star other than Kepler-410A) sets limiting (lower-limit) values for $\log g$ of $\gtrsim 4.51 \pm 0.05$ dex (at 5500 K) and $\gtrsim 4.57 \pm 0.05$ dex (at 5777 K). For higher assumed values for T_{eff}, the limiting values for $\log g$ are inconsistent with allowed combinations for $\log g$ and T_{eff} from stellar evolutionary theory. From these limiting values for $\log g$ any potential second component must necessarily be a small dwarf star.

For Kepler-410 the asteroseismic constraint, together with the geometric constraint, is enough to establish the planetary nature of the transit signal. As shown in Section 4.1.1.1 the signal cannot occur on a star fainter than $K_p = 13$ (limiting the maximum true transit depth) and due to the asteroseismic constraint, any nearby object brighter than this is necessarily small. Since the transit depth is given by the size of the transiting object relative to its host star, the two constraints together limit the size of the transiting object to be smaller than Jupiter. For both constraints, observations in a short-cadence sampling are crucial.

4.1.2 *Scenarios*

We now use the constraints established in the last section to evaluate three possible scenarios which could cause the transit signal; a chance alignment with a background system (Section 4.1.2.1), an unseen companion to Kepler-410 (Section 4.1.2.2), and a planet in orbit around Kepler-410B (Section 4.1.2.3). Given the available data we can rule them out and conclude that the transit signal occurs on Kepler-410A.

4.1.2.1 *Chance alignment*

The scenario of a background system, largely diluted by a much brighter foreground object (Kepler-410A), is disfavored by a combination of the geometric constraints and the additional observations described in Section 4.1.1. With

most of the parameter space ruled out, a relevant system would need to have a K_p between 9.5 and 13 (see Section 4.1.1.1) and a separation less than 0.02″ from Kepler-410A (see Section 4.1.1.3).

A detailed analysis on false positive scenarios can be found in Fressin et al. (2013). Following a similar approach we use the Besançon model of the galaxy (Robin et al. 2003) to simulate the stellar background around Kepler-410. This leads to the prediction of 319 objects brighter than 13th magnitude in the R-band (which is close to the *Kepler* band[5]), in an area of one square degree. This places on average 6×10^{-8} background stars of sufficient brightness in the confusion region of 0.05″around Kepler-410A, the region which is not ruled out by any constraints (see Figure 7). Even without further consideration of whether any background objects could be eclipsing binaries or hosting a transiting planet, we consider this number too small for such a scenario to be feasible. From here on we therefore assume that the transit signal is not caused by a chance alignment of a background system.

4.1.2.2 *Physically associated system*

We now consider the possibility that the transit occurs on a star physically associated to Kepler-410A but not Kepler-410A itself. According to Fressin et al. (2013), transiting planets on a physically associated star are the most likely source of false positives for small Neptunes. Prior to constraints, they estimate $4.7 \pm 1.0\%$ of the small Neptune *Kepler* candidates are misidentified in this way. For Kepler-410 the spatial constraints from the ground-based photometry (see Section 4.1.1.3) are far more strict than what was used by Fressin et al. (2013), who only use the *Kepler* data itself to determine the region of confusion.

From the transit geometry, stars fainter by $\Delta K_p = 3.5$ are already excluded as possible host stars. Since a physical companion would have the same age as Kepler-410A, we can use the mass-luminosity relation for main sequence stars to derive a lower mass limit. We find this to be about 0.5 $M_\odot$. Furthermore, the companion star cannot be more massive than Kepler-410A itself, otherwise it would be more luminous and thereby visible in the spectra and produce an asteroseismic signal.

We proceed with a simple calculation to quantify the chance that Kepler-410 has an unseen companion with a planet that causes the transit signal. As in Fressin et al. (2013), we assign a binary companion to Kepler-410A following the distribution of binary objects from Raghavan et al. (2010); a random mass ratio and eccentricity and a log-normal distribution for the orbital period. We calculate the semi-major axis using Kepler's third law and assign a random

5 *Kepler* magnitudes are nearly equivalent to R band magnitudes (Koch et al. 2010).

inclination angle, argument of periastron, and orbital phase to the system.

From the simulated companions, we reject those with a mass lower than 0.5 $M_\odot$. We calculate their angular separation (using the distance estimate derived in Section 4.2.2, see Table 3) and reject those which would have been detected in the ground-based photometry. Finally, we compute the radial velocity (RV) signal that the companion would produce at the times of the RV measurements (Table 2) and reject those objects inconsistent with the observations. For this, we calculate the χ^2 value for each simulated companion, and assign a chance of rejection to each one based on the χ^2 distribution.

We find that only 0.46% of the simulated objects could pass these tests. The frequency of non-single stars is 44% (Raghavan et al. 2010), resulting in a chance of 0.2% that an undetected star is associated with Kepler-410A. This limit would be even lower if we assume Kepler-410B is physically associated with Kepler-410A, since the probability of additional companions in a multiple system is lower than the value quoted above (an estimated 11% of all stars are triple system or more complex; Raghavan et al. 2010). More elaborate simulations could also further reduce this statistical chance, as we have not taken into account the *Spitzer* transit depth, visibility in spectra, or visibility of asteroseismic features, of this hypothetical companion.

4.1.2.3 *Kepler-410B*

While the nature of Kepler-410B is largely unknown, some information on the star can be derived from the observations by Adams et al. (2012). Using their 2MASS J and Ks magnitude, we can convert the measured brightness difference into a temperature estimate, using color-temperature transformations as described by Casagrande et al. (2010). We find a temperature of around 4850 K, assuming a solar metallicity. This indicates a small (dwarf) star, which is consistent with the non-detection of an asteroseismic signal of the object in the blended *Kepler* light (see Section 4.1.1.6).

There is modulation signal present in the *Kepler* data, which is presumably caused by the rotation of Kepler-410B. It indicates a brightness variation of the object of $\approx$ 2.5% (assuming the brightness contrast by Adams et al. 2012, see Section 4.1.1.3), over a rotation period of 20 days. In fact, the modulation signal has previously been mis-attributed to Kepler-410A (McQuillan et al. 2013), resulting in a rotation period inconsistent with what we derive through asteroseismology (5.25 ± 0.16 days, see also Chapter 9).

The different colors of Kepler-410A and Kepler-410B can be used to rule out Kepler-410B as a host star, by comparing the transit depth measured in the *Spitzer* IRAC band with the depth as measured by *Kepler*. Kepler-410B

is 2.7 magnitudes fainter than Kepler-410A in the Kepler band (Adams et al. 2012). The flux of Kepler-410B is $\approx$ 8% the flux of Kepler-410A. In 2MASS Ks (2.1 µm) the magnitude difference reduces to 1.9 ($\approx$ 17% flux). We conservatively assume that in *Spitzer*'s IRAC band (4.5 µm), $\Delta m \leqslant 1.9$. Using this assumption, a transit occurring on Kepler-410A would be blended somewhat more in the *Spitzer* observations (depth $\leqslant$ 300 ppm), while a transit occurring on Kepler-410B would only be diluted by less than half the dilution in the *Kepler* light (depth $\geqslant$ 600 ppm).

A measured *Spitzer* transit depth of 240 ± 90 ppm distinctly (at a 4σ level) rules out Kepler-410B as a potential host star to the transiting planet and is consistent with the planet occurring on Kepler-410A (see Figure 8). From here on, we assume that the transits occur on Kepler-410A.

4.2 KNOWING THE STAR: ASTEROSEISMOLOGY

Using asteroseismology, I now derive detailed stellar parameters for Kepler-410A. In Section 4.2.1, I explain how the star's oscillation frequencies are measured, and in Section 4.2.2 I describe how those frequencies are used to determine the star's parameters. The splitting of frequencies under the influence of rotation is also used to determine the star's inclination and constrain the obliquity of the system, but that discussion is postponed to Chapter 9. An introduction to asteroseismology can be found in Section 2.3.

4.2.1 *Frequency analysis*

Kepler-410 was observed in short-cadence mode for the entire duration of the *Kepler* mission, except during the second quarter of observations (Q2) where the long cadence mode was used. The latter observations are not included in the asteroseismic analysis, and we use short-cadence simple aperture photometry (SAP) data from Q0-Q1 and Q3-Q13. Before using the data as input for asteroseismology, it is de-trended and normalized using a specifically designed median filter to remove all transit features from the time series. The resulting time series is then used to derive a power spectrum[6], which is shown in Figure 9.

The extraction of mode parameters for the asteroseismic analysis was performed by *peak-bagging* the power spectrum (see e. g., Appourchaux 2003). This was done by making a global optimization of the power spectrum using

6 The power spectrum was calculated using a sine-wave fitting method (see e. g., Kjeldsen 1992; Frandsen et al. 1995) which is normalized according to the amplitude-scaled version of Parseval's theorem (see e.g. Kjeldsen and Frandsen 1992), in which a sine wave of peak amplitude A will have a corresponding peak in the power spectrum of A^2.

a *Markov Chain Monte Carlo* (MCMC) routine[7], including a parallel tempering scheme to better search the full parameter space (see Handberg and Campante 2011). In the fit the following model was used for the power spectrum:

$$\mathcal{P}(\nu_j;\Theta) = \sum_{n=n_a}^{n_b} \sum_{\ell=0}^{2} \sum_{m=-\ell}^{\ell} \frac{\mathcal{E}_{\ell m}(i)\tilde{V}_\ell^2 \alpha_{n\ell}}{1+\frac{4}{\Gamma_{n\ell}^2}(\nu-\nu_{n\ell m})^2} + B(\nu), \tag{4.3}$$

here n_a and n_b represent respectively the first and last radial order included from the power spectrum. We include modes of degree $\ell = 0-2$. Each mode is described by a Lorentzian profile (see e.g. Anderson et al. 1990; Gizon and Solanki 2003) due to the way in which the p-modes are excited, namely stochastically by the turbulent convection in the outer envelope upon which they are intrinsically damped (Goldreich et al. 1994). In this description $\nu_{n\ell m}$ is the frequency of the mode while $\Gamma_{n\ell}$ is a measure for the damping[8] rate of the mode and equals the full width at half maximum of the Lorentzian. $\mathcal{E}_{\ell m}(i)$ is a function that sets the relative heights between the azimuthal m-components in a split multiplet as a function of the stellar inclination (see e.g. Dziembowski 1977; Gizon and Solanki 2003). The factor $\tilde{V}_\ell^2$ is the relative visibility (in power) of a mode relative to the radial and non-split $\ell = 0$ modes. The factor $\alpha_{n\ell}$ represents an amplitude modulation which mainly depends on frequency and is generally well approximated by a Gaussian. The granulation background signal is given by $B(\nu)$, which we describe as a sum of powerlaws (Harvey 1985; Karoff 2008). We refer to Van Eylen et al. (2014) for more details. The frequencies of the individual modes in the interval $1370-2630$ μHz found from this optimization (see Figure 9) are used in the stellar modeling which is described in Section 4.2.2.

4.2.2 *Asteroseismic modeling*

The stellar parameters were determined based on grids of models constructed using the GARching STellar Evolution Code (GARSTEC, Weiss and Schlattl 2008). The input physics consists of the NACRE compilation of nuclear reaction rates (Angulo et al. 1999), the Grevesse and Sauval (1998) solar mixture, OPAL opacities (Iglesias and Rogers 1996) for high temperatures complemented by low-temperature opacities from Ferguson et al. (2005), the 2005 version of the OPAL equation of state (Rogers et al. 1996), and the mixing-length theory of convection as described in Kippenhahn et al. (2013). One grid of models also included the effect of convective overshooting from the stellar core when present. This is implemented in GARSTEC as an exponential decay of the convective velocities in the radiative region, and the used

7 The program StellarMC was used, which was written and is maintained by Rasmus Handberg.

8 The mode life time is given by $\tau = 1/\pi\Gamma_{n\ell}$.

efficiency of mixing is the one calibrated to reproduce the color-magnitude diagram of open clusters (e.g. Magic et al. 2010). Diffusion of helium and heavy elements was not considered.

Our grid of models spans a mass range between 1.10-1.40 $M_\odot$ in steps of 0.02 $M_\odot$, and comprises five different compositions for each mass value spanning the 1-σ uncertainty in metallicity as found from spectroscopy by Huber et al. (2013b), see Table 1. We chose this set of atmospheric constraints for the host star since they were derived using an asteroseismic determination of the surface gravity to avoid degeneracies from the correlations between T_{eff}, log g, and [Fe/H] (see Torres et al. 2012, for a thorough discussion). While the relative abundance of heavy elements over hydrogen can be directly determined from the measured [Fe/H] value, the assumption of a galactic chemical evolution law of $\Delta Y/\Delta Z = 1.4$ (e.g., Casagrande et al. 2007) allows a complete determination of the chemical composition. For both grids of models we computed frequencies of oscillations using the Aarhus Adiabatic Oscillations Package (ADIPLS, Christensen-Dalsgaard 2008), and determined the goodness of fit by calculating a χ^2 fit to the spectroscopic data and frequency combinations sensitive to the interior as described in Silva Aguirre et al. (2013). Final parameters and uncertainties were obtained by a weighted mean and standard deviation using the χ^2 values of the grid without overshooting, and we added in quadrature the difference between these central values and those from the grid with overshooting to encompass in our error bar determinations the systematics introduced by the different input physics.

By combining the Casagrande et al. (2010) implementation of the InfraRed Flux Method (IRFM) with the asteroseismic determinations as described in Silva Aguirre et al. (2011, 2012), it is possible to obtain a distance to the host star which is in principle accurate to a level of ~5%. Since the photometry of the host star might be contaminated by the close companion, we carefully checked the 2MASS photometry used in the implementation of the IRFM for warnings in the quality flags. The effective temperature determined by this method, $T_{eff} = 6273 \pm 140$K, is in excellent agreement with those given in Table 1, giving us confidence that the distance to the host star is accurately determined. The final parameters of the star, including this distance, are given in Table 3.

In Figure 10 the échelle diagram (Grec et al. 1983) is shown, with observations overlaid by the frequencies from the best stellar model after the above iteration. For the sake of the comparison in the échelle diagram a surface correction has been applied to the model frequencies following the procedure of Kjeldsen et al. (2008)[9]. Note, that the surface correction is not needed for the

9 As reference frequency we use the mean value of the radial modes, while b is set to the solar calibrated value of 4.823 (Mathur et al. 2012)

model optimization as frequency ratios, unaffected by the surface layers, are used rather than the actual frequencies. The splitting of the $\ell = 1$ modes is clearly visible, with mode power mainly contained in the sectoral $m = \pm 1$ azimuthal components around the zonal $m = 0$ components found in the peak-bagging and the modeling. This distribution of power between the azimuthal components is a function of the stellar inclination angle (see e.g. Gizon and Solanki 2003), where we indeed for i close to 90° (as found for Kepler-410) should expect to see power mainly in the sectoral components of $\ell = 1$ (see Van Eylen et al. (2014) and Chapter 9 for details).

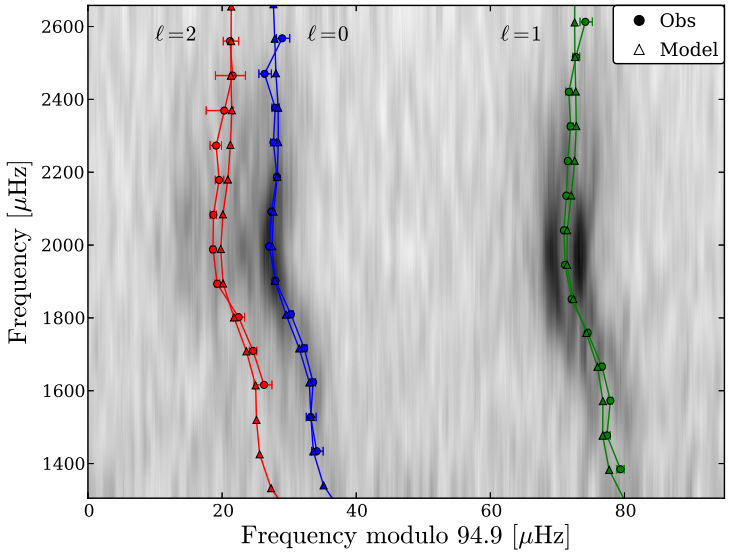

Figure 10 – Echelle diagram showing, in gray scale, the power spectrum of Kepler-410A. Overlaid are the frequencies estimated from the MCMC peak-bagging (circles), along with the frequencies from the best-fitting stellar model after a surface correction (triangles). The frequencies estimated from the peak-bagging are the $m = 0$ components, while $|m| > 0$ components are included in Equation 4.3 by the splitting. For an inclination close to 90° as found for Kepler-410 (see Chapter 9) mode power will for $\ell = 1$ modes mainly be contained in the $m = \pm 1$ components, whereby the estimated $m = 0$ component needed for the asteroseismic modeling should be found in between the $m = \pm 1$ power concentrations, as is observed.

4.3 KNOWING THE PLANET

For the planetary analysis, we start from the same dataset as for the asteroseismic analysis (see Section 4.2), where we normalize the planetary transits by fitting a second-order polynomial to the transit wings. To determine the planetary parameters we first create a phase folded high signal-to-noise light curve out of the *Kepler* light curve (see Section 4.4 for the exact procedure). The period-folded data are then used to determine the planetary parameters. The blending from Kepler-410B (see Section 4.1.1.3) needs to be taken into account before estimating the planetary parameters, so we subtract the esti-

Stellar parameters	Kepler-410A
Mass [$M_\odot$]	1.214 ± 0.033
Radius $R_\star$ [$R_\odot$]	1.352 ± 0.010
log g [cgs]	4.261 ± 0.007
ρ [g cm^{-3}]	0.693 ± 0.009
Age [Gyr]	2.76 ± 0.54
Luminosity [$L_\odot$]	2.72 ± 0.18
Distance [pc]	132 ± 6.9
Inclination $i_\star$ [°]	$82.5^{+7.5}_{-2.5}$
Rotation period, P_{rot} [days]	5.25 ± 0.16
Planetary parameters	**Kepler-410A b**
Period [days]	17.833648 ± 0.000054
Radius R_p [$R_\oplus$]	2.838 ± 0.054
Semi-major axis a [AU]	0.1226 ± 0.0047
Eccentricity e	$0.17^{+0.07}_{-0.06}$
Inclination i_p [°]	$87.72^{+0.13}_{-0.15}$
Model parameters	
a/R_*	$19.50^{+0.68}_{-0.77}$
R_p/R_*	$0.01923^{+0.00034}_{-0.00033}$
Linear LD	$0.57^{+0.22}_{-0.28}$
Quad LD	$-0.04^{+0.26}_{-0.22}$

Table 3 – Stellar parameters are derived from asteroseismic modeling (Section 4.2.2). Values are from the best fitting model without overshoot; the differences between these values and the ones from the best fitting model including overshoot are taken as a measure of the systematic error from differing input physics in the modeling; this difference is added in quadrature to the uncertainties from the grid optimization. The measurement of inclination and rotation period is discussed in Chapter 9 but included here for completeness. Planetary values are derived from transit modeling (Section 4.3) combined with asteroseismic results.

mated flux due to Kepler-410B (8%) from the light curve before starting our analysis.

The transits are fitted using the Transit Analysis Package (TAP) which is freely available (Gazak et al. 2012). An MCMC analysis is carried out, using the analytical model of Mandel and Agol (2002). An orbital eccentricity of zero is assumed for the entire fitting procedure. Flat priors were imposed on the limb darkening coefficients, and they were simply treated as free parameters in our approach. The folded datasets were binned to improve the speed of the MCMC procedure. Figure 6 shows the transit curve. A list of all param-

eters is provided in Table 3.

We finally note that the true errors are likely to be slightly larger than the formal errors reported in Table 3. These are the result of the MCMC fitting procedure, and do not take into account systematics in the *Kepler* data (see Chapter 6 and Van Eylen et al. 2013), or the uncertainty in the flux contribution by the blended light from Kepler-410B, both of which could affect the transit depth.

Because we have access to a transit light curve of excellent quality, and an independent measurement of the stellar density through asteroseismology, the eccentricity of the planet can be estimated. By carefully measuring the transit duration we find that the planet's orbit cannot be circular. The exact value of the orbital eccentricity is correlated to the angle of periastron, which is unknown, but by integrating over the possible angles a statistical constraint on eccentricity can nevertheless be derived, and is listed in Table 3. The reader is referred to Van Eylen et al. (2014) for more information, and to Chapter 10 for a description of the determination of eccentricity from transit photometry in much more detail.

4.4 TRANSIT TIMING VARIATIONS: A SECOND PLANET?

Transit timing variations (TTVs) are detected for Kepler-410A b, which indicate the likely presence of one or more additional planets (see Section 2.2.3 for more details about TTVs). We use the following procedure to measure the TTV signal:

1. Estimate the planetary period and produce a phase-folded light curve;
2. Use the phase-folded light curve as an empirical model for the shape of the transit and use this model to determine individual transit times;
3. Repeat the first two steps until convergence is reached;
4. Determine TTVs and produce a phase-folded lightcurve which takes this into account.

We find the usage of the phase-folded light curve as an empirical model for the transit quite efficient in determining the times of individual transits. The time for an individual transit event is determined by shifting the empirical model around the predicted transit time. The new time for the transit event is determined by comparing data points with the time-shifted empirical model and minimizing χ^2. Based on the new transit times, a new period estimate can be made and the procedure can be repeated. Following this approach, we reached convergence after only two iterations.

After convergence is reached on determining transit times of individual transit events, the planetary period can be determined. Under the assumption of a perfectly Keplerian orbit, the planetary period is given by a linear interpolation of the transit times:

$$T(n) = T(0) + n \times \text{Period}, \tag{4.4}$$

where $T(n)$ and $T(0)$ refer to the nth and 0th transit times (taking into account possible data gaps). The period found in this way is 17.833648 ± 0.000054 days. Subsequently, we produce an O-C ($Observed - Calculated$) diagram in which for each transit the calculated transit time is subtracted from the observed transit time, and which we present in Figure 11. TTVs are clearly visible.

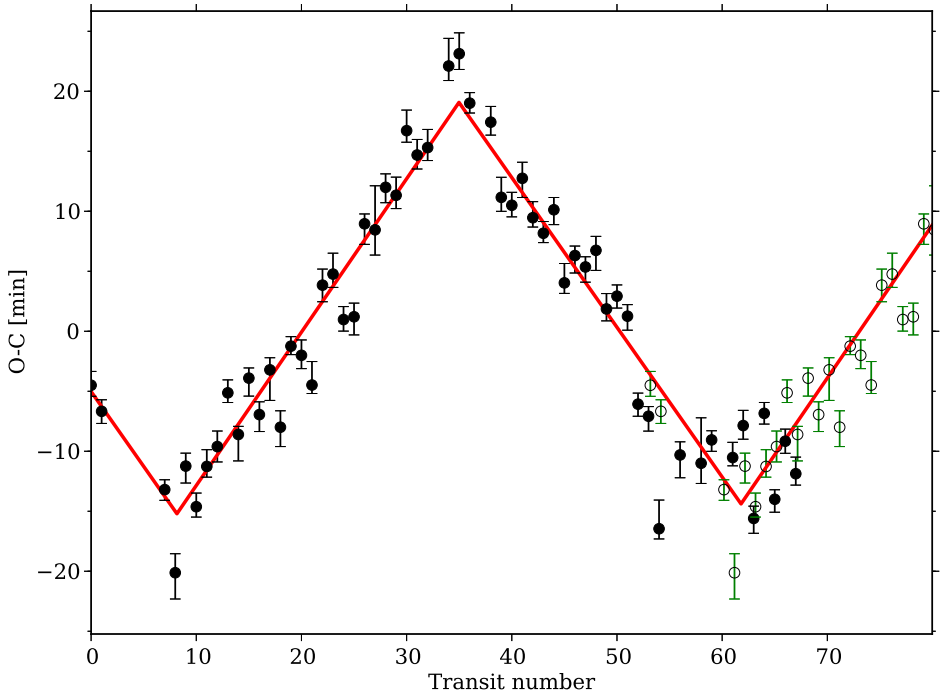

Figure 11 – O-C diagram showing the observed transit times minus the calculated transit times following a Keplerian orbit (Equation 4.4). The black points represent individual transit measurements (with their error bars), the green dots are a copy of the observed data points, offset by one full period. They are for illustration only, and were not included in the fit. A clear trend is visible, which is fitted by a model with discontinuities at the turning points.

The interpretation of TTVs is difficult. Short-period trends can be caused by stellar variability (e. g. stellar spots causing an apparent TTV signal), while longer-period trends such as here are in most cases attributed to a third body (e.g. a planet), whose gravitational influence causes the deviation from the strictly Keplarian orbit.

The signal can be highly degenerate, with bodies in or close to different resonance orbits resulting in very similar TTV signals. Attempts of interpretations have been made by performing three-body simulations, with unique solutions for non-transiting objects in only a limited number of cases (see e. g., Nesvorný et al. 2013). TTVs have been successfully used to characterize systems with multiple transiting exoplanets, by studying their mutual gravitational influence (e.g. Carter et al. 2012). We have made a visual inspection of the time series to look for additional transit signals, but found none.

Based on limited data, Ford et al. (2011) reported a possible detection of TTVs in the orbit of Kepler-410, and a study of TTVs on the full sample of KOIs (Mazeh et al. 2013) resulted in an amplitude of 13.95 ± 0.86 minutes and a period of 990 days (no error given) for Kepler-410, using a sinusoidal model. We find a peak-to-peak amplitude of 0.023 days (33 minutes), and a period of 957 days, not using a sinusoidal but a *zigzag* model, as indicated in Figure 11 by the solid line. It is not immediately clear what is causing the seemingly non-sinusoidal shape of the TTVs (see e. g. Nesvorný 2009, for a discussion). A similar shape is seen for Kepler-36 (Carter et al. 2012), where discontinuities occur when the planets are at conjunction. We speculate that the mild eccentricity of Kepler-410A b could be influencing the shape.

4.5 SUMMARY

In this chapter I described the discovery of Kepler-410A b, a Neptune-sized planet in a 17.8 day orbit around Kepler-410A. Kepler-410A is a bright star (V = 9.4) which has a close companion star (Kepler-410B), which was ruled out as the host of the transit signal using a combination of *Kepler* and *Spitzer* observations, in combination with a number of other constraints. The properties of Kepler-410A are accurately determined using asteroseismology, with an uncertainty of $\approx$ 1% on the radius, $\approx$ 3% on the mass, $\approx$ 20% on the age and $\approx$ 6% on the distance. As a result, the planetary parameters are also determined very accurately, e.g. the planetary radius is known to $\approx$ 2%. TTVs were detected and signal the presence of one or more additional planets in the system. The splitting of stellar oscillation frequencies also allowed the measurement of the stellar rotation rate and inclination angle, but this is discussed in detail in Chapter 9.

5 KNOWING THE STAR, FINDING THE PLANET

In this chapter I make use of detailed knowledge of the interiors of stars in combination with a careful analysis of transit photometry, to validate new planets. The technique relies on knowledge of the mean stellar density, which can be achieved highly accurately using asteroseismology, and a precise measurement of the transit duration and shape. The combination of those two things allows the validation (or falsification) of a star as the host star of a planetary candidate, at least for multi-planet systems where the eccentricity is known to be low. The technique is explained in Section 5.1, and used to find six new planets in Section 5.2. A brief discussion in Section 5.3 concludes this chapter.

5.1 HOW TO USE THE TRANSIT DURATION TO FIND THE HOST STAR

Multi-planet systems can often be confirmed based on statistical grounds because their multiplicity makes false positive scenarios very unlikely (Rowe et al. 2014; Lissauer et al. 2014). However, this is no longer generally true if the light curve consists of two or more blended stars of different magnitudes, because it can be difficult to tell at which object the transits occur (see e.g. Section 4.1).

In principle, transit durations can be used to assess the validity of a transiting planet candidate, when the stellar density ($\rho_\star$) of the suspected host star is known as well as the orbital eccentricity (e) of the planet (e.g. Tingley and Sackett 2005). To make this statement more intuitive, I combine Equation 2.5 and Equation 2.6 to find an approximate expression for the stellar density as a function of the transit duration and eccentricity:

$$\rho_\star \approx \frac{3P}{\pi^2 G T^3}(1-b^2)^{3/2}\frac{(1-e^2)^{3/2}}{(1+e\sin\omega)^3}. \tag{5.1}$$

As a reminder, the orbital period P, the transit duration T and the impact parameter b can all be constrained from the transit photometry. This implies that if e and ω are known, the stellar density can be measured by the transit photometry. This estimate of the stellar density can be compared with an independent measurement to see if the transit appears to occur on the suspected host star or not.

In general, the eccentricity is not known, and it is difficult to distinguish between eccentric planets and false positives, although statistical claims can sometimes be made (see e.g. Sliski and Kipping 2014). However, in the case

of systems with multiple transiting planets the eccentricity was determined by Van Eylen and Albrecht (2015) to be very low (see Chapter 10), so this complication does not arise for these systems. Consequently, transit durations can be readily used to assess the validity of transit signals in these systems.

5.2 APPLICATION: SIX NEW PLANETS

I now apply the method to validate new planets in multi-planet systems. I discuss four systems with multiple planets, which were not previously validated but where a stellar density is available from asteroseismology (Huber et al. 2013b; Silva Aguirre et al. 2015). The transits are modeled using the Mandel and Agol (2002) analytical equations, where the optimal solution is found using a Markov Chain Monte Carlo (MCMC) algorithm that allows the measurement of reliable uncertainties and parameter correlations. The data analysis is described in detail in Section 10.2.

The stellar density derived from modeling the planetary candidates is compared with the asteroseismic density of the brightest star in the system. Any mismatch would be a strong indication that the star is not the true host. A clear agreement is strong evidence the star is the true host, especially if any other star in the system has a very different density. A density ratio (the asteroseismic stellar density divided by the density derived from the transit) is calculated and a value close to unity indicates evidence that the star is the true host star.

Here I discuss four multi-planet systems for which asteroseismic constraints are available but where planets were not previously validated or confirmed. These results were first announced by Van Eylen and Albrecht (2015). KOI-5 is presented in Section 5.2.1, KOI-285 (Kepler-92) in Section 5.2.2, KOI-270 (Kepler-449) in Section 5.2.3, and KOI-279 (Kepler-450) in Section 5.2.4. I discuss the results in Section 5.3.

5.2.1 *KOI-5*

KOI-5 contains two transiting planet candidates which have not been validated or confirmed as true planets. The inner planet candidate has an orbital period of 4.8 days and a 7.9 $R_\oplus$ radius, while the second planet candidate orbits in 7 days and is much smaller (0.6 $R_\oplus$). The reason the candidates have not been validated is the presence of a second, fainter companion star which is physically associated (Wang et al. 2014; Kolbl et al. 2015). We refer to it here as KOI-5B.

We take a 6% flux dilution (Wang et al. 2014; Kolbl et al. 2015) caused by KOI-5B into account before modeling the planet candidates assuming they orbit the bright star (KOI-5A). The density ratio is $[0.76, 0.93]$ at 68% confidence, and $[0.72, 0.88]$ to 95% confidence, which implies that if the planet candidate is orbiting KOI-5A, it would have a non-zero eccentricity. This is suspicious, in particular given the short orbital period of the candidate, and a possible explanation is that the candidate does not transit KOI-5A but rather KOI-5B instead. Because KOI-5B is much fainter, the candidate would consequentially be larger and might not be planetary in nature.

The second candidate's posterior distribution gives a density ratio $\in [0.45, 1.11]$ (to 68% confidence), which is consistent with a planet on a circular orbit around KOI-5A. This could imply that this candidate is a genuine planet orbiting KOI-5A. However, due to the large error bar caused by the small size of the planet, it is difficult to exclude KOI-5B as a host for this candidate without knowing more about this companion star.

5.2.2 *Kepler-92 (KOI-285)*

Kepler-92 contains three planets, of which the inner two (13 and 26 day periods) were validated based on their TTV signal (Xie 2014). The eccentricity of the planets could not be determined due to a mass-eccentricity degeneracy (Xie 2014). Due to a limited amount of short cadence data, we pick up only a hint of the TTVs and we choose not to include them. The planets are consistent with circularity ($[0, 0.27]$ and $[0, 0.25]$ at 68% confidence, respectively), following the methods described in Section 10.2.

There's a third planetary candidate (KOI-285.03) observed transiting every 49 days, which has not yet been validated or confirmed as true planet orbiting Kepler-92. We model the transit under the assumption that it does. We find a density ratio of $[1.01, 1.56]$ at 68% confidence, consistent with a planet orbiting the star in an orbit which is (almost) circular. Adaptive optics observations have revealed two other stars at 1.4 and 2.3 arcsec, the brightest is estimated to be 5.6 magnitudes fainter in the *Kepler* bandpass (Adams et al. 2012) so that their flux contributions are negliglible. Given the planet candidate's period and similar size to the two confirmed planets, as well as their agreement with the stellar density for (close to) circular orbits, all planets are likely to orbit the same star (Kepler-92), and KOI-285.03 is subsequently validated and named Kepler-92d.

5.2.3 *Kepler-449 (KOI-270)*

KOI-270 contains two transiting planet candidates which transit every 12 and 33 days, thus far unconfirmed. KOI-270 has a stellar companion, separated by only 0.05 arcsec and with the same magnitude in both J and Ks band (Adams et al. 2012). Therefore KOI-270 appears to consist of two very similar stars and we dilute the light curve by a factor two to account for this. We find no evidence for TTVs but note that only limited short-cadence data is available.

After accounting for the flux dilution, the planetary radii are 2.1 and 2.8 $R_\oplus$. The density ratio intervals are $[0.94, 1.29]$ and $[0.80, 1.11]$ respectively. Both candidates are likely true planets and KOI-270A is a plausible planet host star. However, with KOI-270B presumably very similar to KOI-270A, we cannot rule out the planets orbit this star instead. In this case the transits would still be caused by genuine planets with similar properties, so we find that KOI-270's two candidates are indeed planets orbiting either KOI-270A or KOI-270B, and the planets are further referred to as Kepler-449b and Kepler-449c.

5.2.4 *Kepler-450 (KOI-279)*

KOI-279 contains three planetary candidates which transit every 7.5, 15 and 28 days, previously unconfirmed as planets. For the outer planet, a long period TTV signal was clearly measured and included (with a period of 1008 days and an amplitude of 2 minutes, see also Section 10.3.2), while for the inner two planets no sinusoidal TTVs were included although an increased scatter in the transit times of the middle planet was seen.

The reason for the lack of confirmation for this system is the presence of a second star (at 0.9 arcsec) to which we refer as KOI-279B which is significantly fainter and contributes 6% flux[1]. After removing this flux contamination assuming the candidates orbit KOI-279A and including the TTV signal for the outer planet candidate we proceed to model the transits. We find density ratios of $[0.88, 1.08]$, $[0.90, 1.13]$ and $[0.56, 1.51]$ respectively. The range of periods and the TTV signal is further evidence that the planets orbit the same star. We find that the three candidates are indeed planets orbiting KOI-279(A), and they are subsequently named Kepler-450b, Kepler-450c and Kepler-450d.

5.3 DISCUSSION

In this chapter I applied a method to connect the properties of transits, specifically their duration, to the density of the host star to validate or falsify plan-

1 Based on WIYN Speckle images and Keck spectra; Mark Everett and David R. Ciardi, from https://cfop.ipac.caltech.edu

etary candidates. In general, this method is complicated by the orbital eccentricity, which also influences the duration and is usually unknown, but for the sample of *Kepler* stars with multiple transiting planets it turns out the eccentricity is generally be very low (see Chapter 10).

In KOI-5, a clear conclusion cannot be drawn because only one of the planets provides meaningful constraints. For KOI-270, I could confirm that the transits are caused by true planets which could orbit either KOI-270A or KOI-270B, two stars which are very similar, and the new planets are named Kepler-449b and Kepler-449c. The three planet candidates for KOI-279 are genuine planets orbiting KOI-279A and are named Kepler-450b, Kepler-450c and Kepler-450d. Finally, I also confirm a third planet orbiting Kepler-92, a system where two other planets were previously confirmed.

This proves that with appropriate constraints on stellar density and orbital eccentricity, this method can indeed work to (help) validate planet candidates. The method is particularly powerful in systems where more than one star is known, because it has the potential to distinguish between potential host stars, something that is otherwise difficult to do. The method may also be used in the future to validate interesting planet candidates, such as planets in the habitable zone where liquid water may exist. Because of the long orbital period of these planets, the transit photometry often has a low signal-to-noise ratio, and the RV signal they induce is also difficult to detect. Consequentially, these planets are interesting but difficult to validate or confirm, and this method may help with that in the future.

6 SYSTEMATIC EFFECTS IN *KEPLER* DATA

In this chapter I take an excursion to look into the characteristics of *Kepler* data themselves. The main drive behind this data investigation is the question whether years of *Kepler* photometry can allow for the detection of astrophysical variability over time. Such variability could be interesting, for example in exoplanet phase curves. These phase curves occur for the closest-in exoplanets, where the flux is variable over the period of the planet, e.g. due to reflected star light. This reflected light may itself vary over time, if the planet contains some kind of 'weather'. Variability of brown dwarfs has been a source of extensive study and weather effects have been detected in a number of instances (e.g. Metchev et al. 2015). Another time-variable effect is the precession of a misaligned rotating exoplanet, which could cause the observed transit depth to vary over time, an effect which could in principe be used to constrain the oblateness of the planet (e.g. Carter and Winn 2010). Could such effects in principle be detected with *Kepler* observations? In attempting to answer this question, I investigated the transit depth of HAT-P-7b. This system contains a large hot Jupiter planet which orbits a bright star. This makes it ideal to look for temporal variations, as the deep transits make variations easier to measure, and the short orbital period gives more transits to measure the depth so there are more data points to compare.

The study of the transit depths of HAT-P-7b revealed a striking feature: the transit depths are variable, but the variability coincides with quarters of observations. Such quarters, each containing three months of data, are separated by a 'roll' of the spacecraft as it continues to observe the target. As a result, the observed variability is clearly instrumental. Because it is of the order of 1%, this finding implies that any measurements related to *Kepler* amplitudes, such as transit depths, cannot be measured more reliably than this. Therefore, an immediate conclusion of this work is that care needs to be taken when averaging observations obtained over different quarters, and stating error bars based on that. A different study later confirmed the systematic effect using a different method, studying the variability of M giant stars (Bányai et al. 2013). The derived properties for HAT-P-7b have also since been used in other studies, performing asteroseismology on HAT-P-7 (Lund et al. 2014b; Benomar et al. 2014) and into obliquity evolution (Valsecchi and Rasio 2014). In my study, I also noticed an asymmetric shape in the transit light curve (see Figure 12), which may be attributed to gravity darkening and has since been the subject of studies to constrain the obliquity of the planet (Masuda 2015). The work was first published by Van Eylen et al. (2013) and is republished here, edited only for formatting. This chapter is more technical than other parts of this thesis and some readers may wish to skip it.

Investigation of Systematic Effects in Kepler Data: Seasonal Variations in the Light Curve of HAT-P-7b

Vincent Van Eylen, Michael Lindholm Nielsen, Brian Hinrup, Brandon Tingley, and Hans Kjeldsen.
Astrophysical Journal Letters, Volume 774, Issue 2, article id. L19, 6 pp. (2013)

With years of *Kepler* data currently available, it can now be attempted to measure variations in planetary transit depths over time. To do so, it is of primary importance to understand which systematic effects may affect the measurement of transits. We aim to measure the stability of *Kepler* measurements over years of observations. We present a study of the depth of about 500 transit events of the Hot Jupiter HAT-P-7b, using 14 quarters (Q0-Q13) of data from the *Kepler* Satellite. We find a systematic variation in the depth of the primary transit, related to quarters of data and recurring yearly. These seasonal variations are about 1%. Within seasons, we find no evidence for trends. We speculate that the cause of the seasonal variations could be unknown field crowding or instrumental artifacts. Our results show that care must be taken when combining transits throughout different quarters of *Kepler* data. Measuring the relative planetary radius of HAT-P-7b without taking these systematic effects into account leads to unrealistically low error estimates. This effect could be present in all *Kepler* targets. If so, relative radius measurements of all Hot Jupiters to a precision much better than 1% are unrealistic.

6.1 INTRODUCTION

The *Kepler Satellite* was launched on March 6, 2009 and operates from an Earth-trailing orbit around the Sun. The satellite continually measures the brightness of about 150,000 stars in a long-cadence mode (sampled every 29.4 minutes), and a subset of stars are sampled in a short-cadence of 58.8 seconds (Borucki et al. 2008). The primary scientific goal of the *Kepler* Mission is to discover transiting exoplanets, identifying 2740 exoplanet candidates to date (Borucki et al. 2011; Batalha and Kepler Team 2012).

The photometry from the mission can be used to characterize many parameters of a star-planet system, e.g. star-to-planet radius ratio, planetary inclination angle, semi-major axis and stellar limb darkening coefficients. For close-in Hot Jupiter planets, the phase curve and planetary occultation may also contain information about the planetary emission and reflection (e.g. Borucki et al. 2009a; Van Eylen et al. 2012) and in some cases even about ellipsoidal variations and Doppler beaming (Welsh et al. 2010; Jackson et al. 2012). More-

over, if the data is short-cadence, the photometry can also be used to study the host star using asteroseismology (Christensen-Dalsgaard et al. 2010; Van Eylen et al. 2012).

Previous studies show that the various system parameters become better constrained as the amount of data increases (e.g. Van Eylen et al. 2012; Morris et al. 2013). In this paper, we investigate the limits to this ever-increasing accuracy. Ultimately, the accuracy with which parameters can be determined depends on the systematic noise sources, including the instrumental stability of the satellite. This is an important line of research, because such systematic changes could in principle be mistaken for actual changes in the star-planet system, e.g. changes in the planetary atmosphere. We propose therefore to probe these limits by tracking changes in transit depth. Given that *Kepler* rotates 90° every three months, with each new pointing assigned a new quarter (Q) number and each orientation a season (every fourth quarter), we explore the changes with this in mind, as these pointing changes are the most likely source of systematic noise.

The HAT-P-7 system (Pál et al. 2008) is an ideal target for the study of transit variations. It is a relatively bright star (apparent magnitude of $m_V = 10.5$), orbited by a Hot Jupiter, whose short period (2.2 days) and large radius (1.4 R_J) result in many deep transits – all observed with short-cadence. In this paper, we analyze *Kepler* data (Q0-Q13) for this exoplanet, searching for significant quarter-by-quarter or seasonal variations.

In Section 6.2, we describe the data reduction procedure. In Section 6.3, we present our results. We discuss these results in Section 6.4, exploring possible causes and testing to see if our results are specific or general. Finally, we conclude in Section 6.5.

6.2 OBSERVATIONS

We choose to start with the raw *Kepler* data, despite the existence of the Presearch Data Conditioned data, desiring to tailor the analysis to the peculiarities of this system. We detrend the raw light curve following three steps: (i) we identify all transit-like features and temporarily mask them off, (ii) fit a fourth-order polynomial to the remaining data in one-month sections (this choice is somewhat arbitrary, as using third- or fifth-order polynomials produces no significant differences), then (iii) remove the long-term trends by dividing the data (including the transits) by the fitted curve. This results in a normalized, detrended light curve, which we can then clean for short-term instrumental effects such as outliers, jumps or drifts with local median filtering. We use this cleaned light curve in the subsequent analyses – first to get the global parameters, then using these global parameters to search for variations.

6.3 RESULTS

6.3.1 *Global transit modeling*

Assuming a perfectly Keplerian orbit, the orbital period is found by applying a linear fit to the centers of the individual transits. The resulting orbital period is 2.204 735 40(9) days. This value is in agreement with other recent period determinations (e.g. Van Eylen et al. 2012), consistent with and refining values based on more limited datasets (e.g. Borucki et al. 2009b). We test for deviations from linearity (transit timing variations, see e.g. Mazeh et al. 2013), but find no evidence. We place an upper limit of just 3 seconds, as the strongest possible amplitude of a sinusoidal variation.

Having established the absolute periodicity of HAT-P-7, we used the Transit Analysis Package (TAP) (Gazak et al. 2012) on the phase-folded data, binned to a temporal resolution of ~ 20 s. TAP uses Markov Chain Monte Carlo (MCMC) simulations to fit the transit signature with the analytical methods described in Mandel and Agol (2002). When fitting, we used no priors for the limb darkening (LD) coefficients; they were treated as free parameters. The transit light curve and the corresponding fit are shown in Figure 12, with the resulting global planetary parameters listed in Table 4. These values are in excellent agreement with Esteves et al. (2013). The limb darkening parameters can be compared to predictions from stellar atmospheres, even though they are known to disagree (Howarth 2011). Using the stellar parameters by Van Eylen et al. (2012), linear and quadratic values of respectively 0.3201 and 0.4297 are predicted (Neilson and Lester 2013), for spherically symmetric model atmospheres. The residuals from the transit fit (Fig. 12) exhibit an asymmetric trend, also visible in Esteves et al. (2013). This may be due to planet-induced gravitational darkening, as suggested by Morris et al. (2013).

Parameter	Value
Period P (days)	2.20473540 (9)
Inclination i (°)	$83.151\ ^{+0.030}_{-0.033}$
Rel. semi-major axis $a/R_\star$	$4.1547\ ^{+0.0040}_{-0.0042}$
Rel. radius $R_p/R_\star$	$0.077462\ ^{+0.000034}_{-0.000034}$
Linear Limb Darkening	$0.3440\ ^{+0.0064}_{-0.0065}$
Quad. Limb Darkening	$0.1843\ ^{+0.0098}_{-0.0096}$

Table 4 – Summary of all parameters for HAT-P-7b.

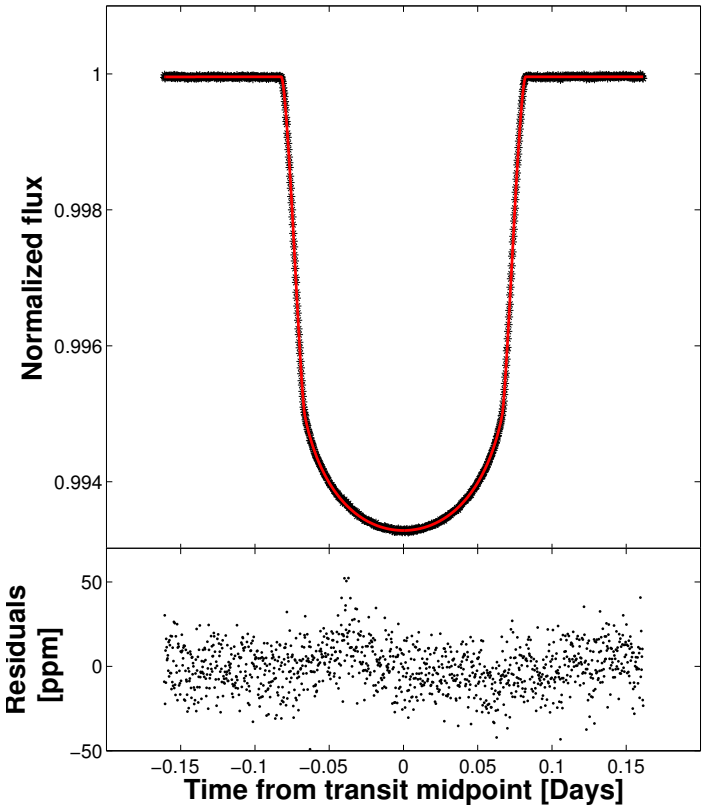

Figure 12 – *Upper*: Phase folded and binned data near the transit of HAT-P-7b. Individual bins are shown as black dots and the best fit model from TAP is shown in red. *Lower*: Residuals between the binned data and the TAP model.

From these parameters a mean stellar density $\bar{\rho}_\star$ can be derived directly (Tingley et al. 2011):

$$\bar{\rho}_\star = \frac{3\pi}{GP^2}\left(\frac{a}{R_\star}\right)^3 - \left(\frac{R_p}{R_\star}\right)^3 \bar{\rho}_p, \tag{6.1}$$

where $\bar{\rho}_p$ is the average planetary density, G the gravitational constant, and all other symbols as defined in Table 4. The second term on the right hand side is often neglected, since the planetary radius is so much smaller than the stellar radius, however we include it in this case. We find $\bar{\rho}_\star = 0.2787 \pm 0.0008$ g cm^{-3}, with the second term contributing 0.0004 g cm^{-3}. This is consistent with stellar densities obtained with asteroseismology: 0.2712 ± 0.003 g cm^{-3} (Christensen-Dalsgaard et al. 2010) and 0.2781 ± 0.0017 g cm^{-3} (Van Eylen et al. 2012).

6.3.2 *Transit depth variations*

Having obtained the global transit depth, we now measure the depth of individual transits. The depth as measured here is defined (somewhat arbitrarily) as the average of the in-transit obserations within 65 minutes from the transit center, compared with the average flux level at the transit wings (taking the same amount of data points in and out of transit). We find that the transit depth is dependent on the data quarter, as can be seen in Figure 13. The figure shows the relative depth measurements for individual transits, as well as the average transit depth per quarter of *Kepler* data. To avoid making assumptions about the distribution of the measurements, the error bars are calculated using a bootstrap procedure. A variation in transit depth is clearly visible, with a recurring trend every fourth quarter (every year) – a seasonal variation. To ensure the crude way of estimating a transit depth is adequate, we also show a quarterly median in Figure 13 (top panel).

Season	Module	Channel	'Depth' (ppm)	Rel. 'depth'	'Depth' diff. (%)	$R_p/R_\star$
1	17	58	6557.2 ± 3.5	1.00869 ± 0.00054	0.869± 0.054	$0.077618\ ^{+0.000073}_{-0.000073}$
2	19	66	6491.8 ± 4.5	0.99863 ± 0.00068	-0.137± 0.068	$0.077355\ ^{+0.000035}_{-0.000035}$
3	9	26	6475.9 ± 6.0	0.99618 ± 0.00091	-0.382± 0.091	$0.077330\ ^{+0.000056}_{-0.000059}$
4	7	18	6461.1 ± 4.7	0.99392 ± 0.00071	-0.608± 0.071	$0.077229\ ^{+0.000044}_{-0.000043}$

Table 5 – HAT-P-7b measurements per season. The transit 'depth' is measured directly as an average of in-transit data points, the relative and per cent depths are calculated by dividing by the average 'depth' (6500.7 ppm). $R_p/R_\star$ is calculated from fitting a physical model to the transits, allowing only this parameter to vary.

Season	Module	Channel	RMS Amplitude (ppm)	Relative difference	Difference (%)
1	8	23	270723 ± 176	1.0092 ± 0.0007	0.92 ± 0.07
2	12	39	268014 ± 109	0.9991 ± 0.0004	-0.09 ± 0.04
3	18	63	266843 ± 312	0.9948 ± 0.0012	-0.52 ± 0.12
4	14	47	267414 ± 1164	0.9969 ± 0.0043	-0.31 ± 0.43

Table 6 – Measurements of pulsation amplitude of FN Lyr (KIC 6936115) per season. The relative difference and per cent difference are calculated by dividing by the average RMS amplitude (268249 ppm).

Subsequently, we split the data into four sets of quarters (seasons): a dataset for Q0-1-5-9-13, for Q2-6-10, for Q3-7-11 and finally for Q4-8-12. The resulting average transits, rebinned for clarity, are shown in Figure 13. This figure confirms that the transit depth is dependent on the season of observation. The figure also shows that the *shape* of the transit is seemingly unaffected.

The average depth per quarter is also shown in Table 5, as well as the average depth per quarter divided by the average depth for the combined dataset,

showing differences of 1.5% between Season 1 and Season 4, with differences of at least 3σ between any two seasons. To investigate this effect further, we fit the individual seasons using the TAP as described in Section 6.3.1, but only allowed the planetary radius to be free, fixing all other parameters to our earlier derived values. The results are also shown in Table 5. For verification purposes, we also performed this analysis on the PDC *Kepler* light curve and found similar results.

6.4 DISCUSSION

6.4.1 *The true planetary radius*

While Figure 13 shows a clear change in depth per *Kepler* quarter, the impact on the planetary radius is less severe (see Table 5). The reason for this is two-fold. Firstly, using a full physical description to model the transit increases the size of the error bars than simply measuring the average of all in-transit data points. As a result, the radius difference is statistically less significant than the depth difference. The other reason is the fact that the radius scales with the square root of the transit depth, and is therefore less affected.

Even so, when comparing Season 1 to Season 4, the radius found for HAT-P-7b is different by 6σ. It is not immediately clear which season is the most accurate. While the true depth may be somewhere in the middle of all seasonal depths, it is also possible that one specific season represents the correct transit depth – or none at all. Indeed, one might speculate that all of the seasons are to some extent affected by this apparent systematic error. The true transit depth can also be important for studies of exoplanet atmospheres, where a different radius is expected in different wavelengths as a consequense of haze or dust (e.g. Pont et al. 2008). The reported effect shows care must be taken when comparing *Kepler* values with measurements in other wavelengths. Regardless of the true planetary size, it is clear from Table 4 that the resulting value from a naïve fit to the combined *Kepler* photometry ($R_p/R_\star = 0.077462 \pm 0.000034$) underestimates the true error bars of the relative planetary radius by an order of magnitude.

6.4.2 *Other targets*

A full comparison of the seasonal variations of the *Kepler* satellite is outside the scope of this paper. Even so, we attempted to confirm this effect in other targets.

The non-Blazhko ab-type RR Lyr star KIC 6936115, also known as FN Lyr (Nemec et al. 2011) is a very stable pulsating star. Its pulsation amplitude

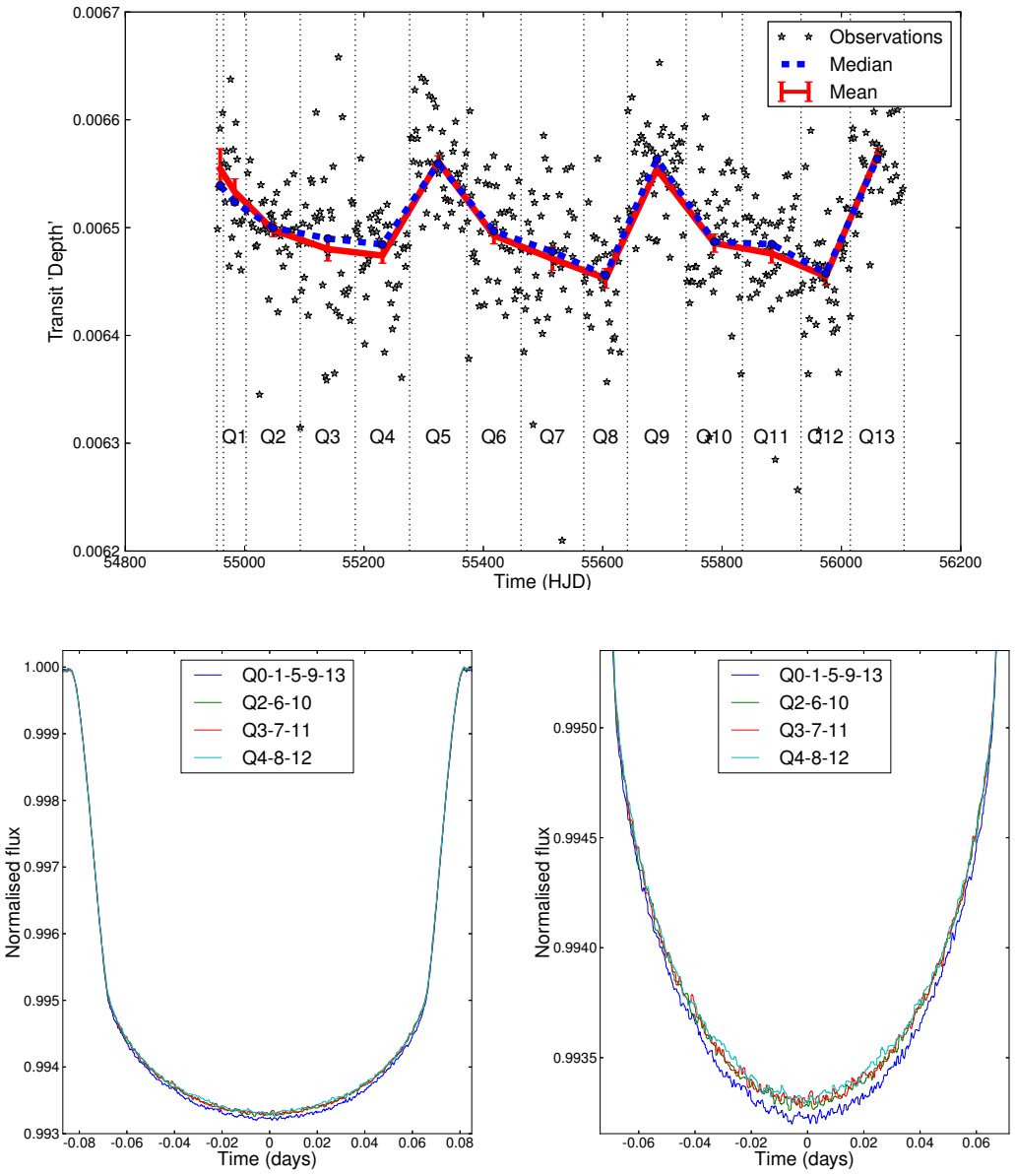

Figure 13 – Top: Transit depth per quarter, as measured directly from averaging in-transit data points. The measured depth of individual transits (blue dots) is plotted. The green dotted line shows the median per quarter. The red solid line shows the mean and standard deviation per quarter, calculated from non-parametric bootstrapping of the observations. **Bottom:** Transit depth as binned per season. From the left figure, it is clear that the different seasons show the same transit shape. The right figure (zoom) shows the change in depth for different seasons. The observations were binned for clarity.

(which should be constant) was therefore used to search for seasonal dependences in *Kepler* data. The RMS amplitude is calculated from the raw time series. Instead of extracting amplitudes from Fourier Analysis by measuring the amplitude of the different oscillation modes we calculated the RMS amplitude directly from the time series. First, we corrected for the slow sensitivity variation by calculating the moving median of the time series and divide the time series with the moving median series, then we calculated the average RMS amplitude for each quarter (Qo-Q14) and season (shown in Table 6). The relative amplitude of the pulsations differs from season to season by up to 1% with a high level of significance. It is clear from the table that the seasonal variations in this target are real: the offset of Season 1 is separated by 13 sigma from the average. As with HAT-P-7, we have repeated the analysis, replacing the raw *Kepler* data by PDC processed data. The level of our error bars increases slightly (the PDC pipeline is not normally used for studying pulsation amplitudes), but our findings remain intact.

The seasonal differences seem to agree quantitatively with our findings for HAT-P-7b's transit depth, with peak-to-peak variations of 1.5 per cent. It is tempting to interpret this as proof that these seasonal variation occur in all *Kepler* targets. However, it turns out to be complicated to confirm: testing relative stability to a percentage level requires physical events that are stable to this level over a few years. Most stellar pulsations do not fall into this category, and most planetary transits are not as deep or as frequently occurring as HAT-P-7b's.

One alternative to planetary transits are transits caused by eclipsing binary stars, which have even deeper transits than HAT-P-7b. Slawson et al. (2011) mention, for example, that potential quarter-to-quarter systematics may be present in their catalogue of 2165 *Kepler* binary stars. However, the stability of transit depths for binary objects is often not at percentage level, due to various physical phenomena.

6.4.3 *Possible causes*

We speculate on four possible causes for seasonal variations: the first two are systematic errors that are caused by crowding in the field and the applied mask, the other two are related to non-linear behavior of the *Kepler* CCD or its color dependence.

(i) *Field crowding* could potentially explain differences in relative measurements. As the *Kepler* CCDs make a roll maneuver at the end of each quarter, the targets fall on different CCDs and a new optimal aperture is applied. Any nearby targets could introduce flux, which could be different every season. The Pre-search Data Conditioning (PDC) attempts to correct for crowding ef-

fects by estimating a crowding metric, the fraction of light that comes from the actual target star. This is estimated from the distribution of surrounding objects in the *Kepler* Input Catalogue (KIC). The crowding metric is calculated per quarter and therefore in principle has the capability to correct for the observed effects. We have tested our analysis of both HAT-P-7 and FN Lyr on PDC data and found similar results as when using the raw data. However, this does not rule out the possibility of additional crowding of unknown or undetected sources that the PDC data does not correct for.

A nearby target, 4-5 *Kepler* magnitudes fainter than HAT-P-7 (*Kepler* magnitude K_v = 10.5), separated by ~ 10″ from HAT-P-7 so it is close to the edge of the optimal aperture, could reproduce the observed 1.5 per cent peak-to-peak variation. Such an object should be seen in the UKIRT[1] or UBV (Everett et al. 2012) catalogues. A target at a distance of 15″ is seen in both catalogues, estimated to be 5.8 (UKIRT) or 7.2 (UBV) K_v fainter. This target appears to be outside the apertures in all seasons, and is presumably too faint to reproduce the observed effect. Two companion stars are observed at about 3″ (Narita et al. 2010), but fall inside the aperture during all seasons. The brightest of the two is also seen in UKIRT photometry, and with an estimated 6.5 K_v fainter than HAT-P-7, it is anyhow too faint to produce the seasonal variations. All other known objects are too faint and too distant.

(ii) An alternative explanation related to the target mask is the opposite effect: *a differential loss of photons from the target star*, due to a mask that is too small. A simple loss of target photons would not create a difference in the measured transit depth (this is a relative measurement), however, in principle, it is possible that the photon loss is different in-transit compared to out-of-transit, because the transit dims the brightness of the star, changing the way electrons in saturated pixels overflow into their neighbors. An example of this is the observations of RR Lyr in early *Kepler* photometry, where a mask that was too small to capture the brightest stages of the star, caused an underestimated amplitude (Kolenberg et al. 2011). As the dimming due to planetary transits is small, we consider this option rather unlikely. If true, this effect could potentially be mitigated by increasing the size of the mask, assuming there are not too many contaminating sources nearby (Kinemuchi et al. 2012).

(iii) Another possible explanation for our observations is *non-linearities related to the Kepler instrument*. The response to a signal is non-linear to some extent for every CCD and those in *Kepler* are no exception to this rule. The *Kepler* instrument handbook (Van Cleve and Caldwell 2009) states that the observed non-linearity in the *Kepler* focal planes is of order 3%. A similar value

1 http://keplergo.arc.nasa.gov/ToolsUKIRT.shtml

of ± 3%, for both saturated and non-saturated targets, is reported based on the first 43 days of *Kepler* observations (Caldwell et al. 2010a). After a few more months of observations, Caldwell et al. (2010b) report that the non-linearity is possibly lower than 3%, but difficult to measure in-flight. The non-linearity we observe is about 1%, well within what could be expected based on these predictions, giving credibility to this explanation. One could turn this argument around and state that the *Kepler* instrument is *remarkably stable*. Indeed, the non-linearity observed is *only 1%* between seasons, and *essentially full linearity* is measured when observations for the same CCD are compared, even when those observations are years apart.

(iv) A final, albeit somewhat unlikely explanation, is that the effect is caused by a slightly different *color-dependence in the pixel response function (PRF)*. The PRFs for individual *Kepler* channels are available for download. We compared the 'average color' of the channels for FN Lyr, as this is known to scale with pulsation amplitude, and found no correlation between color and measured seasonal amplitude, further decreasing the viability of this explanation.

6.5 CONCLUSIONS

We investigated the transit depth of HAT-P-7b for different quarters and find a statistically significant seasonal trend. We have confirmed a similar trend to be present in the amplitude of FN Lyr and speculate this behavior of the *Kepler* data could be caused by instrumental artifacts or by unaccounted-for crowding in the *Kepler* field.

We find the impact on planetary radius measurements to be relatively small, because they scale with the square root of the transit depth: a difference in relative planetary radius of ± 1% is reported over different seasons. Nevertheless, these results cast doubt over the accuracy of transit depth measurements of *Kepler* targets, which are often reported at a higher precision than this and may be subject to the same systematic effects reported in this paper. Hot Jupiters are of particular concern, as their relative radii are sometimes reported with error bars that are an order of magnitude smaller than the systematic effect we observe in HAT-P-7 and FN Lyr. Apart from underestimating the error bars, we also point out that, in principle, the correct radius might not be the average of the seasonal measurements – they might all be affected by a certain degree of systematic error.

If these seasonal variations are indeed persistent throughout *Kepler* measurements, Hot Jupiters such as HAT-P-7b will make them most visible, as they have many deep transit events. When seeking to compare physical variations of transit depths over time (e.g. caused by planetary weather phenomena or variable atmospheres), it is therefore important to be very careful when

combining measurements throughout different *Kepler* quarters and seasons. However, planetary transits may be the ideal tool to calibrate and correct for these seasonal systematics.

We finally conclude that within seasons, the *Kepler* instrument is remarkably stable, even for observations that were made years apart.

We thank the anonymous referee for valuable comments, Douglas Caldwell, Mia Lundkvist, Mikkel N. Lund, Rasmus Handberg for help in retrieving relevant reference data, and Simon Albrecht and Jens Jessen-Hansen for valuable discussions. Funding for this Discovery mission is provided by NASAâs Science Mission Directorate. The authors wish to thank the entire Kepler team, without whom these results would not be possible. Funding for the Stellar Astrophysics Centre is provided by The Danish National Research Foundation (Grant agreement no.: DNRF106). The research is supported by the ASTERISK project (ASTERoseismic Investigations with SONG and Kepler) funded by the European Research Council (Grant agreement no.: 267864).

7

THE SPECTROSCOPIC FOLLOW-UP OF *K2* OBSERVATIONS

In this chapter I shift away from *Kepler* observations to search for planets using *K2* photometry. The *K2* mission makes use of the *Kepler* spacecraft, but has different observing properties because only two functioning reaction wheels remain (see Section 2.1). As a result, a range of instrumental effects make the quality of the data worse than for the *Kepler* mission, so that a more elaborate data reduction is required. In addition, unlike for *Kepler*, the task of finding and vetting planetary candidates lies exclusively with the community. I am part of an international *K2* collaboration which goes by the name ESPRINT. The first publication by the collaboration was published by Sanchis-Ojeda et al. (2015). In this chapter I present the results from a second publication (Van Eylen et al. 2015), which has been submitted to Astrophysical Journal at the time of writing.

To analyze *K2* observations, I have developed a publicly available code. This code can convert raw *K2* images into light curves by doing simple aperture photometry. In addition, center-of-light positions are measured over time and used to correct for photometric variations caused by movement of the spacecraft, which is crucial to achieve a high photometric accuracy. Finally, a search for transits is performed to discover interesting planetary candidates.

In the publication presented in this chapter, I focus on three systems which were observed in Campaign 1, which is the first scientific campaign of the *K2* mission. Ten such campaigns are planned, with data from the first four available at the time of writing. The transit properties of these planetary candidates were measured using my code, and the three systems were followed-up with a spectroscopic campaign using ground-based instruments, in an attempt to measure their masses to constrain their interior structure. To do so, observations from the FIES (Telting et al. 2014), HARPS-N (Cosentino et al. 2012) and HARPS (Mayor et al. 2003) spectrographs were obtained.

Constraining the mass allows for a measure of the bulk density of the planets. Such measurements are difficult to make for small planets due to the small radial velocity (RV) signal such planets induce on the host stars, but are important to help understand the internal composition of these planets (e.g. Rogers 2015). Only a few dozen small *Kepler* planets have measured masses (e.g. Marcy et al. 2014), because most *Kepler* host stars are faint. Here, the *K2* mission is expected to make a significant contribution, as well as the upcoming transit survey missions TESS (Ricker et al. 2014) and PLATO (Rauer et al. 2014). This chapter is taken from Van Eylen et al. (2015) and is adapted only for formatting.

The K2-ESPRINT Project II: Spectroscopic follow-up of three exoplanet systems from Campaign 1 of K2

Vincent Van Eylen, Grzegorz Nowak, Simon Albrecht, Enric Palle, Ignasi Ribas, Hans Bruntt, Manuel Perger, Davide Gandolfi, Teriyuki Hirano, Roberto Sanchis-Ojeda, Amanda Kiilerich, Jorge P. Arranz, Mariona Badenas, Fei Dai, Hans J. Deeg, Eike W. Guenther, Pilar Montañés-Rodríguez, Norio Narita, Leslie A. Rogers, Víctor J. S. Béjar, Tushar S. Shrotriya, Joshua N. Winn. *Submitted to Astrophysical Journal on 10 September 2015.*

We report on Doppler observations of three transiting planet candidates that were detected during Campaign 1 of the K2 mission. The Doppler observations were conducted with FIES, HARPS-N and HARPS. EPIC 201295312b is smaller than Neptune with an orbital period of 5.66 days, radius $2.69^{+0.24}_{-0.21}$ $R_\oplus$ and mass $4.4^{+7.4}_{-7.3}$ $M_\oplus$, giving a mean density of $1.2^{+2.2}_{-2.0}$ g cm^{-3}. EPIC 201546283b is a warm Neptune orbiting its host star in 6.77 days and has a radius of $4.48^{+0.33}_{-0.33}$ $R_\oplus$ and a mass of $28.5^{+7.2}_{-7.2}$ $M_\oplus$, which leads to a mean density of $1.72^{+0.67}_{-0.52}$ g cm^{-3}. EPIC 201577035b is smaller than Neptune orbiting its host star in 19.3 days, with radius $3.98^{+0.34}_{-0.34}$ $R_\oplus$, mass 21^{+17}_{-16} $M_\oplus$ and mean density $1.8^{+1.7}_{-1.4}$ g cm^{-3}. These measurements join the relatively small collection of planets smaller than Neptune with measured masses and radii. Our code for performing K2 photometry and detecting planetary transits is now publicly available.

7.1 INTRODUCTION

Although data from the K2 mission (Howell et al. 2014) has only been available for six months, it has already led to several notable exoplanet discoveries. For example, a sub-Neptune orbiting a bright star (using only the 9 days of Engineering Test Data Vanderburg et al. 2015), three super-Earths orbiting a bright M dwarf star (Crossfield et al. 2015), a disintegrating rocky planet with a cometary head and tail (Sanchis-Ojeda et al. 2015), two super-Earth planets orbiting a nearby cool star (Petigura et al. 2015) and two additional planets orbiting the known hot Jupiter host star WASP-47 (Becker et al. 2015). Based on the Campaign 1 photometry, the first lists of planetary candidates have been produced (Foreman-Mackey et al. 2015; Montet et al. 2015).

As part of the *Equipo de Seguimiento de Planetas Rocosos INterpretando sus Tránsitos* (ESPRINT) project (see Sanchis-Ojeda et al. 2015), we present our radial velocity follow-up measurements of three Campaign 1 planet candidates (EPIC 201295312, EPIC 201546283, and EPIC 201577035), making use of the FIES (Telting et al. 2014), HARPS-N (Cosentino et al. 2012) and HARPS

(Mayor et al. 2003) spectrographs. Measurements of masses for planets smaller than $4-5$ $R_\oplus$ are notoriously difficult (Marcy et al. 2014), but are of importance to constrain interior models for sub-Neptune planets (e.g. Rogers 2015).

In the next section we present our analysis pipeline for K2 photometry, including aperture photometry, light curve detrending and planet search algorithms (the Python code used for the analysis is publicly available on GitHub[1]). We describe the planet characterization via spectroscopic observations in Section 7.3, and discuss the results in Section 12.5.

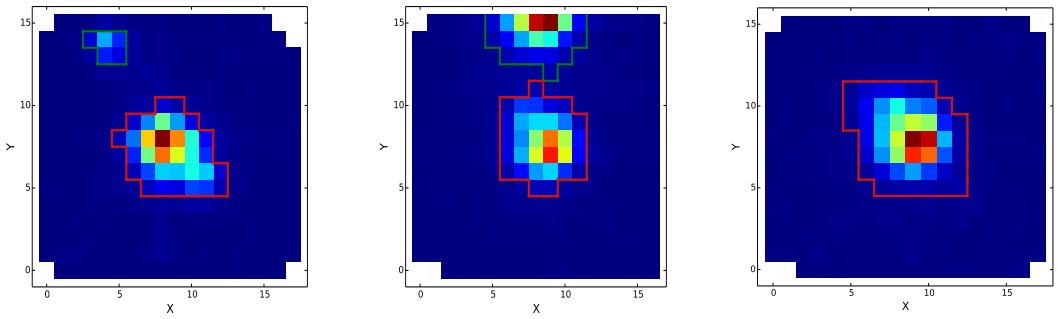

Figure 14 – Pixel masks for EPIC 201295312 (left), EPIC 201546283 (middle) and EPIC 201577035 (right). The colors indicate the electron count, going from red (high) to low (blue). Pixel masks above a threshold electron count are encircled. We use red for those pixels included in the light curve and green for those assumed to be caused by other stars.

7.2 PHOTOMETRY

Unlike for the primary *Kepler* mission, K2 photometry is primarily delivered in the form of pixel files without mission-defined aperture masks, and the task of finding planet candidates rests upon the community rather than upon the mission team. Because the mission operates with only two functioning reaction wheels (Howell et al. 2014) the pointing stability is more limited, which affects the photometric precision. Correction methods make use of the center-of-light offset (Vanderburg and Johnson 2014; Lund et al. 2015) or use trends which are common to many stars (Foreman-Mackey et al. 2015; Angus et al. 2015).

We have developed a photometry pipeline consisting of the following independent modules: (1) Extract aperture photometry; (2) Perform light curve detrending; and (3) Search for transits and perform time-domain transit modeling. We describe these steps in the next sections.

1 https://github.com/vincentvaneylen

Our analysis starts from K2 pixel mask files which can be downloaded from the MAST archive[2]. We perform simple aperture photometry on these pixel masks. First we sum the flux per pixel over the full time series of the K2 campaign. Subsequently, the median flux over the different pixels is calculated. As long as the field is not too crowded the median flux is a fairly good estimate of the background flux. The stellar flux can then be identified as the flux that exceeds the background flux by some predetermined threshold (typically $1.05 \times$ median). We include the pixels exceeding the threshold and group them according to whether they are spatially adjacent. If two or more spatially disjoint groups are detected, the largest pixel group is selected (the other, smaller groups are assumed to be caused by other stars and are ignored). The results are shown in Figure 14 for the three stars discussed in this work. Once the aperture is selected in this way, for each time step the total flux is calculated by summing the flux of all pixels in the aperture, and the flux centroid position is calculated based on the flux-weighted mean X and Y coordinates of the group of pixels. We also subtract the background flux, which is estimated as the median of the pixels after iteratively clipping all 3σ outliers.

For the light curve detrending, we use a linear fit to the centroid positions, a technique first used successfully for *Spitzer* transit observations (e.g. Désert et al. 2009; Van Eylen et al. 2014; Désert et al. 2015), and which is similar to techniques developed for K2 photometry by others (Vanderburg and Johnson 2014; Lund et al. 2015; Sanchis-Ojeda et al. 2015). In summary, the light curve is divided into chunks of specified length (typically 300 data points), and a polynomial function of centroid position and time is fitted to the flux in each chunk. More precisely, for centroid coordinates X_c and Y_c (calculated relative to the mean centroid position), time T, and flux F, we fit the model M:

$$\begin{aligned} M = t_0 + t_1 T + t_2 T^2 + t_3 T^3 + x_1 X_c + x_2 X_c^2 + x_3 X_c^3 \\ + y_1 Y_c + y_2 Y_c^2 + y_3 Y_c^3 + z_1 X_c Y_c, \end{aligned}$$

where t_i, x_i, y_i and z_1 are fitting parameters. For each chunk, the light curve flux is then divided by the model to remove variability caused by spacecraft pointing variations (which cause flux variations due to different pixel sensitivities) as well as long-term astrophysical variations. We have compared this technique with the ones employed by Sanchis-Ojeda et al. (2015) and Vanderburg and Johnson (2014), and found the light curve quality and the transit parameters to be similar.

To search for transit events we subsequently run a "box least square" search on the light curves (Kovács et al. 2002), which detects periodic transit-like

2 See https://archive.stsci.edu/k2/data_search/search.php

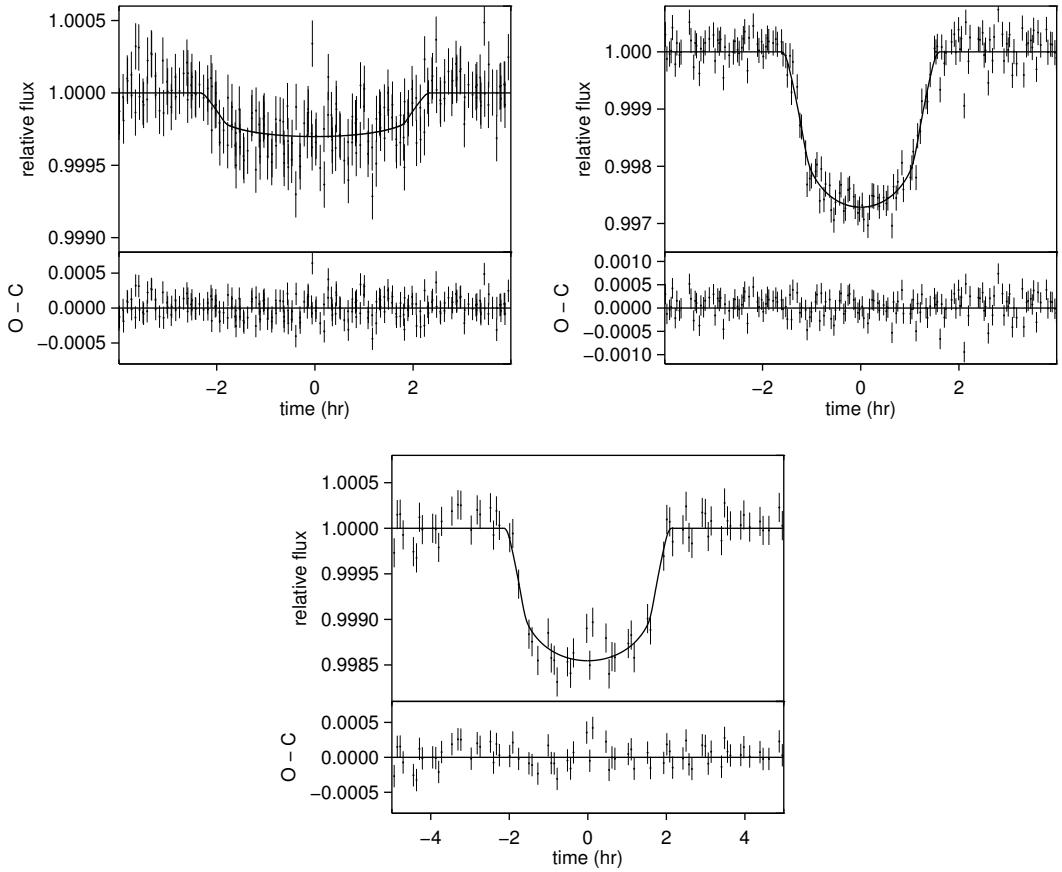

Figure 15 – K2 reduced photometry folded by the best period for EPIC 201295312 (top left), EPIC 201546283 (top right) and EPIC 201577035 (bottom). The best fitted model is shown with a solid line as well as the residuals after subtracting the model.

events[3]. These are then visually inspected in order to check if they are indeed transit-shaped.

7.3 GROUND BASED FOLLOW-UP OBSERVATIONS

Based on an initial analysis of the light curves and ground based imaging, interesting planets were selected for spectroscopic follow-up. Bright planet candidates were observed using the FastCam (FC) lucky imaging camera at the 1.5-m Carlos Sanchez Telescope (TCS) in Tenerife. All images were bias subtracted and then shifted and co-added using FC specific software to produce a final, high SNR, high resolution image. Objects that appeared to be isolated, were then moved forward in the confirmation process to be observed with FIES. We obtained observations (45-60 minute exposures) with the FIES spectrograph for a first detailed stellar characterization and a small number of Radial Velocities (RVs). Systems which show RV scatter less than $20\,\mathrm{m\,s^{-1}}$ are

3 We used an implementation of this algorithm in Python by Ruth Angus and Dan Foreman-Mackey; see https://github.com/dfm/python-bls.

selected for further observations. For Campaign 1, these efforts were focused on EPIC 201295312, EPIC 201546283, and EPIC 201577035.

These systems were recently discussed by Montet et al. (2015). EPIC 201577035 was validated as a genuine planet (also called K2-10b in the NASA Exoplanet Archive[4]), but high-resolution Adaptive Optics images conducted by these authors revealed faint stellar companions for EPIC 201295312 and EPIC 201546283, at distances of 3 and 8 arcsec respectively. This complicates the planet validation because K2 apertures span many pixels (see Figure 14; each pixel measures 3.98×3.98 arcsec). Therefore it can be difficult to be certain that the target star is truly the host of the transiting planet candidate. Consequentially, Montet et al. (2015) were unable to validate the planetary candidates (despite assigning false positive probabilities below 10^{-4} in both cases).

To derive stellar parameters, to measure stellar reflex motion and finally to determine the planetary mass we observed these three systems throughout Spring 2015 with the HARPS-N spectrograph mounted on the TNG on La Palma and the HARPS spectrograph on ESO's 3.6m telescope at La Silla. The exposure times varied between 15 min and 45 min for the different systems and instruments, and we used standard setups. All RVs for the three systems are available in electronic form from the ApJ webpage.

Before modeling the RVs we co-added the available spectra for each system to derive the stellar atmospheric parameters using the VWA software[5] used by Bruntt et al. (2012). With the $T_{\rm eff}$, log g and [Fe/H] as input, we used BaSTI evolution tracks[6] to infer the stellar mass and radius, using the SHOTGUN method (Stello et al. 2009). The parameters obtained this way are consistent with parameters from spectra obtained with HDS at Subaru using a different code (see Takeda et al. 2002; Hirano et al. 2012), with the exception of the radius of EPIC 201295312 (the HDS radius is 1.91 ± 0.11 $R_\odot$, the VWA value adopted is 1.52 ± 0.10 $R_\odot$), possibly due to the use of different isochrones.

We measured RVs using the standard data reduction pipelines for the HARPS and HARPS-N spectrographs. For the case of FIES we used the approach described in Gandolfi et al. (2015). We modeled the K2 light curves together with the RVs obtained from the FIES, HARPS-N, and HARPS spectrographs. For this we use the transit model by Mandel and Agol (2002) and a simple Keplerian RV model. The model parameters mainly constrained by photometry (see Figure 15) include the orbital Period (P), a particular time of mid-transit ($T_{\rm min}$), the stellar radius in units of the orbital semi-major axis ($R_\star/a$), the planetary radius in units of the stellar radius ($R_p/R_\star$), and the cosine of the orbital incli-

4 http://exoplanetarchive.ipac.caltech.edu/
5 https://sites.google.com/site/vikingpowersoftware/home
6 http://albione.oa-teramo.inaf.it/

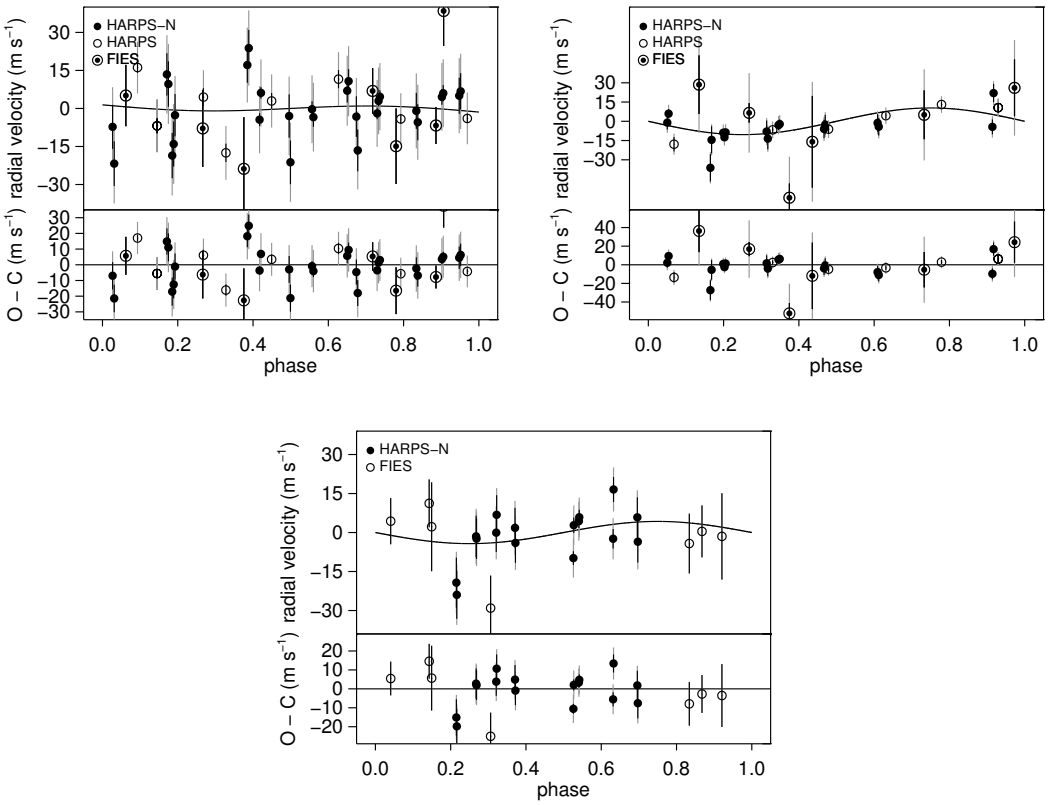

Figure 16 – RV observations (folded by the period) for EPIC 201295312 (top left), EPIC 201546283 (top right) and EPIC 201577035 (bottom). The best fitted model is shown with a solid line as well as the residuals after subtracting the model. The internal RV uncertainties are indicated by the black error bars, while the gray error bars include an additional "stellar jitter" term as explained in the text.

nation ($\cos i_o$). We further assumed quadratic limb-darkening and the parameters u_1 and u_2 were selected from the tables provided by Claret et al. (2013) appropriate for the Kepler bandpass. We placed a Gaussian prior on $u_1 + u_2$ with a width of 0.1. The difference $u_1 - u_2$ was held fixed at the tabulated value, since this combination is weakly constrained by the data. Given the difficulty of constraining the orbital eccentricity from limited datasets such as ours, we provisionally assume the orbits to be circular. This is consistent with what was done by a similar, larger study by Marcy et al. (2014), who found no evidence warranting the inclusion of eccentricity as a free parameter in a study following up 42 transiting *Kepler* candidates with Keck/HIRES. This assumption allows us to use the stellar density derived from the spectra modeling (Table 7) as prior information (see e.g. Van Eylen and Albrecht 2015). We also assumed a linear ephemeris in all three systems as we could detect no sign of significant Transit Timing Variations.

The Keplerian RV model (see Figure 16) introduces additional parameters; the semi-amplitude of the projected stellar reflex motion ($K_\star$), and systemic velocities which were determined as an additive offset for each spectrograph ($\gamma_{\rm spec}$).

We used a Markov Chain Monte Carlo (MCMC) algorithm (see, e.g., Tegmark et al. 2004) to estimate the uncertainty intervals. Before starting the MCMC chain we added "stellar jitter" to the internally estimated uncertainties for HARPS and HARPS-N observations, set by the requirement that the minimum reduced χ^2 value is equal to unity (for FIES observations, no such term was needed).

In Table 7 we report the results derived from the posterior, quoting uncertainties excluding 15.85 % of all values at both extremes, encompassing 68.3 % of the total probability. The key result is $K_\star$, which together with the orbital period, inclination, and stellar mass determines planetary mass and bulk density.

7.4 RESULTS

7.4.1 *EPIC 201295312*

EPIC 201295312b has an orbital period of 5.66 days. We constrain the mass to $4.4^{+7.4}_{-7.3}$ $M_\oplus$ and measure a radius of $2.69^{+0.24}_{-0.21}$ $R_\oplus$, resulting in a planet density of $1.2^{+2.2}_{-2.0}$ g cm^{-3}. We note that our measurement allows for a negative (unphysical) mass, which is necessarily to avoid positively biasing mass measurements for small planets. While this can easily be avoided using a prior that prohibits the unphysical mass regime, it is important not to do so because the negative masses are a statistically important measurement of the planetary mass (see e.g. Marcy et al. 2014, for a detailed discussion). Allowing negative masses accounts naturally for the uncertainty in planet mass due to RV errors, and is key to allow unbiased constraints the interior structure based on a sample of small planets (see e.g. Rogers 2015). A one-sided 95% confidence interval places the $K_\star$ amplitude at 5.5 m s^{-1}, corresponding to a mass upper limit of 16.6 $M_\oplus$. All parameters are available in Table 7. The location of EPIC 201295312b on a planetary mass-radius diagram is indicated in Figure 17.

We note that EPIC 201295312, a subgiant star, has a relatively high stellar jitter (see Table 7). In addition, our HARPS-N observations for this star were clustered around two epochs, each consisting of 1-2 weeks of observations but separated by over a month. There is an effective offset between the two sets of observations of $\approx$ 20 m s^{-1}. We allowed for a linear drift which we find

Parameter	EPIC 201295312	EPIC 201546283	EPIC 201577035
	Basic properties		
2MASS ID	11360278-0231150	11260363+0113505	11282927+0141264
Right Ascension	11 36 02.790	11 26 03.638	11 28 29.269
Declination	-02 31 15.17	+01 13 50.66	+01 41 26.29
Magnitude (*Kepler*)	12.13	12.43	12.30
	Stellar parameters from spectroscopy		
Effective Temperature, $T_{\rm eff}$ (K)	5830 ± 70	5320 ± 70	5620 ± 70
Surface gravity, log g (cgs)	4.04 ± 0.08	4.60 ± 0.08	4.50 ± 0.08
Metallicity, [Fe/H]	0.13 ± 0.07	0.14 ± 0.07	-0.07 ± 0.07
Microturbulence ($\mathrm{km\,s^{-1}}$)	1.2 ± 0.07	0.8 ± 0.07	0.9 ± 0.07
Projected rotation speed, $v \sin i_\star$ ($\mathrm{km\,s^{-1}}$)	5 ± 1	1 ± 1	3 ± 1
Assumed Macroturbulence, ζ ($\mathrm{km\,s^{-1}}$)		2	
Stellar Mass, M_p ($M_\odot$)	1.13 ± 0.07	0.89 ± 0.05	0.92 ± 0.05
Stellar Radius, R_p ($R_\odot$)	1.52 ± 0.10	0.85 ± 0.06	0.98 ± 0.08
Stellar Density, $\rho_\star$ ($\mathrm{g\,cm^{-3}}$)[a]	0.45 ± 0.14	2.04 ± 0.38	1.38 ± 0.34
	Fitting prior parameters		
Limb darkening prior $u_1 + u_2$	0.6752 ± 0.1	0.7009 ± 0.1	0.6876 ± 0.1
Stellar jitter term HARPS ($\mathrm{m\,s^{-1}}$)	10.5	6	—
Stellar jitter term HARPS-N ($\mathrm{m\,s^{-1}}$)	6.5	6	7
Stellar jitter term FIES ($\mathrm{m\,s^{-1}}$)	20	30	5
	Adjusted Parameters from RV and transit fit		
Orbital Period, P (days)	5.65639 ± 0.00075	6.77135 ± 0.00015	19.3044 ± 0.0012
Time of mid-transit, $T_{\rm min}$ (BJD$-$2450000)	6811.7191 ± 0.0049	6812.8451 ± 0.0010	6819.5814 ± 0.0021
Cosine orbital inclination, $\cos i_o$	$0.051^{+0.035}_{-0.029}$	$0.0286^{+0.0079}_{-0.0076}$	$0.0233^{+0.0045}_{-0.0038}$
Scaled Stellar Radius, $R_\star/a$	$0.111^{+0.020}_{-0.009}$	$0.0583^{+0.0042}_{-0.0032}$	$0.0338^{+0.0032}_{-0.0025}$
Fractional Planetary Radius, $R_p/R_\star$	$0.01617^{+0.00089}_{-0.00068}$	$0.0483^{+0.0011}_{-0.0011}$	$0.03717^{+0.00096}_{-0.00090}$
Linear combination limb darkening parameters (prior & transit fit), $u_1 + u_2$,	0.667 ± 0.098	0.667 ± 0.083	0.609 ± 0.091
Stellar Density (prior & transit fit), $\rho_\star$ ($\mathrm{g\,cm^{-3}}$)	$0.44^{+0.13}_{-0.17}$	$2.09^{+0.38}_{-0.39}$	$1.32^{+0.33}_{-0.31}$
Stellar radial velocity amplitude, $K_\star$ ($\mathrm{m\,s^{-1}}$)	$1.5^{+2.4}_{-2.4}$ [(b)]	$10.4^{+2.6}_{-2.6}$	$5.3^{+4.1}_{-4.2}$
Systemic velocity HARPS-N, $\gamma_{\rm HARPS-N}$ ($\mathrm{km\,s^{-1}}$)	44.552 ± 0.002	-37.772 ± 0.002	8.202 ± 0.003
Systemic velocity HARPS, $\gamma_{\rm HARPS}$ ($\mathrm{km\,s^{-1}}$)	44.450 ± 0.008	-37.776 ± 0.003	—
Systemic velocity FIES, $\gamma_{\rm FIES}$ ($\mathrm{km\,s^{-1}}$)	44.456 ± 0.009	-37.979 ± 0.015	8.063 ± 0.004
	Indirectly Derived Parameters		
Impact parameter, b	$0.47^{+0.20}_{-0.25}$	$0.49^{+0.09}_{-0.11}$	$0.689^{+0.063}_{-0.070}$
Planetary Mass, M_p ($M_\oplus$)[c]	$4.4^{+7.4}_{-7.3}$	$28.5^{+7.2}_{-7.2}$	21^{+17}_{-16}

Planetary Radius, R_p ($R_\oplus$)[c]	$2.69^{+0.24}_{-0.21}$	$4.48^{+0.33}_{-0.33}$	$3.98^{+0.34}_{-0.34}$
Planetary Density, ρ_p (g cm^{-3})	$1.2^{+2.2}_{-2.0}$	$1.72^{+0.67}_{-0.52}$	$1.8^{+1.7}_{-1.4}$

NOTES —

[a] This value is used as a prior during the fitting procedure.

[b] This value is derived including a linear offset (see Section 7.4.1 for details).

[c] Adopting an Earth radius of 6371 km and mass of $5.9736 \cdot 10^{24}$ kg.

Table 7 – System parameters.

to be 0.50 ± 0.10 m s^{-1} d^{-1}, and which may be caused by the gravitational influence of an additional body with a longer orbital period. We further note that there is a difference in systemic velocity of 102 m s^{-1} between the HARPS and HARPS-N observations which are separated by about 40 days. If the systemic velocity for HARPS and HARPS-N was set equal, the linear drift would become a curvature trend instead. If we would not allow for any drift, we instead find a $K_\star$ amplitude of 6.2 ± 3.0 m s^{-1} which would correspond to a planet mass of 18.7 ± 9.2 $mathrmM_\oplus$.

7.4.2 *EPIC 201546283*

For EPIC 201546283b, which has an orbital period P of 6.77 days, we obtain a 3σ mass detection of $28.5^{+7.2}_{-7.1}$ $M_\oplus$. This confirms the planetary nature of this candidate. Earlier work detected the transits of this candidate but was unable to confirm the planetary nature on statistical grounds (Montet et al. 2015). We find a planetary radius of $4.48^{+0.33}_{-0.33}$ $R_\oplus$, which taken together with the mass measurement leads to a planet density of $1.72^{+0.67}_{-0.52}$ g cm^{-3}. This makes this planet rather similar to Neptune (which has a density of 1.64 g cm^{-3}). As for EPIC 201295312 we allowed for the presence of a linear drift but found that it did not significantly change the results, and therefore we set it to zero. All parameters for this star and its planet are available in Table 7. The planet is plotted on a mass-radius diagram in Figure 17.

7.4.3 *EPIC 201577035*

EPIC 201577035b (K2-10b) was previously validated to be a true planet by Montet et al. (2015). Here we refine the stellar and planetary parameters and measure the planet's mass. The planet is smaller than Neptune with an orbital period of 19.3 days and a radius of $3.98^{+0.34}_{-0.34}$ $R_\oplus$. We measure its mass to be 21^{+17}_{-16} $M_\oplus$, resulting in a planetary density of $1.8^{+1.7}_{-1.4}$ g cm^{-3}. We found no evidence for a linear drift and set it to zero in the final fit. We note that, due to uncooperative weather, the coverage of this system shows a significant phase gap (see Figure 16). All parameters are listed in Table 7, and the system is indicated on a mass-radius diagram in Figure 17.

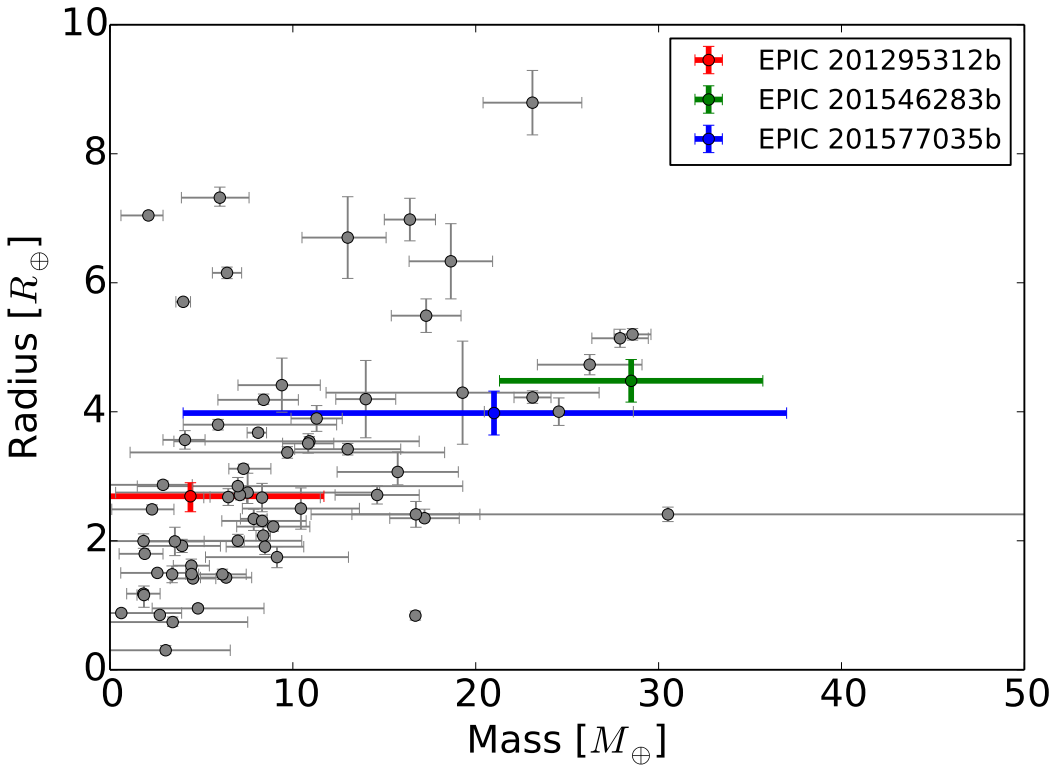

Figure 17 – Mass-radius diagram for transiting exoplanets smaller than 10 $R_\oplus$ and less massive than 50 $M_\oplus$ with masses measured from RV observations (data from exoplanets.org) and TTVs. Our new measurements are indicated.

7.5 DISCUSSION

We have reported our results for three planet candidates observed with K2 during Campaign 1. These planets have been found in the K2 data using two different algorithms and were also discussed by Montet et al. (2015). We measured the mass for the largest of these planets (EPIC 201546283b) and obtain lower significance measurements of the masses and densities of the other two systems (EPIC 201295312b and EPIC 201577035b). The first of these planets is similar to Neptune, while the other two are smaller than Neptune. Relatively few mass measurements are available for sub-Neptunes due to the small RV amplitudes these planets cause. For example, an extensive Keck campaign following up on 22 *Kepler* stars with known transiting planets recently lead to 16 secure mass detections (Marcy et al. 2014) and 26 more marginal measurements or upper limits. Despite thousands of planetary candidates found by the primary *Kepler* mission, many of those are too faint for follow-up measurements. Here, K2 has the potential to make a significant contribution, and our findings for Campaign 1 are encouraging for the yield of the next 11 campaigns of K2 observations. Finally, the significant effort required to measure masses for the planets highlights the need for future missions such as TESS

(Ricker et al. 2014) and PLATO (Rauer et al. 2014) which will observe even brighter stars.

We are grateful for the Python implementation of a BLS algorithm by Ruth Angus and Dan Foreman-Mackey. We are thankful to the GAPS consortium, which kindly agreed to exchange time with us, and the KEST team which shared observations. Based on observations made with the NOT and TNG telescopes operated on the island of La Palma in the Observatorio del Roque de Los Muchachos of the Instituto de Astrofísica de Canarias. Funding for the Stellar Astrophysics Centre is provided by The Danish National Research Foundation (Grant agreement no.: DNRF106). The research is supported by the ASTERISK project (ASTERoseismic Investigations with SONG and Kepler) funded by the European Research Council (Grant agreement no.: 267864). We acknowledge ASK for covering travels in relation to this publication. This research has made use of the Exoplanet Orbit Database and the Exoplanet Data Explorer at exoplanets.org. This work was performed [in part] under contract with the Jet Propulsion Laboratory (JPL) funded by NASA through the Sagan Fellowship Program executed by the NASA Exoplanet Science Institute. I.R. and M.P. acknowledge support from the Spanish Ministry of Economy and Competitiveness (MINECO) and the Fondo Europeo de Desarrollo Regional (FEDER) through grants ESP2013-48391-C4-1-R and ESP2014-57495-C2-2-R. N.N. acknowledges supports by the NAOJ Fellowship, Inoue Science Research Award, and Grant-in-Aid for Scientific Research (A) (JSPS KAKENHI Grant Number 25247026). T.H. is supported by Japan Society for Promotion of Science (JSPS) Fellowship for Research (No.25-3183). L.A.R. gratefully acknowledges support provided by NASA through Hubble Fellowship grant #HF-51313 awarded by the Space Telescope Science Institute, which is operated by the Association of Universities for Research in Astronomy, Inc., for NASA, under contract NAS 5-26555. HD acknowledges support by grant AYA2012-39346-C02-02 of the Spanish Secretary of State for R&D&i (MICINN).

Part II

EXOPLANET DYNAMICS

"We do not ask for what useful purpose the birds do sing, for song is their pleasure since they were created for singing. Similarly, we ought not to ask why the human mind troubles to fathom the secrets of the heavens. The diversity of the phenomena of nature is so great and the treasures hidden in the heavens so rich precisely in order that the human mind shall never be lacking in fresh nourishment."

– Johannes Kepler

8 EXOPLANETS AND THE SOLAR SYSTEM

In the second part of the thesis, I discuss the dynamics of exoplanet systems. Are orbits of planets circular or very elliptical? In multi-planet systems, do all planets orbit in the same plane, and is the rotation of the star aligned with the orbital plane? These are the kind of questions we set out to answer in the subsequent chapters, while this chapter serves as a brief introduction to this topic.

Studying dynamics is important to understand planet formation and evolution. Historically, planet formation theory was constrained by $n = 1$ star-planet systems, i.e. the solar system. After the discovery of the first exoplanets, there were some surprising findings that could not be explained by the theories at the time. Because massive, large exoplanets were discovered earlier, most of the work on exoplanet dynamics has been done for systems with giant, Jupiter-size or -mass planets. In this thesis, I present some of new insights in the dynamics of small exoplanets. As we shall see, these systems may better resemble the solar system than their larger counterparts.

8.1 THE SOLAR SYSTEM

The solar system is sometimes said to be "pancake-flat" because the planets all orbit in nearly the same plane. The planet's mutual alignment is not perfect, but holds to within a few degrees. The angle between the Sun's rotation and the plane of the planet's orbits is called the solar obliquity, a concept which is illustrated in Figure 18. For the solar system, the obliquity is low: the solar rotation axis is aligned with the normal of the Earth's orbital plane to within 7.2° (e.g. Beck and Giles 2005).

The alignment between the Sun's rotation axis and the mutual alignment between the orbits of the solar system planets is not a coincidence. This is thought to date back to the formation of the solar system. The Sun and the planets formed from material which collapsed into a rotating disk. The rotation axis of the Sun and the orbital axes of the planets can be traced back to the angular momentum vector of the disk of material out of which the stars and planets formed. This idea, sometimes called the nebular hypothesis, dates back to Kant (1755) and Laplace (1796).

Eccentricity determines whether an orbit is circular or elliptical (see Figure 19), and is measured on a scale from 0 to 1 where 0 indicates perfect circularity. The orbits of the eight solar system planets have low eccentricities, i.e. they are nearly circular. The Earth has an almost perfectly circular orbit,

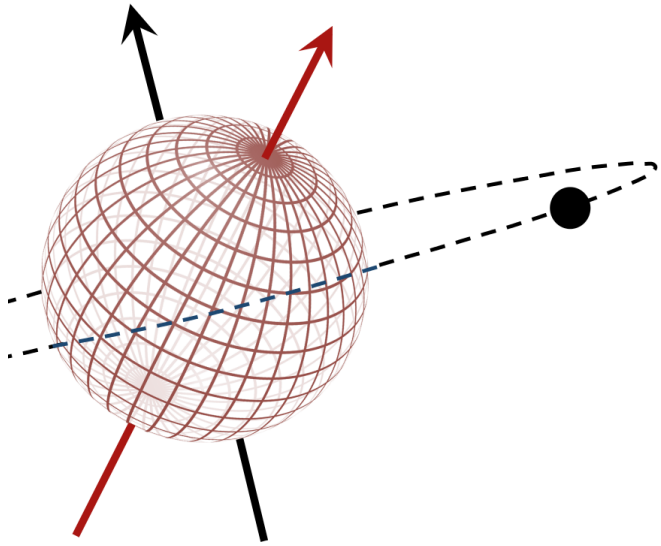

Figure 18 – The stellar obliquity refers to the angle between the stellar rotation axis (in red) and the angular momentum vector of the planet's orbit (in black). When this angle is small, such as for the solar system, we say that a system is well-aligned. When the obliquity is large, we speak of misalignment. Figure courtesy by Josh Winn.

with an eccentricity of only 0.0167. The most eccentric planet in the solar system is Mercury, with an eccentricity of 0.206. The mean eccentricity of all solar system planets is 0.0601.

The dwarf planets have slightly higher eccentricities. Ceres, Makemake and Haumea are less eccentric than Mercury, while Pluto (0.249) and Eris (0.442) have higher eccentricities. The mean eccentricity of all five currently recognized dwarf planets is 0.224. The solar system also contains many moons orbiting the (dwarf) planets. The largest of these all have nearly circular orbits, for instance, the Earth's moon has an eccentricity of 0.0549.

Finally, the solar system contains a large amount of so-called "small solar-system bodies", such as comets and asteroids. While asteroids, many of which are orbiting in the belt between Mars and Jupiter, often have relatively low eccentricities, the picture outlined above does not hold for most comets. These objects can have very high eccentricities, periodically taking them to great distance from the Sun and bringing them very near at other times. In addition, they do not follow the 'pancake structure', with often high inclinations relative to the plane of the planets.

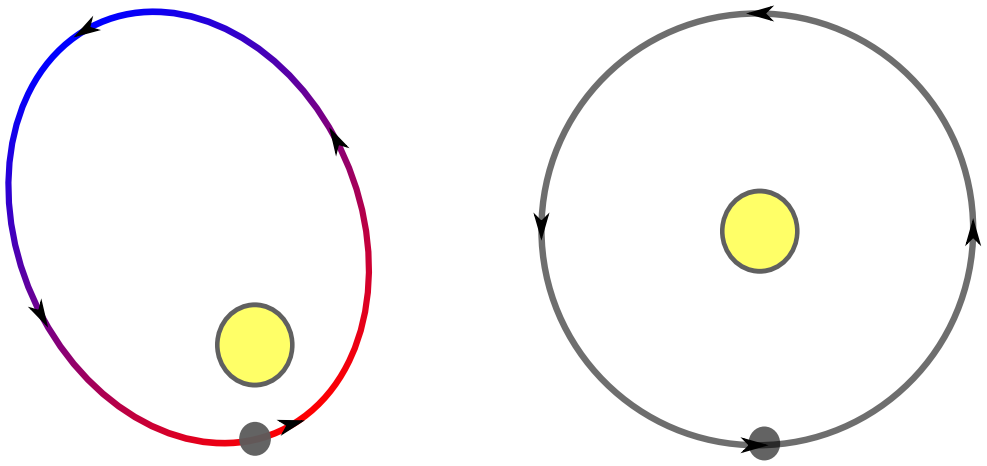

Figure 19 – Illustration of a planet (grey) in orbit around a star (yellow). On the left, an eccentric orbit is shown. In the red part of the orbit, the star-planet separation is low and the planet moves faster than in the slower (blue) part of the orbit. On the right, a circular orbit is shown, where the star-planet distance is always the same and the planet has a constant orbital velocity.

8.2 LARGE EXOPLANETS

For exoplanets, obliquity and eccentricity measurement have sometimes resulted in surprising findings. Historically, most such measurements have been done for large exoplanets, which is the topic of this section. Obliquity is discussed in Section 8.2.1, eccentricity in Section 8.2.2. In Section 8.3 I attempt to interpret these findings and explain the need for measurements of smaller exoplanets.

8.2.1 *Obliquity: the star-planet (mis)alignment*

Measuring obliquities in exoplanet systems is not straightforward. For planets detected only by the radial velocity of the host star, the inclination angle of the orbit is unknown. For transiting planets the situation is better: the orbital inclination is close to 90° and even the exact angle can often be determined from the transit shape (see Section 2.2).

Unfortunately the orientation of the stellar rotation axis is difficult to measure, as nearly all stars are point sources for even the largest telescopes. Nevertheless, there are a few different methods to obtain some information of the stellar rotation axis. The rotation period of a star can sometimes be determined from photometry, when spots rotate in and out of view and cause a semi-periodic variation in the brightness of the star which can be observed over time. Similarly, the projected rotation speed, $v \sin i$, can be determined from spectroscopic observations of a star. Here, v is the rotational velocity

and i the stellar inclination angle, given as the angle from the stellar angular momentum vector to the line-of-sight. This can be observed because rotation causes a broadening of the spectral lines: opposite parts of the star rotate at different (opposite) radial velocities, and the resulting variable Doppler shifts broaden spectral lines.

The main method through which obliquities for exoplanet systems have been determined is known as the Rossiter-McLaughlin effect (Rossiter 1924; McLaughlin 1924), and makes use of spectroscopic distortion of stellar absorption lines during planetary transits. If the orbital and stellar rotation axes are aligned (i.e. the star has a low obliquity), the planet will first cross the part of the star which is blue-shifted because this part is rotating towards the observer. This distorts the spectral lines of the star, as this blue-shifted star light is blocked while the red-shifted light remains fully visible. As the planet continues its transit, the situation reverses, and by the end of the transit the planet is blocking the red-shifted light, coming from the part of the star moving away from the observer. This is illustrated in Figure 20.

By measuring the spectrum of the star over time during transit, one can thus observe if the blue-shifted part is blocked before the red-shifted part, which is indicative of a low obliquity. If this is not the case, misalignment can be detected, for example, in the most extreme case of a retrograde orbit, the most red-shifted area of the star is occulted first and the most blue-shifted part last. The method constrains only the obliquity projected in the plane of the sky, and naturally favors fast-rotating stars (high $v \sin i$), which have the broadest lines so that the distortion is the easiest to detect. Furthermore, Rossiter-McLaughlin measurements are easier for large planets, because they block a larger fraction of light leading to larger distortions.

The method, which was originally used to measure obliquities in eclipsing binaries, was first successfully applied to the exoplanet HD 209458b (Queloz et al. 2000). Subsequently it has been successfully applied to many hot Jupiter planets. A wide range of obliquities has been found, including very well-aligned systems, e.g. HD 189733b (Winn et al. 2006), as well as significantly misaligned systems, e.g. XO-3b (Hébrard et al. 2008; Winn et al. 2009c), HD 80606b (Moutou et al. 2009; Pont et al. 2009; Winn et al. 2009a), and WASP-7b (Albrecht et al. 2012a). Even retrograde systems in which the star appears to spin in the opposite direction compared to the orbit of the planet have been found, e.g. WASP-17b (Triaud et al. 2010) and HAT-P-7b (Winn et al. 2009b).

8.2.2 *Eccentricity: circular and elliptical orbits*

The eccentricity of exoplanets can be dramatically different from the orbits in the solar system which are almost circular. The most straightforward and

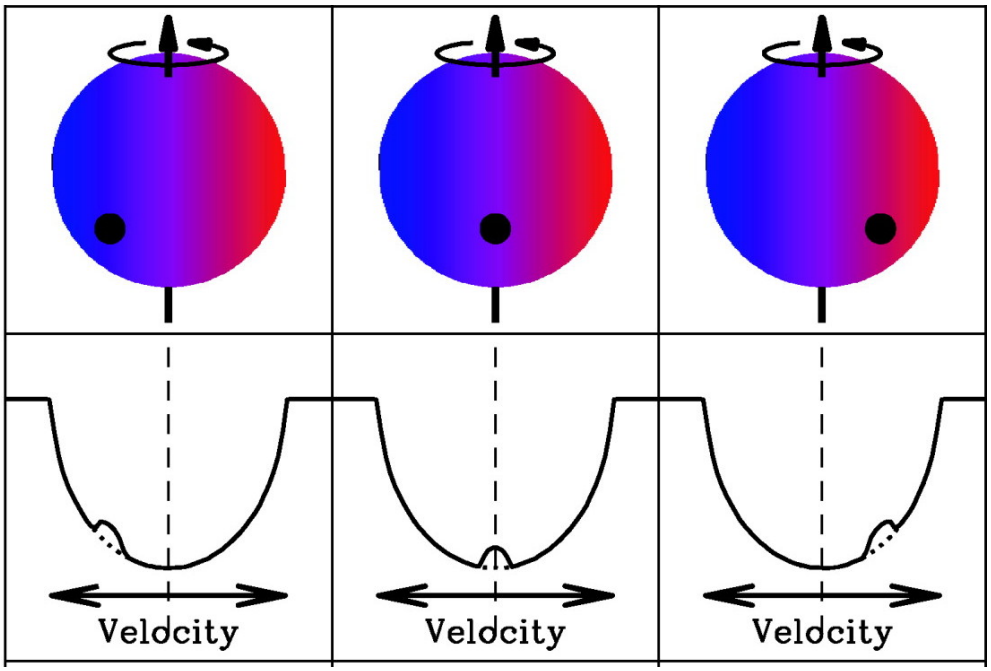

Figure 20 – Illustration of the Rossiter-McLaughlin effect. When a planet which is aligned with the stellar rotation transits the star, it first blocks blue-shifted light and later red-shifted light (top), causing a distortion in the spectral lines (bottom). A different projected obliquity causes a different sequence of distortion. Figure adapted from Gaudi and Winn (2007).

most common way of measuring an exoplanet's eccentricity is through the radial velocity (RV) method. As a planet orbits its star, the star moves around the common center of mass. For circular orbits, the planet's orbit has a constant velocity and the RV signal of the star describes a sinusoid in time. For eccentric orbits, the planet has a higher velocity when close to the star, and orbits slower at a distant part of its orbit. The same is true for the star, and the RV signal is no longer sinusoidal.

Since RV measurements allow an observer to follow the movement of the star at any time during the orbit, data with a high enough time sampling and of high enough quality can in principle measure the eccentricity and orientation (defined by the angle of periastron ω) of any planet. In practice, RV measurements are limited to more massive planets, since the RV amplitude caused by small planets is too low to be detected with current instrumentation (see Equation 2.7).

In Figure 21 the eccentricities for exoplanets measured from RV observations are shown. The difference with the eight solar system planets is striking, with exoplanets spanning the full range of eccentricities.

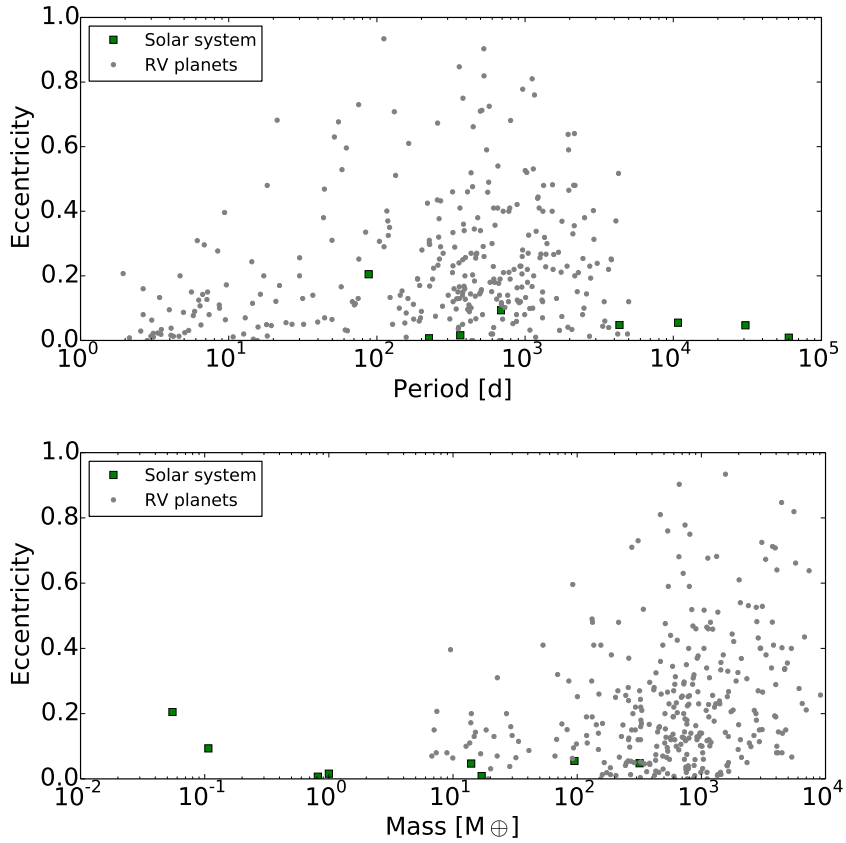

Figure 21 – The eccentricity of exoplanets (taken from exoplanets.org) is shown together with the eight solar system planets. *Left:* Planets as a function of period. *Right:* planets as a function of mass, highlighting the lack of observed eccentricities for exoplanets on the low mass end.

8.3 WHY WE NEED TO OBSERVE DYNAMICS OF SMALL PLANETS

The high variety of obliquities and eccentricities for exoplanets is strikingly different to the seemingly more 'well-behaved' solar system. These findings have inspired a body of theoretical work attempting to provide an explanation in the context of planet formation.

To explain the observed obliquities, very broadly there are two categories of models. A first set of theories assumes that star formation is a chaotic process in which high obliquities naturally occur, and that the stellar rotation axis and the axis of the disc in which planets form can be strongly misaligned (e.g. Bate et al. 2010; Fielding et al. 2015). In the same category there are theories in which the stellar spin axis can become misaligned with the circumstellar disc due to magnetic effects (e.g. Lai et al. 2011). Finally, binary companions may have an influence on the spin axis of the star (e.g. Batygin 2012; Storch et al. 2014).

The second category of explanations assumes it is the planet's orbital plane which has changed, rather than the inclination of the disc out of which it has formed. This is not unreasonable, because many of the Rossiter-McLaughlin measurements are for hot Jupiter planets, which orbit very close to their stars and are not believed to have formed at the orbital distances where they are observed at. Here, obliquities can be the result of planet-planet scattering, a process in which planets interact and may migrate from the location at which they were formed (e.g. Rasio and Ford 1996; Chatterjee et al. 2008). Another way in which hot Jupiters may be misaligned is if their migration is caused by what is known as Kozai-Lidov cycles (Kozai 1962; Lidov 1962), where an outer companion on an inclined orbit perturbs the orbit of the inner body and causes cyclic changes in the orbital inclination and eccentricity (e.g. Mazeh et al. 1997; Fabrycky and Tremaine 2007; Naoz et al. 2011).

Distinguishing between those two broad categories is complicated because measurements of obliquities through the Rossiter-McLaughlin effect are more difficult for smaller planets. Knowledge of the obliquity of systems with (multiple) small planets would help distinguish between those two general scenarios – this is the topic of Chapter 9. I discuss alternative methods of measuring obliquities for small planets, and show the great potential asteroseismology has for doing this. Asteroseismic obliquity measurements are presented and discussed, with a focus on the Kepler-410 system.

A similar situation occurs for observations of exoplanet eccentricities. The most common method, RV observations, is more difficult to use for small planets because small planets cause only a small stellar RV signal. This is evident in Figure 21: eccentricity, a fundamental orbital parameter, is largely unknown for small exoplanets. Making use of transiting planets, and the duration of these transits in combination with stellar properties derived from asteroseismology, I begin to complete Figure 21 on the lower-mass end. Because there may be differences between multi-planet systems and single-planet systems, this work is split over two chapters. In Chapter 10, I present the eccentricity distribution of 74 planets orbiting 28 *Kepler* stars. In Chapter 11, I present the first results of an analysis of the eccentricity of single-planet systems in *Kepler*, which is complicated by the fact that not all such systems are validated or confirmed as genuine planets.

With Rossiter-McLaughlin obliquity measurements of a few dozens of stars, a pattern has emerged in which hot Jupiters orbiting stars with temperatures below 6000-6300 K mostly have low obliquities, while a much broader range of obliquities is observed for hotter stars. This trend is often attributed to the stellar structure (e.g. Winn et al. 2010a; Albrecht et al. 2012b; Dawson 2014), since cool stars have convective outer layers, which favors efficient dissipation of tidal energy, and thereby faster tidal alignment and circularization. To test

this, I look at binary stars. I attempt to reproduce this difference between hot and cool stars, by looking at the orbital eccentricities of *Kepler* eclipsing binaries. If tidal effects are stronger for cool stars than for hot stars, we expect to see a difference in the eccentricities of these two categories of stars. I have analyzed and interpreted the eccentricity of 816 *Kepler* eclipsing binaries and present the results in Chapter 12.

9 STAR-PLANET (MIS)ALIGNMENT

Obliquity measurements for stars with exoplanets have revealed aligned systems, but also many misaligned planet host stars. As explained in Chapter 8, most of the measurements have made use of the Rossiter-McLaughlin effect, which is easier to measure for large planets so that most obliquity measurements are for hot Jupiter systems. This is unfortunate because measurements of obliquities in systems with small planets would help differentiate between planet formation and evolution theories explaining the observation.

Here, asteroseismology turns out to be a great tool. The observed frequencies of stellar oscillations are affected by rotation – in the absence of rotation, modes of different azimuthal order have the same frequency, while with rotation they are split into multiplets (e.g. a triplet or quintuplet, depending on the angular degree of the mode). The fine structure thereby revealed is directly related to the rotation rate of a star. Crucially, for an observer, the relative amplitude of the modes in a multiplet depends on the stellar inclination angle. Therefore, asteroseismology can in principle be used to infer the inclination angle of stars, independent of any planetary properties – this method can even be applied when no planets are present. When the inclination is measured for a star with a transiting planet, the obliquity of the system is constrained. The details of the method are presented in Section 9.1.

Because of stringest requirements on the quality of the data, the method has not yet been widely used. Arguably the best case is that of the bright star Kepler-410A. The obliquity measurement of this system is presented in Section 9.2.1 and was first published in Van Eylen et al. (2014). Other asteroseismic obliquity studies in which I was involved include HAT-P-7 (Lund et al. 2014b) and a statistical study of a sample of *Kepler* planet host stars (Campante et al. 2015b). They are described in Section 9.2.2.

These findings can be taken together with a handful of obliquity measurements for systems with small planets, using other methods. We can then compare the obliquity distribution of small multi-planet systems with that of hot Jupiter systems, and the solar system. Section 9.3 does precisely this and provides an outlook to the future by asking the question: is alignment an emerging trend for small planets in multi-planet systems?

9.1 HOST STAR INCLINATIONS FROM ASTEROSEISMOLOGY

We make use of stellar pulsations to measure the stellar inclination. For more details on the basics of asteroseismology we refer the reader to Section 2.3. It is the *rotational splitting* of solar-like oscillations which provides information on the stellar inclination and the rotation rate. In short, the technique to measure inclinations goes as follows:

1. Observe a star which exhibits solar-like oscillations in a short cadence sampling (e.g. for *Kepler*, a one minute observing cadence), for a sufficiently long time span;
2. Make a power spectrum of the oscillations;
3. Extract frequencies from the power spectrum and compare them to stellar models to determine stellar parameters;
4. Look at smaller effects in the frequencies, which cause the $\ell \neq 0$ (e.g. $\ell = 1$ and $\ell = 2$) modes, where ℓ indicates the number of surface nodal lines, to be split due to stellar rotation, and use these splittings to determine the rotation rate and inclination of the star.

The first three steps are relatively straightforward when high quality photometry (e.g. from *Kepler*) is available, and have been used to measure the stellar properties of hundreds of exoplanet host stars (see e.g. Huber et al. 2013b; Silva Aguirre et al. 2015). The final step is much more difficult because the rotation only causes a smaller effect on the frequencies, for the relatively slow rotation we are interested in here. In practice only a handful of precise measurements have been made so far for exoplanet host stars, all of them using *Kepler* observations, and the technique holds promise for one or two dozen others (see Section 9.2).

I now provide some more details about step 4. As described in Section 2.3, stellar oscillations can be represented by their quantum numbers (n, ℓ, m). The azimuthal order m takes values between $-\ell$ and ℓ, but the frequencies of the oscillation modes with different m-values are degenerate in the absence of rotation. For a rotating star, the degeneracy is lifted such that a frequency $\nu_{n\ell m}$ is given by (Ledoux 1951):

$$\nu_{nlm} = \nu_{nl} + m\Omega(1 - C_{nl}), \tag{9.1}$$

where Ω is the angular velocity and the equation assumes rigid rotation. The factor $m\Omega$ is known as the kinematic splitting and is seen by an observer who is not in a frame that is co-rotating with the star. The factor C_{nl} provides a correction due to the Coriolis force, but this value is typically small (for p

modes in slowly rotating stars). The equation is only true to first order, but holds well for slowly rotating stars (such as the Sun). For faster rotating stars second-order effects have to be taken into account, for example, those due to the centrifugal force which induces distortion.

From Equation 9.1 it can be seen that $\ell = 1$ oscillation modes are split into triplets (with $m = -1, 0, 1$), while $\ell = 2$ modes are split into quintuplets ($m = -2, 1, 0, 1, 2$). Higher degree modes are split into higher order multiplets, but in practice modes with $\ell > 2$ cannot generally be observed with *Kepler* (see Lund et al. 2014a). Equation 9.1 can be used directly to estimate the stellar rotation rate from the frequency splitting.

To determine the inclination angle of a star from its splittings, we turn to the amplitude of the split modes. We assume energy equipartition between modes with different azimuthal order, i.e. we assume modes with different m-values are excited and damped in the same way. This assumption holds well for the Sun and for slowly rotating stars, but may not be valid for faster rotating stars.

Under the equipartition assumption, all frequencies in a multiplet should intrinsically have the same amplitude. However, for an observer these amplitudes may not all look the same. This is due to cancellation effects, as only the disk-integrated flux variation is observed. For $\ell = 1$, the relative visibility of a mode with angular degree ℓ ($\mathcal{E}_{\ell,m}$), is given by

$$\mathcal{E}_{1,0} = \cos^2 i, \qquad \mathcal{E}_{1,\pm1} = \frac{1}{2}\sin^2 i, \tag{9.2}$$

where i is the stellar inclination. For $\ell = 2$, the relative visibilities are

$$\mathcal{E}_{2,0} = \frac{1}{4}(3\cos^2 i - 1)^2, \quad \mathcal{E}_{2,\pm1} = \frac{3}{8}\sin^2(2i), \quad \mathcal{E}_{2,\pm2} = \frac{3}{8}\sin^4 i. \tag{9.3}$$

We refer to Gizon and Solanki (2003) for details and a derivation of these formulae. From Equation 9.2 and 9.3 it can be seen that the relative (observed) amplitudes of the different m components of a rotationally split mode depend on the inclination angle of the star.

In practice, the values for $\mathcal{E}_{\ell,m}$ are fitted for (via i) together with a range of other parameters. The amplitudes of modes with different ℓ values are different themselves, and due to the stochastic nature of stellar oscillations they do not have a single frequency but describe a Lorentzian profile instead. A background, 'noise' contribution has to be taken into account. All the relevant variables are described in Equation 4.3 (Section 4.2.2) and are usually fitted together in an MCMC algorithm to fully map the posterior parameter space and correlations between parameters.

Nevertheless, it is useful to develop some intuition. The separation between different m-values is a proxy for the rotation rate of the star, while the relative amplitude of the m-components can be used to constrain the inclination of the star. The stochastic nature of oscillations, and the resulting Lorentzian profile of a single mode of oscillation, complicates this measurement because the splittings are typically small, i.e. of the order of several μHz. This explains why for many stars it is possible to detect oscillations and model the basic stellar properties, but not determine the inclination and rotation. For the latter, the highest quality photometry is needed, and typically years of observations are required.

Once the stellar inclination is measured, this information can be used to constrain the obliquity of the star. It is important to note that the inclination of the star measured through asteroseismology only describes the inclination projected to the plane of the sky ($i_\star$), while the inclination in the plane of the sky itself remains undetermined (see Figure 22). From an observer's point of view, it is the tilt of the star that is determined, which allows to answer questions like whether it is the star's equator or pole that is pointing towards the observer. However, the star's steering wheel rotation relative to the plane of the planet's orbit, i.e. the projected spin-orbit angle λ, is not observationally constrained. This 'steering wheel axis' is constrained by the Rossiter-McLaughlin effect, which cannot constrain the inclination relative to the plane of the sky. Asteroseismology and the Rossiter-McLaughlin effect together fully constrain the orientation of a star, while one or the other method gives useful partial information. To determine the obliquity (ψ), one further needs to know the orbital inclination of the planet (i_p), but for transiting planets this value is typically well-determined (and in any case close to 90°). The different angles are illustrated in Figure 22 and relate to each other as (Winn et al. 2005):

$$\cos\psi = \sin i_\star \cos\lambda \sin i_p + \cos i_\star \cos i_p. \tag{9.4}$$

9.2 RESULTS

Accurate asteroseismic obliquity measurements have only been made in a handful of cases over the past few years. In Section 9.2.1 I discuss the obliquity measurement of Kepler-410, arguably the best case to measure asteroseismic splittings that can be found in *Kepler* observations. Prior to its publication by Van Eylen et al. (2014), asteroseismic obliquities had only been measured for Kepler-50 and Kepler-65 (Chaplin et al. 2013) and for Kepler-56 (Huber et al. 2013a). In Section 9.2.2 other asteroseismic obliquity results are presented, centered mostly around my involvement in the study of HAT-P-7 (Lund et al. 2014b) and an ensemble study of the best *Kepler* planet host stars (Campante et al. 2015b).

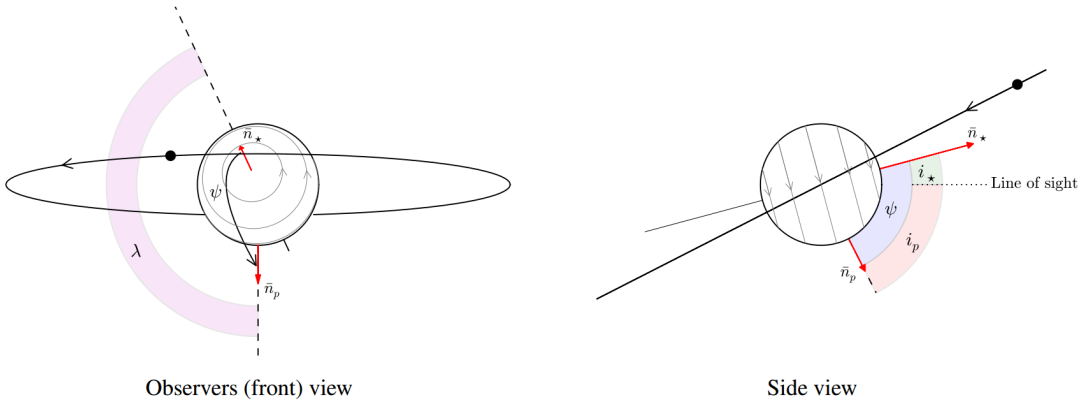

Figure 22 – Illustration of the angles relevant to measuring obliquities. The angle λ measures the projected obliquity (left), while the angle $i_\star$ measures the inclination of the star relative to the plane of the sky (right). On the right, for ease of drawing $\lambda = 180°$, so that i_p and $i_\star$ fall in the same plane. Finally i_p is the inclination of the orbital plane of the planet, which is always close to 90° for transiting planets. Figure courtesy by Lund et al. (2014b).

9.2.1 *The case of Kepler-410*

Kepler-410 is a bright *Kepler* planet host star which has been observed in short-cadence for nearly the entire four years of the *Kepler* mission. This makes it an excellent target for asteroseismic and other studies. The system consists of two distant companion stars, the brightest of which is host to a Neptune-sized transiting planet (Kepler-410A b), and one or more additional planets as revealed through transit timing variations. I refer to Chapter 4 for a detailed description of the star, including a general asteroseismic characterization, as well as the planet validation which made use of *Spitzer* follow-up observations, and to Van Eylen et al. (2014) for the original publication of the results described in this section.

Due to the brightness of the star and the long baseline of observations, Kepler-410 has the clearest rotational splitting signal of all currently known *Kepler* planet host stars. The splittings of individual modes are in several cases visible by eye in the power spectrum of the star. The power spectrum, which was already shown in Figure 9, is repeated in Figure 23, zoomed in on specific oscillation modes. On the left part of the zoom, an $\ell = 1$ triplet is visible, on the right side, an $\ell = 2$ quintuplet and an $\ell = 0$ mode are present (close to each other). The $\ell = 1$ and $\ell = 2$ modes show clear evidence of rotational splitting. From the relative amplitudes of the split components and their separations, the stellar rotation period and inclination can be determined as explained in Section 9.1. Even without any detailed modeling, it can be seen from Figure 23 that the inclination is necessarily close to 90°, because for the $\ell = 1$ triplet the central $m = 0$ mode is hardly visible while the $m = -1$ and $m = 1$ are clearly observed. From Equation 9.2 it then follows that $i_\star \approx 90°$.

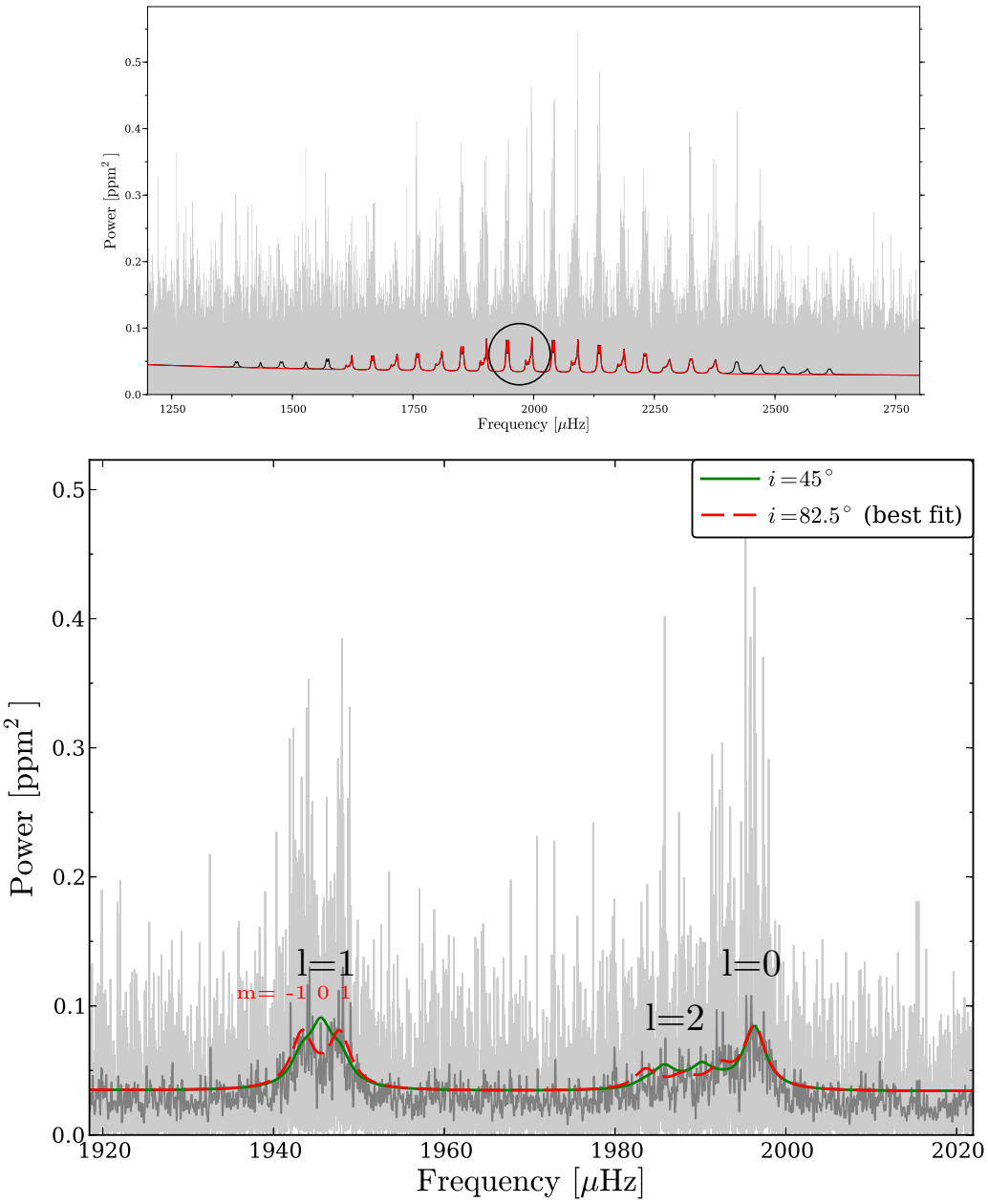

Figure 23 – Top: power spectrum of Kepler-410 (gray). Overlain are the model fits obtained from the MCMC peak-bagging. The black curve gives the model when including modes from the range 1370 – 2630 μHz - all mode frequencies in this range were included in the stellar modeling. The red curve gives the model obtained when excluding the five outermost modes obtained in the first fit (black curve) in each end of the frequency scale. From this fit we get the estimates of the stellar inclination and frequency splitting. In the bottom panel, we zoom in on one order. The dark gray shows the 0.1 μHz smoothed version of the power spectrum. Overlain is the model fit obtained from the MCMC peak-bagging (dashed red), in addition to the spectrum obtained when using an inclination angle of 45° (full green). Figure adapted from Van Eylen et al. (2014)

To illustrate this, a fit using an (arbitrary) stellar inclination of 45° is overplotted in Figure 23, as well as the best fit which has an inclination of 82.5°. The first scenario clearly does not represent the data well. The splitting is also observed for the $\ell = 2$ frequency shown in the figure. In practice, the same splitting is seen for multiple $\ell = 1$ and $\ell = 2$ modes in the power spectrum. To determine the best fitting inclination angle and rotation rate, a simultaneous fit to all $\ell = 1$ and $\ell = 2$ frequencies is made, using an MCMC algorithm, which is described in more detail in Section 4.2.1.

The probability density functions (PDFs) for the splitting and inclination angle which are the result of the MCMC analysis are shown in Figure 24, together with their correlation map. The PDF from the splitting can directly be related to the stellar rotation rate, using the radius of the star, and corresponds to a rotation rate of 5.25 ± 0.16 days. As predicted above, we find an inclination angle close to 90°, i.e. $i_\star = 82.5^{\circ+7.5}_{-2.5}$.

This implies a (nearly) equator-on view of the star. This result can be compared to the orbital inclination of the planet, which is found to be $i_p = 87.72 \pm 0.15°$. This result indicates a low obliquity, but it is important to be careful when interpreting this: as mentioned before, the measured stellar inclination, $i_\star$, gives the angle to the plane of the plane of the sky, while the orientation projected onto the plane of the sky, λ, is unconstrained (see Equation 9.4). Nevertheless, we find that, assuming a uniform distribution in stellar inclination angles, there is only a 17% chance of obtaining the measured inclination as we do - giving credibility to the low-obliquity scenario.

9.2.2 *Other asteroseismic inclination measurements*

An interesting case in which the obliquity could be constrained using asteroseismology is HAT-P-7. The system consists of a relatively bright star with a transiting hot Jupiter planet which was identified prior to the start of the *Kepler* mission (Pál et al. 2008). The system is very well-studied: it has been the subject of several asteroseismic investigations (e.g. Christensen-Dalsgaard et al. 2010; Van Eylen et al. 2012; Lund et al. 2015), there have been studies of the transits and the planet's orbital phase curve (e.g. Welsh et al. 2010; Van Eylen et al. 2013), the planet's atmosphere has been studied (Christiansen et al. 2010) and an associated companion star has been detected (Narita et al. 2012). Most relevant here is that this system has been the target of several Rossiter-McLaughlin studies, which have found a significant obliquity, with the hot Jupiter orbiting in a polar or retrograde orbit (Winn et al. 2009b; Narita et al. 2009; Albrecht et al. 2012b).

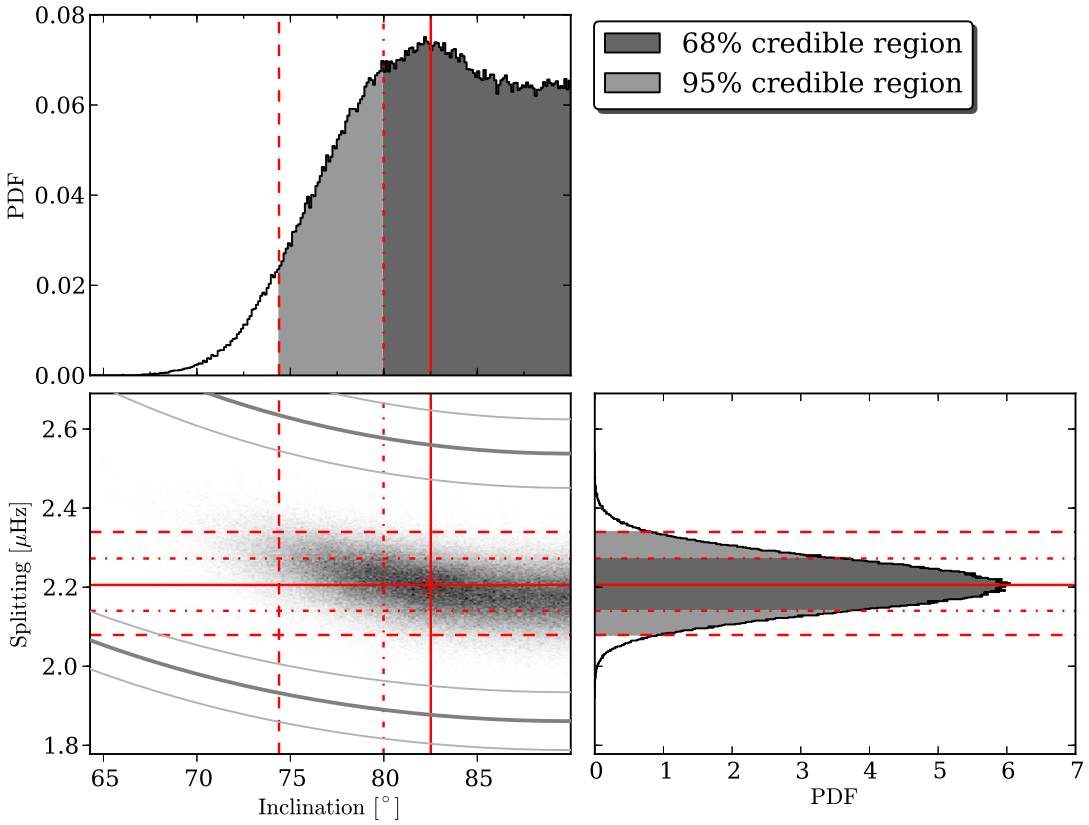

Figure 24 – Rotational splitting and inclination angle for Kepler-410 from an MCMC analysis (see also Section 4.2). The bottom left panel shows the correlation map between the inclination and the rotational splitting, while the panels above (inclination) and to the right (splitting) give the marginal probability density functions (PDFs) for these two parameters. Our estimates for the parameters are given by the median values of their respective PDFs, indicated by the solid lines. The 68% credible regions (found as the highest posterior density credible regions) are indicated by the dark gray part of the PDFs (bounded by dash-dotted lines), while the light gray indicates the additional part of the PDFs covered in a 95% credible regions (bounded by dashed lines). The PDF for the inclination was found after first having folded the part of the full distribution ($0-180°$) in the range $90-180°$ onto the part in the range $0-90°$. In the correlation map we have indicated the splitting as a function of inclination (dark gray), with associated uncertainty (light gray), corresponding to the values of $v\sin(i)$ estimated by Molenda-Żakowicz et al. (2013) (bottom lines) and Huber et al. (2013b) (top lines) and the radius estimate from our analysis. Figure courtesy by Van Eylen et al. (2014).

Using asteroseismic frequency splittings, the inclination angle of the star could be constrained to be $i_\star \leqslant 36.5°$ (Lund et al. 2014b). Although this is a relatively noisy measurement, it is nevertheless interesting because in combination with a determination of the projected obliquity ($\lambda = 155 \pm 37°$, Albrecht et al. 2012b), the true obliquity can be estimated and turns out to be $83° < \psi < 111°$. A simultaneous study of the same system by Benomar et al. (2014) found $i_\star = 33^{+34}_{-20}$, resulting in $\psi = 120^{+26°}_{-18}$. These results indicate the system is strongly misaligned, with the planet having an orbit which is close to polar, but which is more likely not retrograde. HAT-P-7 is one of only two

systems known to date for which both $i_\star$ and λ have been measured. The other system is Kepler-25, host to two planets, and was also studied by Benomar et al. (2014), who found it to be mildly misaligned ($\psi = 26.9^{\circ+7.0}_{-9.2}$).

The only other asteroseismic inclination measurements to date are for Kepler-50 and Kepler-65, both multi-planet systems which were found to be aligned (Chaplin et al. 2013), and Kepler-56 (Huber et al. 2013a). Kepler-56 is a red giant star which was found to be misaligned relative to its two transiting planets. It was found to have a companion in a wide orbit which may be responsible for the misalignment due to torque exerted by the companion. The reason why there are only a handful are the stringent requirements on the photometric quality. Nevertheless, Campante et al. (2015b) investigated if inclinations for any other *Kepler* planet host star could be measured using asteroseismology. Beyond the cases already known, the study finds only weak constraints could be placed on the inclination angle for other stars in the sample. A statistical analysis of the sample revealed that the inclination angles are not consistent with a random inclination (i.e. alignment occurs more often than random chance would suggest), but no significant difference between the multi-planet and single planet systems could be detected.

In the next section, I take the asteroseismic measurements together with obliquity measurements using other methods and attempt to interpret them in the context of planet formation.

9.3 ALIGNMENT: AN EMERGING TREND FOR SMALL PLANETS IN MULTI-PLANET SYSTEMS?

Because the Rossiter-McLaughlin effect is mostly sensitive to large planets, besides asteroseismology some other methods have been developed to measure the alignment for small planets. One technique makes use of star spots. Because spots rotate with the stellar surface, the repeated crossing of a planet over the same spot has been used to determine that the obliquity of Kepler-30 is smaller than 10° (Sanchis-Ojeda et al. 2012). The amplitude of the photometric variation due to spots can in principle also be used to make statistical statements about exoplanet host star's inclinations (Mazeh et al. 2015). Another method measures $\sin i$ by measuring $v \sin i$ (e.g. from spectroscopic measurements) and v (e.g. from photometric spot modulation and stellar properties), but the often significant uncertainties in $v \sin i$ can pose complications (e.g. Schlaufman 2010). This technique allowed Morton and Winn (2014) to make the statistical statement that multi-transiting planets appear to have lower obliquities than systems with only one known transiting planet. For the hot Jupiter Kepler-13, a light curve asymmetry indicates a high obliquity because the asymmetry is caused by the planet transiting over the gravity-darkened pole of the star (Barnes et al. 2011; Szabó et al. 2011), although a degeneracy

between limb darkening and gravity darkening may influence this result (Masuda 2015).

Even though the number of measurements is limited, we can begin to compare the obliquity distribution of systems with multiple small planets with that of hot Jupiter systems which typically have no other transiting planets. As discussed in Section 8.2.1, there has been a substantial number of hot Jupiters obliquity measurements through the Rossiter-McLaughlin effect, with about one in three of these planets showing significant misalignment (see e.g. Winn and Fabrycky 2015). For multi-planet systems, asteroseismology has provided measurements of Kepler-410 (discussed above, see also Van Eylen et al. 2014), Kepler-50 and Kepler-65 (Chaplin et al. 2013), Kepler-56 (Huber et al. 2013a) and Kepler-25 (Benomar et al. 2014). For Kepler-25 the projected obliquity has also been measured using the Rossiter-McLauhglin effect, and such a measurement also exists for Kepler-89 (Hirano et al. 2012; Albrecht et al. 2013). Finally there is the obliquity determination of Kepler-30 using spot-crossings (Sanchis-Ojeda et al. 2012). These measurements are summarized in Figure 25.

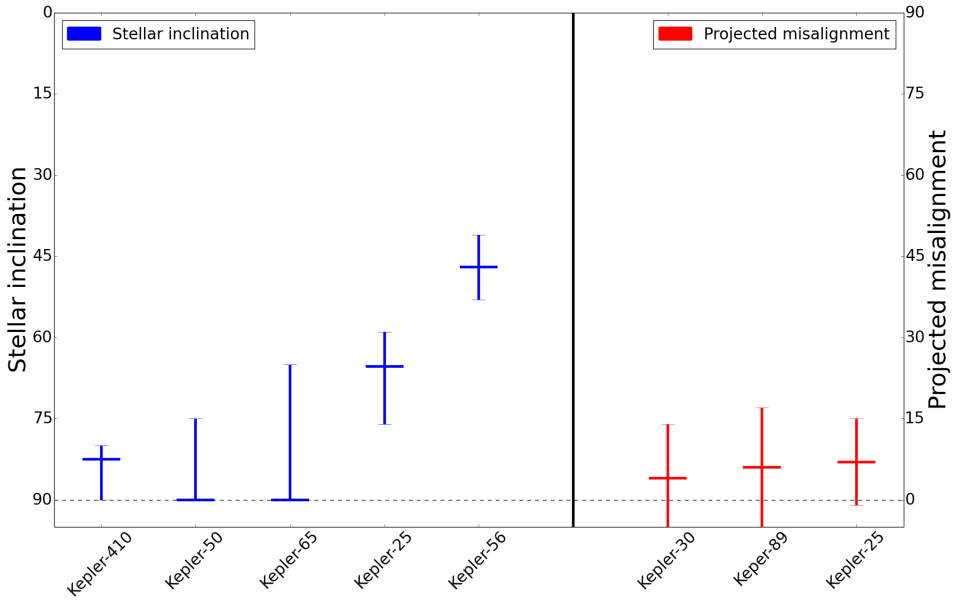

Figure 25 – Obliquity measurements of multi-planet systems to date. On the left hand side in blue are measurements using asteroseismology, which measures the stellar inclination angle, where 90° indicates consistency with alignment. On the right hand side are measurements of the projected obliquity λ, where 0° indicates alignment. Data points from Van Eylen et al. (2014); Chaplin et al. (2013); Benomar et al. (2014); Huber et al. (2013a); Sanchis-Ojeda et al. (2012); Albrecht et al. (2013) (see text for details).

Although the number of data points is limited, the current picture may suggest that alignment is more the norm for multi-planet systems than it is for hot Jupiter systems. Kepler-56 is clearly misaligned, but this misalignment may

be due to the companion which was detected (Huber et al. 2013a). According to Benomar et al. (2014), Kepler-25 may have mildly misaligned stellar inclination angle, but a reanalysis of this system by Campante et al. (2015b) slightly shifts the measurement, so that it is consistent with alignment. The other observations of multi-planet systems are currently consistent with alignment. The statistical study by Morton and Winn (2014) also provides some evidence that multi-planet systems are more likely to be aligned than single-planet systems, consistent with what was seen earlier by Albrecht et al. (2013) using Rossiter-McLaughlin measurements.

If this trends holds under the scrutiny of additional data points, this suggests that a primary path for the misalignment of many hot Jupiters may be orbital migration (e.g. Chatterjee et al. 2008). The misalignment of Kepler-56 may be explained by the influence of the companion through the Kozai-Lidov mechanism (e.g. Fabrycky and Tremaine 2007). If misalignment is a common outcome of planet formation itself (e.g. Bate et al. 2010), we expect to see a similar fraction of misaligned systems as compared to the hot Jupiter systems.

With only a small number of measurements at hand, it is clear that more data points are needed to settle this debate. From Figure 25, it is clear that asteroseismology has already made a key contribution. Unfortunately, the technique is unlikely to yield further results from the *Kepler* data set (Campante et al. 2015b). The upcoming TESS mission (Ricker et al. 2014) is unlikely to add a significant number of asteroseismic inclination measurements due to the short baseline of the observation, so that real progress may have to await the high-quality photometry from the PLATO mission planned for 2024 (Rauer et al. 2014).

10 ECCENTRICITY OF MULTI-PLANET SYSTEMS

In contrast to the solar system, eccentricities for exoplanets have revealed some very elliptical orbits, but unfortunately those measurements were mostly made for large planets because the RV signal they induce is larger than for small planets. In this chapter I make use of transit durations to measure the eccentricity of small transiting planets. The principle behind this method is that for a planet on a specific orbital period, the transit duration is influenced by eccentricity, stellar density, and transit impact parameter. An introduction to physics of transits can be found in Section 2.2.2 and some background on previous eccentricity measurements for exoplanets is provided in Section 8.2.2.

I select a sample for which the stellar density has been measured very accurately using asteroseismology. The mesaurement of transit durations and transit impact parameter turns out to be relatively complex, due to correlations between the parameters, and other aspects such as the unknown angle of periastron and the presence of transit timing variations (TTVs) complicate the measurement.

After addressing these issues, the eccentricity of a selected sample was measured. In this chapter, I focus on planets in multi-planet systems. The eccentricity for 74 planets orbiting 28 stars was measured and they turn out to have nearly circular orbits, which is in contrast to the larger planets with more elliptical orbits measured from RV observations.

The reason for focusing on multi-planet systems is that this sample nearly exclusively consists of confirmed planets. For single-planet systems, many planetary candidates are unconfirmed because such systems are harder to validate (see e.g. Lissauer et al. 2014; Rowe et al. 2014). The presence of potential false positives provides an additional complication, and an analysis of the sample of single-planet candidates is deferred to Chapter 11.

The results in this chapter were published by Van Eylen and Albrecht (2015) and are adapted here. The key results of the publication are adapted here only for formatting, but some results about using the same method to validate new planets were previously presented in Chapter 5, and are omitted here. In addition, Van Eylen and Albrecht (2015) contains an appendix presenting posterior distributions for all individual systems discussed in this work – this appendix is not included here.

Eccentricity from transit photometry: small planets in Kepler multi-planet systems have low eccentricities

Vincent Van Eylen and Simon Albrecht, *Astrophysical Journal 808:126, August 2015*

Solar system planets move on almost circular orbits. In strong contrast, many massive gas giant exoplanets travel on highly elliptical orbits, whereas the shape of the orbits of smaller, more terrestrial, exoplanets remained largely elusive. Knowing the eccentricity distribution in systems of small planets would be important as it holds information about the planet's formation and evolution, and influences its habitability. We make these measurements using photometry from the *Kepler* satellite and utilizing a method relying on Kepler's second law, which relates the duration of a planetary transit to its orbital eccentricity, if the stellar density is known. Our sample consists of 28 bright stars with precise asteroseismic density measurements. These stars host 74 planets with an average radius of 2.6 $R_\oplus$. We find that the eccentricity of planets in *Kepler* multi-planet systems is low and can be described by a Rayleigh distribution with $\sigma = 0.049 \pm 0.013$. This is in full agreement with solar system eccentricities, but in contrast to the eccentricity distributions previously derived for exoplanets from radial velocity studies. Our findings are helpful in identifying which planets are habitable because the location of the habitable zone depends on eccentricity, and to determine occurrence rates inferred for these planets because planets on circular orbits are less likely to transit. For measuring eccentricity it is crucial to detect and remove Transit Timing Variations (TTVs), and we present some previously unreported TTVs. Finally transit durations help distinguish between false positives and true planets and we use our measurements to confirm six new exoplanets.

10.1 INTRODUCTION

In the solar system, the orbit of Mercury has the highest ellipticity with an eccentricity (e) of 0.21, where an eccentricity of 0 indicates a circular orbit, whereas the mean orbital eccentricity of the other seven planets is 0.04. In contrast, Radial Velocity (RV) measurements revealed a wide range of eccentricities for gas giant planets (Butler et al. 2006), where HD 80606b is the current record holder with an eccentricity of 0.927 (Naef et al. 2001). RV surveys also found evidence that orbital eccentricities for sub-Jovian planets reach up to 0.45 (Wright et al. 2009; Mayor et al. 2011). For Earth-sized planets and Super-Earths, RV detections of eccentricities are typically not feasible, even with modern instruments, because of the small orbital RV signal

amplitude K (Marcy et al. 2014), and the fact that the amplitude of the eccentricity scales with $e \times K$ (see e.g. Lucy 2005). One alternative way to measure orbital eccentricities relies on the timing of secondary transits (eclipses), but this method is limited to the hottest and closest-in exoplanets. In some systems with multiple transiting planets Transit Timing Variations (TTVs) can be used to infer planetary mass ratios and orbital eccentricities. While these two parameters are often correlated, sometimes eccentricity information can nevertheless be inferred using statistical arguments (e.g. Lithwick et al. 2012; Wu and Lithwick 2013), or from the "chopping" effect (e.g. Deck and Agol 2015). Low-eccentricity as well as some higher eccentricity systems have been found (Hadden and Lithwick 2014). Unfortunately, TTVs are only detected in a subset of all transiting multiple systems, and the interpretations of the results is complex as systems with TTVs are typically found near resonances, and it's unclear if such systems have undergone the same evolution as systems without such resonances.

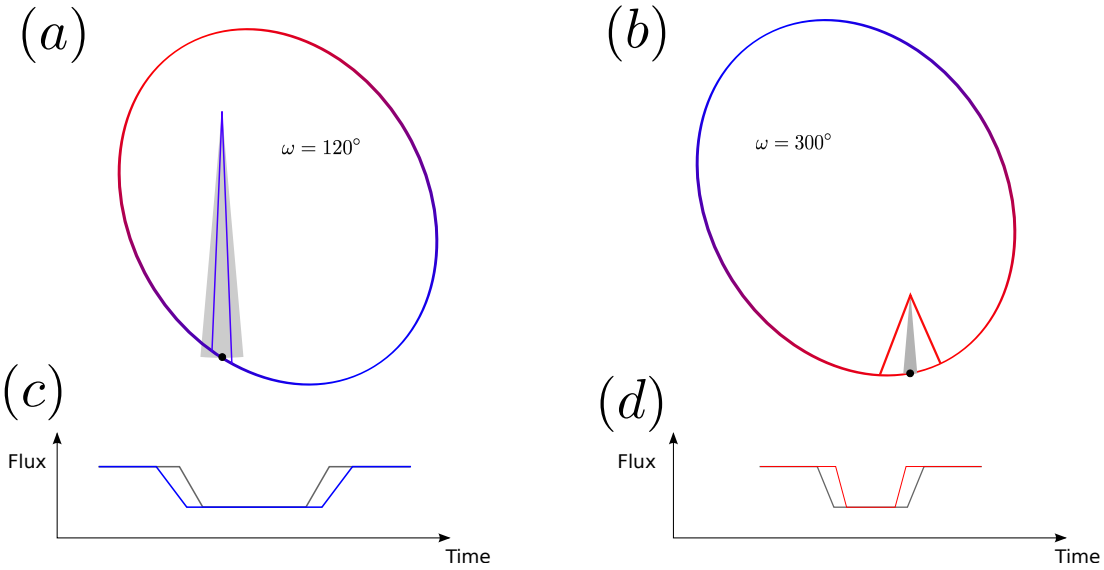

Figure 26 – The left top panel (a) pictures an orbit with $e = 0.6$ and an argument of periastron of 120°. The observer is located below the figure. Panel (b) shows the same orbit, now with $\omega = 300°$. The pies outlined with blue and red lines in the two panels encompass the same surface areas and the corresponding arcs are traveled by the planet during 1/36 of their orbital period. These times are centered around the time of planetary transit. The gray filled pies correspond to the surface areas covered by a planet traveling on a circular orbit with the same apparent $a/R_\star$ ratio. According to Kepler's second law the transit in the eccentric system in panel (a) lasts longer than in the system with the circular orbit. The reverse is true for panel (b). Corresponding schematic light curves are shown in panels (c) and (d).

Here we determine orbital eccentricities of planets making use of Kepler's second law, which states that eccentric planets vary their velocity throughout their orbit. This results in a different duration for their transits relative to the circular case: transits can last longer or shorter depending on the orientation of the orbit in its own plane, the argument of periastron (ω). This is illustrated

in Figure 26. Transit durations for circular orbits are governed by the mean stellar density (Seager and Mallén-Ornelas 2003). Therefore if the stellar density is known from an independent source then a comparison between these two values constrains the orbital eccentricity of a transiting planet independently of its mass (Ford et al. 2008; Tingley et al. 2011).

Using this technique, individual measurements of eccentric orbits were made successfully, making use of high-quality *Kepler* transit observations. For highly eccentric Jupiters, the technique is powerful even when only loose constraints on the 'true' stellar density are available, as shown for Kepler-419 (Dawson and Johnson 2012) and later confirmed by radial velocity observations (Dawson et al. 2014). Kipping et al. (2012) suggested that multiple planets in the same system can be compared to constrain the sum of eccentricities in cases where the stellar density is not known. For close-in hot Jupiters where the orbits are assumed to be circular due to tidal forces, the technique provides stellar densities which rival the accuracy provided by other methods such as asteroseismology, and good agreement is typically found (e.g. HAT-P-7b, Van Eylen et al. 2013). For Kepler-410b, a Super-Earth, a small but significantly non-zero eccentricity ($0.17^{+0.07}_{-0.06}$) was measured, thanks to an accurately determined stellar density from asteroseismology and the brightness of the star (*Kepler* magnitude 9.4, Van Eylen et al. 2014). The orbits of both Kepler-10b (1.4 $R_\oplus$) and Kepler-10c (2.4 $R_\oplus$) were found to be consistent with circularity (Fogtmann-Schulz et al. 2014).

An ensemble study, based on early *Kepler* catalog data and averaging over impact parameters, found the eccentricity distribution of large planet candidates ($\geqslant$ 8 $R_\oplus$) to be consistent with the RV eccentricity distribution, with some evidence that sub-Neptune planets had lower average eccentricities (Kane et al. 2012). However, subsequent ensemble studies have revealed a range of complications, such as a correlation with the transit impact parameter (Huber et al. 2013b), the influence of planetary false positives (Sliski and Kipping 2014) and uncertainties or biases in stellar parameters (Plavchan et al. 2014; Rowe et al. 2014). Price et al. (2015) recently investigated the feasibility of such studies for the smallest planets.[1] Kipping (2014a) identified a number of other mechanisms that influence transit durations, e.g. TTVs. We approach these complications in two ways.

Firstly, we design a data analysis pipeline that allows us to identify and remove TTVs, measure transit parameters and their correlations, and insert and recover artificial transits to test our methods. Secondly, we focus on a sample of 28 bright stars observed by *Kepler* (Borucki et al. 2010): the brightest host

1 We note that the authors made use of *Kepler* 30-minute integration time data in their study, while the data used in this work has a one-minute (short cadence) sampling, which complicates a direct comparison (see also Section 10.2.2.2).

star has a *Kepler* magnitude 8.7 and all but one are brighter than magnitude 13. They have all been observed in short-cadence mode with a one-minute integration time. Their mean stellar density is constrained through asteroseismology. The 17 brightest of these stars were analyzed in Silva Aguirre et al. (2015) and the average accuracy of their mean density measurements is 1.7%. The other 11 stars were previously modeled by Huber et al. (2013b) and the average uncertainty on the mean stellar density of these objects is 6.7%. All 28 stars also have separate mass and radius measurements, while the detailed modeling of individual frequencies by Silva Aguirre et al. (2015) also provides stellar ages with a median uncertainty of 14%. They all contain multiple planets (74 in total) and all but three contain confirmed planets. The planets are small with an average radius of 2.8 $R_\oplus$ and have orbital periods ranging from 0.8 to 180 days.

In Section 10.2 we describe our analysis methods. We present the pipeline developed to model the planetary transits and discuss several important parameter correlations. Our main results are presented in Section 10.3. We present the eccentricity distribution of our sample of planets, as well as homogeneous planetary parameters and several previously unreported transit timing variations. We also validate several previously unconfirmed exoplanets. In Section 12.5 we discuss the implications of our findings in the context of planetary habitability and planetary occurrence rates. Our conclusions are presented in Section 10.5.[2]

10.2 METHODS

We built a customary data reduction and analysis pipeline to measure all transit parameters and their correlations. This also allows us to do transit insertion and recovery tests. In Section 10.2.1 we describe the pipeline and how we extract the relevant parameters. In Section 10.2.2 we discuss parameter correlations. In Section 10.2.3, we present the results of modeling artificial transits that we inserted in the data.

10.2.1 *Pipeline*

The pipeline performed the following main steps:

1. *Kepler* data reduction and normalisation
2. Period determination and Transit Timing Variation (TTV) assessment; data folding

2 Note that an appendix describing individual systems and their posterior distributions in detail can be found in Van Eylen and Albrecht (2015).

3. MCMC transit fit module

We now describe each step in more detail.

10.2.1.1 *Data reduction*

The first part of our pipeline is responsible for reducing and normalising *Kepler* light curves. For a given *Kepler* object of interest (KOI), the pipeline searches for observations in any quarter (Q), between Qo-Q17. Only the quarters which contain short cadence observations are downloaded (in fits-file format), because the one minute sampling is required to resolve the planetary ingress and egress (see Section 10.2.2.2). Our analysis starts with the Presearch Data Conditioning (PDC) version of the data (Smith et al. 2012).

In the following, we only focus on data directly before, during or after the transits (typically encompassing about 5-10 hours before and 5-10 hours after a given transit). An initial estimate of the transit times is calculated with the ephemeris available at the *Kepler* database[3]. From the same source a value for the transit duration is obtained and used to determine the in-transit data points. By default the transit duration is increased by three hours to make sure no in-transit data points are erroneously used for the data normalisation. In case of (previously known or subsequently detected) TTVs, the transit duration is further increased to catch all in-transit data points. The data before and after the transits are then fitted by a second order polynomial which is used to normalise the data.

In a final step, all transits are visually inspected. In some cases, (instrumental or astrophysical) data jumps or gaps can cause the transit fits to fail or the true transit to be poorly determined. These transits are manually removed. Similarly, when multiple transits happen simultaneously, these data points are removed to avoid biasing the transit measurement.

10.2.1.2 *Period and TTV determination*

This part of the pipeline measures times of individual transits and uses them to find the orbital period, as well as detect any TTVs. The measurement of an individual transit time is done by fitting the best transit model to the individual transits, keeping all transit parameters fixed except for the transit mid-time. During the first iteration, the model is based on the parameters extracted from the *Kepler* database, afterwards the best model from the MCMC analysis in Step 3 (transit fit module) is used, a procedure which is repeated until convergence is reached. The uncertainty of each transit-mid time is calculated by first subtracting the best fitting transit model from the original light curve, bootstrapping the residuals with replacement, injecting the best fitting

3 http://exoplanetarchive.ipac.caltech.edu/

transit model and fitting this new light curve. The steps after and including the permutation of the residuals are repeated 200 times for each transit, to calculate the mid-time uncertainty from the spread in these fits.

Now the planetary period is obtained by (weighted) fitting for a linear ephemeris to the individual transit times. From this we calculate the observed minus calculated (O-C) transit times. Next we refit, this time ignoring $3-\sigma$ outliers (as determined by the standard deviation around the linear ephemeris), and repeat until convergence is reached (no more outliers are removed).

Once the linear ephemeris has been determined we perform a search for TTVs as these might cause biases in the eccentricity calculations, as explained below. For this a sinusoidal model is fitted to the O-C diagram. A list of the systems where TTVs were included is given in Table 9. The transits are subsequently folded based on their period and TTVs if present. The folded transit curve is binned to contain a maximum of 6000 data points, which even for the longest transits implies more than 10 data points per minute, which is an oversampling compared to the original one minute *Kepler* sampling.

10.2.1.3 *Transit fit module*

This part of the pipeline consists of a transit fitting module, which makes use of a Markov Chain Monte Carlo (MCMC) algorithm. We choose to employ an Affine-Invariant Ensemble Sampler (Goodman and Weare 2010) as implemented in the Python module *emcee* (Foreman-Mackey et al. 2013). Planetary transits are modeled analytically (Mandel and Agol 2002)[4].

For each planet in the system, we sample five parameters: the impact parameter b, relative planetary radius $R_p/R_\star$, $\sqrt{e}\cos\omega$, $\sqrt{e}\sin\omega$, mid-transit time T_0 and flux offset F. In addition, two stellar limb darkening parameters are adjusted. These are common for all planets in one system, leading to $6n+2$ parameters per planetary system, where n is the amount of planets in the system. The MCMC chains were run using 200 walkers, each producing a chain of 500 000 steps, after a burn-in phase of 150 000 steps was completed.

We sample uniformly in $R_p/R_\star$ and place a uniform prior on T_0 and b, where the latter is sampled between -2 and 2 to allow grazing orbits and avoid border effects around 0. We do not sample directly in e and ω, as this biases the eccentricity results for nearly circular orbits due to the boundary at zero (Lucy and Sweeney 1971; Eastman et al. 2013). Instead we sample uni-

4 We gratefully acknowledge the implementation of planetary transit equations into Python by Ian J. M. Crossfield, upon which our code was based; see http://www.lpl.arizona.edu/~ianc/python/transit.html.

formly in $\sqrt{e}\cos\omega$ and $\sqrt{e}\sin\omega$ (both between -1 and 1), which corresponds to a uniform sampling in $e \in [0,1]$ and $\omega \in [0,360]^\circ$ after conversion and rejection of values corresponding to $e > 1$. The conversion between e and ω and the stellar density ratio is given by (Kipping 2010; Moorhead et al. 2011; Tingley et al. 2011; Dawson and Johnson 2012)

$$\frac{\rho_\star}{\rho_{\star,\mathrm{transit}}} = \frac{(1-e^2)^{3/2}}{(1+e\sin\omega)^3}, \tag{10.1}$$

and this can be further converted into the ratio of semi-major axis to stellar radius $R_\star/a$ using (Seager and Mallén-Ornelas 2003)

$$\rho_{\star,\mathrm{transit}} = \frac{3\pi}{GP^2}\left(\frac{a}{R_\star}\right)^3. \tag{10.2}$$

Here G represents the gravitational constant. It is $R_\star/a$ which is used in the analytical transit model (Mandel and Agol 2002). For circular orbits, $R_\star/a$ directly constrains the stellar density ($\rho_{\star,\mathrm{transit}} = \rho_\star$). In general, when $\rho_\star$ is known (e.g. from asteroseismology (Huber et al. 2013b; Silva Aguirre et al. 2015)), $R_\star/a$ constrains the combination of e and ω given by the right-hand side of Equation 10.1. We note that it is possible to sample directly from the stellar density ratio (or from $R_\star/a$) (Dawson and Johnson 2012; Van Eylen et al. 2014), since the data always constrains a combination of e and ω simultaneously, but doing so makes it more complicated to achieve an uninformative flat prior in e and ω.

Multiple planets around the same star are modeled simultaneously using the same limb darkening parameters. We use a quadratic limb darkening law with parameters u_1 and u_2 ($I(\mu)/I(1) = 1-u_1(1-\mu)+u_2(1-\mu)^2$, where $I(1)$ represents the specific intensity at the centre of the disc and μ the cosine of the angle between the line of sight and the emergent intensity) and place a Gaussian prior with a standard deviation of 0.1 on each parameter, centered on predicted values interpolated for a Kurucz atmosphere (Claret and Bloemen 2011). This is a compromise to avoid fixing the parameters entirely, while still making use of the detailed stellar parameters available for the stars in our sample.

The final part of this module of the pipeline consists of the processing of the MCMC chains. Convergence is checked by visually inspecting traceplots, checking that an increase in burn-in time does not influence the posteriors, and confirming that MCMC chains initialized with different starting conditions give equivalent results. Transit fits for the final parameters are produced. All parameter distributions and their mutual correlations are plotted and visually inspected. A range of statistics, such as the mean, median, mode and

confidence intervals are calculated for each parameter.

The results for our combined sample are presented in terms of the stellar density ratio in Section 10.3.1. The results for all individual systems and parameters are presented in Table 8.

10.2.2 *Parameter correlations*

There are several correlations between eccentricity and other parameters which are addressed here. The most important correlation occurs between eccentricity and angle of periastron ω and was already reported above (Equation 10.1). We explain how this complication can be overcome for a *sample* of systems, by directly using the relative density instead, as well as its influence on eccentricity estimates for individual systems. Another important correlation occurs with impact parameter b. The influence of TTVs is also discussed. The effect of ω, b and TTVs on the eccentricity is summarized in Figure 27. We briefly discuss other commonly anticipated complications.

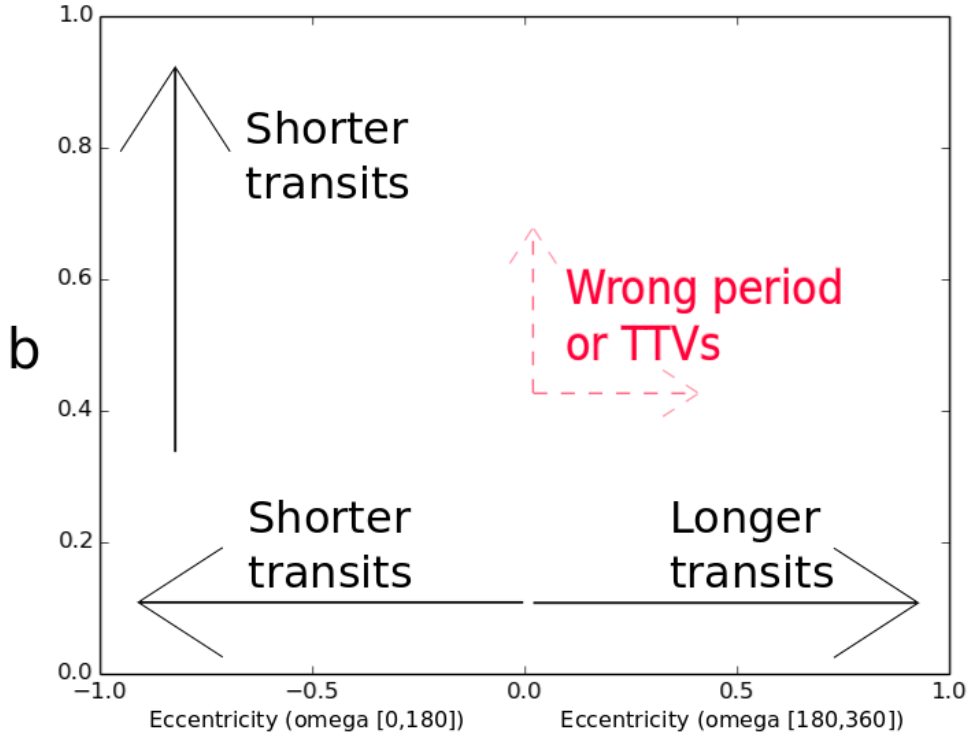

Figure 27 – Illustration showing the influence of impact parameter b and eccentricity e on the transit duration. Misidentified periods or inadequately removed TTV signals cause a bias in b and e.

10.2.2.1 *Correlation with angle of periastron*

When measuring transits, a combination of eccentricity and angle of periastron is constrained, as given by Equation 10.1. The combined influence of e and ω is illustrated in Figure 28. For $\omega \in [0, 180]^\circ$, eccentric orbits lead to shorter transits, while for $\omega \in [180, 360]^\circ$, eccentricity increases the transit duration (see Figure 27). The left-hand side of the equation (the relative density $\rho_{\mathrm{circ.}}/\rho_{\mathrm{transit}}$) is the observable property, i.e. it is used to fit transits. Each relative density corresponds to a given eccentricity but also depends on the angle ω, which is illustrated in Figure 28.

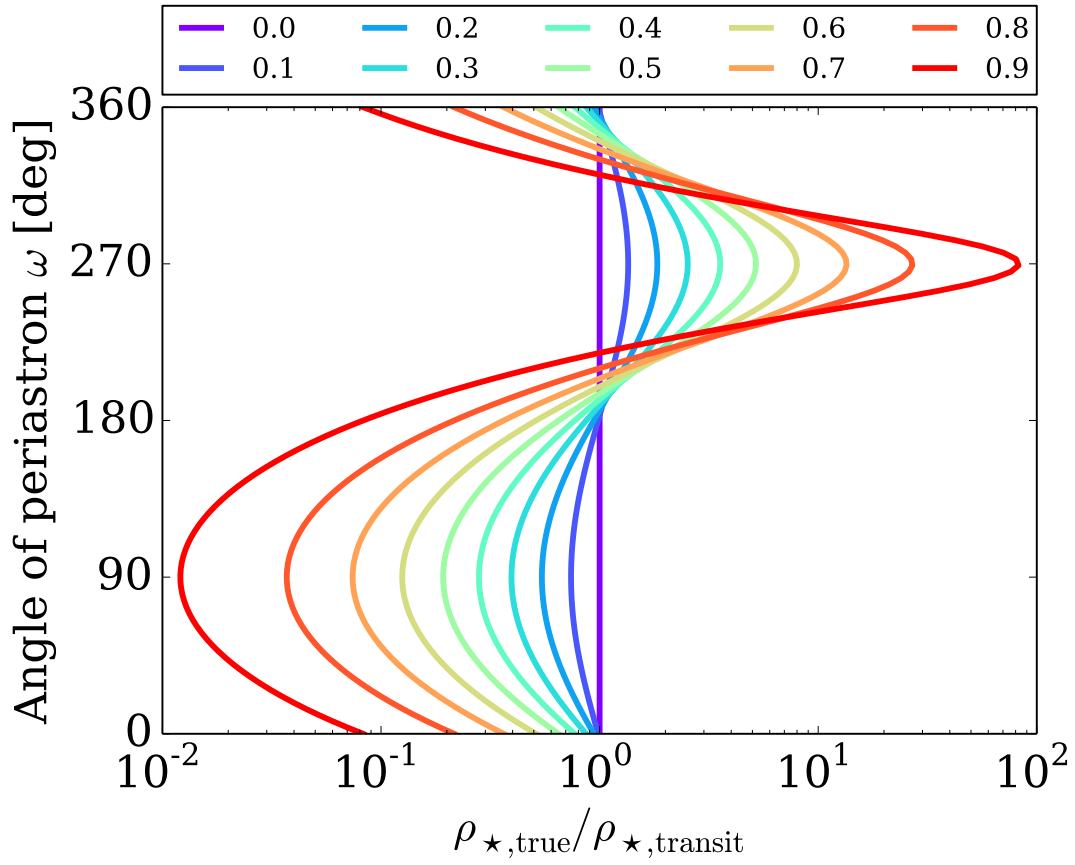

Figure 28 – The influence of e and ω on the relative density measured. The colored lines indicate different eccentricities ranging from 0 (inner) to 0.9 (outer). Different combinations of e and ω can correspond to the same relative density.

When looking at an ensemble of systems, this complication can be avoided by reporting the measured relative densities, which is what we do in Section 10.3.1. This is the true observable (i.e. it influences the transit model), and it holds information on both e and ω in a way that is defined by Equation 10.1. For an ensemble of systems, ω is expected to be randomly distributed[5] so that

5 In general, the transit probability depends itself on ω for eccentric orbits, but given the low eccentricity orbits we find in our sample ω can be assumed to be randomly distributed.

the distribution of relative densities can be directly compared to any anticipated eccentricity distributions.

Note that for individual systems information on e and ω can still be separately extracted, although the incomplete knowledge of ω increases the uncertainty of e. We report eccentricity modal values and highest probability density intervals which represent 68% confidence in Table 8.

10.2.2.2 *Correlation with impact parameter*

Eccentricity can be correlated with the transit impact parameter b. This can be understood by looking at Figure 29, in which the effect of changing impact parameters and eccentricities is plotted for two analytically generated transit curves. While eccentric orbits change transit durations (increasing or decreasing it depending on the angle of periastron), increasing the impact parameters also shortens transits since a smaller part of the stellar disk is being crossed. Fortunately, changing the impact parameter also has the effect of *deforming* the planetary transit. This is caused by the ingress and egress taking up more of the total transit time and leads to the typical V-shaped transits for high impact parameters. However, for smaller planets, ingress/egress times are intrinsically very short and the deformation of the transit shape is therefore far more limited, causing b and e to be more degenerate for smaller planets than for larger planets (see also Ford et al. 2008, and Figure 5 therein). This is why the availability of short cadence observations with a one minute sampling is crucial. Long cadence data, with an integration time of 30 minutes, smears out the ingress and egress of the planet. Therefore measuring eccentricities for small planets is more complicated for two reasons: transits of smaller planets require higher accuracy light curves to obtain the same signal-to-noise ratio in the light curve than needed for larger planets, and for small planets eccentricity and impact parameter are more degenerate. The effect of b and e on the transit duration is illustrated in Figure 27. In a few cases (see Table 8) the correlation between b and e caused the eccentricity range to be uninformative (here defined as an $1-\sigma$ interval larger than 0.4). These 8 systems were excluded from the sample presented in Section 10.3.1 as they do not present any additional information (see e.g. Price et al. 2015).

10.2.2.3 *The influence of TTVs*

Transit timing variations have the potential to influence eccentricity measurements. Contrary to what one might expect, the major issue with TTVs is not that they cause the total transit duration to be mismeasured, but rather that TTVs can cause the impact parameter to be measured wrongly (Kipping 2014a). When combining multiple transits which are not correctly aligned, the best-fit model transit will be more V-shaped (higher impact parameter) than

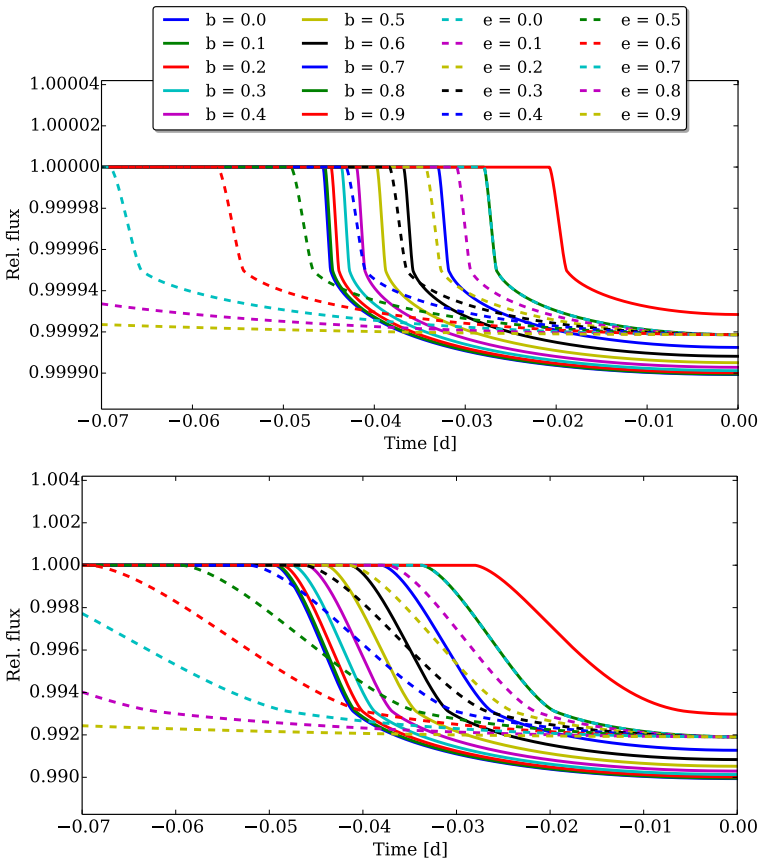

Figure 29 – **Top**: Earth-sized planet, **bottom:** Jupiter-sized planet. Solid lines show transits for different impact parameter b and $e = 0$, dotted lines show transits for different e and $b = 0.8$. All angle of periastron ω are taken to be 270°. In the Earth-size planet case, high b and medium eccentricity look very similar to zero b and zero e, while in the Jupiter-size case, there is much less degeneracy.

the original transit. As high impact parameters typically have shorter transit durations, this bias in b can then be 'compensated' by a higher eccentricity (and an angle of periastron within $[180, 360]°$). Consequently, when TTVs are not properly taken into account, a bias occurs towards the top right on the illustration in Figure 27. This bias due to TTVs can be quite large. For example, we inserted an artificial planet on a circular orbit into the *Kepler* observations and added a sinusoidal TTV signal with an amplitude of 20 minutes and a period of 250 days. An eccentricity of 0.7 was recovered (with small formal uncertainty), while for the same case without TTVs the correct circular orbit was recovered. However, these clear cases of TTVs can easily be measured and removed, which we do in our pipeline.

Smaller TTV signals can be more difficult to detect and adequately remove. With smaller planetary radii (smaller transit depths), the ability to measure individual transit times decreases and therefore also our ability to detect a TTV signal. On the other hand, for the smallest planets, the impact parameter

is typically poorly constrained, making (small) TTVs less important relative to other sources of uncertainties (see Section 10.2.3). It is not always straightforward to determine whether TTVs should be included in the modeling. We found that classic tests such as the likelihood ratio tests or the Bayesian Information Criterium sometimes favor the inclusion of a TTV signal for the smallest planets, on artificial transits inserted without TTVs into real *Kepler* observations. This could be caused by an underestimate of the errors on the transit times for very small planets, or the influence of light curve inperfections (instrumental or astrophysical, e.g. star spots).

In our final analysis we include only clearly detectable sinusoidal TTV signals, after confirming that in cases where there was doubt, the decision to include TTVs or not did not influence the eccentricity measurement (see also Section 10.2.3). A list of systems with included TTVs is given in Table 9 and for Kepler-103, Kepler-126, Kepler-130 and Kepler-278, these TTVs have not been previously reported. Four systems were excluded from our initial sample because their TTVs could not be adequately removed using a sinusoidal model.

10.2.2.4 *Other potential complications*

We briefly discuss several other issues that have been previously identified as potential sources of error for measurements of eccentricities from transit photometry.

False positives can complicate eccentricity measurements. When a planetary transit's host star is misidentified, the true stellar density can differ significantly from the one used to calculate the eccentricity (Sliski and Kipping 2014). In our sample, all but three systems (KOI-5, KOI-270 and KOI-279) contain planets which were previously confirmed or validated as true exoplanets. Kepler-92 contains two confirmed planets and one additional candidate[6]. Therefore our sample is not biased due to false positives.

Similar to planetary false positives is the issue of *light curve dilution*. Here, the planet orbits around its host star, but third light dilutes the light curve, causing the transit depth to be reduced. This results not only in a biased planet radius (Ciardi et al. 2015), but also in a biased impact parameter, which in turn can cause the eccentricity to be wrongly measured. However, most of the targets from our selected sample of bright stars have been followed up with adaptive optics (Adams et al. 2012) and Speckle images (Howell et al. 2011). No significant sources of dilution have been found for any of our confirmed planets. The reported light curve contamination for KOI-5, KOI-270 and KOI-279 is taken into account prior to the modeling. Quarter to quarter

6 The planetary nature of these planet candidates is discussed in Chapter 5

variations in the light curve owing to pixel sensitivity are of the percentage order (Van Eylen et al. 2013) and do not affect our eccentricity measurement.

Stellar *limb darkening* is another potential source of complication. Visual inspection yields no evidence of a correlation with eccentricity (see also Ford et al. 2008). We use a prior on the limb darkening based on stellar atmosphere models (Claret and Bloemen 2011) to speed up MCMC convergeance, but nevertheless allow the limb darkening parameters to vary to avoid this source of complications.

Another potential influence on eccentricity measurements would be a bias in the *stellar densities* determined from asteroseismology. Part of the values from our sample are taken from Silva Aguirre et al. (2015), and are based on individual frequency modeling using several different stellar evolution codes. The remaining densities are taken from (Huber et al. 2013b) and are based on scaling relations. Such relations have been proven accurate and unbiased for dwarfs and subdwarfs, such as the stars considered in this study (Huber et al. 2012; Silva Aguirre et al. 2012; Silva Aguirre et al. 2015).

Finally we note that the *uncertainty in the folded light curve* could be of potential concern. Ideally, all individual transits would be normalised and modeled simultaneously, while also fitting for the period and any potential TTVs and modeling the correlated noise. However, such an approach is computationally unfeasible. Consequentially, these errors are not fully propogated and the resulting uncertainties could be underestimated. In most cases many transits are available, causing the period to be very well determined. Of bigger concern are TTVs, but tests with artificial planetary transits (see Section 10.2.3) show no evidence of any bias or underestimated error bars.

10.2.3 *Transit insertion tests*

We have inserted artificial transits into the data to test the performance of our pipeline. The procedure we used is as follows. First, an artificial planetary transit was generated, and inserted into the light curve that has been observed for one of the stars analyzed in our sample. The lightcurves in which we inserted artificial transits were chosen randomly from our sample of stars with two or three transiting planets (stars with more planets were not chosen to avoid 'crowding' due to the pre-existing planets). Subsequently the procedure described in Section 10.2.1.2 was followed to find the orbital period and potential TTVs and fold the data. The period and ephemeris information of the (genuine) planets already present in the light curve was used to remove overlapping transits, as is done for genuine planets. Finally the folded light curve is modeled as described in Section 10.2.1.3.

The aim of these tests is not to be complete in covering the full parameter space, which is indeed challenging as it spans different stellar and planetary parameters, periods and eccentricities, as well as amplitudes and periods of TTVs, while transit insertion tests are computationally expensive. Rather, the purpose is to evaluate representative cases to understand the performance of our pipeline and judge any potential limitations. A total of 141 artificial transits have been generated, inserted in real *Kepler* data, and modeled. We now describe a few cases in more detail.

In a first number of tests, we generated planets with radii and periods representative for our sample, and assigned a random eccentricity, uniform between 0 and 1, and a random angle of periastron ω. We were able to recover the correct eccentricities within the uncertainties. In another set of tests, we attempted to reproduce our sample of planets more closely. The light curves in which the transits were inserted were drawn randomly from the light curves in our sample. The periods and planetary radii were drawn randomly from our sample of planets (Table 8). The impact parameters were chosen uniformly between 0 and 1 for outer planets, and uniformly within a 1.6° spread for inner planets (Fabrycky et al. 2014). The eccentricities were typically recovered within the uncertainties.

We have also tested the influence of TTVs by adding sinusoidal TTV signals to the inserted transits. The influence of TTVs depends not only on the TTV amplitude, but also on the size of the planet. For example, for a 3.5 $R_\oplus$ planet on a 15 day orbit, a 20 minute TTV signal can have a large influence on the derived eccentricity (see Section 10.2.2.3), but the TTV signal is easily recovered and after removal, the correct eccentricity is determined within the uncertainty (and without bias). For smaller planets, it can be difficult to adequately remove the TTV signal, and it can escape detection entirely. However, we find that in these cases, the influence of TTVs on the eccentricity determination is small because other uncertainties dominate. For example, when inserting a TTV signal with an amplitude of 15 minutes, for a planet of 1.5 $R_\oplus$ with an orbital period of 8 days, we did not recover the TTV signal but were nevertheless able to retrieve the correct eccentricities. Other, similar TTV tests revealed similar results, and we also obtained a similar result when modeling genuine planets: when there was significant doubt about the TTV signal, the decision to include it or not did not influence the outcome of our eccentricity measurement.

10.3 RESULTS

Here we present the results of our analysis. In Section 10.3.1 we report the distribution of eccentricities for the planets in our sample. In Section 10.3.2 we present the other parameters that result from our analysis, such as home-

geneous planetary parameters, a distribution in impact parameters and new and updated TTVs.

10.3.1 *Multi-planet systems with small planets have low eccentricities*

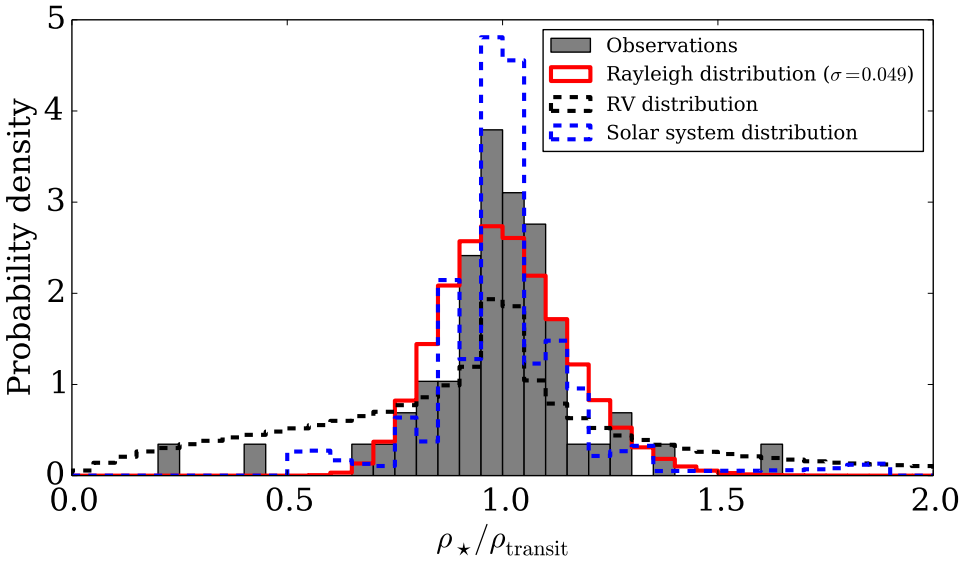

Figure 30 – The stellar density determined from asteroseismology divided by the stellar density determined from the planetary transit if the orbit was circular. Values much smaller than one indicate eccentric orbits with $\omega \in [0, 180]^\circ$ and short transits, while values much larger indicate $\omega \in [180, 360]^\circ$ and longer transits. The best fitted Rayleigh distribution is overplotted and has $\sigma = 0.049$. For illustration the densities which would be observed assuming the RV eccentricity distribution are also indicated, as well as the distribution derived from the Solar System planet's eccentricities.

The stellar density encompasses the combined influence of the orbital eccentricity and angle of periastron on the transit duration as described in Section 10.2.2. In Figure 30 we show a histogram of the ratio of the densities derived from asteroseismology to the densities derived from the transit fits. In this figure large eccentricities would be revealed as very large or small density ratios, depending on the argument of periastron. The absence of such ratios already indicates that low eccentricities are common.

To quantitatively constrain the eccentricity distribution we now assume a Rayleigh distribution for the eccentricities, which provides a best fit to the data for $\sigma = 0.049 \pm 0.013$. The resulting distribution of density ratios is shown in Figure 30. The Rayleigh distribution has the additional advantage that it can be directly compared to some other eccentricity determinations, such as $\sigma = 0.018$ found for some TTV systems (Hadden and Lithwick 2014). Kipping (2013b) suggests the use of a Beta distribution, which has the advantage of being convenient to use as a prior for transit fits. Using this distribution

to model our results we find a good fit to our data with Beta parameters $\alpha = 1.03 \pm 0.15$ and $\beta = 13.6 \pm 2.1$. The best-fit values are calculated by drawing random eccentricity values from the chosen distribution (Rayleigh distribution or Beta distribution) and assigning a random angle of periastron to calculate the corresponding density ratio. The distribution of density ratios is then compared to the observed density ratio distribution, by minimizing the χ^2 when comparing the cumulative density functions, to avoid a dependency of the fit on binning of the data (see e.g. Kipping 2013b). The uncertainty on the parameters is calculating by bootstrapping the observed density ratios (with replacement) and repeating the procedure, and calculating the scatter in the best-fit parameters.

The distribution is similar to that of the Solar System which is plotted in the same figure for comparison (integrated over different angles). In contrast we also plot the relative densities that would have been observed if our sample had the same eccentricity distribution as measured for RV planets (Shen and Turner 2008) in Figure 30. Figure 31 compares the eccentricities in our sample with the solar system planets and the exoplanets with RV observations. The RV observations were taken from exoplanets.org (27 April 2015) and include all data points where the eccentricity was measured (not fixed to zero), and the RV amplitude ('K') divided by its uncertainty ('UK') is greater than ten. The masses for the planets in our sample were estimated based on the radius, using Weiss et al. (2013) for planets with $R \geqslant 4\ R_\oplus$ and following Weiss and Marcy (2014) for planets where $R \leqslant 4\ R_\oplus$.

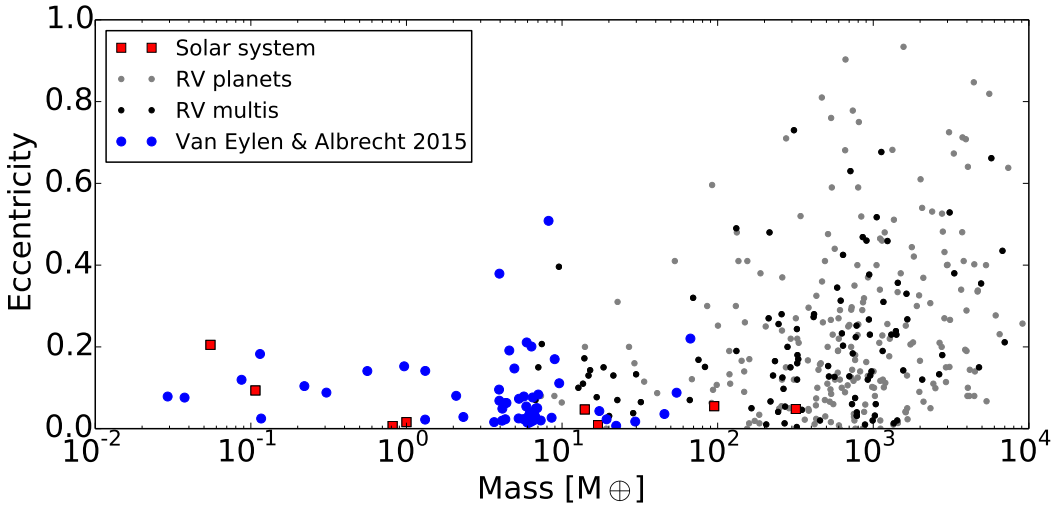

Figure 31 – The eccentricity and mass measurements for exoplanets are plotted as taken from exoplanets.org on 27 April 2015, for planets where both values are determined. Planets which are flagged as multi-planet systems are highlighted. For comparison, the solar system is shown. The eccentricities of the planets in our sample are plotted with their mass estimated based on radius (Weiss et al. 2013; Weiss and Marcy 2014). Error bars are omitted for clarity.

Our sample differs in two important ways from the RV sample: planetary size and planetary multiplicity. These properties are not independent since smaller planets are frequently found in multiple planet systems (Latham et al. 2011). A hint towards smaller eccentricities for smaller/less massive planets and higher multiplicity has already been observed in RV systems. In systems with sub-Jovian mass planets and systems with multiple planets, eccentricities are limited to 0-0.45 (Wright et al. 2009; Mayor et al. 2011). Even so the eccentricities observed in our sample have a much narrower range, possibly because the average size of the planets is much smaller even when compared to the sub-Jovian RV sample (most planets in our sample cannot be detected with RV measurements, and even when RV mass measurements are possible eccentricity determinations are not feasible, Marcy et al. 2014).

Analyzing TTV signals for *Kepler* planets, Hadden and Lithwick (2014) find an rms eccentricity of $0.018^{+0.005}_{-0.004}$. They further note that eccentricities of planets smaller than 2.5 $R_\oplus$ are about twice as large as those larger than this limit, although they caution a TTV detection bias may influence this result. We have compared our eccentricity measurements with the planetary radii in Figure 33 (see also Section 10.3.2) and found no evidence for a correlation. However, the difference between the rms eccentricity for planets smaller and larger than 2.5 $R_\oplus$ is only 0.009 (Hadden and Lithwick 2014), which would likely not be detectable in our sample.

Planet-planet interactions have been brought forward as a mechanism to explain the observed eccentricities in massive planets (Fabrycky and Tremaine 2007; Chatterjee et al. 2008; Nagasawa et al. 2008; Ford and Rasio 2008; Jurić and Tremaine 2008). In this picture gravitational interactions lead to high eccentricities and planetary migration. However, despite finding a small anti-correlation between mass and eccentricity for massive planets, Chatterjee et al. (2008) suggested that damping from residual gas or planetesimals could more effectively reduce the eccentricities of low-mass planets after scattering. Furthermore, it has been suggested that there may exist a dependence of eccentricity on the orbital semi-major axis, because the mean eccentricity depends on the velocity dispersion scaled by the Keplerian velocity (see e.g. Ida et al. 2013; Petrovich et al. 2014). Consequentially the eccentricity may be proportional to the square root of the semi-major axis (Ida et al. 2013). The majority of the planets in our sample have orbital distances that are unlikely to be affected by tidal circularisation, but it was suggested very recently that tidal effects in compact multi-planet systems may propagate further than for single planet systems (Hansen and Murray 2015).

The observed low eccentricities could be related to the planet multiplicity, which was also observed by Limbach and Turner (2015). Highly eccentric planets in multi-planet systems are also less likely to be stable over longer

timescales, which could lead to lower observed eccentricities in compact systems because systems with more eccentric systems would not survive. Pu and Wu (2015) found that planets with circular orbits can be more tightly packed than systems with eccentric planets. The systems in our sample have between 2 and 5 transiting planets but the true multiplicity could be underestimated if additional non-transiting planet are present.

10.3.2 *Homogeneous stellar and planetary parameters and new TTVs*

Next to orbital eccentricities our analysis also yields a homegeneous set of planetary parameters. They are not only derived from homegeneous transit modeling but also from a homegemeous set of stellar parameters, which were all derived from asteroseismology (Huber et al. 2013b; Silva Aguirre et al. 2015). We report the eccentricities and the planetary radii, as well as the stellar masses and radii upon which they were based (Huber et al. 2013b; Silva Aguirre et al. 2015) in Table 8. The modes and 68% highest probability density intervals are quoted for all values. The full posterior distributions, including the correlations between parameters, are available upon request.

We checked the distribution of transit impact parameters and show a histogram in Figure 32. Because we are dealing with multi-transiting systems a bias towards lower impact parameters is expected since such systems are more likely to have multiple planets transiting. When we plot the impact parameter of all planets, low impact parameter values indeed appear favored and the distribution is inconsistent with a homegeneous one between 0 and 1 (KS-test with p-value of 0.003). If we only plot the impact parameters of the outer planet (the longest period) in each system, a distribution which appears uniform in impact parameter is observed (KS-test with p-value of 0.86, see Figure 32). That planets on shorter orbital periods have lower impact parameter than the outer planets in the same system shows that most systems in our sample have very low mutual inclinations, consistent with earlier work (Fabrycky et al. 2014).

We furthermore compared the eccentricity to other parameters and found no correlation (see Figure 33). We plot the eccentricity versus the orbital period and planetary radius. We also compare the eccentricity to stellar temperature and stellar age, two parameters which might influence tidal circularisation. We note that ages are only available for part of our sample (Silva Aguirre et al. 2015). We see no correlations.

We have determined transit times and (re)derived orbital periods in a way that is robust to outliers (see Section 10.2). In several cases, we found clear evidence of TTVs. The TTV periods and amplitudes that were included in our analysis are listed in Table 9. For Kepler-103, Kepler-126, Kepler-130 and

		e (mode)	e (68%)	R_p [$R_\oplus$]	Period [d]	Ref.	$M_\star$ [$M_\odot$]	$R_\star$ [$R_\odot$]	Density [g/cm3]
Kepler-10b	KOI-72.01	0.06	[0, 0.22]	1.473 ± 0.026	0.83749026(29)	(2)	$0.920^{-0.020}_{0.010}$	$1.0662^{-0.0075}_{0.0069}$	$1.0679^{-0.012}_{0.0072}$
Kepler-10c	KOI-72.02	0.05	[0, 0.25]	2.323 ± 0.028	45.294292(97)	(2)	$0.920^{-0.020}_{0.010}$	$1.0662^{-0.0075}_{0.0069}$	$1.0679^{-0.012}_{0.0072}$
Kepler-23b	KOI-168.03	0.06	[0, 0.32]	1.694 ± 0.076	7.106995(73)	(1)	$1.078^{-0.077}_{0.077}$	$1.548^{-0.048}_{0.048}$	$0.410^{-0.023}_{0.023}$
Kepler-23c	KOI-168.01	0.02	[0, 0.41]	3.12 ± 0.10	10.742434(39)	(1)	$1.078^{-0.077}_{0.077}$	$1.548^{-0.048}_{0.048}$	$0.410^{-0.023}_{0.023}$
Kepler-23d	KOI-168.02	0.08	[0, 0.32]	2.235 ± 0.088	15.27429(17)	(1)	$1.078^{-0.077}_{0.077}$	$1.548^{-0.048}_{0.048}$	$0.410^{-0.023}_{0.023}$
Kepler-25b	KOI-244.02	0.05	[0, 0.16]	2.702 ± 0.037	6.2385369(33)	(2)	$1.160^{-0.050}_{0.040}$	$1.299^{-0.016}_{0.015}$	$0.7454^{-0.0098}_{0.0093}$
Kepler-25c	KOI-244.01	0.01	[0, 0.08]	5.154 ± 0.060	12.7203678(35)	(2)	$1.160^{-0.050}_{0.040}$	$1.299^{-0.016}_{0.015}$	$0.7454^{-0.0098}_{0.0093}$
Kepler-37b	KOI-245.03	0.08	[0, 0.29]	0.354 ± 0.014	13.36805(38)	(2)	$0.810^{-0.010}_{0.020}$	$0.7725^{-0.0063}_{0.0051}$	$2.486^{-0.025}_{0.022}$
Kepler-37c	KOI-245.02	0.09	[0, 0.27]	0.705 ± 0.012	21.302071(92)	(2)	$0.810^{-0.010}_{0.020}$	$0.7725^{-0.0063}_{0.0051}$	$2.486^{-0.025}_{0.022}$
Kepler-37d	KOI-245.01	0.15	[0.05, 0.22]	1.922 ± 0.024	39.792232(54)	(2)	$0.810^{-0.010}_{0.020}$	$0.7725^{-0.0063}_{0.0051}$	$2.486^{-0.025}_{0.022}$
Kepler-65b	KOI-85.02	0.02	[0, 0.19]	1.409 ± 0.017	2.1549156(25)	(2)	$1.199^{-0.030}_{0.030}$	$1.401^{-0.014}_{0.013}$	$0.6158^{-0.0079}_{0.0071}$
Kepler-65c	KOI-85.01	0.08	[0, 0.2]	2.571 ± 0.033	5.8599408(23)	(2)	$1.199^{-0.030}_{0.030}$	$1.401^{-0.014}_{0.013}$	$0.6158^{-0.0079}_{0.0071}$
Kepler-65d	KOI-85.03	0.10	[0, 0.33]	1.506 ± 0.040	8.131231(21)	(2)	$1.199^{-0.030}_{0.030}$	$1.401^{-0.014}_{0.013}$	$0.6158^{-0.0079}_{0.0071}$
Kepler-68b	KOI-246.01	0.02	[0, 0.15]	2.354 ± 0.020	5.3987533(13)	(2)	$1.070^{-0.020}_{0.010}$	$1.2379^{-0.0051}_{0.0067}$	$0.7949^{-0.011}_{0.0052}$
Kepler-68c	KOI-246.02	0.42	[0.32, 0.83]	0.927 ± 0.025	9.604979(45)	(2)	$1.070^{-0.020}_{0.010}$	$1.2379^{-0.0051}_{0.0067}$	$0.7949^{-0.011}_{0.0052}$
Kepler-92b	KOI-285.01	0.17	[0, 0.27]	3.65 ± 0.13	13.748933(75)	(2)	$1.209^{-0.030}_{0.020}$	$1.719^{-0.013}_{0.011}$	$0.3355^{-0.0040}_{0.0044}$
Kepler-92c	KOI-285.02	0.04	[0, 0.26]	2.455 ± 0.053	26.72311(19)	(2)	$1.209^{-0.030}_{0.020}$	$1.719^{-0.013}_{0.011}$	$0.3355^{-0.0040}_{0.0044}$
Kepler-92d	KOI-285.03	0.07	[0.03, 0.41]	2.067 ± 0.056	49.3568(24)	(2)	$1.209^{-0.030}_{0.020}$	$1.719^{-0.013}_{0.011}$	$0.3355^{-0.0040}_{0.0044}$
Kepler-100b	KOI-41.02	0.13	[0, 0.40]	1.305 ± 0.030	6.887037(47)	(2)	$1.109^{-0.020}_{0.020}$	$1.5131^{-0.011}_{0.0093}$	$0.4542^{-0.0058}_{0.0043}$
Kepler-100c	KOI-41.01	0.02	[0.01, 0.17]	2.221 ± 0.022	12.815909(26)	(2)	$1.109^{-0.020}_{0.020}$	$1.5131^{-0.011}_{0.0093}$	$0.4542^{-0.0058}_{0.0043}$
Kepler-100d	KOI-41.03	0.38	[0.22, 0.50]	1.514 ± 0.034	35.33313(43)	(2)	$1.109^{-0.020}_{0.020}$	$1.5131^{-0.011}_{0.0093}$	$0.4542^{-0.00579}_{0.00431}$
Kepler-103b	KOI-108.01	0.03	[0, 0.23]	3.476 ± 0.039	15.965316(18)	(2)	$1.099^{-0.030}_{0.019}$	$1.455^{-0.013}_{0.024}$	$0.5070^{-0.0050}_{0.0050}$
Kepler-103c	KOI-108.02	0.02	[0, 0.21]	5.319 ± 0.052	179.6133(47)	(2)	$1.099^{-0.030}_{0.019}$	$1.450^{-0.009}_{0.009}$	$0.5070^{-0.0050}_{0.0050}$
Kepler-107b	KOI-117.03	0.02	[0, 0.22]	1.581 ± 0.056	3.180026(12)	(1)	$1.142^{-0.068}_{0.068}$	$1.411^{-0.047}_{0.047}$	$0.581^{-0.049}_{0.049}$
Kepler-107c	KOI-117.02	0.02	[0, 0.28]	1.664 ± 0.065	4.901441(30)	(1)	$1.142^{-0.068}_{0.068}$	$1.411^{-0.047}_{0.047}$	$0.581^{-0.049}_{0.049}$

Kepler-107d	KOI-117.04	0.14	[0, 0.39]	1.064 ± 0.062	7.95825(11)	(1)	$1.142^{-0.068}_{0.068}$	$1.411^{-0.047}_{0.047}$	$0.581^{-0.049}_{0.049}$
Kepler-107e	KOI-117.01	0.02	[0, 0.20]	2.92 ± 0.10	14.749176(34)	(1)	$1.142^{-0.068}_{0.068}$	$1.411^{-0.047}_{0.047}$	$0.581^{-0.049}_{0.049}$
Kepler-108b	KOI-119.01	0.22	[0.10, 0.41]	9.56 ± 0.53	49.18354(18)	(1)	$1.377^{-0.089}_{0.089}$	$2.19^{-0.12}_{0.12}$	$0.188^{-0.024}_{0.024}$
Kepler-108c	KOI-119.02	0.04	[0, 0.23]	8.23 ± 0.47	190.3214 (n/a)	(1)	$1.377^{-0.089}_{0.089}$	$2.19^{-0.12}_{0.12}$	$0.188^{-0.024}_{0.024}$
Kepler-109b	KOI-123.01	0.21	[0, 0.30]	2.338 ± 0.034	6.4816370(80)	(2)	$1.069^{-0.040}_{0.040}$	$1.339^{-0.015}_{0.017}$	$0.6278^{-0.0068}_{0.0076}$
Kepler-109c	KOI-123.02	0.03	[0, 0.22]	2.634 ± 0.043	21.222620(30)	(2)	$1.069^{-0.040}_{0.040}$	$1.339^{-0.015}_{0.017}$	$0.6278^{-0.0068}_{0.0076}$
Kepler-126b	KOI-260.01	0.07	[0, 0.17]	1.439 ± 0.020	10.495634(30)	(2)	$1.148^{-0.049}_{0.051}$	$1.345^{-0.018}_{0.015}$	$0.666^{-0.010}_{0.010}$
Kepler-126c	KOI-260.03	0.19	[0, 0.37]	1.498 ± 0.062	21.86964(10)	(2)	$1.148^{-0.049}_{0.051}$	$1.345^{-0.018}_{0.015}$	$0.666^{-0.010}_{0.010}$
Kepler-126d	KOI-260.02	0.02	[0, 0.11]	2.513 ± 0.031	100.28208(41)	(2)	$1.148^{-0.049}_{0.051}$	$1.345^{-0.018}_{0.015}$	$0.666^{-0.010}_{0.010}$
Kepler-127b	KOI-271.03	0.47	[0.08, 0.51]	1.52 ± 0.13	14.43577(10)	(1)	$1.240^{-0.086}_{0.086}$	$1.359^{-0.035}_{0.035}$	$0.697^{-0.023}_{0.023}$
Kepler-127c	KOI-271.02	0.03	[0, 0.17]	2.389 ± 0.067	29.39344(17)	(1)	$1.240^{-0.086}_{0.086}$	$1.359^{-0.035}_{0.035}$	$0.697^{-0.023}_{0.023}$
Kepler-127d	KOI-271.01	0.03	[0, 0.31]	2.668 ± 0.084	48.62997(57)	(1)	$1.240^{-0.086}_{0.086}$	$1.359^{-0.035}_{0.035}$	$0.697^{-0.023}_{0.023}$
Kepler-129b	KOI-275.01	0.01	[0, 0.25]	2.409 ± 0.040	15.791619(53)	(2)	$1.159^{-0.030}_{0.030}$	$1.649^{-0.014}_{0.012}$	$0.3659^{-0.0037}_{0.0042}$
Kepler-129c	KOI-275.02	0.20	[0, 0.35]	2.522 ± 0.066	82.1908 (n/a)	(2)	$1.159^{-0.030}_{0.030}$	$1.649^{-0.014}_{0.012}$	$0.3659^{-0.0037}_{0.0042}$
Kepler-130b	KOI-282.02	0.15	[0, 0.29]	0.976 ± 0.045	8.45725(11)	(1)	$0.934^{-0.059}_{0.059}$	$1.127^{-0.033}_{0.033}$	$0.927^{-0.053}_{0.053}$
Kepler-130c	KOI-282.01	0.08	[0, 0.23]	2.811 ± 0.084	27.508686(37)	(1)	$0.934^{-0.059}_{0.059}$	$1.127^{-0.033}_{0.033}$	$0.927^{-0.053}_{0.053}$
Kepler-130d	KOI-282.03	0.80	[0.40, 0.89]	1.31 ± 0.13	87.5211(24)	(1)	$0.934^{-0.059}_{0.059}$	$1.127^{-0.033}_{0.033}$	$0.927^{-0.053}_{0.053}$
Kepler-145b	KOI-370.02	0.43	[0.18, 0.61]	2.56 ± 0.28	22.95102(23)	(2)	$1.419^{-0.030}_{0.030}$	$1.887^{-0.014}_{0.012}$	$0.2976^{-0.0038}_{0.0045}$
Kepler-145c	KOI-370.01	0.11	[0, 0.22]	3.92 ± 0.11	42.88254(15)	(2)	$1.419^{-0.030}_{0.030}$	$1.887^{-0.014}_{0.012}$	$0.2976^{-0.0038}_{0.0045}$
Kepler-197b	KOI-623.03	0.02	[0, 0.25]	1.064 ± 0.038	5.599293(39)	(1)	$0.922^{-0.059}_{0.059}$	$1.120^{-0.033}_{0.033}$	$0.907^{-0.052}_{0.052}$
Kepler-197c	KOI-623.01	0.08	[0, 0.29]	1.208 ± 0.048	10.349711(54)	(1)	$0.922^{-0.059}_{0.059}$	$1.120^{-0.033}_{0.033}$	$0.907^{-0.052}_{0.052}$
Kepler-197d	KOI-623.02	0.03	[0, 0.23]	1.244 ± 0.049	15.67787(13)	(1)	$0.922^{-0.059}_{0.059}$	$1.120^{-0.033}_{0.033}$	$0.907^{-0.052}_{0.052}$
Kepler-197e	KOI-623.04	0.38	[0.21, 0.63]	0.983 ± 0.048	25.2097(14)	(1)	$0.922^{-0.059}_{0.059}$	$1.120^{-0.033}_{0.033}$	$0.907^{-0.052}_{0.052}$
Kepler-278b	KOI-1221.01	0.04	[0, 0.37]	4.59 ± 0.26	30.15856(91)	(1)	$1.298^{-0.076}_{0.076}$	$2.935^{-0.066}_{0.066}$	$0.07240^{-0.00094}_{0.00094}$
Kepler-278c	KOI-1221.02	0.51	[0.39, 0.70]	3.31 ± 0.12	51.0851(35)	(1)	$1.298^{-0.076}_{0.076}$	$2.935^{-0.066}_{0.066}$	$0.07240^{-0.00094}_{0.00094}$
Kepler-338b	KOI-1930.01	0.04	[0, 0.31]	2.58 ± 0.13	13.72699(47)	(1)	$1.142^{-0.084}_{0.084}$	$1.735^{-0.082}_{0.082}$	$0.309^{-0.034}_{0.034}$

Kepler-338c	KOI-1930.02	0.03	[0, 0.27]	2.48 ± 0.14	24.31168(87)	(1)	$1.142^{-0.084}_{0.084}$	$1.735^{-0.082}_{0.082}$	$0.309^{-0.034}_{0.034}$
Kepler-338d	KOI-1930.03	0.03	[0, 0.25]	2.66 ± 0.15	44.4287(16)	(1)	$1.142^{-0.084}_{0.084}$	$1.735^{-0.082}_{0.082}$	$0.309^{-0.034}_{0.034}$
Kepler-338e	KOI-1930.04	0.05	[0, 0.28]	1.587 ± 0.083	9.34149(40)	(1)	$1.142^{-0.084}_{0.084}$	$1.735^{-0.082}_{0.082}$	$0.309^{-0.034}_{0.034}$
Kepler-444b	KOI-3158.01	0.08	[0, 0.30]	0.381 ± 0.021	3.600125(28)	(2)	$0.740^{-0.010}_{0.010}$	$0.7492^{-0.0040}_{0.0046}$	$2.498^{-0.025}_{0.018}$
Kepler-444c	KOI-3158.02	0.12	[0, 0.29]	0.490 ± 0.024	4.545817(44)	(2)	$0.740^{-0.010}_{0.010}$	$0.7492^{-0.0040}_{0.0046}$	$2.498^{-0.025}_{0.018}$
Kepler-444d	KOI-3158.03	0.18	[0, 0.34]	0.530 ± 0.025	6.189512(54)	(2)	$0.740^{-0.010}_{0.010}$	$0.7492^{-0.0040}_{0.0046}$	$2.498^{-0.025}_{0.018}$
Kepler-444e	KOI-3158.04	0.02	[0, 0.29]	0.533 ± 0.019	7.74350(10)	(2)	$0.740^{-0.010}_{0.010}$	$0.7492^{-0.0040}_{0.0046}$	$2.498^{-0.025}_{0.018}$
Kepler-444f	KOI-3158.05	0.58	[0.21, 0.70]	0.679 ± 0.008	9.740529(36)	(2)	$0.740^{-0.010}_{0.010}$	$0.7492^{-0.0040}_{0.0046}$	$2.498^{-0.025}_{0.018}$
Kepler-449b	KOI-270.01	0.03	[0, 0.31]	2.056 ± 0.069	12.58242(27)	(1)	$0.969^{-0.053}_{0.053}$	$1.467^{-0.033}_{0.033}$	$0.439^{-0.016}_{0.016}$
Kepler-449c	KOI-270.02	0.05	[0, 0.29]	2.764 ± 0.086	33.6727(10)	(1)	$0.969^{-0.053}_{0.053}$	$1.467^{-0.033}_{0.033}$	$0.439^{-0.016}_{0.016}$
Kepler-450b	KOI-279.01	0.02	[0, 0.16]	6.14 ± 0.33	28.454851(25)	(1)	$1.346^{-0.084}_{0.084}$	$1.570^{-0.085}_{0.085}$	$0.478^{-0.064}_{0.064}$
Kepler-450c	KOI-279.02	0.02	[0, 0.19]	2.62 ± 0.14	15.413135(85)	(1)	$1.346^{-0.084}_{0.084}$	$1.570^{-0.085}_{0.085}$	$0.478^{-0.064}_{0.064}$
Kepler-450d	KOI-279.03	0.14	[0, 0.38]	0.837 ± 0.068	7.51464(23)	(1)	$1.346^{-0.084}_{0.084}$	$1.570^{-0.085}_{0.085}$	$0.478^{-0.064}_{0.064}$
	KOI-5.01	0.09	[0, 0.27]	7.87 ± 0.14	4.78032767(84)	(2)	$1.199^{-0.030}_{0.020}$	$1.795^{-0.014}_{0.015}$	$0.2920^{-0.0034}_{0.0027}$
	KOI-5.02	0.10	[0, 0.40]	0.642 ± 0.061	7.05174(13)	(2)	$1.199^{-0.030}_{0.020}$	$1.795^{-0.014}_{0.015}$	$0.2920^{-0.0034}_{0.0027}$

Table 8 – Planetary and stellar parameters for all planets analyzed. The source of the stellar parameters is indicated in the ref. column: (1) Huber et al. (2013b); (2) Silva Aguirre et al. (2015).

Kepler-278, these TTVs have not been previously reported. In some cases, hints of small TTVs were found, in which cases we have checked that the decision whether or not to include them had no significant influence on the derived eccentricity, and ultimately did not include any TTVs in the final analysis. All measured times of individual transits are available upon request.

	TTV period [d]	TTV amplitude [min]
Kepler-23b	433	21.8
Kepler-23c	472	23.0
Kepler-23d	362	22.3
Kepler-25b	327	3.8
Kepler-25c	348	1.1
Kepler-36b	449	166.5
Kepler-36c	446	116.2
Kepler-50b	2127	61.0
Kepler-50c	739	8.7
Kepler-103b	264	2.7
Kepler-103c	514	22.2
Kepler-126b	2052	9.4
Kepler-126c	372	8.0
Kepler-126d	1052	6.4
Kepler-128b	413	55.2
Kepler-128c	355	103.7
Kepler-130b	2043	53.8
Kepler-130c	491	2.8
Kepler-278c	464	88.5
KOI-279.01	1008	2.0

Table 9 – Overview of the period and amplitude of sinusoidal transit timing variations which were included in the modeling. The transit times and the best model fits are shown in Figure 34.

10.4 DISCUSSION

We discuss two important implications of our eccentricity distribution here. In Section 10.4.1 we discuss the influence of orbital eccentricity on habitability. In Section 10.4.2 the consequences of the orbital eccentricity distribution on exoplanet occurrence rates is discussed.

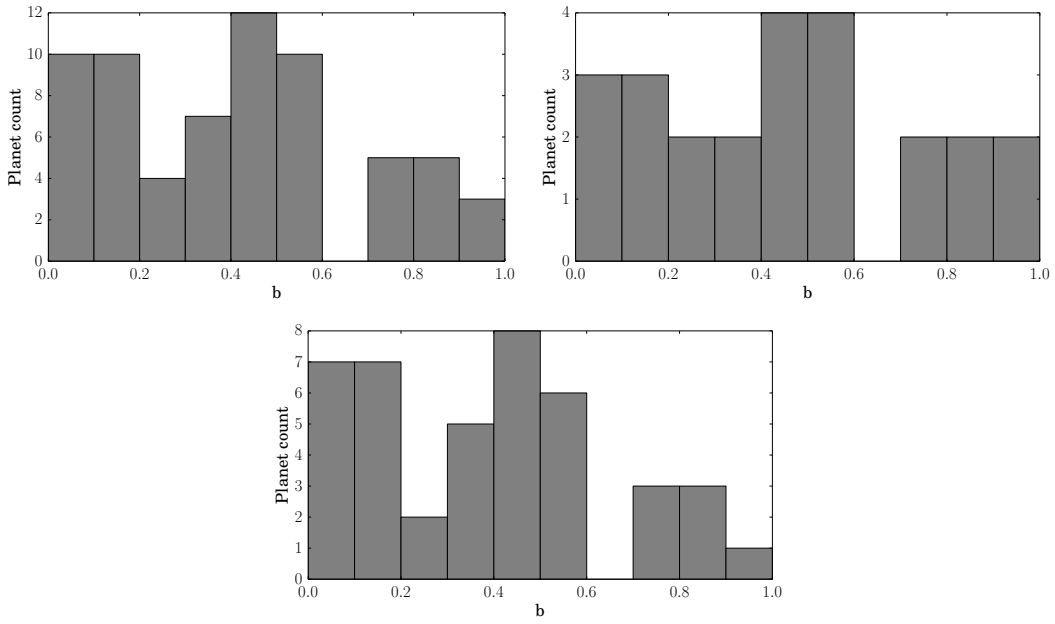

Figure 32 – Histogram of the modes of the impact parameters for individual planets. **Top left:** all planets, **top right:** only outer planets, **bottom:** planets that are not the outer transiting planet.

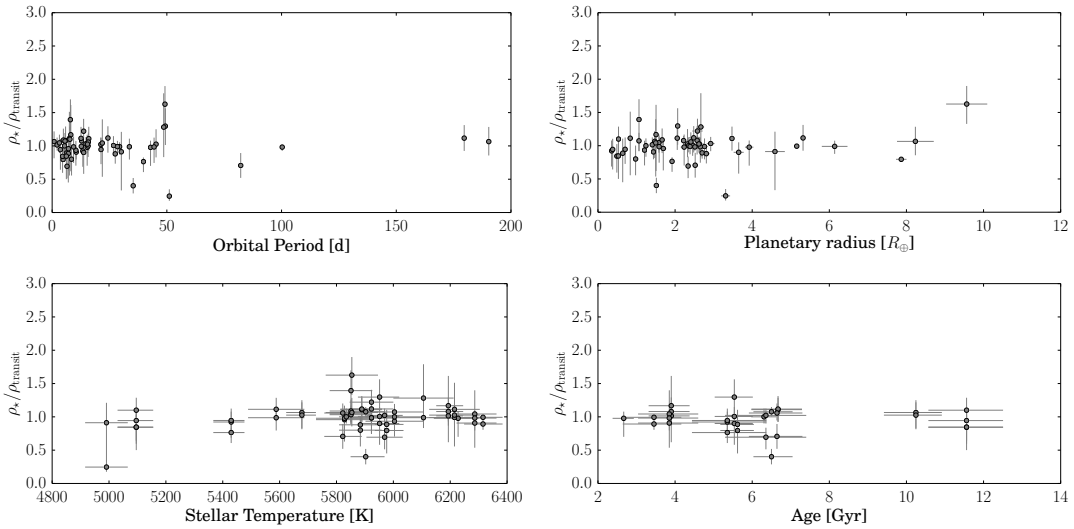

Figure 33 – The orbital period and planetary radius of planets in our sample and the stellar temperature and age, plotted versus the measured relative density (where one indicates a circular orbit).

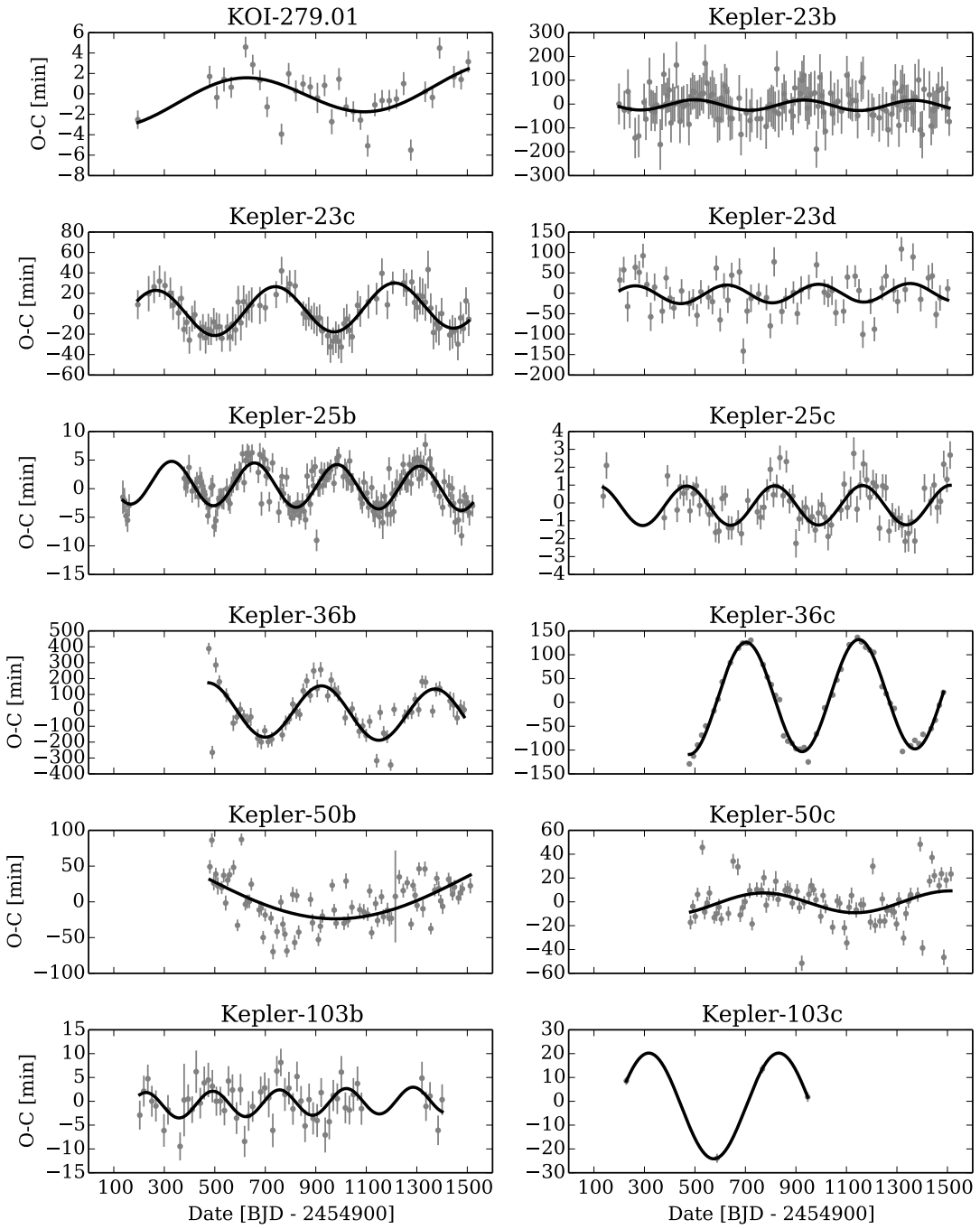

Figure 34 – The observed minus calculated transit times are shown for systems with detected TTVs. A sinusoidal fit to the O-C times is shown.

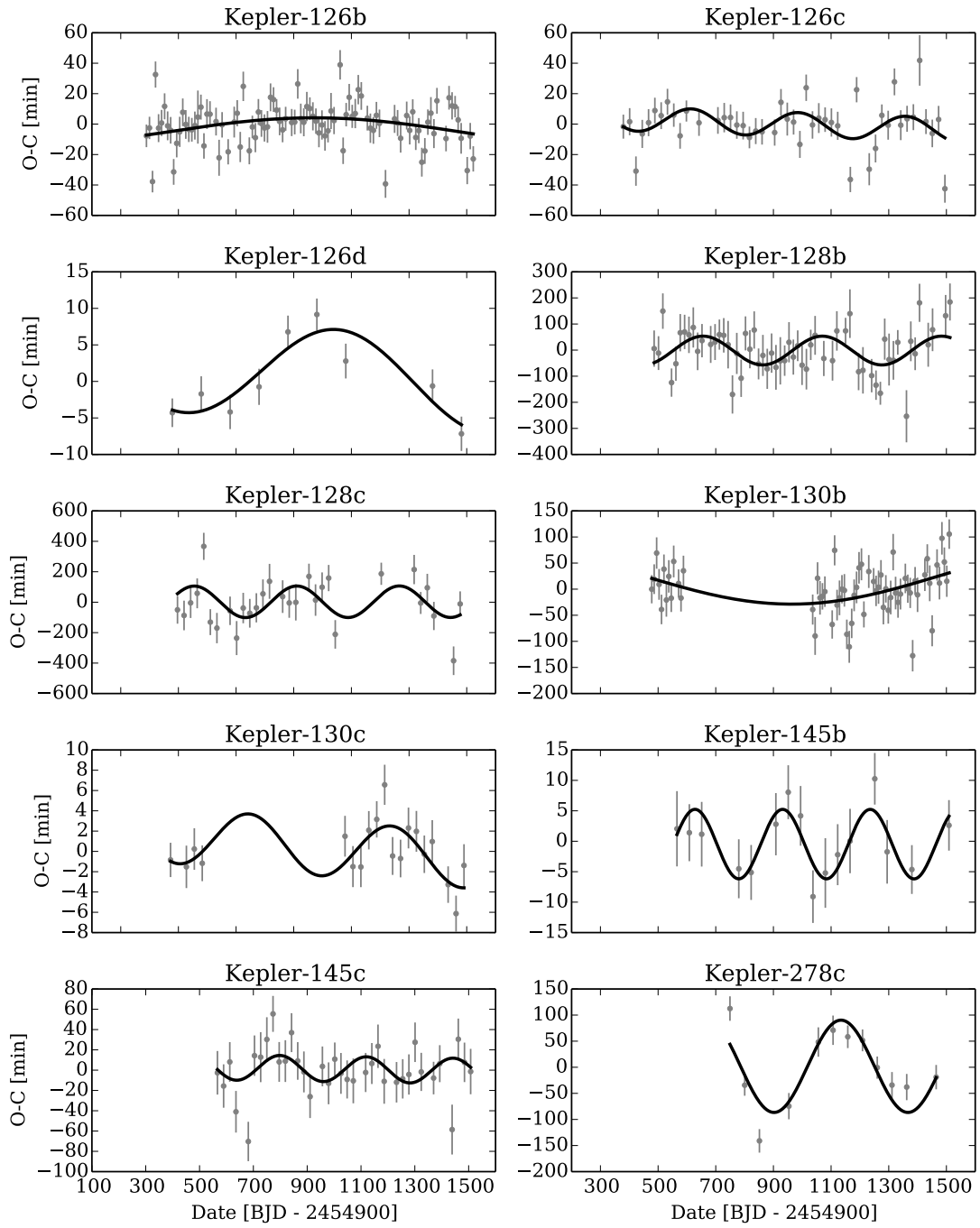

Figure 34 – (Continued) The observed minus calculated transit times are shown for systems with detected TTVs. A sinusoidal fit to the O-C times is shown.

10.4.1 *Habitability*

Earth's orbit is almost circular with a current eccentricity (e) of 0.017. The influence of the orbital eccentricity on habitability has been investigated using planet climate models (Williams and Pollard 2002; Dressing et al. 2010). Our results allow one of the first looks at the orbital eccentricities of small and potentially rocky planets and indicate that low eccentricities are the rule. In fact we can not find a clear candidate for a planet on an elliptic orbit among the 74 planets in our sample. The few planets with densities away from unity Figure 30 also have the largest uncertainties (see Table 8 for an overview).

If this extends to planets on longer orbital periods or to planets orbiting lower mass stars (the planets in our sample are all outside the habitable zone) then this influences habitability in two ways. Planets on circular orbits have more stable climates than planets on eccentric orbits which can have large seasonal variations, even though large oceans might temper the climate impact of moderate eccentricities (Williams and Pollard 2002). Secondly the location of the habitable zone itself depends on the orbital eccentricity. For moderately eccentric orbits the outer edge of the habitable zone is increased (Spiegel et al. 2010; Dressing et al. 2010; Kopparapu et al. 2013), i.e. moderately eccentric planets could be habitable further away from the host star than planets on circular planets. However our results suggest that this might not occur.

10.4.2 *Occurrence rates*

The eccentricity distribution is a key parameter needed to reliably estimate planetary occurrence rates inferred from transit surveys. This is because the transit probability depends on eccentricity (Barnes 2007). Planets on orbits with $e = 0.5$ are 33% more likely to transit, and in the extreme case of HD 80606b ($e = 0.92$) (Naef et al. 2001) the transit probability increased by 640%. A recent estimate based on the eccentricity distribution derived from RV observations shows that the overall transit probability changes by 10% (Kipping 2014b). This can significantly change the planet occurrence estimate, e.g. the number of planets smaller than 4 $R_\oplus$ around cool stars is estimated to 3% precision before the effect of eccentricity is taken into account (Dressing and Charbonneau 2013). Our analysis shows that neglecting eccentricity is a valid assumption when considering transiting multiple planet systems.

Beyond the influence on the global occurrence rate the eccentricity distribution also influences the relative occurrence between different types of planets. Because single more massive planets show a wider range of eccentricities than multi-planet systems with smaller planets, the occurrence of larger planets is overestimated compared to smaller planets. These effects are important when

comparing occurrence rates of different types of planets but have so far not been taken into account (Petigura et al. 2013; Foreman-Mackey et al. 2014).

10.5 CONCLUSIONS

We have measured the eccentricity distribution of 74 planets orbiting 28 stars, making use of photometry alone. For this we made use of the influence of eccentricity on the duration of planetary transits. Several complications are avoided by carefully selecting this sample. Planetary false positives and third light blending are sidestepped in our selection of (primarily) confirmed multi-transiting planet systems around bright host stars. Issues due to inaccurate stellar parameters are overcome owing to the power of asteroseismology to determine stellar densities and other stellar parameters. The use of short cadence data, newly derived orbital periods and a careful analysis of possible TTVs prevent a bias towards high impact parameters.

We find that most of the systems we considered are likely to reside on orbits which are close to circular. The eccentricity is well-described by a Rayleigh distribution with $\sigma = 0.049 \pm 0.013$. This is distinctly different from RV measurements (Wright et al. 2009; Latham et al. 2011; Mayor et al. 2011), possibly due to the smaller planets in our sample. It is similar to low eccentricities reported for TTV systems (Hadden and Lithwick 2014) and to the eccentricities found in the solar system.

Our findings have important consequences:

- Constraining orbital eccentricities is an important step towards understanding planetary formation. Several mechanisms for eccentricity excitation and damping have previously been suggested based on evidence of eccentric orbits from RV observations. If planet-planet scattering (Ford and Rasio 2008) is important, it appears to result in low eccentricity in systems with multiple planets, at least for those systems with low mutual inclinations. This could be related to the small planet size, the planetary multiplicity or the orbital distance, or a combination of these.

- While no Earth twins are present in our sample, our findings cover planets with small radii and a wide range of orbital periods. It seems plausible that low eccentricity orbits would also be common in solar system analogues, influencing habitability and the location of the habitable zone.

- Orbital eccentricities influence planet occurrence rates derived from transit surveys because eccentric planets are more likely to transit. Our find-

ings indicate that the transit probability of multi-planet systems is different from that of systems with single, massive planets.

- We have compared the individual eccentricity estimates with accurately determined stellar parameters, such as the stellar temperature (Huber et al. 2013b; Silva Aguirre et al. 2015) and age (Silva Aguirre et al. 2015), and found no trend. It would be interesting to compare the eccentricity measurements with measurements of stellar inclination, which might be possible using asteroseismology (e.g. Chaplin et al. 2013; Van Eylen et al. 2014; Lund et al. 2014b) for some stars in our sample.

- With circular orbits common in systems with multiple transiting planets, the stellar density can be reliably estimated from transit observations of such systems (see Chapter 5 for details). This can be used to characterize the host stars of such systems and to rule out planetary false positives. We use this to validate planets in two systems with planetary candidates (KOI-270, now Kepler-449, and KOI-279, now Kepler-450), as well as one planet in a system with previously known planets (KOI-285.03, now Kepler-92d).

- We anticipate that the methods used here will be useful in the context of the future photometry missions *TESS* (Ricker et al. 2014) and *PLATO* (Rauer et al. 2014), both of which will allow for asteroseismic studies of a large number of targets. Transit durations will be useful to confirm the validity of transit signals in compact multi-planet systems, in particular for the smallest and most interesting candidates that are hardest to confirm using other methods. For systems where independent stellar density measurements exist the method will also provide further information on orbital eccentricities.

We are grateful to Victor Silva Aguirre for making available an early version of the asteroseismic parameters to us. We thank Mikkel N. Lund for suggestions in the early stage of this work, and Josh Winn for fruitful discussions as well as suggestions on the manuscript. We are grateful for the many valuable suggestions by the anonymous referee, which have significantly improved this manuscript. We thank David Kipping, Dan Fabrycky and Daniel Huber for insightful comments and suggestions. Part of this manuscript was written at MIT and I appreciate the hospitality of the researchers and staff at the Institute for Astrophysics and Space Research. This research made use of the Grendel HPC-cluster for computations. Funding for the Stellar Astrophysics Centre is provided by The Danish National Research Foundation (Grant agreement no.: DNRF106). The research is supported by the ASTERISK project (ASTERoseismic Investigations with SONG and Kepler) funded by the European Research Council (Grant agreement no.: 267864). We acknowledge ASK for covering travels in relation to this publication.

11 ECCENTRICITY OF SINGLE-PLANET SYSTEMS

In Chapter 10, I determined that the eccentricity distribution of small transiting planets in multi-planet systems is very low, similar to the solar system, but different from the much higher eccentricities that occur for larger planets. What exactly is causing these low eccentricities? Is it the relatively small size of the planets in multi-planet systems, or is it the multiplicity that limits the range of eccentricities? To answer these questions, I now focus on the eccentricity of systems with only a single transiting planet.

The techniques used to measure the eccentricities of systems with a single transiting planets are very similar to those used for multi-planet systems in Chapter 10. As I did in the previous chapter, I focus on a subset of transiting *Kepler* planets for which the mean densities of the host stars have been measured through asteroseismology. This allows the orbital eccentricity to be measured by carefully modeling the planetary transits.

In comparison with the multi-planet systems discussed in Chapter 10, there are several additional complications for single-planet systems. The most important complication is that single-planet candidates are harder to validate statistically. This implies that any randomly selected sample of single-planet systems contains a substantial amount of unconfirmed planet candidates, carrying the risk that some of these candidates are false positives. This complicates the determination of the underlying eccentricity distribution of the planets in the sample. One way to increase the number of confirmed planets is by focusing on a subset of short-period planets, such as hot Jupiters. These objects often occur in single-planet systems, and are often confirmed as genuine planets. This is due to the fact that they are relatively easy to confirm, because of the high amplitude RV signal they induce on their stars. Unfortunately, hot Jupiters have experienced strong tidal effects, so that most such systems have nearly circular orbits.

Another complication arises in the interpretation of these results. The transit probability for any given planet is low, because only a small range of orbital inclinations result in the occurrence of transits. Consequentially, not all systems which have a single transiting planet are necessarily truly single-planet systems, because some of these systems may have additional planets which escaped detection, due to an unfavorable orbital inclination. Nevertheless, as I will show, there is some evidence that at least some of the systems with a single transiting planet are dynamically different from the compact multi-planet systems such as those discussed in Chapter 10. For the remainder of this chapter, I use the term single-planet system as a shorthand for systems

which have only a single transiting planet, regardless of the true amount of planets in the system, which is always unknown.

This chapter is structured as follows. In Section 11.1 I present the sample of *Kepler* single-planet candidates, and address the two complications raised above: the influence of false positives, and the fraction of additional, non-transiting planets. I summarize the key aspects of the method in Section 11.2. I present the results in Section 11.3, where I separate the sample in two: short-period planets which may have undergone significant tidal circularisation, and other planets which presumably have not. I also discuss constraints on the entire sample and compare with previous eccentricity measurements for other samples, such as the multi-planet systems by Van Eylen and Albrecht (2015). Finally, in Section 11.4, I discuss the findings and outline the next steps for further investigation.

11.1 SAMPLE OF "SINGLE-PLANET" SYSTEMS

I start from a sample of 64 planet candidates, for which the stellar parameters were determined in a homogeneous asteroseismic analysis by Lundkvist et al. (2015). Out of these candidates, 9 planets are excluded because they have only a few months of *Kepler* short cadence data available. For five more candidates, KOI-268, KOI-2706, KOI-2720, KOI-3165, and KOI-5086, the transit signal could not be unambiguously modeled, which may be due to the presence of a strong star spot signal, or because these candidates could be false positives. These systems warrant further investigation, however, they are excluded from our sample at this point. Out of the remaining 50 planet candidates, 16 are validated or confirmed planets, while 34 are currently planet candidates which could not yet be confirmed or falsified.

I now discuss the presence of potential false positives in Section 11.1.1, and the influence of additional non-transiting planets in Section 11.1.2.

11.1.1 *False positives*

The majority of the planet candidates in our sample, 34 out of 50, are currently unconfirmed. Nevertheless, the amount of false positives is likely low, because the general *Kepler* false positive rate is thought to be low and because our sample consists of high signal-to-noise planetary candidates, which have already undergone significant vetting.

A study of the average *Kepler* false positive rate by Morton and Johnson (2011) find it to be below 10%, while a more elaborate analysis by Fressin et al. (2013) measured it to be 9.4%. Similarly, a *Spitzer* follow-up study of *Kepler* planets found that at least 90% of the *Kepler* signals could be planetary (Désert et al. 2015).

Such numbers suggest that our sample contains only a handful of false positives, while the overwhelming majority of candidates are genuine planets. Nevertheless, the false positive rate is dependent on stellar and planetary properties. Since our sample was selected based on stellar properties, i.e. the presence of stellar oscillations, its false positive rate need not be the same as the overall false positive rate. In fact, it seems reasonable to assume that our sample has a lower than average false positive rate, because our sample consists of very bright stars, which are observed to have a false positive rate several times lower than fainter stars (Désert et al. 2015).

Furthermore, our sample has already undergone significant vetting, i.e. some false positives have already been removed. The sample selection by Lundkvist et al. (2015) already assures that only high signal-to-noise candidates are included, due to the stringent requirements on the data to achieve an asteroseismic detection. Furthermore, known false positives were not included in the sample. Because all planets in our sample are partially observed using short-cadence data, most of them were discovered relatively early during the *Kepler* mission. Consequentially, many of the systems have been targeted with follow-up studies, e.g. to detect companion stars, or rule out high-amplitude RV signals indicative of eclipsing binary stars rather than planets. To illustrate this, it is good to look at the part of our sample which was the study of a previous transit duration investigation. Sliski and Kipping (2014) analyzed the transit duration of single-planet systems in a sample of stars with asteroseismic stellar densities measured by Huber et al. (2013b). They studied 31 dwarf stars, of which 27 are also included in our sample. For the remaining 4, at least three are false positives (KOI-113, KOI-263, and KOI-1924), while one other (KOI-64) remains as a candidate, although RV follow-up observations have been unable to measure the mass of the planet and a deep secondary eclipse suggests it may be a self-luminous object (Esteves et al. 2013). This illustrates that some of the false positives, which were initially present in our sample, have already been discarded. Furthermore, as described above, five planets were removed from our analysis because their transits gave reason to doubt the candidate's validity, while all other candidates could be reliably modeled under the assumption they are genuine planets.

Therefore, we further operate under the assumption that almost all of the remaining planet candidates in our sample are genuine planets.

11.1.2 *Single-planet systems vs. multi-planet systems*

Not all single-planet candidates are truly single, because what we refer to here as single-planet systems only means that only a single planet candidate is seen transiting, while additional non-transiting planets may be present. In fact, in several cases, there is proof of additional (non-transiting) planets: six

of the candidates exhibit TTVs (see Table 10) and several of the other candidates have long-term RV variations indicative of (distant) additional planets.

The prevalence of *Kepler* multi-planet systems suggests that at least some of these systems should be observed as systems where only a single planet transits. Because the planets in such compact multi-planet systems are mutually aligned within a few degrees (e.g. Fabrycky et al. 2014; Van Eylen and Albrecht 2015), one expects to see the inner planets in such systems to transit more often than more outer planets, because the transit probability decreases with increasing orbital period.

Nevertheless, there is evidence that not all single-transiting planets can be explained by this scenario. Lissauer et al. (2011) first noted a ratio of single-transiting to multi-transiting systems that is too large to be explained by geometric considerations alone. Simulations by Hansen and Murray (2013) suggest there are roughly 50% more single-planet candidates, compared to multi-planet systems, than are predicted by in situ formation models. This suggests that these single-planet candidates either had other planets which were destroyed or were scattered to higher mutual inclinations, so they would not be seen transiting. Similarly, Ballard and Johnson (2014) find that $0.55^{+0.23}_{-0.12}$ of the single-transiting systems are either truly alone, or have additional planets with mutual inclinations larger than those seen in compact multi-planet systems. These findings imply that at least some of the single-planet systems are dynamically different from the *Kepler* multi-planet systems, although this does not prove those single-planet systems are truly alone, as they may still have misaligned, or distant companions which are not transiting.

11.2 ANALYSIS METHOD

The eccentricity of the planet candidate systems is analyzed following the procedure by Van Eylen and Albrecht (2015), which was described in detail in Section 10.2. The key aspects of the analysis are summarized here. *Kepler* short cadence observations are reduced starting from the so-called Presearch Data Conditioning (PDC) data (Smith et al. 2012), and the planetary orbital period is determined together with any potential transit timing variations (TTVs). The latter is important, as not taking into account TTVs has the potential to bias the eccentricity results (see Section 10.2.2.3). In six systems, we find TTVs. They are listed in Table 10 and shown in Figure 35.

The data are then folded, making use of the determined period and a sinusoidal TTV model when TTVs are detected, and modeled using a Markov Chain Monte Carlo (MCMC) algorithm, specifically a Affine-Invariant Ensemble Sampler (Goodman and Weare 2010) implemented in Python as `emcee` (Foreman-Mackey et al. 2013). We use the analytical equations by Mandel and

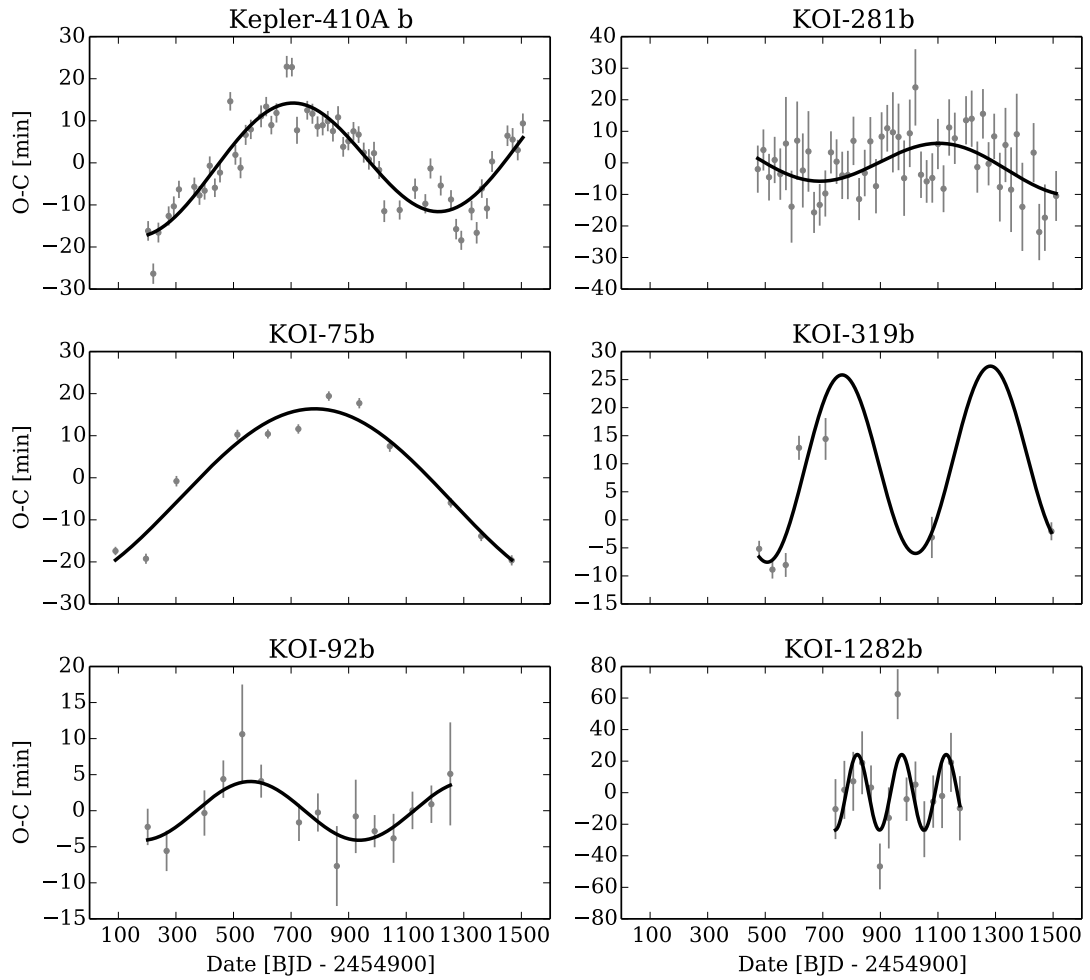

Figure 35 – The observed minus calculated transit times are shown for systems with detected TTVs. A sinusoidal fit to the O-C times is shown.

Agol (2002) to model the transit light curves. Eight parameters are sampled, i.e. the impact parameter (b), planetary relative to stellar radius ($R_p/R_\star$), two combinations of e and ω ($\sqrt{e}\cos\omega$ and $\sqrt{e}\sin\omega$), the mid-transit time (T_0), the flux offset (F), and two stellar limb darkening parameters (u_1 and u_2).

All parameters are sampled uniformly (using a flat prior), with the exception of the limb darkening coefficients for which a Gaussian prior is employed, which is centered at values predicted from a Kurucz atmosphere table (Claret and Bloemen 2011) and has a standard deviation of 0.1. We sample in $\sqrt{e}\cos\omega$ and $\sqrt{e}\sin\omega$ rather than in e and ω directly to avoid a bias due to a boundary condition at zero eccentricity (see e.g. Lucy and Sweeney 1971; Eastman et al. 2013) and convert those values into stellar density ratios used in the transit equations (see e.g. Kipping 2010; Moorhead et al. 2011; Van Eylen and Albrecht 2015).

	TTV period [d]	TTV amplitude [min]
Kepler-410A b	1055	14.4
KOI-75b	1892	21.7
KOI-92b	756	4.1
KOI-281b	884	7.1
KOI-319b	515	16.3
KOI-1282b	154	23.9

Table 10 – Overview of the period and amplitude of sinusoidal transit timing variations which were included in the modeling. The transit times and the best model fits are shown in Figure 35.

There are important correlations between the eccentricity and other parameters, which are detailed in Section 10.2.2. First of all, it is important to take into account TTVs, as is done here prior to the transit modeling. Furthermore, a correlation occurs between ω and e, such that these parameters cannot be independently determined, except when invoking statistical arguments on ω. Another important correlation occurs between e and b, an issue which in a few cases can prohibit meaningful eccentricity measurements. In both cases the MCMC algorithm takes those correlations into account. A histogram of the modes of the impact parameters for the planets in our sample is shown in Figure 36. The fact that the impact parameters appear to be roughly uniformly distributed, as expected, gives confidence that the modeling is performed as it should.

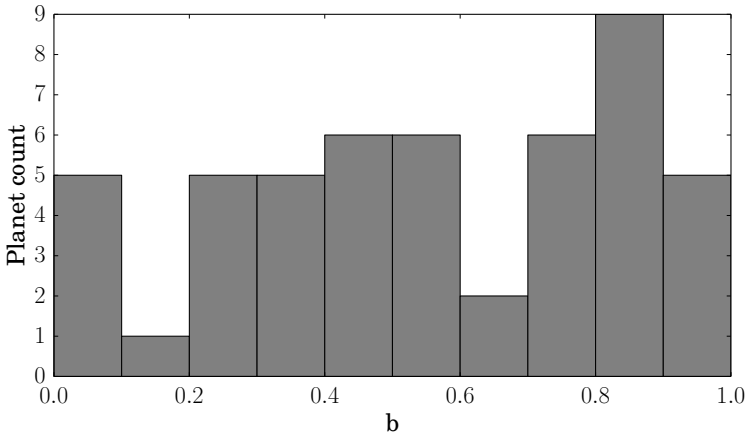

Figure 36 – A histogram showing the modal values for the impact parameter for the planet in our sample. This serves as a sanity check that the modeling is done correctly, as impact parameters should be distributed uniformly, as they indeed are.

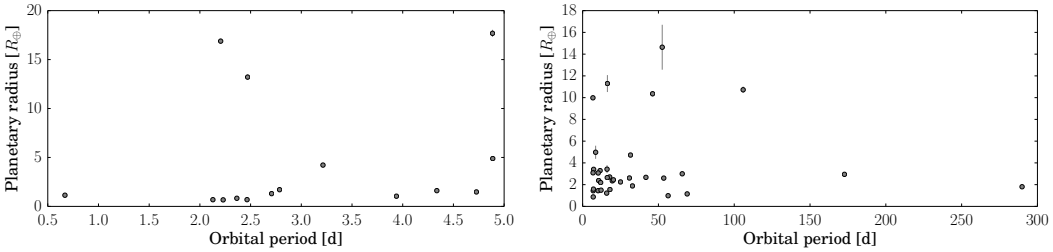

Figure 37 – The radius and period for planets in the sample. **Left:** the sample of short-period planets (P $<$ 5 days); **right:** longer period planets.

11.3 RESULTS

Because several planets in our sample have very short-period orbits, where tidal effects are strong and expected to lead to significant circularisation, I split the sample into two subsets. First, I consider the hot, short period planets, defined here somewhat arbitrarily as planets with periods lower than 5 days. They are discussed in Section 11.3.1. After that, I discuss longer-period planets in Section 11.3.2. Finally, the eccentricity distribution of single-planet systems is modeled in Section 11.3.3.

11.3.1 *Short-period planets*

The subset of our sample with periods less than 5 days consists of 15 planets. Some of those planets are hot Jupiters, while others are hot super-Earths or hot Neptunes, as shown in Figure 37.

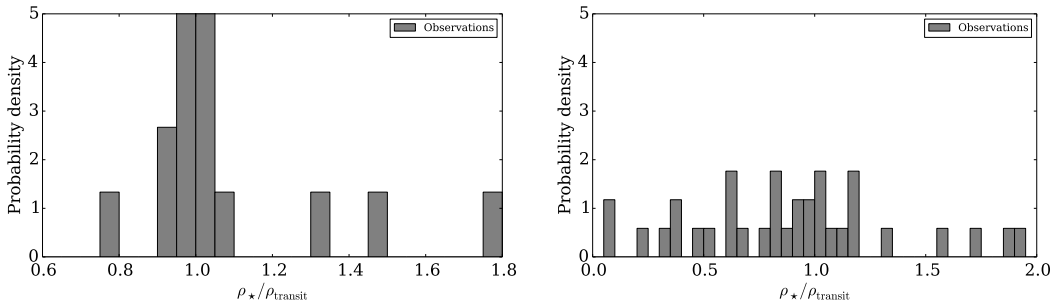

Figure 38 – A histogram indicating the measured density ratios. **Left:** short-period planets, where, as expected, most values are close to one. This indicates circularity, which is consistent with tidal effects circularising the orbits of these planets. **Right:** longer period planets, which show a wider range of density ratios, indicating a wider range of eccentricity values.

As expected, these planets generally have (close to) circular orbits because the strong tidal interaction with the host star presumably rapidly circularizes their orbits. A histogram of density ratios is shown in Figure 38. Values close to unity indicate consistency with circularity. There are four apparent ex-

ceptions: KOI-3, KOI-975, KOI-1612 and KOI-2956. For KOI-1612 (Kepler-408) and KOI-2956, the large uncertainties in the measurement are responsible for this, and allow for a large degeneracy between e and b, effectively spanning the full parameter space of both e and b at 95% confidence. HAT-P-11 (KOI-3) and Kepler-21 (KOI-975) are more interesting and are discussed below. A list of the parameters for all planet candidates is provided in Table 11.

11.3.1.1 *HAT-P-11 (KOI-3)*

HAT-P-11b is a Neptune-sized planet orbiting its star each 4.9 days. Its eccentricity is found to have a modal value at 0.09, with a 68% confidence interval of $[0.06, 0.27]$. This is small, but distinctly non-zero, as even at 95% confidence the eccentricity is found to be within $[0.06, 0.59]$, indicating that tides have not had a chance to fully circularize the orbit, or that eccentricity is being pumped into the system. HAT-P-11 is also interesting because the obliquity of the system has been measured and the orbit is found to be oblique (Winn et al. 2010b; Sanchis-Ojeda and Winn 2011).

Further evidence that the eccentricity is real is provided from RV observations, which placed the eccentricity at 0.198 ± 0.046 (Bakos et al. 2010). This value, which is fully consistent with our finding, further proves that transit durations can indeed be used to reliable measure even relatively small eccentricities.

11.3.1.2 *Kepler-21 (KOI-975)*

Kepler-21b is a super-Earth orbiting its star each 2.8 days, and as such it is expected to have a circular orbit. The modal eccentricity value is 0.26, with a 68% confidence interval placing the eccentricity at $[0.11, 0.49]$. This is surprising, given the short period, but some caution is warranted: Kepler-21 is a spotted star, complicating the measurement. In addition, the 95% confidence interval includes a circular orbit, and measures the eccentricity between $[0, 0.80]$. As a result, it is unclear at this stage whether Kepler-21 has an eccentric orbit or not.

11.3.2 *Longer period single-planet systems*

The sample of longer period planets ($P > 5$ days) consists of 35 planet candidates. The radii and periods of the sample are shown in Figure 37. The density ratio of the candidates is shown in Figure 38. In comparison to the shorter period planets, the density ratios for these planets span a wider range of values, and they do not display a clear peak around unity. This is indicative of non-circular orbits. Some interesting cases are discussed below, while a full list of parameters for all planet candidates is provided in Table 11.

Short-period systems		e (mode)	e (68%)	R_p [$R_\oplus$]	Period [d]	$M_\star$ [$M_\odot$]	$R_\star$ [$R_\odot$]	$\rho_\star$ [g/cm3]
TrES-2	KOI-1.01	0.01	[0.0, 0.1]	13.21 ± 0.28	2.47061340(20)	$0.97^{-0.08}_{0.08}$	$0.96^{-0.02}_{0.02}$	$1.54809^{-0.04226}_{0.04226}$
HAT-P-7	KOI-2.01	0.01	[0.0, 0.13]	16.88 ± 0.26	2.204735430(30)	$1.55^{-0.1}_{0.1}$	$1.99^{-0.03}_{0.03}$	$0.27891^{-0.01409}_{0.01409}$
HAT-P-11	KOI-3.01	0.09	[0.06, 0.27]	4.887 ± 0.065	4.88780240(15)	$0.86^{-0.06}_{0.06}$	$0.76^{-0.01}_{0.01}$	$2.74262^{-0.0817}_{0.0817}$
Kepler-4	KOI-7.01	0.02	[0.0, 0.21]	4.22 ± 0.12	3.21367134(91)	$1.09^{-0.07}_{0.07}$	$1.55^{-0.04}_{0.04}$	$0.40991^{-0.01831}_{0.01831}$
Kepler-93	KOI-69.01	0.02	[0.0, 0.18]	1.477 ± 0.033	4.72673930(86)	$0.89^{-0.07}_{0.07}$	$0.91^{-0.02}_{0.02}$	$1.64247^{-0.0493}_{0.0493}$
Kepler-7	KOI-97.01	0.01	[0.0, 0.15]	17.68 ± 0.36	4.8854862(12)	$1.28^{-0.07}_{0.07}$	$1.97^{-0.04}_{0.04}$	$0.23665^{-0.01409}_{0.01409}$
Kepler-21	KOI-975.01	0.26	[0.11, 0.49]	1.707 ± 0.043	2.78581(10)	$1.27^{-0.08}_{0.08}$	$1.85^{-0.03}_{0.03}$	$0.28454^{-0.0155}_{0.0155}$
Kepler-407	KOI-1442.01	0.02	[0.0, 0.3]	1.141 ± 0.041	0.6693127(60)	$1.02^{-0.07}_{0.07}$	$1.02^{-0.02}_{0.02}$	$1.34384^{-0.03522}_{0.03522}$
Kepler-408	KOI-1612.01	0.67	[0.47, 0.87]	0.689 ± 0.017	2.465024(17)	$1.02^{-0.07}_{0.07}$	$1.21^{-0.02}_{0.02}$	$0.8156^{-0.02536}_{0.02536}$
	KOI-1618.01	0.03	[0.0, 0.33]	0.828 ± 0.049	2.364388(32)	$1.29^{-0.09}_{0.09}$	$1.5^{-0.03}_{0.03}$	$0.53669^{-0.02395}_{0.02395}$
	KOI-1883.01	0.14	[0.0, 0.36]	1.304 ± 0.072	2.707295(36)	$1.09^{-0.18}_{0.18}$	$1.48^{-0.07}_{0.07}$	$0.46767^{-0.02676}_{0.02676}$
	KOI-1890.01	0.07	[0.0, 0.32]	1.609 ± 0.046	4.336422(31)	$1.18^{-0.07}_{0.07}$	$1.54^{-0.02}_{0.02}$	$0.45217^{-0.0155}_{0.0155}$
	KOI-1964.01	0.13	[0.0, 0.37]	0.668 ± 0.029	2.2293226(85)	$0.93^{-0.11}_{0.11}$	$0.88^{-0.03}_{0.03}$	$1.89744^{-0.05775}_{0.05775}$
	KOI-2792.01	0.04	[0.0, 0.35]	0.684 ± 0.052	2.128229(24)	$0.99^{-0.15}_{0.15}$	$1.3^{-0.06}_{0.06}$	$0.63107^{-0.02958}_{0.02958}$
	KOI-2956.01	0.04	[0.0, 0.45]	1.04 ± 0.11	3.93800(32)	$1.51^{-0.21}_{0.21}$	$1.98^{-0.08}_{0.08}$	$0.27609^{-0.03522}_{0.03522}$
Long-period systems		e (mode)	e (68%)	R_p [$R_\oplus$]	Period [d]	$M_\star$ [$M_\odot$]	$R_\star$ [$R_\odot$]	$\rho_\star$ [g/cm3]
Kepler-410	KOI-42.01	0.2	[0.14, 0.43]	2.704 ± 0.045	17.833613(47)	$1.22^{-0.07}_{0.07}$	$1.35^{-0.02}_{0.02}$	$0.70009^{-0.02958}_{0.02958}$
Kepler-22	KOI-87.01	0.38	[0.0, 0.45]	1.806 ± 0.029	289.8655(19)	$0.85^{-0.05}_{0.05}$	$0.83^{-0.01}_{0.01}$	$2.12704^{-0.05916}_{0.05916}$
Kepler-14	KOI-98.01	0.11	[0.05, 0.32]	9.98 ± 0.20	6.7901237(20)	$1.34^{-0.08}_{0.08}$	$2.02^{-0.04}_{0.04}$	$0.2282^{-0.01409}_{0.01409}$
Kepler-95	KOI-122.01	0.39	[0.26, 0.56]	3.290 ± 0.094	11.5230844(97)	$1.12^{-0.08}_{0.08}$	$1.45^{-0.04}_{0.04}$	$0.5226^{-0.01831}_{0.01831}$
Kepler-96	KOI-261.01	0.39	[0.31, 0.58]	2.647 ± 0.088	16.2384819(93)	$1.03^{-0.1}_{0.1}$	$0.94^{-0.03}_{0.03}$	$1.73967^{-0.05071}_{0.05071}$
Kepler-432	KOI-1299.01	0.41	[0.29, 0.62]	14.635 ± 2.066	52.5018(11)	$1.69^{-0.6}_{0.6}$	$4.51^{-0.63}_{0.63}$	$0.02536^{-0.00423}_{0.00423}$
Kepler-409	KOI-1925.01	0.05	[0.0, 0.42]	1.148 ± 0.048	68.95825(29)	$0.95^{-0.08}_{0.08}$	$0.9^{-0.02}_{0.02}$	$1.82419^{-0.05353}_{0.05353}$
	KOI-75.01	0.02	[0.0, 0.18]	10.72 ± 0.29	105.88162(75)	$1.32^{-0.07}_{0.07}$	$2.58^{-0.07}_{0.07}$	$0.10847^{-0.00986}_{0.00986}$
	KOI-92.01	0.37	[0.26, 0.69]	3.00 ± 0.13	65.70453(17)	$1.08^{-0.11}_{0.11}$	$1.05^{-0.03}_{0.03}$	$1.31567^{-0.03803}_{0.03803}$

KOI-107.01	0.11	[0.0, 0.3]	3.406 ± 0.097	7.257038(45)	$1.2^{-0.08}_{0.08}$	$1.6^{-0.04}_{0.04}$	$0.41132^{-0.01831}_{0.01831}$
KOI-118.01	0.23	[0.0, 0.4]	2.248 ± 0.088	24.99337(21)	$1.01^{-0.07}_{0.07}$	$1.36^{-0.04}_{0.04}$	$0.56205^{-0.02395}_{0.02395}$
KOI-257.01	0.02	[0.0, 0.21]	3.088 ± 0.082	6.8834081(26)	$1.23^{-0.1}_{0.1}$	$1.2^{-0.03}_{0.03}$	$1.00577^{-0.03803}_{0.03803}$
KOI-269.01	0.03	[0.0, 0.46]	1.549 ± 0.047	18.01181(12)	$1.33^{-0.08}_{0.08}$	$1.45^{-0.02}_{0.02}$	$0.62262^{-0.03381}_{0.03381}$
KOI-273.01	0.04	[0.0, 0.35]	2.38 ± 0.094	10.573754(12)	$1.15^{-0.11}_{0.11}$	$1.1^{-0.03}_{0.03}$	$1.20439^{-0.0324}_{0.0324}$
KOI-276.01	0.44	[0.01, 0.47]	2.67 ± 0.20	41.746009(97)	$1.05^{-0.07}_{0.07}$	$1.19^{-0.02}_{0.02}$	$0.88603^{-0.02536}_{0.02536}$
KOI-280.01	0.1	[0.0, 0.35]	2.190 ± 0.068	11.872877(11)	$1.03^{-0.09}_{0.09}$	$1.04^{-0.02}_{0.02}$	$1.28186^{-0.03803}_{0.03803}$
KOI-281.01	0.14	[0.09, 0.62]	2.350 ± 0.077	19.556464(62)	$0.81^{-0.11}_{0.11}$	$1.38^{-0.04}_{0.04}$	$0.43245^{-0.02536}_{0.02536}$
KOI-288.01	0.17	[0.07, 0.43]	3.073 ± 0.052	10.275375(31)	$1.41^{-0.08}_{0.08}$	$2.09^{-0.03}_{0.03}$	$0.21693^{-0.00986}_{0.00986}$
KOI-319.01	0.02	[0.0, 0.22]	10.356 ± 0.249	46.15113(37)	$1.29^{-0.06}_{0.06}$	$2.08^{-0.04}_{0.04}$	$0.20144^{-0.01268}_{0.01268}$
KOI-367.01	0.77	[0.73, 0.84]	4.72 ± 0.15	31.578671(12)	$1.11^{-0.09}_{0.09}$	$1.03^{-0.03}_{0.03}$	$1.43822^{-0.03662}_{0.03662}$
KOI-374.01	0.04	[0.0, 0.53]	2.947 ± 0.064	172.70681(75)	$0.88^{-0.06}_{0.06}$	$1.15^{-0.02}_{0.02}$	$0.80715^{-0.03099}_{0.03099}$
KOI-674.01	0.27	[0.21, 0.49]	11.29 ± 0.78	16.338888(59)	$1.27^{-0.22}_{0.22}$	$2.78^{-0.19}_{0.19}$	$0.08311^{-0.00563}_{0.00563}$
KOI-974.01	0.14	[0.0, 0.32]	2.60 ± 0.06	53.50593(20)	$1.21^{-0.08}_{0.08}$	$1.85^{-0.04}_{0.04}$	$0.26905^{-0.0169}_{0.0169}$
KOI-1282.01	0.04	[0.0, 0.39]	2.611 ± 0.095	30.8633(10)	$1.08^{-0.07}_{0.07}$	$1.59^{-0.03}_{0.03}$	$0.37611^{-0.0169}_{0.0169}$
KOI-1314.01	0.34	[0.03, 0.5]	4.98 ± 0.60	8.57522(22)	$1.69^{-0.5}_{0.5}$	$3.88^{-0.43}_{0.43}$	$0.04085^{-0.00423}_{0.00423}$
KOI-1537.01	0.06	[0.0, 0.35]	1.445 ± 0.074	10.19233(54)	$1.31^{-0.09}_{0.09}$	$1.79^{-0.03}_{0.03}$	$0.3254^{-0.01409}_{0.01409}$
KOI-1613.01	0.33	[0.03, 0.5]	1.221 ± 0.064	15.86631(51)	$0.99^{-0.08}_{0.08}$	$1.34^{-0.03}_{0.03}$	$0.58036^{-0.02395}_{0.02395}$
KOI-1621.01	0.43	[0.09, 0.59]	2.44 ± 0.11	20.30895(73)	$1.22^{-0.08}_{0.08}$	$1.93^{-0.04}_{0.04}$	$0.23947^{-0.0155}_{0.0155}$
KOI-1962.01	0.81	[0.61, 0.96]	1.88 ± 0.11	32.85861(58)	$1.04^{-0.07}_{0.07}$	$1.5^{-0.04}_{0.04}$	$0.4395^{-0.01972}_{0.01972}$
KOI-2390.01	0.63	[0.37, 0.85]	3.42 ± 0.37	16.1046(12)	$1.38^{-0.5}_{0.5}$	$2.68^{-0.25}_{0.25}$	$0.10142^{-0.02395}_{0.02395}$
KOI-2462.01	0.06	[0.0, 0.35]	1.491 ± 0.083	12.14533(70)	$1.19^{-0.1}_{0.1}$	$1.71^{-0.04}_{0.04}$	$0.33244^{-0.0155}_{0.0155}$
KOI-2545.01	0.03	[0.0, 0.37]	1.441 ± 0.071	6.98156(21)	$1.38^{-0.07}_{0.07}$	$2.16^{-0.04}_{0.04}$	$0.19298^{-0.01127}_{0.01127}$
KOI-2632.01	0.19	[0.0, 0.39]	1.588 ± 0.089	7.12836(47)	$1.37^{-0.17}_{0.17}$	$2.16^{-0.07}_{0.07}$	$0.19157^{-0.02395}_{0.02395}$
KOI-2801.01	0.03	[0.0, 0.37]	0.87 ± 0.061	6.99180(16)	$1.12^{-0.17}_{0.17}$	$1.45^{-0.06}_{0.06}$	$0.51274^{-0.02676}_{0.02676}$
KOI-3168.01	0.23	[0.14, 0.57]	0.982 ± 0.074	56.383(45)	$1.03^{-0.16}_{0.16}$	$1.55^{-0.07}_{0.07}$	$0.3916^{-0.02536}_{0.02536}$

Table 11 – Determined parameters for the short-period (top) and long-period planet candidates in our sample. The stellar parameters ($M_\star$, $R_\star$ and $\rho_\star$) are from Lundkvist et al. (2015).

11.3.2.1 *Kepler-410 (KOI-42)*

The Kepler-410 system consists of a transiting planet on a 17.8 day orbit, and an additional planet, which is revealed by transit timing variations (see Figure 35), as well as a nearby companion star. The system was discussed at length in Chapter 4. We find the orbit to be eccentric, with a modal value of 0.2 and a 68% confidence interval of $[0.14, 0.43]$. This is fully consistent with the findings by Van Eylen et al. (2014), although in that case the TTVs were modeled using a zigzag-shaped model rather than the sinusoidal model employed here (see Chapter 4).

11.3.2.2 *Kepler-14 (KOI-98)*

Kepler-14b is a Jupiter-sized planet on a 6.8 day orbit which is found to be slightly eccentric (with a 68% confidence interval of $[0.05, 0.32]$). However, a close examination of the system reveals that care needs to be taken interpreting these measurements, because a nearby companion star, which is only 0.5 magnitudes fainter, contributes a significant fraction of the flux (Buchhave et al. 2011). This influences the measured radii, but also has the potential to influence the eccentricity determination through its influence on the transit shape. This implies that this system should be remodeled after correcting for the flux dilution, and caution is warranted interpreting the current findings.

11.3.2.3 *Kepler-95 (KOI-122)*

Kepler-95b is a super-Earth orbiting with a period of 11.5 days. With a 68% confidence interval for eccentricity of $[0.26, 0.56]$, the planet's orbit is distinctly eccentric. The planet was confirmed by RV follow-up observations, which measured its mass to be 13.0 ± 2.9 $M_\oplus$ (Marcy et al. 2014). This measurement implies a low density for the planet, which must have a large fraction of volatiles. No companion stars were detected. We note that due to the low RV amplitude, this planet was fitted assuming a circular orbit. Now that the transit provides evidence for a non-circular orbit, it may be interesting to fit the transit and the RV observations together to improve the estimate.

11.3.2.4 *Kepler-96 (KOI-261)*

Kepler-96b is a super-Earth with an orbital period of 16.3 days, and we find a relatively large eccentricity with a 68% confidence interval of $[0.31, 0.58]$. Its mass was measured by Marcy et al. (2014) to be 8.46 ± 0.22 $M_\oplus$. A companion star was also detected by Marcy et al. (2014), but this object is 7 magnitudes fainter and consequentially unlikely to influence our measurement. The RV signal was modeled assuming a circular orbit, and it may be interesting to reanalyze the RV data allowing for an eccentric planetary orbit.

It is further of interest that Hirano et al. (2012) find the star to be oriented pole-on, by comparing the rotation period from *Kepler* photometry to spectroscopic $v \sin i$ measurements, suggesting that perhaps the high obliquity and relatively high eccentricity have a common origin.

11.3.2.5 *Kepler-432 (KOI-1299)*

Kepler-432b is a Jupiter-sized planet orbiting its host star with a period of 52.5 days. The star itself is evolved and has a radius of 4.5 $R_\odot$. We find an eccentricity of 0.41, with a 68% confidence interval at $[0.29, 0.62]$.

This system was the object of three recent and simultaneous studies, which monitored the RV signal of the star. This resulted in planetary mass estimates of 4.87 ± 0.48 M_J (Ciceri et al. 2015), 5.84 ± 0.05 M_J (Ortiz et al. 2015), and $5.41^{+0.32}_{-0.18}$ M_J (Quinn et al. 2015). These authors also constrained the eccentricity to respectively 0.535 ± 0.030, 0.478 ± 0.004, and $0.5134^{+0.0098}_{-0.0089}$, measurements which are fully consistent with our findings.

Quinn et al. (2015) also measured the stellar parameters using asteroseismology, and used the stellar density to constrain the eccentricity from the transit photometry, in a method that is similar to what is employed here. From this, they find the eccentricity to be $0.507^{+0.039}_{-0.114}$, which is consistent with our measurement. Notably, it appears the stellar spin is well aligned with the orbit of the planet (Quinn et al. 2015). Finally, a long-period planet companion was also detected from RV observations, orbiting with a period of 406 days (Quinn et al. 2015).

11.3.2.6 *KOI-367*

KOI-367b is a Neptune-sized planet candidate orbiting its host star each 31.6 days. We find a very high eccentricity, with a modal value of 0.77 and a 68% confidence interval of $[0.73, 0.84]$. Adding to the interest of the system, Hirano et al. (2012) find that the star's spin-orbit is likely misaligned. Nevertheless, a word of caution is required since this object is currently a planet candidate, so that the very short transit duration may be indicative of a false positive rather than a high eccentricity. RV follow-up observations of this system may be able to confirm the planet's presence, as well as measure its mass and refine its eccentricity measurement.

11.3.2.7 *KOI-674*

KOI-674b is a Jupiter-sized planet candidate orbiting its host star in 16.3 days. We find a modal eccentricity value of 0.27, and a 68% confidence interval of $[0.21, 0.49]$, indicating that the orbit of this planetary candidate deviates significantly from circularity. An alternative explanation for the measured stellar

density and transit properties is that this object is a false positive. RV observations may be able to confirm or falsify this candidate.

11.3.3 *Eccentricity distribution*

We now attempt to determine the eccentricity distribution of transiting single-planet systems. We established in Section 11.1 that our sample likely consists of a large majority of real planets, with not more than a few false positives. Some of these candidates may be part of compact multi-planet systems, while the others are part of a different set of planets, which are either alone or have distant or significantly misaligned additional planets.

By looking at the eccentricity distribution, we find additional evidence that (some of) the single-planet systems are different from the multi-planet systems. By comparing the density ratios of the (long-period) candidates in Figure 38 with those for the multi-planet systems determined by Van Eylen and Albrecht (2015), which are shown in Figure 30, it is immediately clear that the two distributions are different. From all multi-planet systems presented in Chapter 10, there are no examples which are clearly eccentric. By contrast, in the sample presented in Table 11, there are numerous examples of clearly eccentric cases, including some confirmed planet cases such as Kepler-95, Kepler-410, and Kepler-432.

To make this more quantitative, we fit the eccentricity of the distribution in the same manner as described in Section 10.3.1 for multi-planet systems. We find that the best-fitting Rayleigh parameter for the long-period, single-planet systems is $\sigma = 0.248 \pm 0.067$. This value is significantly different from what is found for multi-planet systems, which is described by a Rayleigh function with $\sigma = 0.049 \pm 0.013$.

In Figure 39, we show the determined eccentricities as a function of period and compare with the solar system, with RV measurements for exoplanets, and with transiting exoplanets with eccentricities determined by Van Eylen and Albrecht (2015). Distinctly higher eccentricities are apparent for the single-planet systems than for the previously determined multi-planet systems. Qualitatively, the single-planet systems appear similar to the eccentricity distribution of RV planets. Quantitatively, the eccentricity distribution of the latter can be reasonably well described by a Rayleigh distribution with $\sigma = 0.3$, although more complicated distributions are usually used to model the RV eccentricity distribution (Jurić and Tremaine 2008).

It is also instructive to plot the eccentricity as a function of mass, which is what is done in Figure 40. The masses for the transiting planets are estimated based on their radii following Weiss et al. (2013) and Weiss and Marcy (2014).

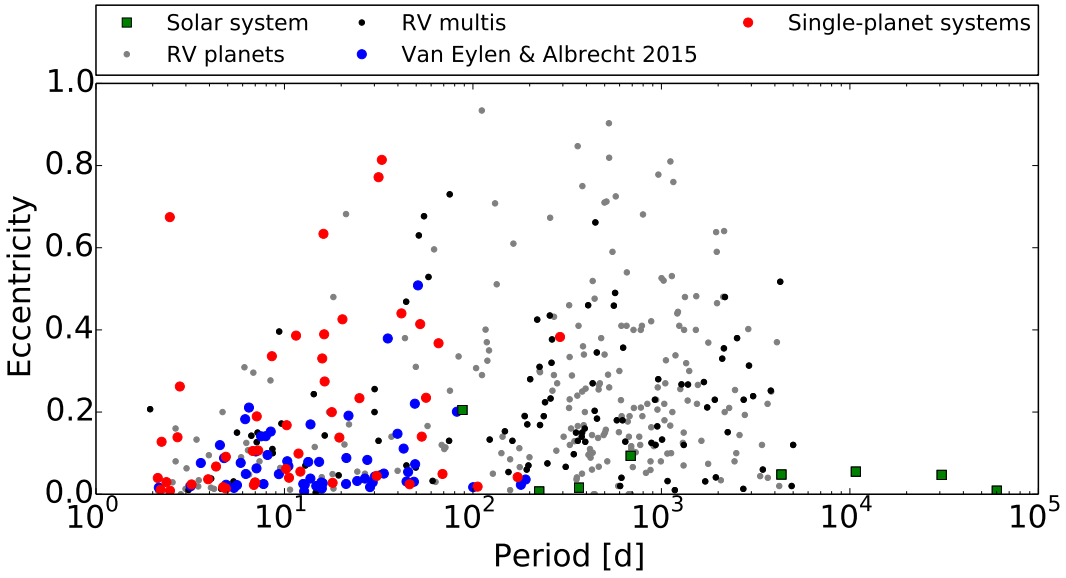

Figure 39 – The eccentricity and period measurements for exoplanets are plotted as taken from exoplanets.org on 27 April 2015, for planets where both values are determined. Planets which are flagged as multi-planet systems are highlighted. For comparison, the solar system is shown. The eccentricities of multi-planet systems determined by Van Eylen and Albrecht (2015) are shown in blue (see Section 10.3.1). The eccentricities of the planets in our sample are plotted in red. Error bars are omitted for clarity.

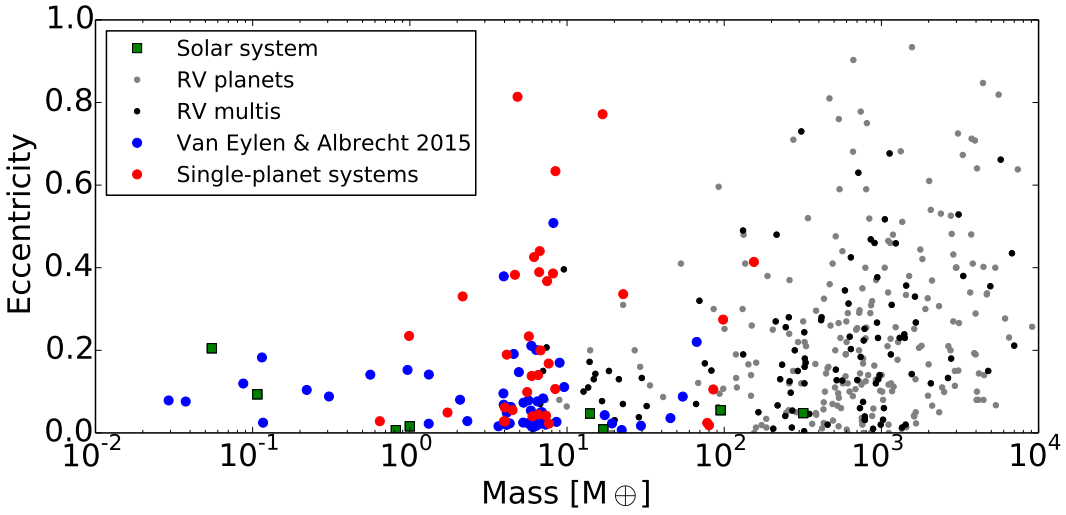

Figure 40 – The eccentricity and mass measurements for exoplanets are plotted as taken from exoplanets.org on 27 April 2015, for planets where both values are determined. Planets which are flagged as multi-planet systems are highlighted. For comparison, the solar system is shown. The eccentricities of multi-planet systems determined by Van Eylen and Albrecht (2015) are shown in blue (see Section 10.3.1). The eccentricities of the planets in our sample are plotted in red, with their mass estimated based on radius (Weiss et al. 2013; Weiss and Marcy 2014), and only the planets with orbital periods longer than five days are plotted. Error bars are omitted for clarity.

Here, it is clear that the single-planet systems on average consist of higher-mass planets than the transiting multi-planet investigated by Van Eylen and Albrecht (2015), while RV observations have been used to determine the eccentricities of planets that are even more massive. The figure suggests a trend of increasing eccentricity with increasing mass, which may enhance the eccentricity difference between single-planet and multi-planet systems.

11.4 DISCUSSION

In this chapter I have measured the eccentricity of *Kepler* single-planet candidates, making use of accurate stellar densities determined by Lundkvist et al. (2015), in combination with a careful modeling of the transit photometry. I find that the eccentricity distribution can be modeled using a Rayleigh distribution with $\sigma = 0.248 \pm 0.067$, which points towards significantly higher eccentricities than for a similar sample of multi-planet systems, which were modeled in Chapter 10 with a Rayleigh distribution with $\sigma = 0.049 \pm 0.013$.

Since I argue that the false positive rate of planets in this sample is low, this provides further evidence that single-planet systems are a sample that is distinct from multi-planet systems, rather than consisting exclusively of aligned multi-planet systems of which only one planet is seen transiting. Nevertheless, single-planet systems are defined here as having a single planet which transits, which does not imply that no other planets may be present in the system. Indeed, for six planets I find TTVs indicating the presence of at least one additional planet.

There are several possible interpretations for these findings. A first option is that the compact multi-planet systems analysed in Chapter 10 are only stable at very low eccentricities (see e.g. Pu and Wu 2015), so that the very low observed eccentricities for these systems is the result of an observational bias, in which only systems which are dynamically stable are observed. The single-planet systems are, on average, more massive than the multi-planet systems (see e.g. Latham et al. 2011). Consequently, it is also possible that the different eccentricity distribution is related to a difference in mass distribution, or that both have a common cause.

Another interpretation is that planet-planet scattering causes excitation of eccentricity as well as increases the mutual inclination, so that additional planets in systems with a single transiting planet are present, but do not transit because of their different inclination angle. In this picture, multi-planet systems would not have undergone strong scattering effects, so that their orbits have remained mutually aligned and nearly circular. Evidence for lower obliquities for multi-planet systems as compared to single planet systems (Albrecht

et al. 2013; Morton and Winn 2014) speaks in favor of this theory.

It would be useful to attempt to detect additional planets present in the single-planet systems, as well as measure the inclinations of these planets. The latter is generally quite difficult for non-transiting planets. One possibility may be for single-planet systems in which TTVs are detected, and where an analysis of the TTV signal, possibly in combination with RV follow-up, may be able to determine the mass and inclination of additional planets.

Modeling the eccentricity using a Rayleigh distribution, as is done here, is illustrative but may not be fully adequate. To model the eccentricity distribution based on RV planets, some authors have suggested using a Rayleigh distribution in combination with an exponential function (Shen and Turner 2008), while others have advocated the use of a Beta function (Kipping 2013b). It may be useful to model the planets discussed here using these distributions, and compare the models to find out which model represents the data most adequately.

Although the different distribution in eccentricity for single-planet systems and multi-planet systems is unlikely to be caused by false positives, it would still be useful to investigate the false positive ratio of planets in this sample in more detail. Even beyond measuring the overall false positive ratio, it would be useful to attempt the measurement of the RV signal of some of the most interesting planet candidates in this sample, which would be able to confirm them as genuine planets, measure their masses and further constrain their eccentricities. The different eccentricity distribution between single-planet and multi-planet systems proves that not all single-planet systems are comparable in architecture those with multiple transiting planets, but because of geometric considerations at least some of the former systems are likely to be multi-planet systems of which only the inner planet is observed to transit. As a result, it would be useful to model the eccentricity of single-planet systems using a distribution which allows for a subset of the planets to follow the multi-planet eccentricity distribution derived by Van Eylen and Albrecht (2015). Such a hybrid distribution may even be able to constrain the fraction of planets that are part of that category.

12 ECCENTRICITY OF BINARY STARS

The final scientific chapter of this thesis deals with eclipsing binaries rather than with transiting exoplanets. From an observational point of view, there are many similarities between the two, and both can be observed using *Kepler* data. Because eclipsing binaries consist of two bright bodies eclipsing each other, rather than a star and a dark planet, usually a primary and secondary eclipse are observed rather than a single 'primary' transit. In this chapter, I constrain the eccentricity of binary star systems from the relative timing of their primary and secondary eclipses.

This line of research has a direct connection with dynamics of exoplanets. As outlined in Section 8.3, the obliquity of hot Jupiters appears to be correlated with stellar temperature. Stars hotter than approximately 6250 K display a wider range of obliquities than stars cooler than this temperature (Winn et al. 2010a; Albrecht et al. 2012b). This trend is sometimes attributed to the difference in stellar structure, because hot stars have radiative outer layers while cool stars have convective outer layers, and the latter may be more tidally efficient.

If it is true that the stellar structure causes hot stars to be less efficient at tidally aligning nearby exoplanets, a similar effect should be seen in binary stars. In addition, tidal effects not only work to align bodies, but also to circularize orbits. Therefore, measuring the eccentricity of both hot and cool stars may be a way to compare the tidal efficiency of both groups of stars.

Eclipsing binaries reveal the eccentricity through the relative transit durations of both eclipses, and through their relative timing. The latter proves to be easier to measure, and more reliable, but only provides information on $e \cos \omega$. Fortunately, there are thousands of known eclipsing binaries observed by *Kepler*, so that statistical statements can be made by comparing groups of binaries rather than individual systems. Even so, complications can arise, such as the fact that hot stars are on average younger than cool stars, giving those stars less time to circularize.

The results of the investigation described here point towards a small but measurable difference in eccentricity distribution between hot and cool stars, which is attributed to a combination of age effects and tidal efficiency. The work presented in this chapter is currently unpublished, but is structured in the form of a manuscript that can be used as a draft for a future publication.

Orbital circularization of hot and cool Kepler eclipsing binaries

Vincent Van Eylen, Joshua N. Winn & Simon Albrecht

The rate of tidal circularization is predicted to be faster for relatively cool stars with convective outer layers, compared to hotter stars with radiative outer layers. Before *Kepler* it was difficult to observe this effect clearly, due to the lack of large homogeneous samples of binaries including both hot and cool stars. Here we seek evidence for the predicted dependence of circularization upon stellar type, using a sample of 802 eclipsing binaries observed by *Kepler*. For each binary we measure $e \cos \omega$ based on the relative timing of the primary and secondary eclipses. We examine the distribution of $e \cos \omega$ as a function of period for binaries composed of hot stars, cool stars, and mixtures of the two types. Hot-hot binaries are more likely to be eccentric at the shortest periods, in agreement with theoretical expectations based on both the weaker dissipation and younger ages of hot stars. For hot-hot, hot-cool, and cool-cool binaries, respectively, significant eccentricities occur only for periods greater than 3.63 ± 0.89 d, 4.95 ± 0.49 d, and 6.74 ± 0.42 d.

12.1 INTRODUCTION

Binary stars make up over half of all stars in the universe, and their orbital properties have been studied for many decades (see, e.g. Kopal 1956). In close binary systems, tidal forces distort the shapes of stars and cause oscillations. The gradual dissipation of energy associated with those fluid motions ultimately leads to coplanarization and synchronization of rotational and orbital motion, as well as circularization of the binary orbit (see, e.g., Mazeh 2008, and references therein).

One interesting aspect of tidal circularization theory is that the dissipation rate is a very strong function of the orbital semi-major axis, and thereby on the orbital period (see, e.g., Zahn 1975). Many efforts have been made to determine the so-called "cut-off period" (see, e.g., Mayor and Mermilliod 1984), which characterizes the transition between mainly-circular and mainly-eccentric orbits. It has also been suggested that the cut-off period can serve as a proxy for age in star clusters (Mathieu and Mazeh 1988), and indeed there is evidence for a linear trend between the cut-off period and the age of binary stars in different clusters (e.g. Meibom and Mathieu 2005).

Another interesting aspect of the theory is that the circularization timescale is also predicted to depend strongly on stellar type. Stars with thick exterior convective zones are expected to experience more rapid tidal dissipation than

stars with mainly-radiative exteriors (Zahn 1975). On the main sequence, the transition between the convective and radiative regimes occurs at a photospheric effective temperature of approximately 6250 K. For simplicity we will refer to stars as "cool" or "hot" depending on whether the effective temperature is lower or higher than this nominal boundary.

The literature does provide some evidence for the expected dependence of the cut-off period on stellar type, but mainly through the comparison of different samples that have been analyzed in different ways. This is at least partly because cool stars and hot stars have been studied by different communities using different techniques. For hot stars, Giuricin et al. (1984) found circularization below a period of 2 days for a sample of about 200 binary stars, which is seemingly consistent with the tidal friction theory of Zahn (1977). A similar result was arrived at more recently by Khaliullin and Khaliullina (2010), who compiled a catalogue of about 100 eclipsing binaries from different sources. For cool stars, Koch and Hrivnak (1981) investigated binaries with periods shorter than 20 days, and found reasonable agreement with theory. Abt (2006) collected eccentricities for cool stars and find cut-off periods at around 4 days. Pourbaix et al. (2004) maintain a large catalog of eclipsing binaries including both hot and cool stars, but the catalog is an inhomogeneous concatenation of various sources, and does not lend itself to statistical studies.

Our interest in this topic was heightened by some recent developments in exoplanetary science. The obliquities of the host stars of close-in giant planets have been observed to have different distributions for hot and cool stars (Winn 2010; Albrecht et al. 2012b). It has been proposed that these differences are due to tidal dissipation, perhaps in conjunction with magnetic braking (Dawson et al. 2014). Investigating these possibilities led us to search the literature for clear observational evidence of the dependence of tidal dissipation rates on effective temperature, where we encountered the apparent inhomogeneity of previous studies.

Exoplanetary science has also provided a new opportunity to perform a more homogeneous study. The NASA *Kepler* mission (Borucki et al. 2010) was designed to find transiting planets, and also discovered thousands of eclipsing binaries (Prša et al. 2011; Slawson et al. 2011). The *Kepler* photometry can be used to precisely determine one component of orbital eccentricity: $e \cos \omega$, the product of the eccentricity and the cosine of the argument of pericenter, which is related to the relative timing of the primary and secondary eclipses. The measured eclipse durations can also be used to determine $e \sin \omega$, though this is less straightforward. These photometric constraints on eccentricity are much easier to obtain than the task of measuring the orbital eccentricity through radial-velocity monitoring (see, e.g., Mazeh et al. 2006). Slawson et al. (2011) modeled a large number of *Kepler* EBs but the results for eccentricity

were not reliable, presumably because their neural-network approach was designed to measure many different properties for a wide variety of binary stars, and was not trained specifically to determine eccentricities.

Here, we employ a simpler method to measure $e \cos \omega$ reliably, based only on the relative timing of the primary and secondary eclipses. We combine these measurements with published effective temperatures for the binary components (Armstrong et al. 2014) to divide our sample into hot-hot, hot-cool, and cool-cool binaries. We then compare the observed $e \cos \omega$–period diagrams for these different categories of EBs.

This paper is organized as follows. Section 12.2 provides the basic theoretical expectations for the differences between the samples, based not only on different tidal dissipation rates but also on systematic differences in stellar age. Section 12.3 describes our sample, and measurement techniques. Section 12.4 presents the results, and Section 12.5 discusses these results in light of the theoretical expectations.

12.2 THEORETICAL EXPECTATIONS

The observed eccentricity of an EB depends on its initial eccentricity, the rate of tidal circularization, and the time interval over which circularization has taken place, i.e., the age of the system. For simplicity we assume that the initial eccentricity distribution is broad and is the same for binaries of all types (although we are not aware of any firm observational support for this latter assumption). Thus, in our model, any differences in eccentricity distributions between samples of EBs come from differences in tidal dissipation rates and ages.

To calculate the expected timescales for tidal circularization for convective stars (τ_{conv}) and for radiative stars (τ_{rad}), we follow Claret and Cunha (1997) and use the formulas

$$\tau_{circ,\,conv} = (1.99 \times 10^3 \text{ yr}) M^3 \frac{(1+q)^{5/3}}{q} L^{-1/3} \lambda_2^{-1} \frac{P^{16/3}}{R^{22/3}} \tag{12.1}$$

and

$$\tau_{circ,\,rad} = (1.71 \times 10^1 \text{ yr}) M^3 \frac{(1+q)^{5/3}}{q} E_2^{-1} \frac{P^7}{R^9}, \tag{12.2}$$

where M and R are the total stellar mass and radius in solar units, q is the mass ratio of the two stars, and L is the total luminosity relative to the Sun's luminosity. For simplicity we assume the main-sequence relations $L \propto M^{3.9}$ and $R \propto M^{0.8}$, and we set $q = 1$. We use representative values for E_2 and λ_2 (Claret and Cunha 1997, ; see their Figures 1 and 3). We can now calculate the

circularization timescale for convective and radiative stars of different masses and periods.

As for the age, our estimate is based on the simple and approximate main-sequence relationship, $\tau_\star = (10^{10}\ \mathrm{yr})(M/M_\odot)^{-2.9}$. While ages of individual *Kepler* EBs are typically unknown, on average the hot stars are expected to be systematically more massive, faster-evolving, and younger, giving them less time for tidal dissipation to circularize their orbits.

We can now calculate the relative circularization time $\tau_{\mathrm{circ}}/\tau_\star$ as a function of period for different systems. Figure 41 shows some illustrative results. For values of $\tau_{\mathrm{circ}}/\tau_\star$ greatly exceeding unity, we expect to observe a broad distribution of eccentricities because the lifetime of the system is too short to have allowed for significant circularization. For values of $\tau_{\mathrm{circ}}/\tau_\star$ well below unity, the opposite is true, and we expect most binaries to have circular orbits.

According to the results of this rough calculation, we should expect to find a critical circularization period for cool stars in the neighborhood of 5 days ($\log P = 0.7$). For hot stars we should find a shorter circularization period depending more strongly on mass, ranging from about 1.3 days for 10 $M_\odot$ to 3 days for 2 $M_\odot$.

To isolate the theoretical effect of tidal dissipation, as opposed to stellar age, Figure 41 shows the results after setting $\tau_\star$ equal to the Hubble time for all cases. Here there are no relative age effects at play. By comparing the two panels in this figure we see that the effect of age is important for the most massive stars (which are on average the youngest). For the hot stars, replacing the stellar age with the much longer Hubble time results in longer circularization periods. Thus, in this simple picture, stars with a mass of 5 $M_\odot$ have a similar tidal dissipation rate as cooler, lower-mass stars with thick convective zones, but we should nevertheless observe such stars to have a shorter circularization period because of their younger ages. For even more massive stars the age effect becomes even more dominant. For the case of 10 $M_\odot$, the circularization period actually *exceeds* that of the cooler stars. On the other hand, for stars of mass 2 $M_\odot$, age effects are much less important. This is understandable, since the typical lifetime of such stars is only a few times shorter than that of subsolar mass stars.

These theoretical considerations show that for the purpose of observing the specific dependence of tidal dissipation rates on stellar type, it is important to focus on stars that are not too massive (too hot). We are thereby led to limit our sample to $M \leqslant 3\ M_\odot$. Since $T_{\mathrm{eff}}/T_{\mathrm{eff},\odot} \approx \sqrt{M/M_\odot}$ on the main sequence, this is achieved by restricting $T_{\mathrm{eff}} \leqslant 10,000$ K.

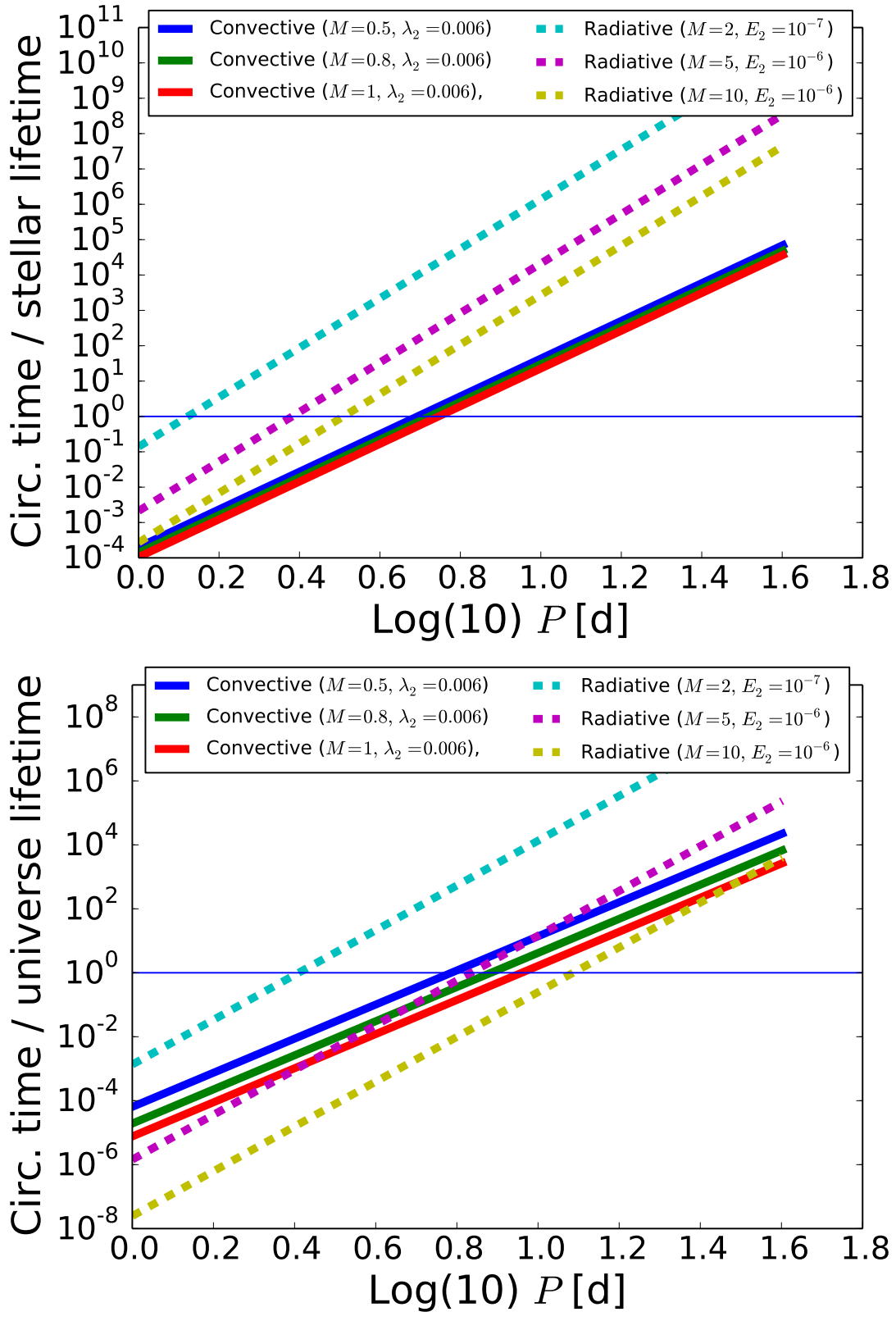

Figure 41 – Top: The circularization time scales for convective (Equation 12.1) and radiative (Equation 12.2) stars, divided by the typical lifetime of such a star. Numbers above unity indicate that most of these systems haven't had time to circularize, while numbers below unity indicate a circularization timescale shorter than the lifetime of the system. **Bottom:** Rather than dividing by the stellar lifetime, we have now divided by the age of the universe. If the most massive stars would live this long, they would circularize up to longer periods than they do, but stars of a few solar masses are much less affected.

12.3 METHODS

12.3.1 *Measuring* $e \cos \omega$

To create our sample we begin with the EB catalog by Slawson et al. (2011), of which the latest updated version is available online[1]. We use the periods given in this catalog. We rely on the effective temperatures for the primary and secondary stars, T_1 and T_2, that were determined by Armstrong et al. (2014) by fitting the observed spectral energy distributions. As described in Section 12.2, we descrict our sample to $T_{\rm eff} \leqslant 10,000$ K. To measure $e \cos \omega$, we determine the times of primary and secondary eclipses, using the procedure described below.

The *Kepler* observations are separated into different quarters (Q), each representing about three months of data. The data from each quarter is provided in three separate files, each containing one month of data. Our starting point is the pre-search data conditioning (PDC) photometry, from which some of the instrumental trends have been removed (Smith et al. 2012). For normalization, we divide the flux data from each month by the mean monthly flux level. The data is then folded based on the period reported in the Villanova EB catalog (Slawson et al. 2011), and the orbital phase data are binned by a factor of 50.

Subsequently we determine the times of the primary and secondary eclipses. We do so as follows: first, we locate the approximate time of the deepest eclipse (t_1). The time interval containing this eclipse is then ignored, and we determine the approximate time of the second eclipse (t_2). We determine the precise times by fitting a second-order polynomial function of time to the data near minimum light. We then find $e \cos \omega$, using

$$e \cos \omega \approx \frac{\pi(t_2 - t_1)}{2P} - \pi/4 \tag{12.3}$$

where P is the orbital period[2] The method is illustrated in Figure 42.

We apply this method to all stars in the EB catalog (Slawson et al. 2011). However, for subsequent analysis we only use the EBs with periods longer than 2 days. Below this period, not all binaries are detached, which complicates the measurements. For the non-detached binaries tidal effects are expected to be so strong that circularity should anyhow be expected.

In some cases, our automated method fails to pick up the correct eclipse times due to data artifacts. In other cases there are no secondary eclipses,

1 http://keplerebs.villanova.edu/, accessed on 9 March 2015.

2 Note that this equation is only approximate and correction factors apply for high eccentricity; see e.g. Sterne (1940).

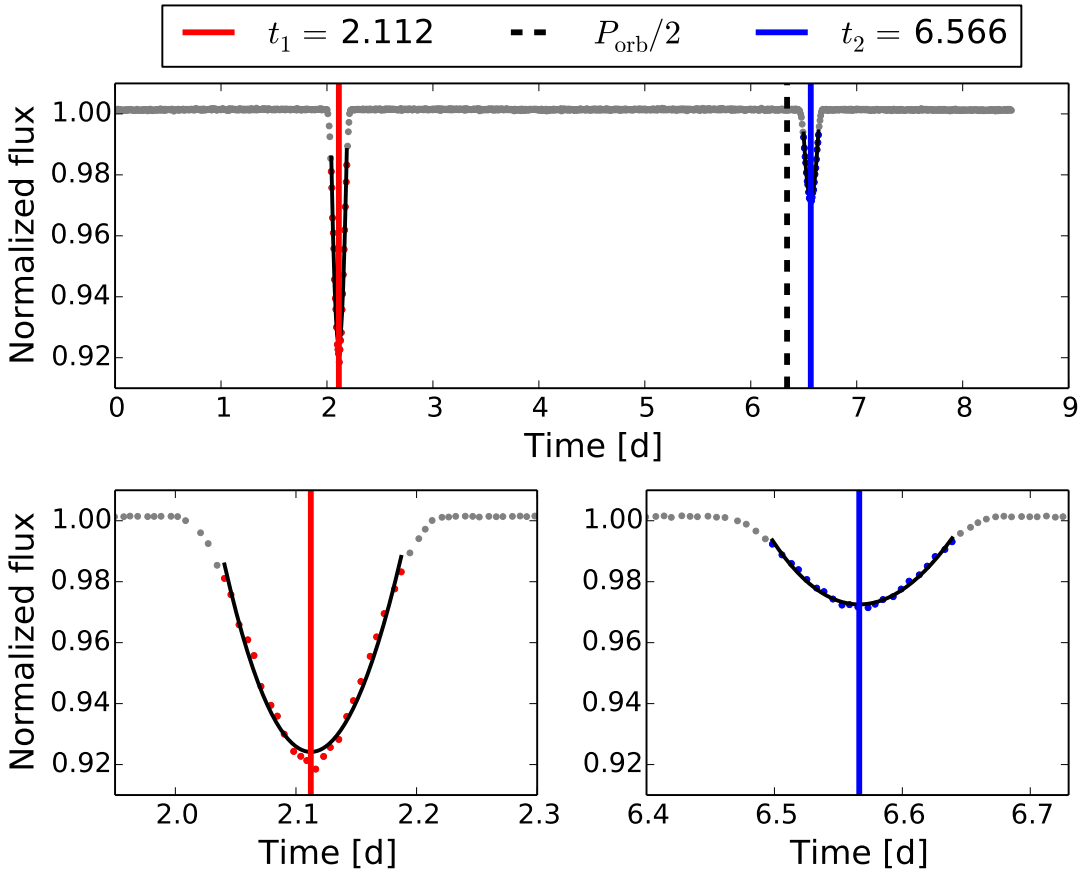

Figure 42 – Example showing how to find the primary and secondary eclipse times. The colored data points are used to determine the best transit time fit, which is indicated by full vertical lines. The dotted vertical line indicates where the secondary transit would be expected in case of circularity. The bottom panels show a zoom of the primary and secondary eclipses.

or no primary eclipses. We remove these cases from consideration, through visual inspection of all the folded light curves. We do not think that these omissions produce any significant bias relating to stellar effective temperature, although we caution that highly eccentric binaries are more likely to only show either primary or secondary eclipses, which means the overall distribution of $e \cos \omega$ (for all stellar temperatures) may be biased towards lower values.

12.4 RESULTS

The main result of our analysis are measurements of $e \cos \omega$ that are associated with the previously determined orbital period P (from Slawson et al. 2011) and the stellar temperatures of the two components (from Armstrong et al. 2014). Figure 43 shows the measurements of $e \cos \omega$ as a function of P, with the color of each circle encoding the effective temperatures of the components. We use 6250 K as the boundary between hot and cool stars, as stars

hotter than this temperature are expected to have mainly radiative outer layers. A binary is designated "hot-hot" if both stars have estimated effective temperatures exceeding this boundary value. Likewise, "cool-cool" binaries have two cooler stars, and "hot-cool" binaries have one hot star and one cool star. We present results for 109 hot-hot binaries, 234 hot-cool binaries and 459 cool-cool binaries.

Figure 43 shows that the distribution of $e\cos\omega$ is roughly symmetric around zero, as would be expected for a uniform random distribution of ω, the argument of pericenter. At the shortest periods, it is clear that most binaries are circular or nearly circular. The spread in eccentricity increases with increasing orbital period. This is consistent with what is expected from tidal circularization at short periods, and with previous studies of other samples.

To investigate any potential differences between the three different subsamples, we fit for the cut-off period P_0, i.e. the period beyond which eccentric binaries are observed to occur. For this we fit the functional form devised by Meibom and Mathieu (2005):

$$\begin{aligned} e(P) &= 0 && \text{for } P \leqslant P_0 \\ e(P) &= \alpha\left[1 - e^{0.14(P_0 - P)}\right] && \text{for } P > P_0 \end{aligned} \tag{12.4}$$

Although Meibom and Mathieu (2005) used the value $\alpha = 0.35$, we adopt $\alpha = 0.35(2/\pi) \approx 0.22$ because we are fitting the distribution of $|e\cos\omega|$ rather than eccentricity.[3] The resulting fits for hot-hot, hot-cool and cool-cool EBs are shown in Figure 43. We find the best-fit cut-off periods to be 3.63 ± 0.89 d, 4.95 ± 0.49 d, and 6.74 ± 0.42 d for hot-hot, hot-cool, and cool-cool systems, respectively.

Figure 44 shows the fraction of EBs that are significantly eccentric, within different period bins. In this analysis, significant eccentricity is defined as $e\cos\omega \geqslant 0.02$. The error bars displayed on the bins represent only the uncertainty due to Poisson (counting) statistics. It is clear that beyond 10-15 days, the large majority of binaries are eccentric regardless of the temperature. At shorter periods, this is not the case. The fraction of eccentric binaries decreases with decreasing period, and it does so at different rates for different temperature classes: the hot-hot binaries have a greater fraction of eccentric systems at a given period, down to the shortest periods examined.

Based on Figure 41 we expected that cool-cool binaries would be mainly circular below ≈5 days ($\log P = 0.7$), with the precise "cut-off" period almost independent of stellar mass. For hot-hot binaries we expected that for periods exceeding 2-3 days ($\log P = 0.3 - 0.5$), some systems could remain

3 For a uniform random distribution in ω, the expectation value of $|\cos\omega|$ is $2/\pi$.

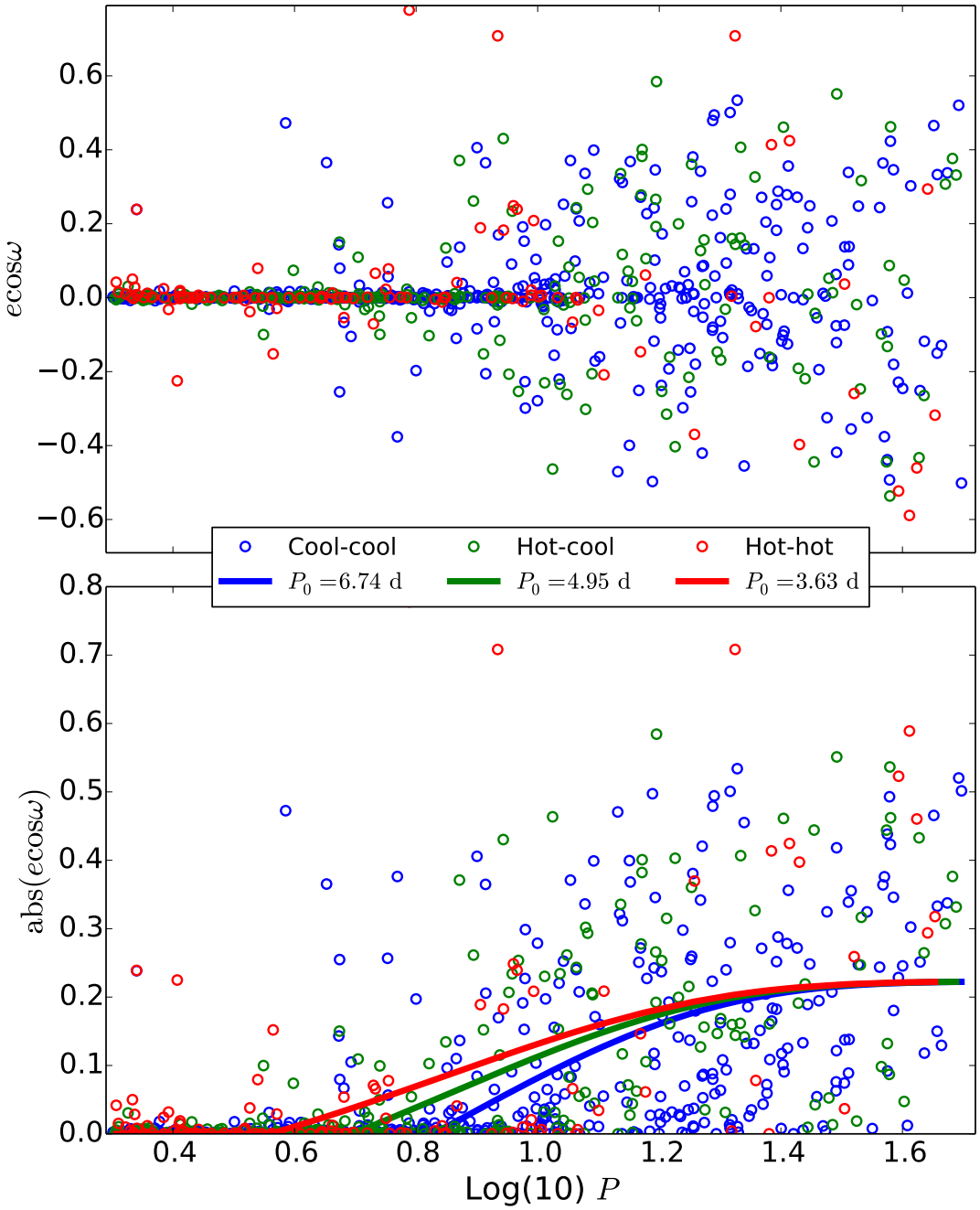

Figure 43 – Measurements of $e\cos\omega$ as function of orbital period. The red circles represent "hot-hot" binaries in which both stars have $T_{eff} > 6250$ K. Blue circles are for "cool-cool" binaries, and green circles are for binaries with one hot star and one cool star. The lines illustrate the cut-off period for the different categories, using Equation 12.4, and are fitted to $|e\cos\omega|$.

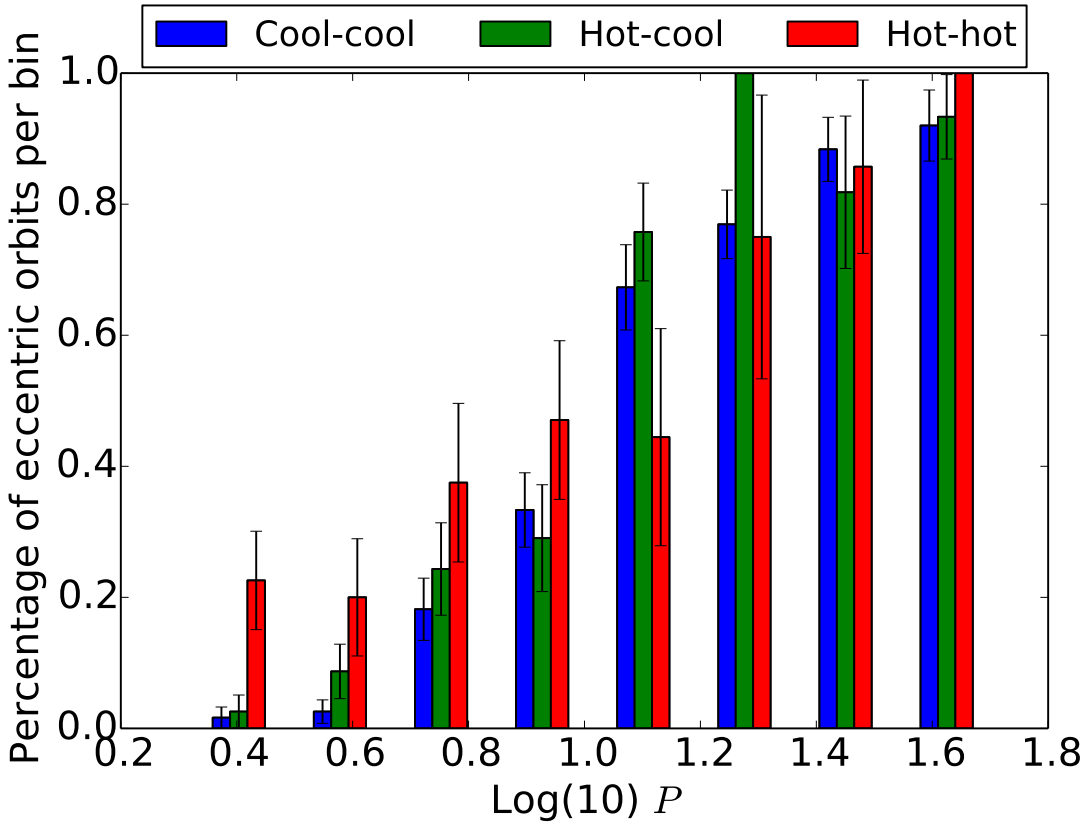

Figure 44 – The fraction of eccentric binaries $e \cos \omega \geqslant 0.02$ in (logarithmic) period bins, divided in hot-hot, hot-cool and cool-cool binaries using the same criteria as for Figure 43.

eccentric, with the precise cut-off period depending more strongly on stellar mass, leading to a greater scatter. This are indeed the trends that are observed in Figure 44.

12.5 DISCUSSION

This work represents an attempt to compare the degree to which tidal circularization has taken place in binaries with hot and cool stars, using a large and homogeneous sample of *Kepler* eclipsing binaries. The observations displayed in Figure 43 and Figure 44 agree remarkably well with the predictions in Figure 41, despite the obvious limitations and simplicity of our crude theoretical calculations.

This suggests that we have indeed detected the dependence of orbital circularization on stellar type, due to the combination of age effects and differing tidal dissipation rates. The observations alone cannot tell us which of these two factors — age or tidal dissipation — is more important. However, as pointed out in Section 12.2, for stars cooler than about 10,000 K, age effects are not expected to be dominant; the main effect should be tidal dissipation

rates. Another suggestion that the differences in cut-off periods between the samples cannot be caused exclusively by differences in age is provided by the "mixed" binaries. In these cases one of the stars is hot and therefore evolving rapidly, causing these binary systems to be systematically younger than cool-cool binaries. Thus, in terms of age, the mixed binaries should be comparable to the hot-hot systems. However, we observe their eccentricity fraction at short periods to be lower than that of the hot-hot systems, which (in our admittedly simple framework) can only be explained by the higher tidal dissipation rate of the cool component in these systems.

Despite the advantages of a homogeneous and relatively large sample, there are also important limitations of our study. Rather than eccentricity itself, we chose to focus on $e \cos \omega$, because this parameter is so readily determined from the existing *Kepler* photometry. After some preliminary efforts, we abandoned the attempt to measure $e \sin \omega$, which can in principle be derived from the relative duration of the primary and secondary eclipses. We found that such measurements are considerably more complicated to make reliably, due to the covariance of this parameter with the semi-major axis, orbital inclination, and limb-darkening parameters. Even in favorable cases the precision in $e \sin \omega$ is typically an order of magnitude worse than in $e \cos \omega$. Nevertheless, it is likely that the measurements of both $e \cos \omega$ and $e \sin \omega$ can be improved upon for individual systems of interest. In addition, radial-velocity observations could be undertaken to validate these determinations.

Another important caveat related to the input data is that we did not take into account the uncertainties in the stellar temperatures given by Armstrong et al. (2014). In some cases the uncertainties are substantial: the mean uncertainty for primary stars is 370 K. Undoubtedly some of the objects in our sample have been misclassified. This situation will improve after the EBs are studied spectroscopically.

There are also some issues to keep in mind regarding the theoretical interpretation. As pointed out in Section 12.2, we have assumed the initial eccentricity distribution is the same for all stellar types, which is not necessarily the case. In addition, we do not generally know the age of individual binary stars. At this point we can only make general statements about systematic differences between our samples. In some cases the individual system ages could be derived from isochrone fitting, asteroseismology or gyrochronology, although deriving ages for all EBs in the sample would require a considerable effort. Furthermore, in our interpretation we have assumed that all stars in our sample are on the main-sequence, by using the scaling relations presented in Section 12.2. This is certainly not the case in reality, particularly for the hotter and faster-evolving stars.

We have attributed the differences in the eccentricity distribution, in part, to tidal effects, using simplified equations drawn from equilibrium and dynamical tidal circularization theory, as brought forward by Zahn (1975). In reality, the tidal circularization efficiency is probably itself a function of stellar evolution, i.e. it is not necessarily the same throughout the evolution of the system. We have furthermore neglected the possibility of additional stars in the systems, which may affect the eccentricity in individual cases (Mazeh and Shaham 1979). The probability of having third bodies is itself a (decreasing) function of orbital period (Tokovinin et al. 2006). It may be interesting to analyze the shortest-period binaries with non-zero eccentricities, to see if they can be explained by the presence of a third companion.

Despite this long list of limitations, we have shown in a relatively direct and homogeneous manner that the eccentricity distribution of hot-hot and cool-cool binaries are significantly different as a function of orbital period. This is likely caused by a combination of the different age of the systems and a different tidal circularization efficiency. We anticipate that more detailed studied of (subsamples of) the *Kepler* EB sample will further constrain tidal circularization theory. We also expect our findings to be of interest in the context of tidal theory for stellar obliquities in double star systems (e.g. Albrecht et al. 2014) and in exoplanet systems (e.g. Winn 2010; Albrecht et al. 2012b) as well as for exoplanet eccentricities (e.g. Van Eylen and Albrecht 2015).

We thank Kevin Schlaufman and Saul Rappaport for helpful comments and suggestions. Part of this manuscript was written at MIT and VVE appreciates the hospitality of the researchers and staff at the MIT Kavli Institute for Astrophysics and Space Research. Work by JNW was partly supported by funding from the NASA Origins program (grant ID NNX11AG85G). Funding for the Stellar Astrophysics Centre is provided by The Danish National Research Foundation (Grant agreement no.: DNRF106). The research is supported by the ASTERISK project (ASTERoseismic Investigations with SONG and Kepler) funded by the European Research Council (Grant agreement no.: 267864). We acknowledge ASK for covering travels in relation to this publication.

13 CONCLUSIONS AND OUTLOOK

In this chapter I draw a few main conclusions about the work presented in this thesis. Which questions have been answered? What has been learned? This thesis has contributed some new pieces to a puzzle, which eventually will lead to a detailed knowledge of alien planets. Most importantly, this chapter aims at placing this thesis into context, linking it to existing exoplanet knowledge and showing directions for future research.

The discussion is centered on a few different topics which form the core of this thesis. I start by focusing on exoplanet discovery and characterization, which was the topic of the first part of this thesis. Subsequently, I discuss the results on exoplanet dynamics presented in the second part of this thesis. I continue by discussing the role of asteroseismology in the context of exoplanets. Finally, I argue that exoplanet research will move towards brighter, more nearby systems, which is good news for research focusing on exoplanet interiors and atmospheres.

FROM DISCOVERY TO CHARACTERIZATION AND BACK AGAIN

Despite a growing number of planet detections, not all categories of planets are equally represented among these discoveries. The radial velocity method is sensitive to planetary mass and has discovered mostly massive planets. The transit method, which has discovered the majority of planets during the past years, is sensitive to planet size, but space-based photometry has allowed detections of planets as small as Earth. However, the detection of a transit is not enough to claim the discovery of a new planet since some transits are false positives, e.g. when they are caused by a background eclipsing binary star. Typically, planet candidates are confirmed or validated using RV follow-up measurements, or making use of statistical arguments.

The latter have been particularly powerful for planets where TTVs are seen (e.g. Steffen et al. 2013), or for multi-planet systems (e.g. Lissauer et al. 2014), which have been validated as genuine planets in large numbers (Rowe et al. 2014). By contrast, only 73 out of more than 1000 currently confirmed *Kepler* exoplanets are known as single-planet systems. Interesting but complicated cases, such as planets orbiting stars that are part of binary or multiple systems, are often left as unconfirmed planetary candidates. This hampers the study of such objects. In this thesis, I've employed two separate methods to validate such 'complicated cases'.

The first method uses transit observations in two colors to determine which of two unresolved stars is being transited (see Chapter 4). This method relies on the fact that in different wavelength bands, the blending of two different stars is different, causing the transit depth to change depending on the star at which the transit occurs. This method is particularly suited to distinguish between two well-known, but spatially nearby, host stars, such as Kepler-410A and Kepler-410B (Van Eylen et al. 2014). A similar technique was used more generally to constrain the overall false-positive rate of a sample of 51 *Kepler* stars with *Spitzer* observations (Désert et al. 2015), and *Spitzer* transit measurements have been previously used to aid confirmation of *Kepler* planets (e.g. Fressin et al. 2011; Ballard et al. 2011; Barclay et al. 2013).

The second validation method developed in this thesis relies on transit durations and carefully measured stellar densities, in combination with knowledge of the eccentricity distribution of planets. Here this method was used to validate six new planets, all in multi-planet systems (see Chapter 5, and Van Eylen and Albrecht 2015). For five of these planets, orbiting Kepler-449 and Kepler-450, the reason they had not been previously validated is the presence of a companion star. This highlights one of the most powerful features of the method: distinguishing between different potential host stars. In the future, the method may prove useful to help validate interesting long-period planets, e.g. those which may be habitable. Such planets are the hardest to confirm, due to their long periods and shallow transits, which typically results in a low signal-to-noise ratio as well as a low RV amplitude. Here, constraints on the transit duration may provide crucial additional information to aid the validation.

Key to these studies is that apart from the discovery of new planets, the host stars are well-characterized leading to accurate planetary parameters. In this context, I have also investigated the detailed characteristics of *Kepler* observations (see Chapter 6 and Van Eylen et al. 2013). Transiting planets do not generally reveal their mass. I have performed a radial velocity (RV) follow-up study to measure the masses, and thereby mean densities, of three planets observed transiting by *K2* (Chapter 7 and Van Eylen et al. 2015).

Takeaway 1.

During the last few years, many new planets have been discovered, and the total number of known exoplanets has doubled during the last two years only, placing the current count at nearly 2000 exoplanets. In Part I of this thesis, I have contributed to this through the discovery of seven new transiting planets. At least as important is the characterization of these planets and their host stars, something for which I have employed asteroseismology. I have also worked on a radial velocity (RV) study to characterize planetary masses and bulk densities.

DYNAMICS OF SMALL EXOPLANETS

The solar system has a pancake structure, with planets orbiting on mutually aligned and mostly circular orbits, while the Sun's rotation is also aligned to a few degrees with the orbital plane of the planets. For hot Jupiter systems, this is not generally true, as the orbital and stellar rotation angular momentum vectors are not always aligned. Misaligned planets (having a high obliquity) are more common for hot stars, possibly because these stars have radiative outer layers such that tidal effects, resulting in alignment, are slower (Winn et al. 2010a; Albrecht et al. 2012b).

A handful obliquity measurements for multi-planet systems have become available during the last few years, using a variety of methods such as the Rossiter-McLaughlin effect, gravitational darkening, spot-crossing and most recently asteroseismology. Such measurements are important because they have the ability to distinguish between competing theories which can explain the observed obliquity measurements: if obliquity is primordial (i.e. an outcome of planet formation) then multi-planet systems should have a similar obliquity distribution as hot Jupiters, whereas if it is caused by migration and planet-planet interactions multi-planet systems are expected to mostly be aligned. In this thesis I measured the inclination of the multi-planet system Kepler-410A to be consistent with a low obliquity (see Chapter 9).

Another dynamical parameter is the eccentricity of planetary orbits. The solar system planets have low eccentricities, while (large) planets observed using the RV method exhibit a wide range of eccentricities, from almost perfectly circular orbits to extremely eccentric ones. Using transit durations, I measured the eccentricity of small planets. In multi-planet systems, I find a very low eccentricity, based on a sample of 74 planets (see Chapter 10, and also Van Eylen and Albrecht 2015). I also presented first results from my study of systems with single, small transiting planets. They also display low eccentricities, albeit significantly higher than for systems with multiple transiting planets (see Chapter 11).

For the interpretation of the obliquity and eccentricity measurements, it is important to understand the tidal forces which are working in these systems. For this reason, I set out to measure the difference in eccentricity distribution for 802 hot and cool binary stars whose eclipses are observed with *Kepler* (see Chapter 12). Hotter stars (here using a boundary of ≈ 6250 K) have radiative outer layers, while cool stars have significant convective outer layers, such that the latter are expected to exhibit stronger tidal forces. I observe a difference in eccentricity distribution between hot and cool binary stars, consistent with what is expected from simple theoretical considerations. However, the interpretation of this measurement is complicated by systematic age differences between hot and cool stars in the sample.

Despite the limited amount of measurements, the current obliquity and eccentricity observations suggest a trend, in which multi-planet systems resemble the solar system, with relatively circular orbits and aligned host stars. This is in contrast with systems with large planets, which can exhibit a wide range of eccentricities and obliquities. However, with very few measurements currently available it is hard to draw reliable conclusions. In addition, in comparison to the solar system, the multi-planets which were studied have relatively short orbital periods.

Asteroseismology has been successful to measure obliquities in a few cases, but does not immediately provide a way forward. The *Kepler* data are unlikely to yield many more asteroseismic inclination measurements of (main-sequence) planet host stars, and the upcoming *K2* and TESS datasets are not ideally suited for such measurements. One avenue forward may be further Rossiter-McLaughlin measurements, in particular on *K2* and TESS systems with bright host stars, which are easier to observe using ground-based instruments. For further eccentricity measurements, transit surveys will provide eccentricities on a larger scale when brighter host stars are observed, because the stellar bulk density of these stars will generally be well-constrained. However, these measurements will be limited to the relatively short period planets that *K2* and TESS will mainly find. In the more distant future, the PLATO mission will likely provide a wealth of new planets suitable for both eccentricity and obliquity studies.

Takeaway 2.

During the past two decades dynamical studies have revealed striking differences between the solar system and exoplanets, such as misaligned exoplanet systems and exoplanets on highly eccentric orbits. However, such studies have mostly been restricted to systems with large, heavy planets. In the last few years, focus has shifted towards smaller planets – the topic of Part II of this thesis. I have measured the obliquity of Kepler-410A, one of only a handful of multi-planet systems for which the obliquity has been measured. Furthermore, I have measured the eccentricity of small transiting planets in multi-planet systems and found a very low eccentricity, similar to the solar system, but different from what was previously found for more massive exoplanets. For systems with a single (small) transiting planet, my first results indicate an eccentricity which is low, but distinctly higher than for multi-planet systems. Finally, to study the effects of tides, I compared the eccentricity distribution of hot and cool binary stars, and found evidence for a difference, as expected from tidal circularization theory.

ASTEROSEISMOLOGY IN THE EXOPLANET ERA

Throughout both parts of this thesis, I have made extensive use of asteroseismology. Here, I summarize how I have employed asteroseismology to contribute to exoplanet science.

I have used asteroseismology for the characterization of host star properties to help characterize the planet(s). Asteroseismology has been widely applied to do so: using *Kepler* observations, it has been used to measure accurate stellar radii and masses for hundreds of stars (e.g. Huber et al. 2013b), resulting in accurate planet radii from transits, and accurate planet masses when star-planet mass ratios are available from RV follow-up observations. Although other methods are available to measure stellar masses or radii, asteroseismology can do so with an accuracy of a few percent, routinely outperforming other methods. In this thesis, the mass of Kepler-410 was measured to a 3% accuracy, the radius to 1% and the age to 20% (see Chapter 4).

Furthermore, asteroseismology was directly helpful to validate Kepler-410. This is because it was used to place limits on the presence of nearby companion stars, by placing limits on the seismic oscillation signal of potential companion stars. For *Kepler*, one of the limitations is that many stars are observed only in the 30-minute long cadence observing mode. Therefore, limits can only be placed on the presence of giant stars, which have longer oscillation periods. In principle, TESS would be more powerful, with an anticipated 2-minute cadence for all preselected stars, although it is unclear if the signal-to-noise quality of the data will be adequate to detect oscillations for many main-sequence stars. For Kepler-410, asteroseismology was also used in combination with a transit observation in a different color (in this case an infrared transit measurement using *Spitzer* data), to clearly distinguish between muliple potential host stars.

Beyond the discovery and characterization of planets, asteroseismology can be used to constrain the obliquity of planet systems by measuring the inclination of the host star (Chapter 9). This requires very high-quality observations, so that the method has only been used on a handful of systems, all of which are observed with *Kepler*: Kepler-50 and -65 (Chaplin et al. 2013), Kepler-56 (Huber et al. 2013a), Kepler-410 (Van Eylen et al. 2014), HAT-P-7 (Lund et al. 2014b; Benomar et al. 2014) and Kepler-25 (Benomar et al. 2014). A sample analysis placing statistical constraints on the obliquity of 25 stars (including the 6 mentioned above) is underway (Campante et al. 2015b). This technique is insensitive to the size of the planets, making it particularly powerful for systems with small planets, for which the obliquity is otherwise difficult to obtain. For multi-planet systems, which often have small planets, asteroseismic measurements currently make up over half of all obliquity measurements.

Asteroseismology is particularly suited to constrain the mean stellar density, which directly influence transit durations through Kepler's third law. To constrain (or rule out) high eccentricities, stellar densities obtained from other methods (e.g. spectroscopy) are sufficient, as shown for an eccentric Jupiter system (Dawson and Johnson 2012; Dawson et al. 2014, 2015). However, to measure small eccentricities, especially for small planets, the accurate and homogeneous measurement of stellar densities through asteroseismology is the tool of choice (see Chapters 10 and 11). Furthermore, if the eccentricity of a planet is known, the stellar density can be used in combination with the transit duration to validate or falsify planets, as I did for Kepler-92d, Kepler-449b and -c, and Kepler-450b, -c, and -d (see Chapter 5). This method has also been used to assess the overal false positive rate of a sample of *Kepler* single planet systems (Sliski and Kipping 2014).

Further asteroseismic work can be expected utilizing the *Kepler* dataset, while asteroseismology for planet hosts with *K2* will likely be limited mostly to giant stars. This is because the standard observing mode for *K2* is 30 minutes, not allowing for measurements of solar-like oscillations for main-sequence stars. Since the *K2* observing fields are not revisited and the planet host stars are not usually known in advance, it is difficult to preselect the right targets for the short (one minute) cadence mode. The TESS mission will observe many bright stars and no doubt lead to very interesting asteroseismic applications, but the synergy with planets remains unclear: the planet finding part of the mission will focus on K and M dwarf stars, which exhibit very low oscillation amplitudes which are difficult to detect. Once transiting planets around bright stars are found, the SONG telescope network (Grundahl et al. 2006) may be able to measure the RV signal caused by stellar oscillations for very bright planet host stars. A significant breakthrough can be expected for 2024 when the PLATO mission will begin observations – with the planned year(s)-long baselines per field and the anticipated high signal-to-noise photometry the mission will likely allow asteroseismic measurements of thousands of planet host stars. Finally, it is worth pointing out that asteroseismic measurements can serve as a 'ground truth' to calibrate other stellar characterization methods. In this regard, a major advance in understanding of (planet host) stars can be expected once GAIA (Perryman et al. 2001) measurements become available for essentially all nearby stars.

Takeaway 3.

To understand planets, it is crucial to understand their host stars, something for which asteroseismology is a very powerful tool. I have employed asteroseismology to:

- Discover and characterize planets;
- Measure the obliquity of planetary systems;
- Constrain the orbital eccentricity of planets.

TOWARDS BRIGHTER EXOPLANET HOST STARS

Kepler has provided a number of major breakthroughs in exoplanet science. Owing to the mission, hundreds of new exoplanets have been found with many more candidates awaiting confirmation. This has allowed the detection of many interesting planets, such as planets on orbits of only a few hours, multi-planet systems exhibiting dynamical interactions revealed through TTVs, and a number of potentially habitable planets. The mission has also allowed research about the occurrence rate of planets, so that it is now known that exoplanets are relatively common.

With many new planet discoveries, it is a good time to move beyond planet discovery and enhance the focus on planet characterization, because for many of the planets not much is known beyond simple observables such as period and radius. Unfortunately, the *Kepler* dataset is often ill-suited for characterization purposes, because many of the planets observed by *Kepler* orbit distant and thus faint stars. This complicates efforts to measure masses, which are required to measure the bulk density of planets to infer their composition, as well as to measure planet atmospheres, which would give insight in chemical and eventually even biological processes.

However, for transiting exoplanets, *the future looks bright*. The *Kepler* follow-up mission *K2* is observing a number of different fields in the galactic plane, and brighter stars than in the nominal *Kepler* mission are observed. For the main *Kepler* mission, after a significant observational effort masses could be measured for a few dozen small planets (e.g. Marcy et al. 2014). Here, the *K2* observations, which are only now becoming available, are expected to contribute more measurements to this purpose, giving hope of providing stronger constraints on the bulk density of planets. One interesting question to be answered is which planets are rocky. The current data suggests that planets below about 1.5 $R_\oplus$ are rocky, while larger planets contain more volatile elements (e.g. Rogers 2015).

Starting observations in 2017, TESS will find transiting planets around even brighter stars. Within two years the mission will map the entire sky. Each field will be observed for at least 30 days, so that all short-period transiting planets orbiting the brightest and most nearby stars are expected to be discovered. Beyond contributing to the measurement of planetary bulk densities, the discovery of a number of habitable planets around the closest cool stars is expected to make it possible for the first time to probe the atmospheres of potentially habitable planets. In 2024 the PLATO mission will provide high-quality photometry allowing similar measurements to be done for planets on

longer periods, and allowing detailed characterization of the planet host stars using asteroseismology.

I can therefore end this thesis on the positive note that the future indeed looks bright for exoplanet research. During the next decade(s), we can expect real progress towards answering an exciting and intriguing question.

Are we alone in the universe?

DANSK RESUMÉ

Er vi alene i Universet? Indtil videre står dette spørgsmål ubesvaret hen, men et betydeligt fremskridt blev opnået for to årtier siden med opdagelsen af den første planet i kredsløb om en anden stjerne end vores Sol. Op mod 2000 exoplaneter er nu blevet detekteret. De har forskellige radier, masser og kredsløbsperioder, men ud over disse basale parametre vides meget lidt om dem. I denne sammenhæng har jeg på den ene side arbejdet med opdagelse og karakterisering af nye interessante planeter, og på den anden side studeret detaljerede egenskaber ved allerede kendte planeter. Jeg vil i denne afhandling gøre brug af transitmetoden, som er baseret på det dyk i en stjernes lysstyrke, der kan måles når en planet passerer foran denne. Denne afhandling består af to dele. Første del fokuserer på opdagelsen af nye planeter og forståelsen af exoplaneters egenskaber. Jeg rapporterer om opdagelsen af planeten Kepler-410A b, en planet med en størrelse som Neptun i et 17 dages kredsløb. Kepler-410 består af to stjerner, en med en planet som transitter stjernen, og en som ikke gør. Den sidstnævnste blev opdaget på grund af dens gravitationelle indvirkning på Kepler-410A b, hvilket forårsager en variation i tidspunkterne, hvor denne passerer foran stjernen. Jeg var i stand til at bestemme hvilken af de to stjerner planeten hører til ved brug af observationer fra rumteleskopet *Kepler* og infrarøde transit målinger fra *Spitzer*. Derudover fandt jeg seks nye planeter, observeret med *Kepler*, som blev opdaget ved præcist at måle deres transittider, for derved at kunne identificere deres værtsstjerner. Jeg bruger asteroseismologi, studiet af stjernesvingninger, til nøjagtigt at bestemme egenskaberne for værtsstjernerne og deres planeter. Et radialhastighedsstudium er præsenteret som opfølgning af planetkandidater, der i *K2* viser transitter. Jeg præsenterer de første resultater fra dette studium med bestemmelse af masser og primære kompositioner af tre planeter. Anden del af afhandlingen fokuserer på dynamik af exoplaneter. Alle planeter i Solsystemet kredser i tæt på det samme plan, og dette plan er tilmed i sammenfaldende med Solens ækvatoriale plan. Dette er ikke tilfældet for alle exoplaneter, hvor tiltede planetbaner og endda retrograde planeter er blevet opdaget. Ved brug af en ny teknik måler jeg inklinationen af Kepler-410A med asteroseismologi og viser, at den er i overensstemmelse med det transittende planets baneplan. Disse målinger danner, sammen med en håndfuld andre lignende målinger, et billede af, at multiplanetsystemer primært befinder sig i samme plan som deres stjernes ækvatoriale plan. Dette favoriserer teorier, som foreslår, at "hot Jupiter" migration ligger til grund for dannelsen af systemer ude af samme plan. Endvidere findes exoplaneter i meget elliptiske kredsløb, ulig planeterne i vores solsystem som alle har næsten cirkulære baner. Jeg præsenterer det første studium af eccentriciteter med fokus på små planeter i multiplanetsystemer og viser, at deres eccentricitet er lav, mens jeg påviser, at eccentriciteter af enkeltplaneter, som transitter, er en smule højere. Disse eccentriciteter er lig dem i vores solsystem, men er forskellige fra nogle af dem, der ses for tunge planeter.

VITAE

The author of this thesis was born in a small village in Belgium named Keerbergen. Initially undecided what to study, I started a bachelor's degree in physics at the University of Leuven. I knew immediately this was a great choice, not in the least because I met some fantastic people to complete my studies with. I got involved in a student society for physics, mathematics and computer science students over which I presided for a year. It is safe to say that during the first years of my time as a student I learned at least as much outside as inside a class room.

For my bachelor's degree in physics I took up a specialisation in mathematics and initially intended to take a master's degree in theoretical physics, but eventually decided to study a master's in astrophysics instead. Even then, I had no intentions to remain in academia and become a researcher, something which changed during my Erasmus exchange stay at Aarhus University. There, I completed a master's thesis bridging the fields of asteroseismology and exoplanets and picked up a real interest in research. After a detour working as a project engineer at a dredging company in Qatar, I returned to Aarhus to start a PhD program.

My PhD research continued along the lines of what got me interested during my master's project: the intersection between stars and their planets, and the interplay between asteroseismology and exoplanets. I also taught courses on classical mechanics, stars, and exoplanets, and served as the advisor for a number of exciting student projects. I have been fortunate to get a chance to experience other environments and spent a month at Sara Seager's research group in Boston during the first year of my research. By the end of my PhD, I returned to MIT for a six month stay at Josh Winn's group.

During my research I've been able to travel a bit of the world. I enjoyed a summer school in Penn State, where I learned about astrostatistics. During another summer school at the Swedish Onsala, I had the best 10 days of my PhD and a chance to operate a radio telescope. I have presented my research at major international conferences in Toulouse, Porto, and Aarhus, as well as in meetings and seminars at Leuven University, Aarhus University, Harvard, MIT, and in London. I appreciate that I had a chance not only to communicate my own research to the press, but also introduce the general public to the exciting world of exoplanets in outreach talks and public lectures.

PUBLICATIONS

PEER-REVIEWED FIRST AUTHOR PUBLICATIONS

- *ESPRINT II: Spectroscopic follow-up of three exoplanet systems from the first K2 campaign*
  V. Van Eylen, G. Nowak, S. Albrecht, E. Palle, I. Ribas, H. Bruntt, M. Perger, D. Gandolfi, T. Hirano, R. Sanchis-Ojeda, A. Kiilerich, J. P. Arranz, M. Badenas, F. Dai, H. J. Deeg, E. W. Guenther, P. Montanes-Rodriguez, N. Narita, L. A. Rogers, V. J. Sanches Bejar, T. S. Shrotriya, J. N. Winn
  Submitted to Astrophysical Journal, September 2015

- *Eccentricity from Transit Photometry: Small Planets in Kepler Multi-planet Systems Have Low Eccentricities*
  V. Van Eylen and S. Albrecht
  Astrophysical Journal 808:126, August 2015

- *What Asteroseismology can do for Exoplanets: Kepler-410A b is a Small Neptune around a Bright Star, in an Eccentric Orbit Consistent with Low Obliquity*
  V. Van Eylen, M. N. Lund, V. Silva Aguirre, T. Arentoft, H. Kjeldsen, S. Albrecht, W. J. Chaplin, H. Isaacson, M. G. Pedersen, J. Jessen-Hansen, B. Tingley, J. Christensen-Dalsgaard, C. Aerts, T. L. Campante, and S. T. Bryson
  Astrophysical Journal 782:14, February 2014

- *Investigation of Systematic Effects in Kepler Data: Seasonal Variations in the Light Curve of HAT-P-7b*
  V. Van Eylen, M. Lindholm Nielsen, B. Hinrup, B. Tingley, and H. Kjeldsen
  Astrophysical Journal Letters 774:L19, September 2013

- *Properties of extrasolar planets and their host stars: A case study of HAT-P-7*
  V. Van Eylen, H. Kjeldsen, J. Christensen-Dalsgaard, and C. Aerts
  Astronomische Nachrichten 333:1088, December 2012

PEER-REVIEWED CO-AUTHORED PUBLICATIONS

- *Spin-orbit alignment of exoplanet systems: ensemble analysis using asteroseismology*
  T. L. Campante, M. N. Lund, J. S.Kuszlewicz, G. R. Davies, W. J. Chaplin,

S. Albrecht, J. N. Winn, T. R.Bedding, O. Benomar, D. Bossini, R. Handberg, A. R. G. Santos, **V. Van Eylen**, and 13 other co-authors.
Submitted to Astrophysical Journal, September 2015

- *Hot super-Earths stripped by their host stars*
M. S. Lundkvist, H. Kjeldsen, S. Albrecht, G. R. Davies, S. Basu, D. Huber, C. Karoff, V. Silva Aguirre, **V. Van Eylen**, and 19 other authors.
Submitted to Nature Communications, September 2015

- *The K2-ESPRINT Project I: Discovery of the Disintegrating Rocky Planet with a Cometary Head and Tail EPIC 201637175b*
R. Sanchis-Ojeda, S. Rappaport, E. Pallé, L. Delrez, J. DeVore, D. Gandolfi, A. Fukui, I. Ribas, K. G. Stassun, S. Albrecht, F. Dai, E. Gaidos, M. Gillon, T. Hirano, M. Holman, A. W. Howard, H. Isaacson, E. Jehin, M. Kuzuhara, A. W. Mann, G. W. Marcy, P. A. Miles-Páez, P. A. Montañés-Rodríguez, F. Murgas, N. Narita, G. Nowak, M. Onitsuka, M. Paegert, **V. Van Eylen**, J. N. Winn, and L. Yu.
Astrophysical Journal, Accepted for publication in September 2015 (arxiv 1504:04379)

- *Ages and fundamental properties of Kepler exoplanet host stars from asteroseismology*
V. Silva Aguirre, G. R. Davies, S. Basu, J. Christensen-Dalsgaard, O. Creevey, T. S. Metcalfe, T. R. Bedding, L. Casagrande, R. Handberg, M. N. Lund, P. E. Nissen, W. J. Chaplin, D. Huber, A. M. Serenelli, D. Stello, **V. Van Eylen**, and 8 other authors. Monthly Notices of the Royal Astronomical Society 452:2127-2148, September 2015

- *Planetary Candidates Observed by Kepler. VI. Planet Sample from Q1–Q16 (47 Months)*
F. Mullally, J. L. Coughlin, S. E. Thompson, J. Rowe, C. Burke, D. W. Latham, N. M. Batalha, S. T. Bryson, J. Christiansen, C. E. Henze, A. Ofir, B. Quarles, A. Shporer, **V. Van Eylen**, and 46 other authors.
Astrophysical Journal Supplements 217:31, April 2015

- *Asteroseismic inference on the spin-orbit misalignment and stellar parameters of HAT-P-7*
M. N. Lund, M. Lundkvist, V. Silva Aguirre, G. Houdek, L. Casagrande, **V. Van Eylen**, T. L. Campante, C. Karoff, H. Kjeldsen, S. Albrecht, W. J. Chaplin, M. B. Nielsen, P. Degroote, G. R. Davies, and R. Handberg.
Astronomy & Astrophysics 570:A54, October 2014

- *Accurate Parameters of the Oldest Known Rocky-exoplanet Hosting System: Kepler-10 Revisited*
A. Fogtmann-Schulz, B. Hinrup, **V. Van Eylen**, J. Christensen-Dalsgaard, H. Kjeldsen, V. Silva Aguirre, and B. Tingley.
Astrophysical Journal 781:67, February 2014

BIBLIOGRAPHY

H. A. Abt. Observed Orbital Eccentricities. II. Late-Type Stars. *Astrophysical Journal*, 651:1151–1154, November 2006.

E. R. Adams, D. R. Ciardi, A. K. Dupree, T. N. Gautier, III, C. Kulesa, and D. McCarthy. Adaptive Optics Images of Kepler Objects of Interest. *Astronomical Journal*, 144:42, August 2012.

C. Aerts, J. Christensen-Dalsgaard, and D. W. Kurtz. *Asteroseismology*. 2010.

E. Agol, J. Steffen, R. Sari, and W. Clarkson. On detecting terrestrial planets with timing of giant planet transits. *Monthly Notices of the Royal Astronomical Society*, 359:567–579, May 2005.

S. Albrecht, J. N. Winn, R. P. Butler, J. D. Crane, S. A. Shectman, I. B. Thompson, T. Hirano, and R. A. Wittenmyer. A High Stellar Obliquity in the WASP-7 Exoplanetary System. *Astrophysical Journal*, 744:189, January 2012a.

S. Albrecht, J. N. Winn, J. A. Johnson, A. W. Howard, G. W. Marcy, R. P. Butler, P. Arriagada, J. D. Crane, S. A. Shectman, I. B. Thompson, T. Hirano, G. Bakos, and J. D. Hartman. Obliquities of Hot Jupiter Host Stars: Evidence for Tidal Interactions and Primordial Misalignments. *Astrophysical Journal*, 757:18, September 2012b.

S. Albrecht, J. N. Winn, G. W. Marcy, A. W. Howard, H. Isaacson, and J. A. Johnson. Low Stellar Obliquities in Compact Multiplanet Systems. *Astrophysical Journal*, 771:11, July 2013.

S. Albrecht, J. N. Winn, G. Torres, D. C. Fabrycky, J. Setiawan, M. Gillon, E. Jehin, A. Triaud, D. Queloz, I. Snellen, and P. Eggleton. The BANANA Project. V. Misaligned and Precessing Stellar Rotation Axes in CV Velorum. *Astrophysical Journal*, 785:83, April 2014.

E. R. Anderson, T. L. Duvall, Jr., and S. M. Jefferies. Modeling of solar oscillation power spectra. *Astrophysical Journal*, 364:699–705, December 1990.

C Angulo, M Arnould, M Rayet, P Descouvemont, D Baye, C Leclercq-Willain, A Coc, S Barhoumi, P Aguer, C Rolfs, R Kunz, J W Hammer, A Mayer, T Paradellis, S Kossionides, C Chronidou, K Spyrou, S Degl'innocenti, G Fiorentini, B Ricci, S Zavatarelli, C Providencia, H Wolters, J Soares, C Grama, J Rahighi, A Shotter, and M Lamehi Rachti. A compilation of charged-particle induced thermonuclear reaction rates. *Nuclear Physics A*, 656:3, August 1999.

R. Angus, D. Foreman-Mackey, and J. A. Johnson. Systematics-insensitive periodic signal search with K2. *ArXiv e-prints*, May 2015.

T. Appourchaux. Peak Bagging for Solar-like Stars. *Astrophysics and Space Science*, 284:109–119, 2003.

D. J. Armstrong, Y. Gómez Maqueo Chew, F. Faedi, and D. Pollacco. A catalogue of temperatures for Kepler eclipsing binary stars. *Monthly Notices of the Royal Astronomical Society*, 437:3473–3481, February 2014.

M. Auvergne, P. Bodin, L. Boisnard, J.-T. Buey, S. Chaintreuil, G. Epstein, M. Jouret, T. Lam-Trong, P. Levacher, A. Magnan, R. Perez, P. Plasson, J. Plesseria, G. Peter, M. Steller, D. Tiphène, A. Baglin, P. Agogué, T. Appourchaux, D. Barbet, T. Beaufort, R. Bellenger, R. Berlin, P. Bernardi, D. Blouin, P. Boumier, F. Bonneau, R. Briet, B. Butler, R. Cautain, F. Chiavassa, V. Costes, J. Cuvilho, V. Cunha-Parro, F. de Oliveira Fialho, M. Decaudin, J.-M. Defise, S. Djalal, A. Docclo, R. Drummond, O. Dupuis, G. Exil, C. Fauré, A. Gaboriaud, P. Gamet, P. Gavalda, E. Grolleau, L. Gueguen, V. Guivarc'h, P. Guterman, J. Hasiba, G. Huntzinger, H. Hustaix, C. Imbert, G. Jeanville, B. Johlander, L. Jorda, P. Journoud, F. Karioty, L. Kerjean, L. Lafond, V. Lapeyrere, P. Landiech, T. Larqué, P. Laudet, J. Le Merrer, L. Leporati, B. Leruyet, B. Levieuge, A. Llebaria, L. Martin, E. Mazy, J.-M. Mesnager, J.-P. Michel, J.-P. Moalic, W. Monjoin, D. Naudet, S. Neukirchner, K. Nguyen-Kim, M. Ollivier, J.-L. Orcesi, H. Ottacher, A. Oulali, J. Parisot, S. Perruchot, A. Piacentino, L. Pinheiro da Silva, J. Platzer, B. Pontet, A. Pradines, C. Quentin, U. Rohbeck, G. Rolland, F. Rollenhagen, R. Romagnan, N. Russ, R. Samadi, R. Schmidt, N. Schwartz, I. Sebbag, H. Smit, W. Sunter, M. Tello, P. Toulouse, B. Ulmer, O. Vandermarcq, E. Vergnault, R. Wallner, G. Waultier, and P. Zanatta. The CoRoT satellite in flight: description and performance. *Astronomy & Astrophysics*, 506:411–424, October 2009.

G. Á. Bakos, G. Torres, A. Pál, J. Hartman, G. Kovács, R. W. Noyes, D. W. Latham, D. D. Sasselov, B. Sipőcz, G. A. Esquerdo, D. A. Fischer, J. A. Johnson, G. W. Marcy, R. P. Butler, H. Isaacson, A. Howard, S. Vogt, G. Kovács, J. Fernandez, A. Moór, R. P. Stefanik, J. Lázár, I. Papp, and P. Sári. HAT-P-11b: A Super-Neptune Planet Transiting a Bright K Star in the Kepler Field. *Astrophysical Journal*, 710:1724–1745, February 2010.

S. Ballard and J. A. Johnson. The Kepler Dichotomy among the M Dwarfs: Half of Systems Contain Five or More Coplanar Planets. *ArXiv:1410.4192*, October 2014.

S. Ballard, D. Fabrycky, F. Fressin, D. Charbonneau, J.-M. Desert, G. Torres, G. Marcy, C. J. Burke, H. Isaacson, C. Henze, J. H. Steffen, D. R. Ciardi, S. B. Howell, W. D. Cochran, M. Endl, S. T. Bryson, J. F. Rowe, M. J. Holman, J. J.

Lissauer, J. M. Jenkins, M. Still, E. B. Ford, J. L. Christiansen, C. K. Middour, M. R. Haas, J. Li, J. R. Hall, S. McCauliff, N. M. Batalha, D. G. Koch, and W. J. Borucki. The Kepler-19 System: A Transiting 2.2 R â Planet and a Second Planet Detected via Transit Timing Variations. *Astrophysical Journal*, 743:200, December 2011.

E. Bányai, L. L. Kiss, T. R. Bedding, B. Bellamy, J. M. Benkő, A. Bódi, J. R. Callingham, D. Compton, I. Csányi, A. Derekas, J. Dorval, D. Huber, O. Shrier, A. E. Simon, D. Stello, G. M. Szabó, R. Szabó, and K. Szatmáry. Variability of M giant stars based on Kepler photometry: general characteristics. *Monthly Notices of the Royal Astronomical Society*, 436:1576–1587, December 2013.

T. Barclay, J. F. Rowe, J. J. Lissauer, D. Huber, F. Fressin, S. B. Howell, S. T. Bryson, W. J. Chaplin, J.-M. Désert, E. D. Lopez, G. W. Marcy, F. Mullally, D. Ragozzine, G. Torres, E. R. Adams, E. Agol, D. Barrado, S. Basu, T. R. Bedding, L. A. Buchhave, D. Charbonneau, J. L. Christiansen, J. Christensen-Dalsgaard, D. Ciardi, W. D. Cochran, A. K. Dupree, Y. Elsworth, M. Everett, D. A. Fischer, E. B. Ford, J. J. Fortney, J. C. Geary, M. R. Haas, R. Handberg, S. Hekker, C. E. Henze, E. Horch, A. W. Howard, R. C. Hunter, H. Isaacson, J. M. Jenkins, C. Karoff, S. D. Kawaler, H. Kjeldsen, T. C. Klaus, D. W. Latham, J. Li, J. Lillo-Box, M. N. Lund, M. Lundkvist, T. S. Metcalfe, A. Miglio, R. L. Morris, E. V. Quintana, D. Stello, J. C. Smith, M. Still, and S. E. Thompson. A sub-Mercury-sized exoplanet. *Nature*, 494:452–454, February 2013.

J. W. Barnes. Effects of Orbital Eccentricity on Extrasolar Planet Transit Detectability and Light Curves. *Publications of the Astronomical Society of the Pacific*, 119:986–993, September 2007.

J. W. Barnes, E. Linscott, and A. Shporer. Measurement of the Spin-Orbit Misalignment of KOI-13.01 from Its Gravity-darkened Kepler Transit Lightcurve. *Astrophysical Journal Supplement Series*, 197:10, November 2011.

N. M. Batalha and Kepler Team. Transiting Planet Candidates Observed by Kepler. In *American Astronomical Society Meeting Abstracts 220*, volume 220 of *American Astronomical Society Meeting Abstracts*, page 306.01, May 2012.

N. M. Batalha, J. F. Rowe, R. L. Gilliland, J. J. Jenkins, D. Caldwell, W. J. Borucki, D. G. Koch, J. J. Lissauer, E. W. Dunham, T. N. Gautier, S. B. Howell, D. W. Latham, G. W. Marcy, and A. Prsa. Pre-spectroscopic False-positive Elimination of Kepler Planet Candidates. *Astrophysical Journal Letters*, 713: L103–L108, April 2010.

N. M. Batalha, J. F. Rowe, S. T. Bryson, T. Barclay, C. J. Burke, D. A. Caldwell, J. L. Christiansen, F. Mullally, S. E. Thompson, T. M. Brown, A. K. Dupree, D. C. Fabrycky, E. B. Ford, J. J. Fortney, R. L. Gilliland, H. Isaacson, D. W. Latham, G. W. Marcy, S. N. Quinn, D. Ragozzine, A. Shporer, W. J. Borucki,

D. R. Ciardi, T. N. Gautier, III, M. R. Haas, J. M. Jenkins, D. G. Koch, J. J. Lissauer, W. Rapin, G. S. Basri, A. P. Boss, L. A. Buchhave, J. A. Carter, D. Charbonneau, J. Christensen-Dalsgaard, B. D. Clarke, W. D. Cochran, B.-O. Demory, J.-M. Desert, E. Devore, L. R. Doyle, G. A. Esquerdo, M. Everett, F. Fressin, J. C. Geary, F. R. Girouard, A. Gould, J. R. Hall, M. J. Holman, A. W. Howard, S. B. Howell, K. A. Ibrahim, K. Kinemuchi, H. Kjeldsen, T. C. Klaus, J. Li, P. W. Lucas, S. Meibom, R. L. Morris, A. Prša, E. Quintana, D. T. Sanderfer, D. Sasselov, S. E. Seader, J. C. Smith, J. H. Steffen, M. Still, M. C. Stumpe, J. C. Tarter, P. Tenenbaum, G. Torres, J. D. Twicken, K. Uddin, J. Van Cleve, L. Walkowicz, and W. F. Welsh. Planetary Candidates Observed by Kepler. III. Analysis of the First 16 Months of Data. *Astrophysical Journal Supplement Series*, 204:24, February 2013.

M. R. Bate, G. Lodato, and J. E. Pringle. Chaotic star formation and the alignment of stellar rotation with disc and planetary orbital axes. *Monthly Notices of the Royal Astronomical Society*, 401:1505–1513, January 2010.

K. Batygin. A primordial origin for misalignments between stellar spin axes and planetary orbits. *Nature*, 491:418–420, November 2012.

J. G. Beck and P. Giles. Helioseismic Determination of the Solar Rotation Axis. *Astrophysical Journal Letters*, 621:L153–L156, March 2005.

J. C. Becker, A. Vanderburg, F. C. Adams, S. A. Rappaport, and H. M. Schwengeler. WASP-47: A Hot Jupiter System with Two Additional Planets Discovered by K2. *ArXiv e-prints*, August 2015.

K. Belkacem, M. J. Goupil, M. A. Dupret, R. Samadi, F. Baudin, A. Noels, and B. Mosser. The underlying physical meaning of the ν_{max} - ν_c relation. *Astronomy & Astrophysics*, 530:A142, June 2011.

B. Benneke. Strict Upper Limits on the Carbon-to-Oxygen Ratios of Eight Hot Jupiters from Self-Consistent Atmospheric Retrieval. *ArXiv e-prints*, April 2015.

B. Benneke and S. Seager. Atmospheric Retrieval for Super-Earths: Uniquely Constraining the Atmospheric Composition with Transmission Spectroscopy. *Astrophysical Journal*, 753:100, July 2012.

O. Benomar, K. Masuda, H. Shibahashi, and Y. Suto. Determination of three-dimensional spin-orbit angle with joint analysis of asteroseismology, transit lightcurve, and the Rossiter-McLaughlin effect: Cases of HAT-P-7 and Kepler-25. *Publications of the Astronomical Society of Japan*, 66:94, October 2014.

J. L. Birkby, R. J. de Kok, M. Brogi, E. J. W. de Mooij, H. Schwarz, S. Albrecht, and I. A. G. Snellen. Detection of water absorption in the day side atmosphere of HD 189733 b using ground-based high-resolution spectroscopy

at 3.2 μm. *Monthly Notices of the Royal Astronomical Society*, 436:L35–L39, November 2013.

W. Borucki, D. Koch, G. Basri, N. Batalha, T. Brown, D. Caldwell, J. Christensen-Dalsgaard, W. Cochran, E. Dunham, T. N. Gautier, J. Geary, R. Gilliland, J. Jenkins, Y. Kondo, D. Latham, J. J. Lissauer, and D. Monet. Finding Earth-size planets in the habitable zone: the Kepler Mission. In Y.-S. Sun, S. Ferraz-Mello, and J.-L. Zhou, editors, *IAU Symposium*, volume 249 of *IAU Symposium*, pages 17–24, May 2008.

W. Borucki, D. Koch, N. Batalha, D. Caldwell, J. Christensen-Dalsgaard, W. D. Cochran, E. Dunham, T. N. Gautier, J. Geary, R. Gilliland, J. Jenkins, H. Kjeldsen, J. J. Lissauer, and J. Rowe. KEPLER: Search for Earth-Size Planets in the Habitable Zone. In F. Pont, D. Sasselov, and M. J. Holman, editors, *IAU Symposium*, volume 253 of *IAU Symposium*, pages 289–299, February 2009a.

W. J. Borucki, D. Koch, J. Jenkins, D. Sasselov, R. Gilliland, N. Batalha, D. W. Latham, D. Caldwell, G. Basri, T. Brown, J. Christensen-Dalsgaard, W. D. Cochran, E. DeVore, E. Dunham, A. K. Dupree, T. Gautier, J. Geary, A. Gould, S. Howell, H. Kjeldsen, J. Lissauer, G. Marcy, S. Meibom, D. Morrison, and J. Tarter. Kepler's Optical Phase Curve of the Exoplanet HAT-P-7b. *Science*, 325:709–, August 2009b.

W. J. Borucki, D. Koch, G. Basri, N. Batalha, T. Brown, D. Caldwell, J. Caldwell, J. Christensen-Dalsgaard, W. D. Cochran, E. DeVore, E. W. Dunham, A. K. Dupree, T. N. Gautier, J. C. Geary, R. Gilliland, A. Gould, S. B. Howell, J. M. Jenkins, Y. Kondo, D. W. Latham, G. W. Marcy, S. Meibom, H. Kjeldsen, J. J. Lissauer, D. G. Monet, D. Morrison, D. Sasselov, J. Tarter, A. Boss, D. Brownlee, T. Owen, D. Buzasi, D. Charbonneau, L. Doyle, J. Fortney, E. B. Ford, M. J. Holman, S. Seager, J. H. Steffen, W. F. Welsh, J. Rowe, H. Anderson, L. Buchhave, D. Ciardi, L. Walkowicz, W. Sherry, E. Horch, H. Isaacson, M. E. Everett, D. Fischer, G. Torres, J. A. Johnson, M. Endl, P. MacQueen, S. T. Bryson, J. Dotson, M. Haas, J. Kolodziejczak, J. Van Cleve, H. Chandrasekaran, J. D. Twicken, E. V. Quintana, B. D. Clarke, C. Allen, J. Li, H. Wu, P. Tenenbaum, E. Verner, F. Bruhweiler, J. Barnes, and A. Prsa. Kepler Planet-Detection Mission: Introduction and First Results. *Science*, 327:977–, February 2010.

W. J. Borucki, D. G. Koch, G. Basri, N. Batalha, T. M. Brown, S. T. Bryson, D. Caldwell, J. Christensen-Dalsgaard, W. D. Cochran, E. DeVore, E. W. Dunham, T. N. Gautier, III, J. C. Geary, R. Gilliland, A. Gould, S. B. Howell, J. M. Jenkins, D. W. Latham, J. J. Lissauer, G. W. Marcy, J. Rowe, D. Sasselov, A. Boss, D. Charbonneau, D. Ciardi, L. Doyle, A. K. Dupree, E. B. Ford, J. Fortney, M. J. Holman, S. Seager, J. H. Steffen, J. Tarter, W. F. Welsh, C. Allen, L. A. Buchhave, J. L. Christiansen, B. D. Clarke, S. Das, J.-M. Désert,

M. Endl, D. Fabrycky, F. Fressin, M. Haas, E. Horch, A. Howard, H. Isaacson, H. Kjeldsen, J. Kolodziejczak, C. Kulesa, J. Li, P. W. Lucas, P. Machalek, D. McCarthy, P. MacQueen, S. Meibom, T. Miquel, A. Prsa, S. N. Quinn, E. V. Quintana, D. Ragozzine, W. Sherry, A. Shporer, P. Tenenbaum, G. Torres, J. D. Twicken, J. Van Cleve, L. Walkowicz, F. C. Witteborn, and M. Still. Characteristics of Planetary Candidates Observed by Kepler. II. Analysis of the First Four Months of Data. *Astrophysical Journal*, 736:19, July 2011.

T. M. Brown, R. L. Gilliland, R. W. Noyes, and L. W. Ramsey. Detection of possible p-mode oscillations on Procyon. *Astrophysical Journal*, 368:599–609, February 1991.

H. Bruntt, S. Basu, B. Smalley, W. J. Chaplin, G. A. Verner, T. R. Bedding, C. Catala, J.-C. Gazzano, J. Molenda-Żakowicz, A. O. Thygesen, K. Uytterhoeven, S. Hekker, D. Huber, C. Karoff, S. Mathur, B. Mosser, T. Appourchaux, T. L. Campante, Y. Elsworth, R. A. García, R. Handberg, T. S. Metcalfe, P.-O. Quirion, C. Régulo, I. W. Roxburgh, D. Stello, J. Christensen-Dalsgaard, S. D. Kawaler, H. Kjeldsen, R. L. Morris, E. V. Quintana, and D. T. Sanderfer. Accurate fundamental parameters and detailed abundance patterns from spectroscopy of 93 solar-type Kepler targets. *Monthly Notices of the Royal Astronomical Society*, 423:122–131, June 2012.

S. T. Bryson, J. M. Jenkins, R. L. Gilliland, J. D. Twicken, B. Clarke, J. Rowe, D. Caldwell, N. Batalha, F. Mullally, M. R. Haas, and P. Tenenbaum. Identification of Background False Positives from Kepler Data. *ArXiv:1303.0052*, February 2013.

L. A. Buchhave, D. W. Latham, J. A. Carter, J.-M. Désert, G. Torres, E. R. Adams, S. T. Bryson, D. B. Charbonneau, D. R. Ciardi, C. Kulesa, A. K. Dupree, D. A. Fischer, F. Fressin, T. N. Gautier, III, R. L. Gilliland, S. B. Howell, H. Isaacson, J. M. Jenkins, G. W. Marcy, D. W. McCarthy, J. F. Rowe, N. M. Batalha, W. J. Borucki, T. M. Brown, D. A. Caldwell, J. L. Christiansen, W. D. Cochran, D. Deming, E. W. Dunham, M. Everett, E. B. Ford, J. J. Fortney, J. C. Geary, F. R. Girouard, M. R. Haas, M. J. Holman, E. Horch, T. C. Klaus, H. A. Knutson, D. G. Koch, J. Kolodziejczak, J. J. Lissauer, P. Machalek, F. Mullally, M. D. Still, S. N. Quinn, S. Seager, S. E. Thompson, and J. Van Cleve. Kepler-14b: A Massive Hot Jupiter Transiting an F Star in a Close Visual Binary. *Astrophysical Journal Supplement Series*, 197:3, November 2011.

C. J. Burke, S. T. Bryson, F. Mullally, J. F. Rowe, J. L. Christiansen, S. E. Thompson, J. L. Coughlin, M. R. Haas, N. M. Batalha, D. A. Caldwell, J. M. Jenkins, M. Still, T. Barclay, W. J. Borucki, W. J. Chaplin, D. R. Ciardi, B. D. Clarke, W. D. Cochran, B.-O. Demory, G. A. Esquerdo, T. N. Gautier, III, R. L. Gilliland, F. R. Girouard, M. Havel, C. E. Henze, S. B. Howell, D. Huber, D. W. Latham, J. Li, R. C. Morehead, T. D. Morton, J. Pepper, E. Quintana, D. Ragozzine, S. E. Seader, Y. Shah, A. Shporer, P. Tenenbaum, J. D.

Twicken, and A. Wolfgang. Planetary Candidates Observed by Kepler IV: Planet Sample from Q1-Q8 (22 Months). *Astrophysical Journal Supplement Series*, 210:19, February 2014.

R. P. Butler, J. T. Wright, G. W. Marcy, D. A. Fischer, S. S. Vogt, C. G. Tinney, H. R. A. Jones, B. D. Carter, J. A. Johnson, C. McCarthy, and A. J. Penny. Catalog of Nearby Exoplanets. *Astrophysical Journal*, 646:505–522, July 2006.

D. A. Caldwell, J. J. Kolodziejczak, J. E. Van Cleve, J. M. Jenkins, P. R. Gazis, V. S. Argabright, E. E. Bachtell, E. W. Dunham, J. C. Geary, R. L. Gilliland, H. Chandrasekaran, J. Li, P. Tenenbaum, H. Wu, W. J. Borucki, S. T. Bryson, J. L. Dotson, M. R. Haas, and D. G. Koch. Instrument Performance in Kepler's First Months. *Astrophysical Journal Letters*, 713:L92–L96, April 2010a.

D. A. Caldwell, J. E. van Cleve, J. M. Jenkins, V. S. Argabright, J. J. Kolodziejczak, E. W. Dunham, J. C. Geary, P. Tenenbaum, H. Chandrasekaran, J. Li, H. Wu, and J. von Wilpert. Kepler instrument performance: an in-flight update. In *Society of Photo-Optical Instrumentation Engineers (SPIE) Conference Series*, volume 7731 of *Society of Photo-Optical Instrumentation Engineers (SPIE) Conference Series*, July 2010b.

T. L. Campante, W. J. Chaplin, M. N. Lund, D. Huber, S. Hekker, R. A. García, E. Corsaro, R. Handberg, A. Miglio, T. Arentoft, S. Basu, T. R. Bedding, J. Christensen-Dalsgaard, G. R. Davies, Y. P. Elsworth, R. L. Gilliland, C. Karoff, S. D. Kawaler, H. Kjeldsen, M. Lundkvist, T. S. Metcalfe, V. Silva Aguirre, and D. Stello. Limits on Surface Gravities of Kepler Planet-candidate Host Stars from Non-detection of Solar-like Oscillations. *Astrophysical Journal*, 783:123, March 2014.

T. L. Campante, T. Barclay, J. J. Swift, D. Huber, V. Z. Adibekyan, W. Cochran, C. J. Burke, H. Isaacson, E. V. Quintana, G. R. Davies, V. Silva Aguirre, D. Ragozzine, R. Riddle, C. Baranec, S. Basu, W. J. Chaplin, J. Christensen-Dalsgaard, T. S. Metcalfe, T. R. Bedding, R. Handberg, D. Stello, J. M. Brewer, S. Hekker, C. Karoff, R. Kolbl, N. M. Law, M. Lundkvist, A. Miglio, J. F. Rowe, N. C. Santos, C. Van Laerhoven, T. Arentoft, Y. P. Elsworth, D. A. Fischer, S. D. Kawaler, H. Kjeldsen, M. N. Lund, G. W. Marcy, S. G. Sousa, A. Sozzetti, and T. R. White. An Ancient Extrasolar System with Five Sub-Earth-size Planets. *Astrophysical Journal*, 799:170, February 2015a.

T. L. Campante, M. N. Lund, J. S. Kuszlewicz, G. R. Davies, W. J. Chaplin, S. Albrecht, J. N. Winn, T. R. Bedding, O. Benomar, D. Bossini, R. Handberg, A. R. G. Santos, V. Van Eylen, and 13 co authors. Spin-orbit alignment of exoplanet systems: ensemble analysis using asteroseismology. *Submitted to ApJ*, 2015b.

J. A. Carter and J. N. Winn. Empirical Constraints on the Oblateness of an Exoplanet. *Astrophysical Journal*, 709:1219–1229, February 2010.

J. A. Carter, E. Agol, W. J. Chaplin, S. Basu, T. R. Bedding, L. A. Buchhave, J. Christensen-Dalsgaard, K. M. Deck, Y. Elsworth, D. C. Fabrycky, E. B. Ford, J. J. Fortney, S. J. Hale, R. Handberg, S. Hekker, M. J. Holman, D. Huber, C. Karoff, S. D. Kawaler, H. Kjeldsen, J. J. Lissauer, E. D. Lopez, M. N. Lund, M. Lundkvist, T. S. Metcalfe, A. Miglio, L. A. Rogers, D. Stello, W. J. Borucki, S. Bryson, J. L. Christiansen, W. D. Cochran, J. C. Geary, R. L. Gilliland, M. R. Haas, J. Hall, A. W. Howard, J. M. Jenkins, T. Klaus, D. G. Koch, D. W. Latham, P. J. MacQueen, D. Sasselov, J. H. Steffen, J. D. Twicken, and J. N. Winn. Kepler-36: A Pair of Planets with Neighboring Orbits and Dissimilar Densities. *Science*, 337:556–, August 2012.

L. Casagrande, C. Flynn, L. Portinari, L. Girardi, and R. Jimenez. The helium abundance and $\Delta Y/\Delta Z$ in lower main-sequence stars. *Monthly Notices of the Royal Astronomical Society*, 382:1516, December 2007.

L. Casagrande, I. Ramírez, J. Meléndez, M. Bessell, and M. Asplund. An absolutely calibrated T_{eff} scale from the infrared flux method. Dwarfs and subgiants. *Astronomy & Astrophysics*, 512:A54, March 2010.

W. J. Chaplin, H. Kjeldsen, T. R. Bedding, J. Christensen-Dalsgaard, R. L. Gilliland, S. D. Kawaler, T. Appourchaux, Y. Elsworth, R. A. García, G. Houdek, C. Karoff, T. S. Metcalfe, J. Molenda-Żakowicz, M. J. P. F. G. Monteiro, M. J. Thompson, G. A. Verner, N. Batalha, W. J. Borucki, T. M. Brown, S. T. Bryson, J. L. Christiansen, B. D. Clarke, J. M. Jenkins, T. C. Klaus, D. Koch, D. An, J. Ballot, S. Basu, O. Benomar, A. Bonanno, A.-M. Broomhall, T. L. Campante, E. Corsaro, O. L. Creevey, L. Esch, N. Gai, P. Gaulme, S. J. Hale, R. Handberg, S. Hekker, D. Huber, S. Mathur, B. Mosser, R. New, M. H. Pinsonneault, D. Pricopi, P.-O. Quirion, C. Régulo, I. W. Roxburgh, D. Salabert, D. Stello, and M. D. Suran. Predicting the Detectability of Oscillations in Solar-type Stars Observed by Kepler. *Astrophysical Journal*, 732:54, May 2011.

W. J. Chaplin, R. Sanchis-Ojeda, T. L. Campante, R. Handberg, D. Stello, J. N. Winn, S. Basu, J. Christensen-Dalsgaard, G. R. Davies, T. S. Metcalfe, L. A. Buchhave, D. A. Fischer, T. R. Bedding, W. D. Cochran, Y. Elsworth, R. L. Gilliland, S. Hekker, D. Huber, H. Isaacson, C. Karoff, S. D. Kawaler, H. Kjeldsen, D. W. Latham, M. N. Lund, M. Lundkvist, G. W. Marcy, A. Miglio, T. Barclay, and J. J. Lissauer. Asteroseismic Determination of Obliquities of the Exoplanet Systems Kepler-50 and Kepler-65. *Astrophysical Journal*, 766:101, April 2013.

D. Charbonneau, T. M. Brown, R. W. Noyes, and R. L. Gilliland. Detection of an Extrasolar Planet Atmosphere. *Astrophysical Journal*, 568:377–384, March 2002.

S. Chatterjee, E. B. Ford, S. Matsumura, and F. A. Rasio. Dynamical Outcomes of Planet-Planet Scattering. *Astrophysical Journal*, 686:580–602, October 2008.

J. Christensen-Dalsgaard. ADIPLS—the Aarhus adiabatic oscillation package. *Ap&SS*, 316:113, August 2008.

J. Christensen-Dalsgaard, H. Kjeldsen, T. M. Brown, R. L. Gilliland, T. Arentoft, S. Frandsen, P.-O. Quirion, W. J. Borucki, D. Koch, and J. M. Jenkins. Asteroseismic Investigation of Known Planet Hosts in the Kepler Field. *Astrophysical Journal Letters*, 713:L164–L168, April 2010.

J. L. Christiansen, S. Ballard, D. Charbonneau, N. Madhusudhan, S. Seager, M. J. Holman, D. D. Wellnitz, D. Deming, M. F. A'Hearn, and EPOXI Team. Studying the Atmosphere of the Exoplanet HAT-P-7b Via Secondary Eclipse Measurements with EPOXI, Spitzer, and Kepler. *Astrophysical Journal*, 710: 97–104, February 2010.

C. Chubak, G. Marcy, D. A. Fischer, A. W. Howard, H. Isaacson, J. A. Johnson, and J. T. Wright. Precise Radial Velocities of 2046 Nearby FGKM Stars and 131 Standards. *ArXiv:1207.6212*, July 2012.

D. R. Ciardi, C. A. Beichman, E. P. Horch, and S. B. Howell. Understanding the Effects of Stellar Multiplicity on the Derived Planet Radii from Transit Surveys: Implications for Kepler, K2, and TESS. *Astrophysical Journal*, 805: 16, May 2015.

S. Ciceri, J. Lillo-Box, J. Southworth, L. Mancini, T. Henning, and D. Barrado. Kepler-432 b: a massive planet in a highly eccentric orbit transiting a red giant. *Astronomy & Astrophysics*, 573:L5, January 2015.

A. Claret. A new non-linear limb-darkening law for LTE stellar atmosphere models III. Sloan filters: Calculations for -5.0 $\leqslant$ log [M/H] $\leqslant$ +1, 2000 K $\leqslant$ T_{eff} $\leqslant$ 50 000 K at several surface gravities. *Astronomy & Astrophysics*, 428: 1001–1005, December 2004.

A. Claret and S. Bloemen. Gravity and limb-darkening coefficients for the Kepler, CoRoT, Spitzer, uvby, UBVRIJHK, and Sloan photometric systems. *Astronomy & Astrophysics*, 529:A75, May 2011.

A. Claret and N. C. S. Cunha. Circularization and synchronization times in Main-Sequence of detached eclipsing binaries II. Using the formalisms by Zahn. *Astronomy & Astrophysics*, 318:187–197, February 1997.

A. Claret, P. H. Hauschildt, and S. Witte. New limb-darkening coefficients for Phoenix/1d model atmospheres. II. Calculations for 5000 K $\leqslant$ T_{eff} $\leqslant$ 10 000 K Kepler, CoRot, Spitzer, uvby, UBVRIJHK, Sloan, and 2MASS photometric systems. *Astronomy & Astrophysics*, 552:A16, April 2013.

R. Cosentino, C. Lovis, F. Pepe, A. Collier Cameron, D. W. Latham, E. Molinari, S. Udry, N. Bezawada, M. Black, A. Born, N. Buchschacher, D. Charbonneau, P. Figueira, M. Fleury, A. Galli, A. Gallie, X. Gao, A. Ghedina, C. Gonzalez, M. Gonzalez, J. Guerra, D. Henry, K. Horne, I. Hughes, D. Kelly,

M. Lodi, D. Lunney, C. Maire, M. Mayor, G. Micela, M. P. Ordway, J. Peacock, D. Phillips, G. Piotto, D. Pollacco, D. Queloz, K. Rice, C. Riverol, L. Riverol, J. San Juan, D. Sasselov, D. Segransan, A. Sozzetti, D. Sosnowska, B. Stobie, A. Szentgyorgyi, A. Vick, and L. Weber. Harps-N: the new planet hunter at TNG. In *Society of Photo-Optical Instrumentation Engineers (SPIE) Conference Series*, volume 8446 of *Society of Photo-Optical Instrumentation Engineers (SPIE) Conference Series*, page 1, September 2012.

I. J. M. Crossfield, E. Petigura, J. E. Schlieder, A. W. Howard, B. J. Fulton, K. M. Aller, D. R. Ciardi, S. Lépine, T. Barclay, I. de Pater, K. de Kleer, E. V. Quintana, J. L. Christiansen, E. Schlafly, L. Kaltenegger, J. R. Crepp, T. Henning, C. Obermeier, N. Deacon, L. M. Weiss, H. T. Isaacson, B. M. S. Hansen, M. C. Liu, T. Greene, S. B. Howell, T. Barman, and C. Mordasini. A Nearby M Star with Three Transiting Super-Earths Discovered by K2. *Astrophysical Journal*, 804:10, May 2015.

R. I. Dawson. On the Tidal Origin of Hot Jupiter Stellar Obliquity Trends. *Astrophysical Journal Letters*, 790:L31, August 2014.

R. I. Dawson and J. A. Johnson. The Photoeccentric Effect and Proto-hot Jupiters. I. Measuring Photometric Eccentricities of Individual Transiting Planets. *Astrophysical Journal*, 756:122, September 2012.

R. I. Dawson, J. A. Johnson, D. C. Fabrycky, D. Foreman-Mackey, R. A. Murray-Clay, L. A. Buchhave, P. A. Cargile, K. I. Clubb, B. J. Fulton, L. Hebb, A. W. Howard, D. Huber, A. Shporer, and J. A. Valenti. Large Eccentricity, Low Mutual Inclination: The Three-dimensional Architecture of a Hierarchical System of Giant Planets. *Astrophysical Journal*, 791:89, August 2014.

R. I. Dawson, R. A. Murray-Clay, and J. A. Johnson. The Photoeccentric Effect and Proto-hot Jupiters. III. A Paucity of Proto-hot Jupiters on Super-eccentric Orbits. *Astrophysical Journal*, 798:66, January 2015.

K. M. Deck and E. Agol. Measurement of Planet Masses with Transit Timing Variations Due to Synodic Chopping Effects. *Astrophysical Journal*, 802:116, April 2015.

K. M. Deck, E. Agol, M. J. Holman, and D. Nesvorný. TTVFast: An Efficient and Accurate Code for Transit Timing Inversion Problems. *Astrophysical Journal*, 787:132, June 2014.

D. Deming, A. Wilkins, P. McCullough, A. Burrows, J. J. Fortney, E. Agol, I. Dobbs-Dixon, N. Madhusudhan, N. Crouzet, J.-M. Desert, R. L. Gilliland, K. Haynes, H. A. Knutson, M. Line, Z. Magic, A. M. Mandell, S. Ranjan, D. Charbonneau, M. Clampin, S. Seager, and A. P. Showman. Infrared Transmission Spectroscopy of the Exoplanets HD 209458b and XO-1b Using the Wide Field Camera-3 on the Hubble Space Telescope. *Astrophysical Journal*, 774:95, September 2013.

B.-O. Demory, M. Gillon, D. Deming, D. Valencia, S. Seager, B. Benneke, C. Lovis, P. Cubillos, J. Harrington, K. B. Stevenson, M. Mayor, F. Pepe, D. Queloz, D. Ségransan, and S. Udry. Detection of a transit of the super-Earth 55 Cancri e with warm Spitzer. *Astronomy & Astrophysics*, 533:A114, September 2011.

B.-O. Demory, J. de Wit, N. Lewis, J. Fortney, A. Zsom, S. Seager, H. Knutson, K. Heng, N. Madhusudhan, M. Gillon, T. Barclay, J.-M. Desert, V. Parmentier, and N. B. Cowan. Inference of Inhomogeneous Clouds in an Exoplanet Atmosphere. *Astrophysical Journal Letters*, 776:L25, October 2013.

J.-M. Désert, A. Lecavelier des Etangs, G. Hébrard, D. K. Sing, D. Ehrenreich, R. Ferlet, and A. Vidal-Madjar. Search for Carbon Monoxide in the Atmosphere of the Transiting Exoplanet HD 189733b. *Astrophysical Journal*, 699: 478–485, July 2009.

J.-M. Désert, D. Charbonneau, G. Torres, F. Fressin, S. Ballard, S. T. Bryson, H. A. Knutson, N. M. Batalha, W. J. Borucki, T. M. Brown, D. Deming, E. B. Ford, J. J. Fortney, R. L. Gilliland, D. W. Latham, and S. Seager. Low False Positive Rate of Kepler Candidates Estimated From A Combination Of Spitzer And Follow-Up Observations. *Astrophysical Journal*, 804:59, May 2015.

C. D. Dressing and D. Charbonneau. The Occurrence Rate of Small Planets around Small Stars. *Astrophysical Journal*, 767:95, April 2013.

C. D. Dressing, D. S. Spiegel, C. A. Scharf, K. Menou, and S. N. Raymond. Habitable Climates: The Influence of Eccentricity. *Astrophysical Journal*, 721: 1295–1307, October 2010.

W. Dziembowski. Light and radial velocity variations in a nonradially oscillating star. *Acta Astronomica*, 27:203–211, 1977.

J. Eastman, B. S. Gaudi, and E. Agol. EXOFAST: A Fast Exoplanetary Fitting Suite in IDL. *Publications of the Astronomical Society of the Pacific*, 125:83–112, January 2013.

D. Ehrenreich, X. Bonfils, C. Lovis, X. Delfosse, T. Forveille, M. Mayor, V. Neves, N. C. Santos, S. Udry, and D. Ségransan. Near-infrared transmission spectrum of the warm-Uranus GJ 3470b with the Wide Field Camera-3 on the Hubble Space Telescope. *Astronomy & Astrophysics*, 570:A89, October 2014.

L. J. Esteves, E. J. W. De Mooij, and R. Jayawardhana. Optical Phase Curves of Kepler Exoplanets. *Astrophysical Journal*, 772:51, July 2013.

M. E. Everett, S. B. Howell, and K. Kinemuchi. A UBV Photometric Survey of the Kepler Field. *Publications of the Astronomical Society of the Pacific*, 124: 316–322, April 2012.

D. Fabrycky and S. Tremaine. Shrinking Binary and Planetary Orbits by Kozai Cycles with Tidal Friction. *Astrophysical Journal*, 669:1298–1315, November 2007.

D. C. Fabrycky, J. J. Lissauer, D. Ragozzine, J. F. Rowe, J. H. Steffen, E. Agol, T. Barclay, N. Batalha, W. Borucki, D. R. Ciardi, E. B. Ford, T. N. Gautier, J. C. Geary, M. J. Holman, J. M. Jenkins, J. Li, R. C. Morehead, R. L. Morris, A. Shporer, J. C. Smith, M. Still, and J. Van Cleve. Architecture of Kepler's Multi-transiting Systems. II. New Investigations with Twice as Many Candidates. *Astrophysical Journal*, 790:146, August 2014.

G. G. Fazio, J. L. Hora, L. E. Allen, M. L. N. Ashby, P. Barmby, L. K. Deutsch, J.-S. Huang, S. Kleiner, M. Marengo, S. T. Megeath, G. J. Melnick, M. A. Pahre, B. M. Patten, J. Polizotti, H. A. Smith, R. S. Taylor, Z. Wang, S. P. Willner, W. F. Hoffmann, J. L. Pipher, W. J. Forrest, C. W. McMurty, C. R. McCreight, M. E. McKelvey, R. E. McMurray, D. G. Koch, S. H. Moseley, R. G. Arendt, J. E. Mentzell, C. T. Marx, P. Losch, P. Mayman, W. Eichhorn, D. Krebs, M. Jhabvala, D. Y. Gezari, D. J. Fixsen, J. Flores, K. Shakoorzadeh, R. Jungo, C. Hakun, L. Workman, G. Karpati, R. Kichak, R. Whitley, S. Mann, E. V. Tollestrup, P. Eisenhardt, D. Stern, V. Gorjian, B. Bhattacharya, S. Carey, B. O. Nelson, W. J. Glaccum, M. Lacy, P. J. Lowrance, S. Laine, W. T. Reach, J. A. Stauffer, J. A. Surace, G. Wilson, E. L. Wright, A. Hoffman, G. Domingo, and M. Cohen. The Infrared Array Camera (IRAC) for the Spitzer Space Telescope. *Astrophysical Journal Supplement Series*, 154:10–17, September 2004.

J. W. Ferguson, D. R. Alexander, F. Allard, T. Barman, J. G. Bodnarik, P. H. Hauschildt, A. Heffner-Wong, and A. Tamanai. Low-Temperature Opacities. *Astrophysical Journal*, 623:585, April 2005.

D. B. Fielding, C. F. McKee, A. Socrates, A. J. Cunningham, and R. I. Klein. The turbulent origin of spin-orbit misalignment in planetary systems. *Monthly Notices of the Royal Astronomical Society*, 450:3306–3318, July 2015.

D. A. Fischer, M. E. Schwamb, K. Schawinski, C. Lintott, J. Brewer, M. Giguere, S. Lynn, M. Parrish, T. Sartori, R. Simpson, A. Smith, J. Spronck, N. Batalha, J. Rowe, J. Jenkins, S. Bryson, A. Prsa, P. Tenenbaum, J. Crepp, T. Morton, A. Howard, M. Beleu, Z. Kaplan, N. Vannispen, C. Sharzer, J. Defouw, A. Hajduk, J. P. Neal, A. Nemec, N. Schuepbach, and V. Zimmermann. Planet Hunters: the first two planet candidates identified by the public using the Kepler public archive data. *Monthly Notices of the Royal Astronomical Society*, 419:2900–2911, February 2012.

A. Fogtmann-Schulz, B. Hinrup, V. Van Eylen, J. Christensen-Dalsgaard, H. Kjeldsen, V. Silva Aguirre, and B. Tingley. Accurate Parameters of the Oldest Known Rocky-exoplanet Hosting System: Kepler-10 Revisited. *Astrophysical Journal*, 781:67, February 2014.

E. B. Ford and F. A. Rasio. Origins of Eccentric Extrasolar Planets: Testing the Planet-Planet Scattering Model. *Astrophysical Journal*, 686:621–636, October 2008.

E. B. Ford, S. N. Quinn, and D. Veras. Characterizing the Orbital Eccentricities of Transiting Extrasolar Planets with Photometric Observations. *Astrophysical Journal*, 678:1407–1418, May 2008.

E. B. Ford, J. F. Rowe, D. C. Fabrycky, J. A. Carter, M. J. Holman, J. J. Lissauer, D. Ragozzine, J. H. Steffen, N. M. Batalha, W. J. Borucki, S. Bryson, D. A. Caldwell, E. W. Dunham, T. N. Gautier, III, J. M. Jenkins, D. G. Koch, J. Li, P. Lucas, G. W. Marcy, S. McCauliff, F. R. Mullally, E. Quintana, M. Still, P. Tenenbaum, S. E. Thompson, and J. D. Twicken. Transit Timing Observations from Kepler. I. Statistical Analysis of the First Four Months. *Astrophysical Journal Supplement Series*, 197:2, November 2011.

D. Foreman-Mackey, D. W. Hogg, D. Lang, and J. Goodman. emcee: The MCMC Hammer. *Publications of the Astronomical Society of the Pacific*, 125: 306–312, March 2013.

D. Foreman-Mackey, D. W. Hogg, and T. D. Morton. Exoplanet Population Inference and the Abundance of Earth Analogs from Noisy, Incomplete Catalogs. *Astrophysical Journal*, 795:64, November 2014.

D. Foreman-Mackey, B. T. Montet, D. W. Hogg, T. D. Morton, D. Wang, and B. Schölkopf. A systematic search for transiting planets in the K2 data. *ArXiv e-prints*, February 2015.

S. Frandsen, A. Jones, H. Kjeldsen, M. Viskum, J. Hjorth, N. H. Andersen, and B. Thomsen. CCD photometry of the δ-Scuti star κ^2^ Bootis. *Astronomy & Astrophysics*, 301:123, September 1995.

F. Fressin, G. Torres, J.-M. Désert, D. Charbonneau, N. M. Batalha, J. J. Fortney, J. F. Rowe, C. Allen, W. J. Borucki, T. M. Brown, S. T. Bryson, D. R. Ciardi, W. D. Cochran, D. Deming, E. W. Dunham, D. C. Fabrycky, T. N. Gautier, III, R. L. Gilliland, C. E. Henze, M. J. Holman, S. B. Howell, J. M. Jenkins, K. Kinemuchi, H. Knutson, D. G. Koch, D. W. Latham, J. J. Lissauer, G. W. Marcy, D. Ragozzine, D. D. Sasselov, M. Still, P. Tenenbaum, and K. Uddin. Kepler-10 c: a 2.2 Earth Radius Transiting Planet in a Multiple System. *Astrophysical Journal Supplement Series*, 197:5, November 2011.

F. Fressin, G. Torres, D. Charbonneau, S. T. Bryson, J. Christiansen, C. D. Dressing, J. M. Jenkins, L. M. Walkowicz, and N. M. Batalha. The False Positive Rate of Kepler and the Occurrence of Planets. *Astrophysical Journal*, 766:81, April 2013.

D. Gandolfi, H. Parviainen, H. J. Deeg, A. F. Lanza, M. Fridlund, P. G. Prada Moroni, R. Alonso, T. Augusteijn, J. Cabrera, T. Evans, S. Geier, A. P. Hatzes, T. Holczer, S. Hoyer, T. Kangas, T. Mazeh, I. Pagano, L. Tal-Or, and B. Tingley. Kepler-423b: a half-Jupiter mass planet transiting a very old solar-like star. *Astronomy & Astrophysics*, 576:A11, April 2015.

B. S. Gaudi and J. N. Winn. Prospects for the Characterization and Confirmation of Transiting Exoplanets via the Rossiter-McLaughlin Effect. *Astrophysical Journal*, 655:550–563, January 2007.

J. Z. Gazak, J. A. Johnson, J. Tonry, D. Dragomir, J. Eastman, A. W. Mann, and E. Agol. Transit Analysis Package: An IDL Graphical User Interface for Exoplanet Transit Photometry. *Advances in Astronomy*, 2012:697967, 2012.

G. Giuricin, F. Mardirossian, and M. Mezzetti. Orbital circularization in early-type detached close binaries. *Astronomy & Astrophysics*, 134:365–367, May 1984.

L. Gizon and S. K. Solanki. Determining the Inclination of the Rotation Axis of a Sun-like Star. *Astrophysical Journal*, 589:1009–1019, June 2003.

P. Goldreich, N. Murray, and P. Kumar. Excitation of solar p-modes. *Astrophysical Journal*, 424:466–479, March 1994.

J. Goodman and J. Weare. Ensemble samplers with affine invariance. *Commun. Appl. Math. Comput. Sci.*, 5:65, January 2010.

G. Grec, E. Fossat, and M. A. Pomerantz. Full-disk observations of solar oscillations from the geographic South Pole - Latest results. *Solar Physics*, 82:55–66, January 1983.

N Grevesse and A J Sauval. Standard Solar Composition. *Space Sci. Rev.*, 85: 161, May 1998.

F. Grundahl, H. Kjeldsen, S. Frandsen, M. Andersen, T. Bedding, T. Arentoft, and J. Christensen-Dalsgaard. SONG: Stellar Oscillations Network Group – A global network of small telescopes for asteroseismology and planet searches. *Memorie della Società Astronomica Italiana*, 77:458, 2006.

S. Hadden and Y. Lithwick. Densities and Eccentricities of 139 Kepler Planets from Transit Time Variations. *Astrophysical Journal*, 787:80, May 2014.

R. Handberg and T. L. Campante. Bayesian peak-bagging of solar-like oscillators using MCMC: a comprehensive guide. *Astronomy & Astrophysics*, 527: A56, March 2011.

B. M. S. Hansen and N. Murray. Testing in Situ Assembly with the Kepler Planet Candidate Sample. *Astrophysical Journal*, 775:53, September 2013.

B. M. S. Hansen and N. Murray. Secular effects of tidal damping in compact planetary systems. *Monthly Notices of the Royal Astronomical Society*, 448: 1044–1059, April 2015.

J. Harvey. High-resolution helioseismology. In E. Rolfe and B. Battrick, editors, *Future Missions in Solar, Heliospheric & Space Plasma Physics*, volume 235 of *ESA Special Publication*, pages 199–208, June 1985.

G. Hébrard, F. Bouchy, F. Pont, B. Loeillet, M. Rabus, X. Bonfils, C. Moutou, I. Boisse, X. Delfosse, M. Desort, A. Eggenberger, D. Ehrenreich, T. Forveille, A.-M. Lagrange, C. Lovis, M. Mayor, F. Pepe, C. Perrier, D. Queloz, N. C. Santos, D. Ségransan, S. Udry, and A. Vidal-Madjar. Misaligned spin-orbit in the XO-3 planetary system? *Astronomy & Astrophysics*, 488:763–770, September 2008.

T. Hirano, R. Sanchis-Ojeda, Y. Takeda, N. Narita, J. N. Winn, A. Taruya, and Y. Suto. Measurements of Stellar Inclinations for Kepler Planet Candidates. *Astrophysical Journal*, 756:66, September 2012.

M. J. Holman and N. W. Murray. The Use of Transit Timing to Detect Terrestrial-Mass Extrasolar Planets. *Science*, 307:1288–1291, February 2005.

I. D. Howarth. On stellar limb darkening and exoplanetary transits. *Monthly Notices of the Royal Astronomical Society*, 418:1165–1175, December 2011.

S. B. Howell, M. E. Everett, W. Sherry, E. Horch, and D. R. Ciardi. Speckle Camera Observations for the NASA Kepler Mission Follow-up Program. *Astronomical Journal*, 142:19, July 2011.

S. B. Howell, C. Sobeck, M. Haas, M. Still, T. Barclay, F. Mullally, J. Troeltzsch, S. Aigrain, S. T. Bryson, D. Caldwell, W. J. Chaplin, W. D. Cochran, D. Huber, G. W. Marcy, A. Miglio, J. R. Najita, M. Smith, J. D. Twicken, and J. J. Fortney. The K2 Mission: Characterization and Early results. *ArXiv e-prints*, February 2014.

D. Huber, M. J. Ireland, T. R. Bedding, I. M. Brandão, L. Piau, V. Maestro, T. R. White, H. Bruntt, L. Casagrande, J. Molenda-Żakowicz, V. Silva Aguirre, S. G. Sousa, T. Barclay, C. J. Burke, W. J. Chaplin, J. Christensen-Dalsgaard, M. S. Cunha, J. De Ridder, C. D. Farrington, A. Frasca, R. A. García, R. L. Gilliland, P. J. Goldfinger, S. Hekker, S. D. Kawaler, H. Kjeldsen, H. A. McAlister, T. S. Metcalfe, A. Miglio, M. J. P. F. G. Monteiro, M. H. Pinsonneault,

G. H. Schaefer, D. Stello, M. C. Stumpe, J. Sturmann, L. Sturmann, T. A. ten Brummelaar, M. J. Thompson, N. Turner, and K. Uytterhoeven. Fundamental Properties of Stars Using Asteroseismology from Kepler and CoRoT and Interferometry from the CHARA Array. *Astrophysical Journal*, 760:32, November 2012.

D. Huber, J. A. Carter, M. Barbieri, A. Miglio, K. M. Deck, D. C. Fabrycky, B. T. Montet, L. A. Buchhave, W. J. Chaplin, S. Hekker, J. Montalbán, R. Sanchis-Ojeda, S. Basu, T. R. Bedding, T. L. Campante, J. Christensen-Dalsgaard, Y. P. Elsworth, D. Stello, T. Arentoft, E. B. Ford, R. L. Gilliland, R. Handberg, A. W. Howard, H. Isaacson, J. A. Johnson, C. Karoff, S. D. Kawaler, H. Kjeldsen, D. W. Latham, M. N. Lund, M. Lundkvist, G. W. Marcy, T. S. Metcalfe, and J. N. Winn. Stellar Spin-Orbit Misalignment in a Multiplanet System. *ArXiv:1310.4503*, October 2013a.

D. Huber, W. J. Chaplin, J. Christensen-Dalsgaard, R. L. Gilliland, H. Kjeldsen, L. A. Buchhave, D. A. Fischer, J. J. Lissauer, J. F. Rowe, R. Sanchis-Ojeda, S. Basu, R. Handberg, S. Hekker, A. W. Howard, H. Isaacson, C. Karoff, D. W. Latham, M. N. Lund, M. Lundkvist, G. W. Marcy, A. Miglio, V. Silva Aguirre, D. Stello, T. Arentoft, T. Barclay, T. R. Bedding, C. J. Burke, J. L. Christiansen, Y. P. Elsworth, M. R. Haas, S. D. Kawaler, T. S. Metcalfe, F. Mullally, and S. E. Thompson. Fundamental Properties of Kepler Planet-candidate Host Stars using Asteroseismology. *Astrophysical Journal*, 767:127, April 2013b.

S. Ida, D. N. C. Lin, and M. Nagasawa. Toward a Deterministic Model of Planetary Formation. VII. Eccentricity Distribution of Gas Giants. *Astrophysical Journal*, 775:42, September 2013.

C. A. Iglesias and F. J. Rogers. Updated Opal Opacities. *Astrophysical Journal*, 464:943, June 1996.

B. K. Jackson, N. K. Lewis, J. W. Barnes, L. Drake Deming, A. P. Showman, and J. J. Fortney. The EVIL-MC Model for Ellipsoidal Variations of Planet-hosting Stars and Applications to the HAT-P-7 System. *Astrophysical Journal*, 751:112, June 2012.

J. M. Jenkins, D. A. Caldwell, and W. J. Borucki. Some Tests to Establish Confidence in Planets Discovered by Transit Photometry. *Astrophysical Journal*, 564:495–507, January 2002.

D. Jontof-Hutter, J. F. Rowe, J. J. Lissauer, D. C. Fabrycky, and E. B. Ford. The mass of the Mars-sized exoplanet Kepler-138 b from transit timing. *Nature*, 522:321–323, June 2015.

M. Jurić and S. Tremaine. Dynamical Origin of Extrasolar Planet Eccentricity Distribution. *Astrophysical Journal*, 686:603–620, October 2008.

S. R. Kane, D. R. Ciardi, D. M. Gelino, and K. von Braun. The exoplanet eccentricity distribution from Kepler planet candidates. *Monthly Notices of the Royal Astronomical Society*, 425:757–762, September 2012.

I. Kant. *Allgemeine Naturgeschichte und Theorie des Himmels*. 1755.

C. Karoff. PhD thesis, PhD thesis, University of Aarhus, Denmark, (2008), 2008.

K. F. Khaliullin and A. I. Khaliullina. Synchronization and circularization in early-type binaries on main sequence. *Monthly Notices of the Royal Astronomical Society*, 401:257–274, January 2010.

K. Kinemuchi, T. Barclay, M. Fanelli, J. Pepper, M. Still, and S. B. Howell. Demystifying Kepler Data: A Primer for Systematic Artifact Mitigation. *Publications of the Astronomical Society of the Pacific*, 124:963–984, September 2012.

R. Kippenhahn, A. Weigert, and A. Weiss. Stellar Structure and Evolution. *Stellar Structure and Evolution: Astronomy and Astrophysics Library, ISBN 978-3-642-30255-8. Springer-Verlag Berlin Heidelberg*, March 2013.

D. M. Kipping. Investigations of approximate expressions for the transit duration. *Monthly Notices of the Royal Astronomical Society*, 407:301–313, September 2010.

D. M. Kipping. Efficient, uninformative sampling of limb darkening coefficients for two-parameter laws. *Monthly Notices of the Royal Astronomical Society*, 435:2152–2160, November 2013a.

D. M. Kipping. Parametrizing the exoplanet eccentricity distribution with the Beta distribution. *Monthly Notices of the Royal Astronomical Society*, 434: L51–L55, July 2013b.

D. M. Kipping. Characterizing distant worlds with asterodensity profiling. *Monthly Notices of the Royal Astronomical Society*, 440:2164–2184, May 2014a.

D. M. Kipping. Bayesian priors for the eccentricity of transiting planets. *Monthly Notices of the Royal Astronomical Society*, 444:2263–2269, November 2014b.

D. M. Kipping, W. R. Dunn, J. M. Jasinski, and V. P. Manthri. A novel method to photometrically constrain orbital eccentricities: Multibody Asterodensity Profiling. *Monthly Notices of the Royal Astronomical Society*, 421:1166–1188, April 2012.

H. Kjeldsen. PhD thesis, PhD thesis, University of Aarhus, Denmark, (1992), 1992.

H. Kjeldsen and S. Frandsen. High-precision time-resolved CCD photometry. *Publications of the Astronomical Society of the Pacific*, 104:413–434, June 1992.

H. Kjeldsen, T. R. Bedding, and J. Christensen-Dalsgaard. Correcting Stellar Oscillation Frequencies for Near-Surface Effects. *Astrophysical Journal Letters*, 683:L175–L178, August 2008.

H. A. Knutson, D. Charbonneau, L. E. Allen, J. J. Fortney, E. Agol, N. B. Cowan, A. P. Showman, C. S. Cooper, and S. T. Megeath. A map of the day-night contrast of the extrasolar planet HD 189733b. *Nature*, 447:183–186, May 2007.

H. A. Knutson, D. Charbonneau, L. E. Allen, A. Burrows, and S. T. Megeath. The 3.6-8.0 μm Broadband Emission Spectrum of HD 209458b: Evidence for an Atmospheric Temperature Inversion. *Astrophysical Journal*, 673:526–531, January 2008.

D. G. Koch, W. J. Borucki, G. Basri, N. M. Batalha, T. M. Brown, D. Caldwell, J. Christensen-Dalsgaard, W. D. Cochran, E. DeVore, E. W. Dunham, T. N. Gautier, III, J. C. Geary, R. L. Gilliland, A. Gould, J. Jenkins, Y. Kondo, D. W. Latham, J. J. Lissauer, G. Marcy, D. Monet, D. Sasselov, A. Boss, D. Brownlee, J. Caldwell, A. K. Dupree, S. B. Howell, H. Kjeldsen, S. Meibom, D. Morrison, T. Owen, H. Reitsema, J. Tarter, S. T. Bryson, J. L. Dotson, P. Gazis, M. R. Haas, J. Kolodziejczak, J. F. Rowe, J. E. Van Cleve, C. Allen, H. Chandrasekaran, B. D. Clarke, J. Li, E. V. Quintana, P. Tenenbaum, J. D. Twicken, and H. Wu. Kepler Mission Design, Realized Photometric Performance, and Early Science. *Astrophysical Journal Letters*, 713:L79, April 2010.

R. H. Koch and B. J. Hrivnak. On Zahn's theory of tidal friction for cool, main-sequence close binaries. *Astronomical Journal*, 86:438–441, March 1981.

R. Kolbl, G. W. Marcy, H. Isaacson, and A. W. Howard. Detection of Stars Within 0.8 in of Kepler Objects of Interest. *Astronomical Journal*, 149:18, January 2015.

K. Kolenberg, S. Bryson, R. Szabó, D. W. Kurtz, R. Smolec, J. M. Nemec, E. Guggenberger, P. Moskalik, J. M. Benkő, M. Chadid, Y.-B. Jeon, L. L. Kiss, G. Kopacki, J. Nuspl, M. Still, J. Christensen-Dalsgaard, H. Kjeldsen, W. J. Borucki, D. A. Caldwell, J. M. Jenkins, and D. Koch. Kepler photometry of the prototypical Blazhko star RR Lyr: an old friend seen in a new light. *Monthly Notices of the Royal Astronomical Society*, 411:878–890, February 2011.

Z. Kopal. Evolutionary processes in close binary stars. *Annales d'Astrophysique*, 19:298, January 1956.

R. K. Kopparapu, R. Ramirez, J. F. Kasting, V. Eymet, T. D. Robinson, S. Mahadevan, R. C. Terrien, S. Domagal-Goldman, V. Meadows, and R. Desh-

pande. Habitable Zones around Main-sequence Stars: New Estimates. *Astrophysical Journal*, 765:131, March 2013.

G. Kovács, S. Zucker, and T. Mazeh. A box-fitting algorithm in the search for periodic transits. *Astronomy & Astrophysics*, 391:369–377, August 2002.

Y. Kozai. Secular perturbations of asteroids with high inclination and eccentricity. *Astronomical Journal*, 67:591, November 1962.

L. Kreidberg, J. L. Bean, J.-M. Désert, B. Benneke, D. Deming, K. B. Stevenson, S. Seager, Z. Berta-Thompson, A. Seifahrt, and D. Homeier. Clouds in the atmosphere of the super-Earth exoplanet GJ1214b. *Nature*, 505:69–72, January 2014.

D. Lai, F. Foucart, and D. N. C. Lin. Evolution of spin direction of accreting magnetic protostars and spin-orbit misalignment in exoplanetary systems. *Monthly Notices of the Royal Astronomical Society*, 412:2790–2798, April 2011.

P. S. Laplace. Exposition du systeme du monde. 1796.

D. W. Latham, J. F. Rowe, S. N. Quinn, N. M. Batalha, W. J. Borucki, T. M. Brown, S. T. Bryson, L. A. Buchhave, D. A. Caldwell, J. A. Carter, J. L. Christiansen, D. R. Ciardi, W. D. Cochran, E. W. Dunham, D. C. Fabrycky, E. B. Ford, T. N. Gautier, III, R. L. Gilliland, M. J. Holman, S. B. Howell, K. A. Ibrahim, H. Isaacson, J. M. Jenkins, D. G. Koch, J. J. Lissauer, G. W. Marcy, E. V. Quintana, D. Ragozzine, D. Sasselov, A. Shporer, J. H. Steffen, W. F. Welsh, and B. Wohler. A First Comparison of Kepler Planet Candidates in Single and Multiple Systems. *Astrophysical Journal Letters*, 732:L24, May 2011.

P. Ledoux. The Nonradial Oscillations of Gaseous Stars and the Problem of Beta Canis Majoris. *Astrophysical Journal*, 114:373, November 1951.

M. L. Lidov. The evolution of orbits of artificial satellites of planets under the action of gravitational perturbations of external bodies. *Planet. Space Sci.*, 9: 719–759, October 1962.

M. A. Limbach and E. L. Turner. Exoplanet orbital eccentricity: Multiplicity relation and the Solar System. *Proceedings of the National Academy of Science*, 112:20–24, January 2015.

J. J. Lissauer, D. Ragozzine, D. C. Fabrycky, J. H. Steffen, E. B. Ford, J. M. Jenkins, A. Shporer, M. J. Holman, J. F. Rowe, E. V. Quintana, N. M. Batalha, W. J. Borucki, S. T. Bryson, D. A. Caldwell, J. A. Carter, D. Ciardi, E. W. Dunham, J. J. Fortney, T. N. Gautier, III, S. B. Howell, D. G. Koch, D. W. Latham, G. W. Marcy, R. C. Morehead, and D. Sasselov. Architecture and Dynamics of Kepler's Candidate Multiple Transiting Planet Systems. *Astrophysical Journal Supplement Series*, 197:8, November 2011.

J. J. Lissauer, G. W. Marcy, J. F. Rowe, S. T. Bryson, E. Adams, L. A. Buchhave, D. R. Ciardi, W. D. Cochran, D. C. Fabrycky, E. B. Ford, F. Fressin, J. Geary, R. L. Gilliland, M. J. Holman, S. B. Howell, J. M. Jenkins, K. Kinemuchi, D. G. Koch, R. C. Morehead, D. Ragozzine, S. E. Seader, P. G. Tanenbaum, G. Torres, and J. D. Twicken. Almost All of Kepler's Multiple-planet Candidates Are Planets. *Astrophysical Journal*, 750:112, May 2012.

J. J. Lissauer, G. W. Marcy, S. T. Bryson, J. F. Rowe, D. Jontof-Hutter, E. Agol, W. J. Borucki, J. A. Carter, E. B. Ford, R. L. Gilliland, R. Kolbl, K. M. Star, J. H. Steffen, and G. Torres. Validation of Kepler's Multiple Planet Candidates. II. Refined Statistical Framework and Descriptions of Systems of Special Interest. *Astrophysical Journal*, 784:44, March 2014.

Y. Lithwick, J. Xie, and Y. Wu. Extracting Planet Mass and Eccentricity from TTV Data. *Astrophysical Journal*, 761:122, December 2012.

C. Lovis and D. Fischer. *Radial Velocity Techniques for Exoplanets*, pages 27–53. December 2010.

L. B. Lucy. Spectroscopic binaries with elliptical orbits. *Astronomy & Astrophysics*, 439:663–670, August 2005.

L. B. Lucy and M. A. Sweeney. Spectroscopic binaries with circular orbits. *Astronomical Journal*, 76:544–556, August 1971.

M. N. Lund, W. J. Chaplin, and H. Kjeldsen. A new method to detect solar-like oscillations at very low S/N using statistical significance testing. *Monthly Notices of the Royal Astronomical Society*, 427:1784–1792, December 2012.

M. N. Lund, H. Kjeldsen, J. Christensen-Dalsgaard, R. Handberg, and V. Silva Aguirre. Detection of l = 4 and l = 5 Modes in 12 Years of Solar VIRGO-SPM Data–Tests on Kepler Observations of 16 Cyg A and B. *Astrophysical Journal*, 782:2, February 2014a.

M. N. Lund, M. Lundkvist, V. Silva Aguirre, G. Houdek, L. Casagrande, V. Van Eylen, T. L. Campante, C. Karoff, H. Kjeldsen, S. Albrecht, W. J. Chaplin, M. B. Nielsen, P. Degroote, G. R. Davies, and R. Handberg. Asteroseismic inference on the spin-orbit misalignment and stellar parameters of HAT-P-7. *Astronomy & Astrophysics*, 570:A54, October 2014b.

M. N. Lund, R. Handberg, G. R. Davies, W. J. Chaplin, and C. D. Jones. K2P^2 A Photometry Pipeline for the K2 Mission. *Astrophysical Journal*, 806:30, June 2015.

M. S. Lundkvist, H. Kjeldsen, S. Albrecht, G. R. Davies, S. Basu, D. Huber, C. Karoff, V. Silva Aguirre, V. Van Eylen, C. Vang, T. Arentoft, T. Barclay, T. R. Bedding, T. L. Campante, W. J. Chaplin, J. Christensen-Dalsgaard, Y. P. Elsworth, R. L. Gilliland, R. Handberg, S. Hekker, S. D. Kawaler, M. N.

Lund, T. S. Metcalfe, A. Miglio, J. F. Rowe, D. Stello, B. Tingley, and T. R. White. Hot super-Earths stripped by their host stars. *submitted to Nature comm.*, September 2015.

Z. Magic, A. Serenelli, A. Weiss, and B. Chaboyer. On Using the Color-Magnitude Diagram Morphology of M67 to Test Solar Abundances. *Astrophysical Journal*, 718:1378–1387, August 2010.

K. Mandel and E. Agol. Analytic Light Curves for Planetary Transit Searches. *Astrophysical Journal Letters*, 580:L171–L175, December 2002.

G. W. Marcy, H. Isaacson, A. W. Howard, J. F. Rowe, J. M. Jenkins, S. T. Bryson, D. W. Latham, S. B. Howell, T. N. Gautier, III, N. M. Batalha, L. Rogers, D. Ciardi, D. A. Fischer, R. L. Gilliland, H. Kjeldsen, J. Christensen-Dalsgaard, D. Huber, W. J. Chaplin, S. Basu, L. A. Buchhave, S. N. Quinn, W. J. Borucki, D. G. Koch, R. Hunter, D. A. Caldwell, J. Van Cleve, R. Kolbl, L. M. Weiss, E. Petigura, S. Seager, T. Morton, J. A. Johnson, S. Ballard, C. Burke, W. D. Cochran, M. Endl, P. MacQueen, M. E. Everett, J. J. Lissauer, E. B. Ford, G. Torres, F. Fressin, T. M. Brown, J. H. Steffen, D. Charbonneau, G. S. Basri, D. D. Sasselov, J. Winn, R. Sanchis-Ojeda, J. Christiansen, E. Adams, C. Henze, A. Dupree, D. C. Fabrycky, J. J. Fortney, J. Tarter, M. J. Holman, P. Tenenbaum, A. Shporer, P. W. Lucas, W. F. Welsh, J. A. Orosz, T. R. Bedding, T. L. Campante, G. R. Davies, Y. Elsworth, R. Handberg, S. Hekker, C. Karoff, S. D. Kawaler, M. N. Lund, M. Lundkvist, T. S. Metcalfe, A. Miglio, V. Silva Aguirre, D. Stello, T. R. White, A. Boss, E. Devore, A. Gould, A. Prsa, E. Agol, T. Barclay, J. Coughlin, E. Brugamyer, F. Mullally, E. V. Quintana, M. Still, S. E. Thompson, D. Morrison, J. D. Twicken, J.-M. Désert, J. Carter, J. R. Crepp, G. Hébrard, A. Santerne, C. Moutou, C. Sobeck, D. Hudgins, M. R. Haas, P. Robertson, J. Lillo-Box, and D. Barrado. Masses, Radii, and Orbits of Small Kepler Planets: The Transition from Gaseous to Rocky Planets. *Astrophysical Journal Supplement Series*, 210: 20, February 2014.

K. Masuda. Spin-Orbit Angles of Kepler-13Ab and HAT-P-7b from Gravity-darkened Transit Light Curves. *Astrophysical Journal*, 805:28, May 2015.

R. D. Mathieu and T. Mazeh. The circularized binaries in open clusters - A new clock for age determination. *Astrophysical Journal*, 326:256–264, March 1988.

S. Mathur, T. S. Metcalfe, M. Woitaszek, H. Bruntt, G. A. Verner, J. Christensen-Dalsgaard, O. L. Creevey, G. Doğan, S. Basu, C. Karoff, D. Stello, T. Appourchaux, T. L. Campante, W. J. Chaplin, R. A. García, T. R. Bedding, O. Benomar, A. Bonanno, S. Deheuvels, Y. Elsworth, P. Gaulme, J. A. Guzik, R. Handberg, S. Hekker, W. Herzberg, M. J. P. F. G. Monteiro, L. Piau, P.-O. Quirion, C. Régulo, M. Roth, D. Salabert, A. Serenelli, M. J. Thompson,

R. Trampedach, T. R. White, J. Ballot, I. M. Brandão, J. Molenda-Żakowicz, H. Kjeldsen, J. D. Twicken, K. Uddin, and B. Wohler. A Uniform Asteroseismic Analysis of 22 Solar-type Stars Observed by Kepler. *Astrophysical Journal*, 749:152, April 2012.

M. Mayor and J. C. Mermilliod. Orbit Circularization Time in Binary Stellar Systems. In A. Maeder and A. Renzini, editors, *Observational Tests of the Stellar Evolution Theory*, volume 105 of *IAU Symposium*, page 411, 1984.

M. Mayor and D. Queloz. A Jupiter-mass companion to a solar-type star. *Nature*, 378:355–359, November 1995.

M. Mayor, F. Pepe, D. Queloz, F. Bouchy, G. Rupprecht, G. Lo Curto, G. Avila, W. Benz, J.-L. Bertaux, X. Bonfils, T. Dall, H. Dekker, B. Delabre, W. Eckert, M. Fleury, A. Gilliotte, D. Gojak, J. C. Guzman, D. Kohler, J.-L. Lizon, A. Longinotti, C. Lovis, D. Megevand, L. Pasquini, J. Reyes, J.-P. Sivan, D. Sosnowska, R. Soto, S. Udry, A. van Kesteren, L. Weber, and U. Weilenmann. Setting New Standards with HARPS. *The Messenger*, 114:20–24, December 2003.

M. Mayor, M. Marmier, C. Lovis, S. Udry, D. Ségransan, F. Pepe, W. Benz, J. . Bertaux, F. Bouchy, X. Dumusque, G. Lo Curto, C. Mordasini, D. Queloz, and N. C. Santos. The HARPS search for southern extra-solar planets XXXIV. Occurrence, mass distribution and orbital properties of super-Earths and Neptune-mass planets. *ArXiv:1109.2497*, September 2011.

T. Mazeh. Observational Evidence for Tidal Interaction in Close Binary Systems. In M.-J. Goupil and J.-P. Zahn, editors, *EAS Publications Series*, volume 29 of *EAS Publications Series*, pages 1–65, 2008.

T. Mazeh and J. Shaham. The orbital evolution of close triple systems - The binary eccentricity. *Astronomy & Astrophysics*, 77:145–151, August 1979.

T. Mazeh, Y. Krymolowski, and G. Rosenfeld. The High Eccentricity of the Planet Orbiting 16 Cygni B. *Astrophysical Journal Letters*, 477:L103–L106, March 1997.

T. Mazeh, O. Tamuz, and P. North. Automated analysis of eclipsing binary light curves - II. Statistical analysis of OGLE LMC eclipsing binaries. *Monthly Notices of the Royal Astronomical Society*, 367:1531–1542, April 2006.

T. Mazeh, G. Nachmani, T. Holczer, D. C. Fabrycky, E. B. Ford, R. Sanchis-Ojeda, G. Sokol, J. F. Rowe, E. Agol, J. A. Carter, J. J. Lissauer, E. V. Quintana, D. Ragozzine, J. H. Steffen, and W. Welsh. Transit Timing Observations from Kepler. VIII Catalog of Transit Timing Measurements of the First Twelve Quarters. *ArXiv:1301.5499*, January 2013.

T. Mazeh, H. B. Perets, A. McQuillan, and E. S. Goldstein. Photometric Amplitude Distribution of Stellar Rotation of KOIs – Indication for Spin-Orbit Alignment of Cool Stars and High Obliquity for Hot Stars. *Astrophysical Journal*, 801:3, March 2015.

D. B. McLaughlin. Some results of a spectrographic study of the Algol system. *Astrophysical Journal*, 60:22–31, July 1924.

A. McQuillan, T. Mazeh, and S. Aigrain. Stellar Rotation Periods of the Kepler Objects of Interest: A Dearth of Close-in Planets around Fast Rotators. *ArXiv:1308.1845*, August 2013.

S. Meibom and R. D. Mathieu. A Robust Measure of Tidal Circularization in Coeval Binary Populations: The Solar-Type Spectroscopic Binary Population in the Open Cluster M35. *Astrophysical Journal*, 620:970–983, February 2005.

S. A. Metchev, A. Heinze, D. Apai, D. Flateau, J. Radigan, A. Burgasser, M. S. Marley, É. Artigau, P. Plavchan, and B. Goldman. Weather on Other Worlds. II. Survey Results: Spots are Ubiquitous on L and T Dwarfs. *Astrophysical Journal*, 799:154, February 2015.

J. Molenda-Żakowicz, S. G. Sousa, A. Frasca, K. Uytterhoeven, M. Briquet, H. Van Winckel, D. Drobek, E. Niemczura, P. Lampens, J. Lykke, S. Bloemen, J. F. Gameiro, C. Jean, D. Volpi, N. Gorlova, A. Mortier, M. Tsantaki, and G. Raskin. Atmospheric parameters of 169 F-, G-, K- and M-type stars in the Kepler field. *Monthly Notices of the Royal Astronomical Society*, July 2013.

B. T. Montet, T. D. Morton, D. Foreman-Mackey, J. A. Johnson, D. W. Hogg, B. P. Bowler, D. W. Latham, A. Bieryla, and A. W. Mann. Stellar and Planetary Properties of K2 Campaign 1 Candidates and Validation of 17 Planets, Including a Planet Receiving Earth-like Insolation. *Astrophysical Journal*, 809: 25, August 2015.

A. V. Moorhead, E. B. Ford, R. C. Morehead, J. Rowe, W. J. Borucki, N. M. Batalha, S. T. Bryson, D. A. Caldwell, D. C. Fabrycky, T. N. Gautier, III, D. G. Koch, M. J. Holman, J. M. Jenkins, J. Li, J. J. Lissauer, P. Lucas, G. W. Marcy, S. N. Quinn, E. Quintana, D. Ragozzine, A. Shporer, M. Still, and G. Torres. The Distribution of Transit Durations for Kepler Planet Candidates and Implications for Their Orbital Eccentricities. *Astrophysical Journal Supplement Series*, 197:1, November 2011.

B. M. Morris, A. M. Mandell, and D. Deming. Kepler's Optical Secondary Eclipse of HAT-P-7b and Probable Detection of Planet-induced Stellar Gravity Darkening. *Astrophysical Journal Letters*, 764:L22, February 2013.

T. D. Morton and J. A. Johnson. On the Low False Positive Probabilities of Kepler Planet Candidates. *Astrophysical Journal*, 738:170, September 2011.

T. D. Morton and J. N. Winn. Obliquities of Kepler Stars: Comparison of Single- and Multiple-transit Systems. *Astrophysical Journal*, 796:47, November 2014.

C. Moutou, G. Hébrard, F. Bouchy, A. Eggenberger, I. Boisse, X. Bonfils, D. Gravallon, D. Ehrenreich, T. Forveille, X. Delfosse, M. Desort, A.-M. Lagrange, C. Lovis, M. Mayor, F. Pepe, C. Perrier, F. Pont, D. Queloz, N. C. Santos, D. Ségransan, S. Udry, and A. Vidal-Madjar. Photometric and spectroscopic detection of the primary transit of the 111-day-period planet HD 80 606 b. *Astronomy & Astrophysics*, 498:L5–L8, April 2009.

F. Mullally, J. L. Coughlin, S. E. Thompson, J. Rowe, C. Burke, D. W. Latham, N. M. Batalha, S. T. Bryson, J. Christiansen, C. E. Henze, A. Ofir, B. Quarles, A. Shporer, V. Van Eylen, C. Van Laerhoven, Y. Shah, A. Wolfgang, W. J. Chaplin, J.-W. Xie, R. Akeson, V. Argabright, E. Bachtell, T. Barclay, W. J. Borucki, D. A. Caldwell, J. R. Campbell, J. H. Catanzarite, W. D. Cochran, R. M. Duren, S. W. Fleming, D. Fraquelli, F. R. Girouard, M. R. Haas, K. G. Hełminiak, S. B. Howell, D. Huber, K. Larson, T. N. Gautier, III, J. M. Jenkins, J. Li, J. J. Lissauer, S. McArthur, C. Miller, R. L. Morris, A. Patil-Sabale, P. Plavchan, D. Putnam, E. V. Quintana, S. Ramirez, V. Silva Aguirre, S. Seader, J. C. Smith, J. H. Steffen, C. Stewart, J. Stober, M. Still, P. Tenenbaum, J. Troeltzsch, J. D. Twicken, and K. A. Zamudio. Planetary Candidates Observed by Kepler. VI. Planet Sample from Q1–Q16 (47 Months). *Astrophysical Journal Supplement Series*, 217:31, April 2015.

D. Naef, D. W. Latham, M. Mayor, T. Mazeh, J. L. Beuzit, G. A. Drukier, C. Perrier-Bellet, D. Queloz, J. P. Sivan, G. Torres, S. Udry, and S. Zucker. HD 80606 b, a planet on an extremely elongated orbit. *Astronomy & Astrophysics*, 375:L27–L30, August 2001.

M. Nagasawa, S. Ida, and T. Bessho. Formation of Hot Planets by a Combination of Planet Scattering, Tidal Circularization, and the Kozai Mechanism. *Astrophysical Journal*, 678:498–508, May 2008.

S. Naoz, W. M. Farr, Y. Lithwick, F. A. Rasio, and J. Teyssandier. Hot Jupiters from secular planet-planet interactions. *Nature*, 473:187–189, May 2011.

N. Narita, B. Sato, T. Hirano, and M. Tamura. First Evidence of a Retrograde Orbit of a Transiting Exoplanet HAT-P-7b. *Publications of the Astronomical Society of Japan*, 61:L35–L40, October 2009.

N. Narita, B. Sato, T. Hirano, J. N. Winn, W. Aoki, and M. Tamura. Spin-Orbit Alignment of the TrES-4 Transiting Planetary System and Possible Additional Radial-Velocity Variation. *Publications of the Astronomical Society of Japan*, 62:653–, June 2010.

N. Narita, Y. H. Takahashi, M. Kuzuhara, T. Hirano, T. Suenaga, R. Kandori, T. Kudo, B. Sato, R. Suzuki, S. Ida, M. Nagasawa, L. Abe, W. Brandner, T. D. Brandt, J. Carson, S. E. Egner, M. Feldt, M. Goto, C. A. Grady, O. Guyon, J. Hashimoto, Y. Hayano, M. Hayashi, S. S. Hayashi, T. Henning, K. W. Hodapp, M. Ishii, M. Iye, M. Janson, G. R. Knapp, N. Kusakabe, J. Kwon, T. Matsuo, S. Mayama, M. W. McElwain, S. M. Miyama, J.-I. Morino, A. Moro-Martin, T. Nishimura, T.-S. Pyo, E. Serabyn, H. Suto, M. Takami, N. Takato, H. Terada, C. Thalmann, D. Tomono, E. L. Turner, M. Watanabe, J. P. Wisniewski, T. Yamada, H. Takami, T. Usuda, and M. Tamura. A Common Proper Motion Stellar Companion to HAT-P-7. *Publications of the Astronomical Society of Japan*, 64:L7, December 2012.

H. R. Neilson and J. B. Lester. Spherically symmetric model stellar atmospheres and limb darkening. II. Limb-darkening laws, gravity-darkening coefficients and angular diameter corrections for FGK dwarf stars. *Astronomy & Astrophysics*, 556:A86, August 2013.

J. M. Nemec, R. Smolec, J. M. Benkő, P. Moskalik, K. Kolenberg, R. Szabó, D. W. Kurtz, S. Bryson, E. Guggenberger, M. Chadid, Y.-B. Jeon, A. Kunder, A. C. Layden, K. Kinemuchi, L. L. Kiss, E. Poretti, J. Christensen-Dalsgaard, H. Kjeldsen, D. Caldwell, V. Ripepi, A. Derekas, J. Nuspl, F. Mullally, S. E. Thompson, and W. J. Borucki. Fourier analysis of non-Blazhko ab-type RR Lyrae stars observed with the Kepler space telescope. *Monthly Notices of the Royal Astronomical Society*, 417:1022–1053, October 2011.

D. Nesvorný. Transit Timing Variations for Eccentric and Inclined Exoplanets. *Astrophysical Journal*, 701:1116–1122, August 2009.

D. Nesvorný, D. M. Kipping, L. A. Buchhave, G. Á. Bakos, J. Hartman, and A. R. Schmitt. The Detection and Characterization of a Nontransiting Planet by Transit Timing Variations. *Science*, 336:1133–, June 2012.

D. Nesvorný, D. Kipping, D. Terrell, J. Hartman, G. Á. Bakos, and L. A. Buchhave. KOI-142, The King of Transit Variations, is a Pair of Planets near the 2:1 Resonance. *Astrophysical Journal*, 777:3, November 2013.

A. Ofir and S. Dreizler. An independent planet search in the Kepler dataset. I. One hundred new candidates and revised Kepler objects of interest. *Astronomy & Astrophysics*, 555:A58, July 2013.

M. Ortiz, D. Gandolfi, S. Reffert, A. Quirrenbach, H. J. Deeg, R. Karjalainen, P. Montañés-Rodríguez, D. Nespral, G. Nowak, Y. Osorio, and E. Palle. Kepler-432 b: a massive warm Jupiter in a 52-day eccentric orbit transiting a giant star. *Astronomy & Astrophysics*, 573:L6, January 2015.

A. Pál, G. Á. Bakos, G. Torres, R. W. Noyes, D. W. Latham, G. Kovács, G. W. Marcy, D. A. Fischer, R. P. Butler, D. D. Sasselov, B. Sipőcz, G. A. Esquerdo,

G. Kovács, R. Stefanik, J. Lázár, I. Papp, and P. Sári. HAT-P-7b: An Extremely Hot Massive Planet Transiting a Bright Star in the Kepler Field. *Astrophysical Journal*, 680:1450–1456, June 2008.

M. A. C. Perryman, K. S. de Boer, G. Gilmore, E. Høg, M. G. Lattanzi, L. Lindegren, X. Luri, F. Mignard, O. Pace, and P. T. de Zeeuw. GAIA: Composition, formation and evolution of the Galaxy. *Astronomy & Astrophysics*, 369:339–363, April 2001.

E. A. Petigura, A. W. Howard, and G. W. Marcy. Prevalence of Earth-size planets orbiting Sun-like stars. *Proceedings of the National Academy of Science*, 110:19273–19278, November 2013.

E. A. Petigura, J. E. Schlieder, I. J. M. Crossfield, A. W. Howard, K. M. Deck, D. R. Ciardi, E. Sinukoff, K. N. Allers, W. M. J. Best, M. C. Liu, C. A. Beichman, H. Isaacson, B. M. S. Hansen, and S. Lépine. Two Transiting Earth-size Planets Near Resonance Orbiting a Nearby Cool Star. *Astrophysical Journal*, 811:102, October 2015.

C. Petrovich, S. Tremaine, and R. Rafikov. Scattering Outcomes of Close-in Planets: Constraints on Planet Migration. *Astrophysical Journal*, 786:101, May 2014.

P. Plavchan, C. Bilinski, and T. Currie. Investigation of Kepler Objects of Interest Stellar Parameters from Observed Transit Durations. *Publications of the Astronomical Society of the Pacific*, 126:34–47, January 2014.

F. Pont, H. Knutson, R. L. Gilliland, C. Moutou, and D. Charbonneau. Detection of atmospheric haze on an extrasolar planet: the 0.55-1.05 μm transmission spectrum of HD 189733b with the HubbleSpaceTelescope. *Monthly Notices of the Royal Astronomical Society*, 385:109–118, March 2008.

F. Pont, G. Hébrard, J. M. Irwin, F. Bouchy, C. Moutou, D. Ehrenreich, T. Guillot, S. Aigrain, X. Bonfils, Z. Berta, I. Boisse, C. Burke, D. Charbonneau, X. Delfosse, M. Desort, A. Eggenberger, T. Forveille, A.-M. Lagrange, C. Lovis, P. Nutzman, F. Pepe, C. Perrier, D. Queloz, N. C. Santos, D. Ségransan, S. Udry, and A. Vidal-Madjar. Spin-orbit misalignment in the HD 80606 planetary system. *Astronomy & Astrophysics*, 502:695–703, August 2009.

D. Pourbaix, A. A. Tokovinin, A. H. Batten, F. C. Fekel, W. I. Hartkopf, H. Levato, N. I. Morrell, G. Torres, and S. Udry. S_{B⁹}: The ninth catalogue of spectroscopic binary orbits. *Astronomy & Astrophysics*, 424:727–732, September 2004.

E. M. Price, L. A. Rogers, J. A. Johnson, and R. I. Dawson. How Low Can You go? The Photoeccentric Effect for Planets of Various Sizes. *Astrophysical Journal*, 799:17, January 2015.

A. Prša, N. Batalha, R. W. Slawson, L. R. Doyle, W. F. Welsh, J. A. Orosz, S. Seager, M. Rucker, K. Mjaseth, S. G. Engle, K. Conroy, J. Jenkins, D. Caldwell, D. Koch, and W. Borucki. Kepler Eclipsing Binary Stars. I. Catalog and Principal Characterization of 1879 Eclipsing Binaries in the First Data Release. *Astronomical Journal*, 141:83, March 2011.

B. Pu and Y. Wu. Spacing of Kepler Planets: Sculpting by Dynamical Instability. *ArXiv:1502.05449*, February 2015.

D. Queloz, A. Eggenberger, M. Mayor, C. Perrier, J. L. Beuzit, D. Naef, J. P. Sivan, and S. Udry. Detection of a spectroscopic transit by the planet orbiting the star HD209458. *Astronomy & Astrophysics*, 359:L13–L17, July 2000.

S. N. Quinn, T. R. White, D. W. Latham, W. J. Chaplin, R. Handberg, D. Huber, D. M. Kipping, M. J. Payne, C. Jiang, V. Silva Aguirre, D. Stello, D. H. Sliski, D. R. Ciardi, L. A. Buchhave, T. R. Bedding, G. R. Davies, S. Hekker, H. Kjeldsen, J. S. Kuszlewicz, M. E. Everett, S. B. Howell, S. Basu, T. L. Campante, J. Christensen-Dalsgaard, Y. P. Elsworth, C. Karoff, S. D. Kawaler, M. N. Lund, M. Lundkvist, G. A. Esquerdo, M. L. Calkins, and P. Berlind. Kepler-432: A Red Giant Interacting with One of its Two Long-period Giant Planets. *Astrophysical Journal*, 803:49, April 2015.

D. Raghavan, H. A. McAlister, T. J. Henry, D. W. Latham, G. W. Marcy, B. D. Mason, D. R. Gies, R. J. White, and T. A. ten Brummelaar. A Survey of Stellar Families: Multiplicity of Solar-type Stars. *Astrophysical Journal Supplement Series*, 190:1–42, September 2010.

F. A. Rasio and E. B. Ford. Dynamical instabilities and the formation of extrasolar planetary systems. *Science*, 274:954–956, November 1996.

H. Rauer, C. Catala, C. Aerts, T. Appourchaux, W. Benz, A. Brandeker, J. Christensen-Dalsgaard, M. Deleuil, L. Gizon, M.-J. Goupil, M. Güdel, E. Janot-Pacheco, M. Mas-Hesse, I. Pagano, G. Piotto, D. Pollacco, Ċ. Santos, A. Smith, J.-C. Suárez, R. Szabó, S. Udry, V. Adibekyan, Y. Alibert, J.-M. Almenara, P. Amaro-Seoane, M. Ammer-von Eiff, M. Asplund, E. Antonello, S. Barnes, F. Baudin, K. Belkacem, M. Bergemann, G. Bihain, A. C. Birch, X. Bonfils, I. Boisse, A. S. Bonomo, F. Borsa, I. M. Brandão, E. Brocato, S. Brun, M. Burleigh, R. Burston, J. Cabrera, S. Cassisi, W. Chaplin, S. Charpinet, C. Chiappini, R. P. Church, S. Csizmadia, M. Cunha, M. Damasso, M. B. Davies, H. J. Deeg, R. F. Díaz, S. Dreizler, C. Dreyer, P. Eggenberger, D. Ehrenreich, P. Eigmüller, A. Erikson, R. Farmer, S. Feltzing, F. d. Oliveira Fialho, P. Figueira, T. Forveille, M. Fridlund, R. A. García, P. Giommi, G. Giuffrida, M. Godolt, J. Gomes da Silva, T. Granzer, J. L. Grenfell, A. Grotsch-Noels, E. Günther, C. A. Haswell, A. P. Hatzes, G. Hébrard, S. Hekker, R. Helled, K. Heng, J. M. Jenkins, A. Johansen, M. L. Khodachenko, K. G. Kislyakova, W. Kley, U. Kolb, N. Krivova,

F. Kupka, H. Lammer, A. F. Lanza, Y. Lebreton, D. Magrin, P. Marcos-Arenal, P. M. Marrese, J. P. Marques, J. Martins, S. Mathis, S. Mathur, S. Messina, A. Miglio, J. Montalban, M. Montalto, M. J. P. F. G. Monteiro, H. Moradi, E. Moravveji, C. Mordasini, T. Morel, A. Mortier, V. Nascimbeni, R. P. Nelson, M. B. Nielsen, L. Noack, A. J. Norton, A. Ofir, M. Oshagh, R.-M. Ouazzani, P. Pápics, V. C. Parro, P. Petit, B. Plez, E. Poretti, A. Quirrenbach, R. Ragazzoni, G. Raimondo, M. Rainer, D. R. Reese, R. Redmer, S. Reffert, B. Rojas-Ayala, I. W. Roxburgh, S. Salmon, A. Santerne, J. Schneider, J. Schou, S. Schuh, H. Schunker, A. Silva-Valio, R. Silvotti, I. Skillen, I. Snellen, F. Sohl, S. G. Sousa, A. Sozzetti, D. Stello, K. G. Strassmeier, M. Švanda, G. M. Szabó, A. Tkachenko, D. Valencia, V. Van Grootel, S. D. Vauclair, P. Ventura, F. W. Wagner, N. A. Walton, J. Weingrill, S. C. Werner, P. J. Wheatley, and K. Zwintz. The PLATO 2.0 mission. *Experimental Astronomy*, September 2014.

G. R. Ricker, J. N. Winn, R. Vanderspek, D. W. Latham, G. Á. Bakos, J. L. Bean, Z. K. Berta-Thompson, T. M. Brown, L. Buchhave, N. R. Butler, R. P. Butler, W. J. Chaplin, D. Charbonneau, J. Christensen-Dalsgaard, M. Clampin, D. Deming, J. Doty, N. De Lee, C. Dressing, E. W. Dunham, M. Endl, F. Fressin, J. Ge, T. Henning, M. J. Holman, A. W. Howard, S. Ida, J. Jenkins, G. Jernigan, J. A. Johnson, L. Kaltenegger, N. Kawai, H. Kjeldsen, G. Laughlin, A. M. Levine, D. Lin, J. J. Lissauer, P. MacQueen, G. Marcy, P. R. McCullough, T. D. Morton, N. Narita, M. Paegert, E. Palle, F. Pepe, J. Pepper, A. Quirrenbach, S. A. Rinehart, D. Sasselov, B. Sato, S. Seager, A. Sozzetti, K. G. Stassun, P. Sullivan, A. Szentgyorgyi, G. Torres, S. Udry, and J. Villasenor. Transiting Exoplanet Survey Satellite (TESS). In *Society of Photo-Optical Instrumentation Engineers (SPIE) Conference Series*, volume 9143 of *Society of Photo-Optical Instrumentation Engineers (SPIE) Conference Series*, page 20, August 2014.

A. C. Robin, C. Reylé, S. Derrière, and S. Picaud. A synthetic view on structure and evolution of the Milky Way. *Astronomy & Astrophysics*, 409:523–540, October 2003.

F. J. Rogers, F. J. Swenson, and C. A. Iglesias. OPAL Equation-of-State Tables for Astrophysical Applications. *Astrophysical Journal*, 456:902, 1996.

L. A. Rogers. Most 1.6 Earth-radius Planets are Not Rocky. *Astrophysical Journal*, 801:41, March 2015.

R. A. Rossiter. On the detection of an effect of rotation during eclipse in the velocity of the brigher component of beta Lyrae, and on the constancy of velocity of this system. *Astrophysical Journal*, 60:15–21, July 1924.

J. F. Rowe, S. T. Bryson, G. W. Marcy, J. J. Lissauer, D. Jontof-Hutter, F. Mullally, R. L. Gilliland, H. Issacson, E. Ford, S. B. Howell, W. J. Borucki, M. Haas,

D. Huber, J. H. Steffen, S. E. Thompson, E. Quintana, T. Barclay, M. Still, J. Fortney, T. N. Gautier, III, R. Hunter, D. A. Caldwell, D. R. Ciardi, E. Devore, W. Cochran, J. Jenkins, E. Agol, J. A. Carter, and J. Geary. Validation of Kepler's Multiple Planet Candidates. III. Light Curve Analysis and Announcement of Hundreds of New Multi-planet Systems. *Astrophysical Journal*, 784:45, March 2014.

J. F. Rowe, J. L. Coughlin, V. Antoci, T. Barclay, N. M. Batalha, W. J. Borucki, C. J. Burke, S. T. Bryson, D. A. Caldwell, J. R. Campbell, J. H. Catanzarite, J. L. Christiansen, W. Cochran, R. L. Gilliland, F. R. Girouard, M. R. Haas, K. G. Hełminiak, C. E. Henze, K. L. Hoffman, S. B. Howell, D. Huber, R. C. Hunter, H. Jang-Condell, J. M. Jenkins, T. C. Klaus, D. W. Latham, J. Li, J. J. Lissauer, S. D. McCauliff, R. L. Morris, F. Mullally, A. Ofir, B. Quarles, E. Quintana, A. Sabale, S. Seader, A. Shporer, J. C. Smith, J. H. Steffen, M. Still, P. Tenenbaum, S. E. Thompson, J. D. Twicken, C. Van Laerhoven, A. Wolfgang, and K. A. Zamudio. Planetary Candidates Observed by Kepler. V. Planet Sample from Q1-Q12 (36 Months). *Astrophysical Journal Supplement Series*, 217:16, March 2015.

R. Sanchis-Ojeda and J. N. Winn. Starspots, Spin-Orbit Misalignment, and Active Latitudes in the HAT-P-11 Exoplanetary System. *Astrophysical Journal*, 743:61, December 2011.

R. Sanchis-Ojeda, D. C. Fabrycky, J. N. Winn, T. Barclay, B. D. Clarke, E. B. Ford, J. J. Fortney, J. C. Geary, M. J. Holman, A. W. Howard, J. M. Jenkins, D. Koch, J. J. Lissauer, G. W. Marcy, F. Mullally, D. Ragozzine, S. E. Seader, M. Still, and S. E. Thompson. Alignment of the stellar spin with the orbits of a three-planet system. *Nature*, 487:449–453, July 2012.

R. Sanchis-Ojeda, S. Rappaport, J. N. Winn, M. C. Kotson, A. Levine, and I. El Mellah. A Study of the Shortest-period Planets Found with Kepler. *Astrophysical Journal*, 787:47, May 2014.

R. Sanchis-Ojeda, S. Rappaport, E. Pallé, L. Delrez, J. DeVore, D. Gandolfi, A. Fukui, I. Ribas, K. G. Stassun, S. Albrecht, F. Dai, E. Gaidos, M. Gillon, T. Hirano, M. Holman, A. W. Howard, H. Isaacson, E. Jehin, M. Kuzuhara, A. W. Mann, G. W. Marcy, P. A. Miles-Páez, P. A. Montañés-Rodríguez, F. Murgas, N. Narita, G. Nowak, M. Onitsuka, M. Paegert, V. Van Eylen, J. N. Winn, and L. Yu. The K2-ESPRINT Project I: Discovery of the Disintegrating Rocky Planet with a Cometary Head and Tail EPIC 201637175b. *ArXiv e-prints*, April 2015.

K. C. Schlaufman. Evidence of Possible Spin-orbit Misalignment Along the Line of Sight in Transiting Exoplanet Systems. *Astrophysical Journal*, 719: 602–611, August 2010.

M. E. Schwamb, J. A. Orosz, J. A. Carter, W. F. Welsh, D. A. Fischer, G. Torres, A. W. Howard, J. R. Crepp, W. C. Keel, C. J. Lintott, N. A. Kaib, D. Terrell, R. Gagliano, K. J. Jek, M. Parrish, A. M. Smith, S. Lynn, R. J. Simpson, M. J. Giguere, and K. Schawinski. Planet Hunters: A Transiting Circumbinary Planet in a Quadruple Star System. *Astrophysical Journal*, 768:127, May 2013.

S. Seager and D. Deming. Exoplanet Atmospheres. *Annual Review of Astronomy & Astrophysics*, 48:631–672, September 2010.

S. Seager and J. J. Lissauer. *Introduction to Exoplanets*, pages 3–13. December 2010.

S. Seager and G. Mallén-Ornelas. A Unique Solution of Planet and Star Parameters from an Extrasolar Planet Transit Light Curve. *Astrophysical Journal*, 585:1038–1055, March 2003.

S. Seager and D. D. Sasselov. Theoretical Transmission Spectra during Extrasolar Giant Planet Transits. *Astrophysical Journal*, 537:916–921, July 2000.

S. Seager, M. Schrenk, and W. Bains. An Astrophysical View of Earth-Based Metabolic Biosignature Gases. *Astrobiology*, 12:61–82, January 2012.

Y. Shen and E. L. Turner. On the Eccentricity Distribution of Exoplanets from Radial Velocity Surveys. *Astrophysical Journal*, 685:553–559, September 2008.

V. Silva Aguirre, W. J. Chaplin, J. Ballot, S. Basu, T. R. Bedding, A. M. Serenelli, G. A. Verner, A. Miglio, M. J. Monteiro, A. Weiss, T. Appourchaux, A. Bonanno, A. M. Broomhall, H. Bruntt, T. L. Campante, L. Casagrande, E. Corsaro, Y. Elsworth, R. A. García, P. Gaulme, R. Handberg, S. Hekker, D. Huber, C. Karoff, S. Mathur, B. Mosser, D. Salabert, R. Schönrich, S. G. Sousa, D. Stello, T. R. White, J. Christensen-Dalsgaard, R. L. Gilliland, S. D. Kawaler, H. Kjeldsen, G. Houdek, T. S. Metcalfe, J. Molenda-Żakowicz, M. J. Thompson, D. A. Caldwell, J. L. Christiansen, and B. Wohler. Constructing a One-solar-mass Evolutionary Sequence Using Asteroseismic Data from Kepler. *Astrophysical Journal Letters*, 740:L2, October 2011.

V. Silva Aguirre, L. Casagrande, S. Basu, T. L. Campante, W. J. Chaplin, D. Huber, A. Miglio, A. M. Serenelli, J. Ballot, T. R. Bedding, J. Christensen-Dalsgaard, O. L. Creevey, Y. Elsworth, R. A. García, R. L. Gilliland, S. Hekker, H. Kjeldsen, S. Mathur, T. S. Metcalfe, M. J. P. F. G. Monteiro, B. Mosser, M. H. Pinsonneault, D. Stello, A. Weiss, P. Tenenbaum, J. D. Twicken, and K. Uddin. Verifying asteroseismically determined parameters of Kepler stars using Hipparcos parallaxes: self-consistent stellar properties and distances. *Astrophysical Journal*, 757(1):99, September 2012.

V. Silva Aguirre, S. Basu, I. M. Brandão, J. Christensen-Dalsgaard, S. Deheuvels, G. Doğan, T. S. Metcalfe, A. M. Serenelli, J. Ballot, W. J. Chaplin,

M. S. Cunha, A. Weiss, T. Appourchaux, L. Casagrande, S. Cassisi, O. L. Creevey, R. A. García, Y. Lebreton, A. Noels, S. G. Sousa, D. Stello, T. R. White, S. D. Kawaler, and H. Kjeldsen. Stellar ages and convective cores in field main-sequence stars: first asteroseismic application to two Kepler targets. *Astrophysical Journal*, 769(2):141, May 2013.

V. Silva Aguirre, G. R. Davies, S. Basu, J. Christensen-Dalsgaard, O. Creevey, T. S. Metcalfe, T. R. Bedding, L. Casagrande, R. Handberg, M. N. Lund, P. E. Nissen, W. J. Chaplin, D. Huber, A. M. Serenelli, D. Stello, V. Van Eylen, T. L. Campante, Y. Elsworth, R. L. Gilliland, S. Hekker, C. Karoff, S. D. Kawaler, H. Kjeldsen, and M. S. Lundkvist. Ages and fundamental properties of Kepler exoplanet host stars from asteroseismology. *ArXiv:1504.07992*, April 2015.

R. W. Slawson, A. Prša, W. F. Welsh, J. A. Orosz, M. Rucker, N. Batalha, L. R. Doyle, S. G. Engle, K. Conroy, J. Coughlin, T. A. Gregg, T. Fetherolf, D. R. Short, G. Windmiller, D. C. Fabrycky, S. B. Howell, J. M. Jenkins, K. Uddin, F. Mullally, S. E. Seader, S. E. Thompson, D. T. Sanderfer, W. Borucki, and D. Koch. Kepler Eclipsing Binary Stars. II. 2165 Eclipsing Binaries in the Second Data Release. *Astronomical Journal*, 142:160, November 2011.

D. H. Sliski and D. M. Kipping. A High False Positive Rate for Kepler Planetary Candidates of Giant Stars using Asterodensity Profiling. *Astrophysical Journal*, 788:148, June 2014.

J. C. Smith, M. C. Stumpe, J. E. Van Cleve, J. M. Jenkins, T. S. Barclay, M. N. Fanelli, F. R. Girouard, J. J. Kolodziejczak, S. D. McCauliff, R. L. Morris, and J. D. Twicken. Kepler Presearch Data Conditioning II - A Bayesian Approach to Systematic Error Correction. *Publications of the Astronomical Society of the Pacific*, 124:1000–1014, September 2012.

I. A. G. Snellen, R. J. de Kok, E. J. W. de Mooij, and S. Albrecht. The orbital motion, absolute mass and high-altitude winds of exoplanet HD209458b. *Nature*, 465:1049–1051, June 2010.

D. S. Spiegel, S. N. Raymond, C. D. Dressing, C. A. Scharf, and J. L. Mitchell. Generalized Milankovitch Cycles and Long-Term Climatic Habitability. *Astrophysical Journal*, 721:1308–1318, October 2010.

J. H. Steffen, D. C. Fabrycky, E. Agol, E. B. Ford, R. C. Morehead, W. D. Cochran, J. J. Lissauer, E. R. Adams, W. J. Borucki, S. Bryson, D. A. Caldwell, A. Dupree, J. M. Jenkins, P. Robertson, J. F. Rowe, S. Seader, S. Thompson, and J. D. Twicken. Transit timing observations from Kepler - VII. Confirmation of 27 planets in 13 multiplanet systems via transit timing variations and orbital stability. *Monthly Notices of the Royal Astronomical Society*, 428: 1077–1087, January 2013.

D. Stello, W. J. Chaplin, H. Bruntt, O. L. Creevey, A. García-Hernández, M. J. P. F. G. Monteiro, A. Moya, P.-O. Quirion, S. G. Sousa, J.-C. Suárez, T. Appourchaux, T. Arentoft, J. Ballot, T. R. Bedding, J. Christensen-Dalsgaard, Y. Elsworth, S. T. Fletcher, R. A. García, G. Houdek, S. J. Jiménez-Reyes, H. Kjeldsen, R. New, C. Régulo, D. Salabert, and T. Toutain. Radius Determination of Solar-type Stars Using Asteroseismology: What to Expect from the Kepler Mission. *Astrophysical Journal*, 700:1589–1602, August 2009.

T. E. Sterne. On the Determination of the Orbital Elements of Eccentric Eclipsing Binaries. *Proceedings of the National Academy of Science*, 26:36–40, January 1940.

N. I. Storch, K. R. Anderson, and D. Lai. Chaotic dynamics of stellar spin in binaries and the production of misaligned hot Jupiters. *Science*, 345:1317–1321, September 2014.

G. M. Szabó, R. Szabó, J. M. Benkő, H. Lehmann, G. Mező, A. E. Simon, Z. Kővári, G. Hodosán, Z. Regály, and L. L. Kiss. Asymmetric Transit Curves as Indication of Orbital Obliquity: Clues from the Late-type Dwarf Companion in KOI-13. *Astrophysical Journal Letters*, 736:L4, July 2011.

Y. Takeda, M. Ohkubo, and K. Sadakane. Spectroscopic Determination of Atmospheric Parameters of Solar-Type Stars: Description of the Method and Application to the Sun. *Publications of the Astronomical Society of Japan*, 54:451–462, June 2002.

M. Tegmark, M. A. Strauss, M. R. Blanton, K. Abazajian, S. Dodelson, H. Sandvik, X. Wang, D. H. Weinberg, I. Zehavi, N. A. Bahcall, F. Hoyle, D. Schlegel, R. Scoccimarro, M. S. Vogeley, A. Berlind, T. Budavari, A. Connolly, D. J. Eisenstein, D. Finkbeiner, J. A. Frieman, J. E. Gunn, L. Hui, B. Jain, D. Johnston, S. Kent, H. Lin, R. Nakajima, R. C. Nichol, J. P. Ostriker, A. Pope, R. Scranton, U. Seljak, R. K. Sheth, A. Stebbins, A. S. Szalay, I. Szapudi, Y. Xu, J. Annis, J. Brinkmann, S. Burles, F. J. Castander, I. Csabai, J. Loveday, M. Doi, M. Fukugita, B. Gillespie, G. Hennessy, D. W. Hogg, Ž. Ivezić, G. R. Knapp, D. Q. Lamb, B. C. Lee, R. H. Lupton, T. A. McKay, P. Kunszt, J. A. Munn, L. O'Connell, J. Peoples, J. R. Pier, M. Richmond, C. Rockosi, D. P. Schneider, C. Stoughton, D. L. Tucker, D. E. vanden Berk, B. Yanny, and D. G. York. Cosmological parameters from SDSS and WMAP. *Phys. Rev. D*, 69(10):103501, May 2004.

J. H. Telting, G. Avila, L. Buchhave, S. Frandsen, D. Gandolfi, B. Lindberg, H. C. Stempels, S. Prins, and NOT staff. FIES: The high-resolution Fiber-fed Echelle Spectrograph at the Nordic Optical Telescope. *Astronomische Nachrichten*, 335:41, January 2014.

B. Tingley and P. D. Sackett. A Photometric Diagnostic to Aid in the Identification of Transiting Extrasolar Planets. *Astrophysical Journal*, 627:1011–1018, July 2005.

B. Tingley, A. S. Bonomo, and H. J. Deeg. Using Stellar Densities to Evaluate Transiting Exoplanetary Candidates. *Astrophysical Journal*, 726:112, January 2011.

A. Tokovinin, S. Thomas, M. Sterzik, and S. Udry. Tertiary companions to close spectroscopic binaries. *Astronomy & Astrophysics*, 450:681–693, May 2006.

G. Torres, D. A. Fischer, A. Sozzetti, L. A. Buchhave, J. N. Winn, M. J. Holman, and J. A. Carter. Improved Spectroscopic Parameters for Transiting Planet Hosts. *Astrophysical Journal*, 757:161, October 2012.

A. H. M. J. Triaud, A. Collier Cameron, D. Queloz, D. R. Anderson, M. Gillon, L. Hebb, C. Hellier, B. Loeillet, P. F. L. Maxted, M. Mayor, F. Pepe, D. Pollacco, D. Ségransan, B. Smalley, S. Udry, R. G. West, and P. J. Wheatley. Spin-orbit angle measurements for six southern transiting planets. New insights into the dynamical origins of hot Jupiters. *Astronomy & Astrophysics*, 524:A25, December 2010.

F. Valsecchi and F. A. Rasio. Tidal Dissipation and Obliquity Evolution in Hot Jupiter Systems. *Astrophysical Journal*, 786:102, May 2014.

J. E. Van Cleve and D. A. Caldwell. Kepler Instrument Handbook. 2009.

V. Van Eylen and S. Albrecht. Eccentricity from Transit Photometry: Small Planets in Kepler Multi-planet Systems Have Low Eccentricities. *Astrophysical Journal*, 808:126, August 2015.

V. Van Eylen, H. Kjeldsen, J. Christensen-Dalsgaard, and C. Aerts. Properties of extrasolar planets and their host stars: A case study of HAT-P-7. *Astronomische Nachrichten*, 333:1088, December 2012.

V. Van Eylen, M. Lindholm Nielsen, B. Hinrup, B. Tingley, and H. Kjeldsen. Investigation of Systematic Effects in Kepler Data: Seasonal Variations in the Light Curve of HAT-P-7b. *Astrophysical Journal Letters*, 774:L19, September 2013.

V. Van Eylen, M. N. Lund, V. Silva Aguirre, T. Arentoft, H. Kjeldsen, S. Albrecht, W. J. Chaplin, H. Isaacson, M. G. Pedersen, J. Jessen-Hansen, B. Tingley, J. Christensen-Dalsgaard, C. Aerts, T. L. Campante, and S. T. Bryson. What Asteroseismology can do for Exoplanets: Kepler-410A b is a Small Neptune around a Bright Star, in an Eccentric Orbit Consistent with Low Obliquity. *Astrophysical Journal*, 782:14, February 2014.

V. Van Eylen, G. Nowak, S. Albrecht, E. Palle, I. Ribas, H. Bruntt, M. Perger, D. Gandolfi, T. Hirano, R. Sanchis-Ojeda, A. Kiilerich, J. P. Arranz, M. Badenas, F. Dai, H. J. Deeg, P. Montañés-Rodríguez, N. Narita, L. A. Rogers, V. J. Sánches Béjar, T. S. Shrotriya, and J. N. Winn. ESPRINT II: Spectroscopic follow-up of three exoplanet systems from the first K2 campaign*. *Submitted to ApJ Letters*, 2015.

A. Vanderburg and J. A. Johnson. A Technique for Extracting Highly Precise Photometry for the Two-Wheeled Kepler Mission. *Publications of the Astronomical Society of the Pacific*, 126:948–958, November 2014.

A. Vanderburg, B. T. Montet, J. A. Johnson, L. A. Buchhave, L. Zeng, F. Pepe, A. Collier Cameron, D. W. Latham, E. Molinari, S. Udry, C. Lovis, J. M. Matthews, C. Cameron, N. Law, B. P. Bowler, R. Angus, C. Baranec, A. Bieryla, W. Boschin, D. Charbonneau, R. Cosentino, X. Dumusque, P. Figueira, D. B. Guenther, A. Harutyunyan, C. Hellier, R. Kuschnig, M. Lopez-Morales, M. Mayor, G. Micela, A. F. J. Moffat, M. Pedani, D. F. Phillips, G. Piotto, D. Pollacco, D. Queloz, K. Rice, R. Riddle, J. F. Rowe, S. M. Rucinski, D. Sasselov, D. Ségransan, A. Sozzetti, A. Szentgyorgyi, C. Watson, and W. W. Weiss. Characterizing K2 Planet Discoveries: A Super-Earth Transiting the Bright K Dwarf HIP 116454. *Astrophysical Journal*, 800:59, February 2015.

A. Vidal-Madjar, A. Lecavelier des Etangs, J.-M. Désert, G. E. Ballester, R. Ferlet, G. Hébrard, and M. Mayor. An extended upper atmosphere around the extrasolar planet HD209458b. *Nature*, 422:143–146, March 2003.

G. Walker, J. Matthews, R. Kuschnig, R. Johnson, S. Rucinski, J. Pazder, G. Burley, A. Walker, K. Skaret, R. Zee, S. Grocott, K. Carroll, P. Sinclair, D. Sturgeon, and J. Harron. The MOST Asteroseismology Mission: Ultraprecise Photometry from Space. *Publications of the Astronomical Society of the Pacific*, 115:1023–1035, September 2003.

J. Wang, J.-W. Xie, T. Barclay, and D. A. Fischer. Influence of Stellar Multiplicity on Planet Formation. I. Evidence of Suppressed Planet Formation due to Stellar Companions within 20 AU and Validation of Four Planets from the Kepler Multiple Planet Candidates. *Astrophysical Journal*, 783:4, March 2014.

Achim Weiss and Helmut Schlattl. GARSTEC—the Garching Stellar Evolution Code. The direct descendant of the legendary Kippenhahn code. *Ap&SS*, 316:99, August 2008.

L. M. Weiss and G. W. Marcy. The Mass-Radius Relation for 65 Exoplanets Smaller than 4 Earth Radii. *Astrophysical Journal Letters*, 783:L6, March 2014.

L. M. Weiss, G. W. Marcy, J. F. Rowe, A. W. Howard, H. Isaacson, J. J. Fortney, N. Miller, B.-O. Demory, D. A. Fischer, E. R. Adams, A. K. Dupree, S. B. Howell, R. Kolbl, J. A. Johnson, E. P. Horch, M. E. Everett, D. C. Fabrycky, and S. Seager. The Mass of KOI-94d and a Relation for Planet Radius, Mass, and Incident Flux. *Astrophysical Journal*, 768:14, May 2013.

W. F. Welsh, J. A. Orosz, S. Seager, J. J. Fortney, J. Jenkins, J. F. Rowe, D. Koch, and W. J. Borucki. The Discovery of Ellipsoidal Variations in the Kepler Light Curve of HAT-P-7. *Astrophysical Journal Letters*, 713:L145–L149, April 2010.

M. W. Werner, T. L. Roellig, F. J. Low, G. H. Rieke, M. Rieke, W. F. Hoffmann, E. Young, J. R. Houck, B. Brandl, G. G. Fazio, J. L. Hora, R. D. Gehrz, G. Helou, B. T. Soifer, J. Stauffer, J. Keene, P. Eisenhardt, D. Gallagher, T. N. Gautier, W. Irace, C. R. Lawrence, L. Simmons, J. E. Van Cleve, M. Jura, E. L. Wright, and D. P. Cruikshank. The Spitzer Space Telescope Mission. *Astrophysical Journal Supplement Series*, 154:1–9, September 2004.

D. M. Williams and D. Pollard. Earth-like worlds on eccentric orbits: excursions beyond the habitable zone. *International Journal of Astrobiology*, 1:61–69, January 2002.

J. N. Winn. Transits and Occultations. *ArXiv 1001:2010*, January 2010.

J. N. Winn and D. C. Fabrycky. The Occurrence and Architecture of Exoplanetary Systems. *Annual Review of Astronomy & Astrophysics*, 53:409–447, August 2015.

J. N. Winn, R. W. Noyes, M. J. Holman, D. Charbonneau, Y. Ohta, A. Taruya, Y. Suto, N. Narita, E. L. Turner, J. A. Johnson, G. W. Marcy, R. P. Butler, and S. S. Vogt. Measurement of Spin-Orbit Alignment in an Extrasolar Planetary System. *Astrophysical Journal*, 631:1215–1226, October 2005.

J. N. Winn, J. A. Johnson, G. W. Marcy, R. P. Butler, S. S. Vogt, G. W. Henry, A. Roussanova, M. J. Holman, K. Enya, N. Narita, Y. Suto, and E. L. Turner. Measurement of the Spin-Orbit Alignment in the Exoplanetary System HD 189733. *Astrophysical Journal Letters*, 653:L69–L72, December 2006.

J. N. Winn, A. W. Howard, J. A. Johnson, G. W. Marcy, J. Z. Gazak, D. Starkey, E. B. Ford, K. D. Colón, F. Reyes, L. Nortmann, S. Dreizler, S. Odewahn, W. F. Welsh, S. Kadakia, R. J. Vanderbei, E. R. Adams, M. Lockhart, I. J. Crossfield, J. A. Valenti, R. Dantowitz, and J. A. Carter. The Transit Ingress and the Tilted Orbit of the Extraordinarily Eccentric Exoplanet HD 80606b. *Astrophysical Journal*, 703:2091–2100, October 2009a.

J. N. Winn, J. A. Johnson, S. Albrecht, A. W. Howard, G. W. Marcy, I. J. Crossfield, and M. J. Holman. HAT-P-7: A Retrograde or Polar Orbit, and a Third Body. *Astrophysical Journal Letters*, 703:L99–L103, October 2009b.

J. N. Winn, J. A. Johnson, D. Fabrycky, A. W. Howard, G. W. Marcy, N. Narita, I. J. Crossfield, Y. Suto, E. L. Turner, G. Esquerdo, and M. J. Holman. On the Spin-Orbit Misalignment of the XO-3 Exoplanetary System. *Astrophysical Journal*, 700:302–308, July 2009c.

J. N. Winn, D. Fabrycky, S. Albrecht, and J. A. Johnson. Hot Stars with Hot Jupiters Have High Obliquities. *Astrophysical Journal Letters*, 718:L145–L149, August 2010a.

J. N. Winn, J. A. Johnson, A. W. Howard, G. W. Marcy, H. Isaacson, A. Shporer, G. Á. Bakos, J. D. Hartman, and S. Albrecht. The Oblique Orbit of the Super-Neptune HAT-P-11b. *Astrophysical Journal Letters*, 723:L223–L227, November 2010b.

A. Wolszczan and D. A. Frail. A planetary system around the millisecond pulsar PSR1257 + 12. *Nature*, 355:145–147, January 1992.

J. T. Wright, S. Upadhyay, G. W. Marcy, D. A. Fischer, E. B. Ford, and J. A. Johnson. Ten New and Updated Multiplanet Systems and a Survey of Exoplanetary Systems. *Astrophysical Journal*, 693:1084–1099, March 2009.

Y. Wu and Y. Lithwick. Density and Eccentricity of Kepler Planets. *Astrophysical Journal*, 772:74, July 2013.

J.-W. Xie. Transit Timing Variation of Near-resonance Planetary Pairs. II. Confirmation of 30 Planets in 15 Multiple-planet Systems. *Astrophysical Journal Supplement Series*, 210:25, February 2014.

J.-P. Zahn. The dynamical tide in close binaries. *Astronomy & Astrophysics*, 41: 329–344, July 1975.

J.-P. Zahn. Tidal friction in close binary stars. *Astronomy & Astrophysics*, 57: 383–394, May 1977.